

Faculty of Science
Department of Imaging and Applied Physics

**Characterization of Thermal Stability, Microstructures and
Properties of Al_2TiO_5 - and Ti_3SiC_2 - Based Ceramics**

Zeya Oo

**This thesis is presented for the Degree of
Doctor of Philosophy
of
Curtin University**

September 2013

DECLARATION

To the best of my knowledge and belief, this thesis contains no material previously published by any other person except where due acknowledgement has been made. This thesis contains no material which has been accepted for the award of any other degree or diploma in any university.

Zeya Oo.

A handwritten signature in black ink, appearing to read 'Zeya Oo.', written in a cursive style with a long horizontal stroke at the end.

Signature:

Date: 28 September 2013

To my beloved family

ABSTRACT

This thesis focused on the diffraction study of thermal stability in functionally-graded aluminium titanate (Al_2TiO_5) and titanium silicon carbide (Ti_3SiC_2) based ceramic composites, and the oxidation properties of Ti_3SiC_2 . The main aims of the research were: (a) to study the parameters that control the thermal stability of Al_2TiO_5 - and Ti_3SiC_2 -based ceramics, (b) to evaluate the effect of atmospheres, oxygen partial pressures, temperatures and annealing time on the rate of isothermal decomposition, and (c) to investigate the oxidation behavior of Ti_3SiC_2 at elevated temperatures. These functionally-graded Al_2TiO_5 - and Ti_3SiC_2 -based ceramics have been characterized by X-ray diffraction (XRD), neutron diffraction (ND), synchrotron radiation diffraction (SRD), scanning electron microscope (SEM), secondary ion mass spectroscopy (SIMS), differential thermal analysis (DTA) and thermo-gravimetric analysis (TGA). The relative abundances of phase analysis were calculated by the Rietveld method and the thermochemical reactions were monitored by DTA in decomposed Al_2TiO_5 .

A high-temperature vacuum annealing process was proposed for the design of functionally graded Al_2TiO_5 - and Ti_3SiC_2 - based ceramics. The structural changes occurring during phase decomposition in real time was observed; in addition, the effect of the atmospheres (air, argon and 50 % oxygen, 50% argon) on the isothermal stability of Al_2TiO_5 at 1100°C and its decomposition behavior in the temperature range of $20\text{--}1400^\circ\text{C}$ were characterized by ND. There was no decomposition of Al_2TiO_5 in air and argon, as well as oxygen partial pressure of up to 1100°C , but it occurred between 1150 and 1300°C . It was shown that the process of decomposition in Al_2TiO_5 is reversible at temperatures above 1350°C with phase abundance of Al_2TiO_5 restored to 80 wt%.

A high-temperature vacuum annealing process had also been proposed for the designing of $\text{Ti}_3\text{SiC}_2\text{--TiC}$ composites with graded interfaces. In the presence of vacuum or controlled atmosphere of low oxygen partial pressure, it was found that Ti_3SiC_2

decomposed to form a surface layer of nonstoichiometric TiC and / or $\text{Ti}_5\text{Si}_3\text{C}$ at temperatures above 1200°C . Also, the composition depth profiling at the near surface of the vacuum-annealed Ti_3SiC_2 by XRD and SIMS, revealed composition gradation in the phase distribution of TiC and $\text{Ti}_5\text{Si}_3\text{C}$. The results showed that the phase stability and transition of Ti_3SiC_2 at elevated temperatures were strongly dependent on the oxygen partial pressure of the annealing atmosphere of the furnace.

The in-situ thermal stability of impure Ti_3SiC_2 in argon and air was investigated by ND in the temperature range of $23^\circ\text{--}1400^\circ\text{C}$ and analysed using the Rietveld method. The results showed that the partial pressure of oxygen plays an important role in the chemistry of thermal dissociation in argon and diffusion-controlled oxidation in air. Phases of rutile (TiO_2), TiO and cristobalite (SiO_2) were detected at 1000, 1250 and 1300°C respectively, when Ti_3SiC_2 was exposed to an oxygen-rich environment. Ti_3SiC_2 was oxidized in air at 1200°C ; SIMS analysis of the oxidation results showed a gradation in phase composition at the interface of the homogeneous rutile and heterogeneous cristobalite-rutile layers.

ACKNOWLEDGEMENTS

This thesis would not have been possible without the guidance and help of several individuals who in one way or another have contributed and extended their valuable assistance in the preparation and completion of this research.

First, I would like to express my sincere gratitude to my principal supervisor Professor I. M (Jim) Low, Department of Imaging and Applied Physics, Curtin University, Bentley campus, Perth, WA, for his continuous guidance, encouragement, support and the tremendous knowledge that he has shared with me, not only in Materials Science, but also in all aspects of my thesis.

I am also very grateful to Emeritus Professor Brian O' Connor, Associate Supervisor, Department of Imaging and Applied Physics, Curtin University, Bentley campus, Perth, WA, for his continuous guidance on Rietveld data analysis. My gratitude also goes to Associate Professor Bob Loss, Head of Department of Imaging and Applied Physics, and Ms Camel McManus, ex-secretary of Department of Imaging and Applied Physics, Curtin Bentley campus for allowing me to use the facilities therein to conduct the required experimental work.

I would like to thank Professor Dr. Alexander Gorin, Ex-Associate Supervisor, Head of Department of Chemical Engineering, Swinburne University of Technology, Sarawak Malaysia, and Associate Professor Barbara Stauble (Ex-Director of Research and Development and also Ex-Associate supervisor), for their constant encouragement and support.

My earnest thanks also goes to Associate Professor Dr. Chua Han Bing, Head of Department of Chemical Engineering, and Mr. Rajalingam Sökkalingam, Mr. Veeramani S, Mr Lenin Gopal, Mr Rajamohan Ganesan, Dr Perumal Kumar, Senior Lecturers, and Dr Nagarajan R, Head of Department of Applied Geology, School of Engineering and Science, Curtin University Sarawak Malaysia, for their continuous encouragement, insightful comments and motivation for me to complete the thesis on schedule.

I am deeply indebted to Associate Professor Dr. Jeanne Dawson, Director of the Learning Centre, Curtin University, Bentley campus, Perth, Dr. Tan Chong Keng, Senior Lecturer, Department of Electrical and Computer Engineering, Curtin University Sarawak, Ms Serina Ann Doss, Lecturer, The Learning Centre, Curtin University Sarawak Malaysia, Dr M. V. Prasanna, Senior Lecturer, Department of Applied Geology, Curtin University Sarawak Malaysia, for their kind assistance in reviewing my draft thesis.

As for my colleagues in the Department of Imaging and Applied Physics, Curtin Bentley and School of Engineering and Science, Curtin University Sarawak, I am thankful to them for their continuous support during the many years it took me to complete the analysis work.

I would like to express my sincere gratitude to Curtin University Sarawak Malaysia, Staff Study Support Program for the finance supporting to pursue PhD study in Curtin University, Bentley campus, Perth, Australia.

I am also very grateful to Madam Sheila Gopinath for her continuous unfailing advice, encouragement, constructive ideas and inspiration for the professional proof reading of my thesis.

Last but not least, none of this work would have been possible without the love and patience of my family. To my mother, Madam Phwa Tha, and my lovely wife, Dr Thein Thein Kyaw --- I could not have done this without you --- you are my inspiration and my guiding light.

Zeya Oo

September 2013

LIST OF PUBLICATIONS INCLUDED AS PART OF THE THESIS

LOW, I. M. & OO, Z. 2002. Diffraction Studies of a Novel Ti_3SiC_2 -TiC System with Graded Interfaces, *Journal of the Australian Ceramic Society*, 38, 112-116.

OO, Z., LOW, I. M. & O'CONNOR, B. H. 2006. Dynamic Study of the Thermal Stability of Impure Ti_3SiC_2 in Argon and Air by Neutron Diffraction, *Physica B*, 385-386, 499-501.

LOW, I. M., OO, Z. & O'CONNOR, B. H. 2006. Effect of Atmospheres on the Thermal Stability of Aluminium Titanate, *Physica B*, 385-386, 502-504.

LOW, I. M., OO, Z. & PRINCE, K. E. 2007. Effect of Vacuum Annealing on the Phase Stability of Ti_3SiC_2 , *Journal of the American Ceramic Society*, 90, 2610-2614.

LOW, I. M. & OO, Z. 2008. Reformation of Phase Composition in Decomposed Aluminium Titanate, *Materials Chemistry and Physics*, 111, 9-12.

LOW, I. M. & OO, Z. 2008. In Situ Diffraction Study of Self-Recovery in Aluminium Titanate, *Journal of the American Ceramic Society*, 91, 1027-1029.

Statement of Contribution of Others

Zeya Oo's input into this project and the associated papers included the execution of all the experimental work, and a dominant contribution to the intellectual input involved in the project. As is almost always the case in the physical sciences, other scientists made contributions to the work that were significant enough to warrant co authorship on the resulting journal articles. These are specific below:

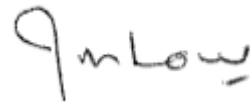
I.M. Low, provided project supervision and manuscript editing.

B.H. O'Connor, provided specialist technical advice and manuscript editing.

K.E. Prince, provided specialist technical advice and instrument usage (Dynamics SIMS at ANSTO).



Zeya Oo



Prof It Meng Low

**LIST OF PUBLICATIONS BY THE CANDIDATE RELEVANT TO THE THESIS
BUT NOT FORMING PART OF IT.**

OO, Z., LOW, I. M. & O'CONNOR, B. H. 2004. In-Situ study of the Phase Stability of Ti_3SiC_2 in Argon by Neutron Diffraction, Proceedings of *AUSTCERAM & the 3rd International Conference on Advanced Materials Processing*, Melbourne, Australia, 132-133.

OO, Z., CHEN-TAN, N. & LOW, I. M. 2004. Indentation Responses of Functionally-graded $Al_2O_3-Al_2TiO_5$ Bi-layers, Proceedings of *AUSTCERAM & the 3rd International Conference on Advanced Materials Processing*, Melbourne, Australia, 121-122.

LOW, I.M., **OO, Z.**, O'CONNOR, B. H. & SMITH, R. I. 2004. Effect of Ageing on the Thermal Stability of Aluminium Titanate, Proceedings of *AUSTCERAM & the 3rd International Conference on Advanced Materials Processing*, Melbourne, Australia, 74-75.

LOW, I. M. & **OO, Z.** 2004. X-ray and Neutron Diffraction Studies on a Functionally Graded Ti_3SiC_2 -TiC System, Proceedings of 28th International Cocoa Beach Conference on Advanced Ceramics & Composites: A & B. (E. Lara-Curzio & Readey, Eds) CESP, Vol 25, Issue 3 & 4. 183-188.

LOW, I. M., **OO, Z.** & O'CONNOR, B. H. 2005. Effect of Oxygen Partial Pressure on the Phase Stability of Ti_3SiC_2 , 29th *Cocoa Beach Conference on Advanced Ceramics and Composites*, Florida, United States, CESP Vol 26. Number 3, 323-330.

OO, Z., LOW, I. M. & O'CONNOR, B. H. 2005. Data Analysis of In-Situ Study of the Phase Stability of Ti_3SiC_2 in argon by using Rietveld Method, Proceedings of 3rd International Conference on Computer Applications, University of Computer Studies, Yangon, Myanmar, 173-178.

OO, Z., LOW, I. M., PALMQUIST, J-P., PANG, W. K. & AVDEEV, M. 2008. Mapping of Composition, Phase Transitions and Properties in Oxidized Ti_3SiC_2 , *Key Engineering Materials*, 368-372, 986-988.

LOW, I. M. & **OO, Z.** 2010. Dynamic Neutron Diffraction study of Thermal Stability and Self-Recovery in Aluminium Titanate, *Ceramic Engineering and Science Proceedings*, (Edited by W. M. Kriven, Y. Zhou, M. Radovic, S. Mathur and T. Ohji), John Wiley & Sons, Inc., Hoboken, NJ, USA, doi: 10.1002/9780470944103.ch14, 31 (10), 139-149.

LIST OF BOOK-CHAPTERS

W.K. Pang, **Z. Oo**, J.V. Hanna, and I.M. Low (2012), Oxidation characteristics of Ti_3AlC_2 , Ti_3SiC_2 and Ti_2AlC . Chapter 12 in *Advances in Science and Technology of $M_{n+1}AX_n$ Phases*. I.M. Low (Ed). Woodhead Publishing Ltd. (UK). pp. 289-322.

W.K. Pang, **Z. Oo**, V.K. Peterson, and I.M. Low (2012), Phase and thermal stability in Ti_3SiC_2 and $\text{Ti}_3\text{SiC}_2/\text{TiC}/\text{TiSi}_2$ systems. Chapter 15 in *Advances in Science and Technology of $M_{n+1}AX_n$ Phases*. I.M. Low (Ed). Woodhead Publishing Ltd. (UK). pp. 389-413.

LIST OF FIGURES

Figure 1.1	Flowchart of experimental design for characterization of Al_2TiO_5	7
Figure 1.2	(a) Flowchart of experimental design for characterisation of oxidized Ti_3SiC_2	8
Figure 1.2	(b) Flowchart of experimental design for characterization techniques for vacuum-annealed Ti_3SiC_2	9
Figure 1.3	(a) Structure of FGM showing composition variations, and (b) Structure of non-FGM showing composition uniformity. Legend: Ceramics (O), metal (\bullet), fiber ($\diamond +$) and micropore (\circ). (Koizumi and Niino, 1995)	11
Figure 1.4	Variations in properties of a functionally-graded material (FGM). (Koizumi and Niino, 1995)	11
Figure 1.5	Crystal structure of α -alumina. The parameters are based on Model ICSD # 73725. (Maslen et al. 1993) Legend: Al^{3+} (red) and O^{2-} (blue) (Kraus and Nolze, 1999)	14
Figure 1.6	Orthorhombic crystal structure of aluminium titanate (Al_2TiO_5) based on the model of Epicier et al. (1991). Legend: red is Al, blue is O and green is Ti. (Kraus and Nolze, 1999)	16
Figure 1.7	A polyhedral representation of the pseudobrookite-type β - Al_2TiO_5 crystal structure(Austin & Schwartz, 1953)	18
Figure 1.8	(a) The basic unit cell crystal structures of TiO_2 (a) rutile (b) anatase. (Cromer and Harrington, 1954)	21
Figure 1.9	Unit cell of Ti_3SiC_2 crystal structure. Legend: Blue is Si, red is Ti and black is C. (Barsoum et al. 2000)	24
Figure 1.10	The crystal structure of TiC. (Li et al. 2008)	26
Figure 1.11	Microstructure (BS-SEM) of Al_2TiO_5 after (a) 1h, (b) 8h, and (c) 25h annealing at 1100°C . (Legend: TiO_2 , rutile is white, Al_2TiO_5 is light gray, Al_2O_3 is dark gray and black are pores and cracks). (Buscaglia and Nanni, 1998)	37

Figure 1.12	Schematic diagram showing the possible decomposition mechanisms of Al_2TiO_5 (Buscaglia. and Nanni, 1998)	38
Figure 1.13	A schematic showing the thermal stability of MAX phases at elevated temperature in different conditions of vacuum (Low and Pang 2013)	40
Figure 1.14	Phase abundance as a function of temperature for the decomposition of (a) Ti_3SiC_2 , (b) $\text{Ti}_3\text{Si}_{0.95}\text{Al}_{0.05}\text{C}_2$, (c) Ti_3AlC_2 , (d) Ti_2AlC_2 , (e) Ti_2AlN and (f) Ti_4AlN_3 in vacuum (Low and Pang 2013)	42
Figure 1.15	Variation of weight loss as a function of temperature for Ti_4AlN_3 (■) and Ti_2AlN (◆) (Low and Pang 2013)	43
Figure 1.16	Vapour pressure of selected elements at various temperatures (www.veeco.com/library/Learning_Centre/Growth_Information/Vapor_Pressure_Data_For_Selected_Elements/Index.aspx).	45
Figure 1.17	Scanning electron micrographs of the surface microstructures of vacuum-decomposed MAX phases; (a) Ti_2AlN , (b) Ti_4AlN_3 , (c) Ti_3SiC_2 , and (d) Ti_3AlC_2 (Low and Pang 2013)	47
Figure 1.18	Time-dependent phase abundance and Avrami fit isothermal decomposition of (a) Ti_2AlN , (b) Ti_3SiC_2 at 1550°C in vacuum (Low and Pang 2013)	48
Figure 5.1	Neutron diffraction (MRPD) Rietveld difference plot for Al_2TiO_5 in air at 1100°C for 2 h	112
Figure 5.2	Neutron diffraction (MRPD) Rietveld difference plot for Al_2TiO_5 in argon at 1100°C for 2 h	114
Figure 5.3	Neutron diffraction Rietveld difference plot for Al_2TiO_5 in air at room temperature	117
Figure 5.4	Neutron diffraction Rietveld difference plot for Al_2TiO_5 in air at 1400°C for 2 h	117
Figure 5.5	ND diffraction Rietveld difference plots for isothermal stability Al_2TiO_5 at 1100°C in an atmosphere of 50% of oxygen and 50% of argon for (a) 1 h, and (b) 16 h . Legend: AT = Al_2TiO_5 , Al = Al_2O_3	120

Figure 5.6	ND Rietveld difference plots for Al_2TiO_5 at (a) room temperature, (b) 1450°C for 2 h, and (c) 1500°C for 2 h. Wavelength for ND is 1.665\AA	124
Figure 5.7	Phase abundance versus temperature for the formation of Al_2TiO_5 from room temperature to 1500°C . (a) re-heating from room temperature to 1450°C , and (b) controlled cooling from 1450°C to room temperature. Error bars indicate two estimated standard deviations $\pm 2\sigma$. Legend: $\text{Al}_2\text{TiO}_5 = \blacksquare$, $\text{Al}_2\text{O}_3 = \blacklozenge$, $\text{TiO}_2 = \blacktriangle$	127
Figure 5.8	(a) and (b): XRD Rietveld difference plot for Ti_3SiC_2 first-depth ($0\ \mu\text{m}$ thick) and sixth-depth ($50\ \mu\text{m}$ thick) Legend: + = Measured pattern, Solid Red = Calculated pattern, Blue = (Vertical lines) Allowable peak positions for each of the phases, Green = Intensity differences between the two patterns	130
Figure 5.9	Neutron diffraction Rietveld difference plot for Ti_3SiC_2 annealed at 1200°C in argon for 2 h	135
Figure 5.10	Stacking ND diffraction patterns for the Ti_3SiC_2 during heat treatment in argon from room temperature to 1400°C . The measured and calculated patterns are indicated by crosses (black) and solid line (red) respectively Legend: 1 = Ti_3SiC_2 , 2 = TiC , 3 = $\text{Ti}_5\text{Si}_3\text{C}$, 4 = Al_2O_3 , 5 = TiO_2	136
Figure 5.11	(a) Neutron diffraction Rietveld difference plot for the Ti_3SiC_2 oxidised in air at 1350°C Legend: From top to bottom T = TiC , A = TiO_2 (rutile), C = SiO_2 (Cristobalite), O = TiO	140
Figure 5.11	(b) Neutron diffraction Rietveld profile plot for the Ti_3SiC_2 oxidised in air cooling from 1350°C to room temperature Legend: From top to bottom T = TiC , A = TiO_2 (rutile) C = SiO_2 , (Cristobalite), Tr = SiO_2 (Trydimite) and O = TiO	140
Figure 5.12	(a) Neutron diffraction Rietveld difference plot for the as-received Maxthal Ti_3SiC_2 at air for room temperature	145
Figure 5.12	(b) Neutron diffraction Rietveld difference plots for Maxthal Ti_3SiC_2 oxidized in air at 1400°C for 2 h	145

Figure 5.12	(c) Neutron diffraction Rietveld difference plots for Maxthal Ti_3SiC_2 oxidized in air at 1400°C and then cooled to 23°C Legend: SiO_2 (C) = Cristobalite, SiO_2 (T) = Tridymite	146
Figure 5.13	Variations of phase evolution during the in-situ oxidation of Ti_3SiC_2 (Maxthal 312) as revealed by neutron diffraction Legend: $\text{Ti}_3\text{SiC}_2 = \blacklozenge$, $\text{TiC} = \blacksquare$, TiO_2 rutile = \blacktriangle , $\text{TiSi}_2 = \blacklozenge$, SiO_2 cristobalite = \bullet	149
Figure 5.14	Optical micrograph showing the microstructural details of Ti_3SiC_2 oxidized at 1300°C for 20 min in air	150
Figure 5.15	XRD Rietveld diffraction pattern for Ti_3SiC_2 (40 micron)	151
Figure 5.16	XRD depth-profiling of phase abundances for Ti_3SiC_2 oxidized at 1300°C for 15 min in air Legend: $\text{TiO}_2 = \blacksquare$, $\text{Ti}_3\text{SiC}_2 = \blacklozenge$, SiO_2 (Cristobalite) = \blacktriangle	153
Figure 5.17	Schematic diagram for the Secondary Ion Mass Spectroscopy (SIMS) Source: Institute for Research in Materials, Dalhousie University, Canada. (http://www.hiden.com.cn)	170

LIST OF TABLES

Table 1.1	Different types of FGM (Sakai and Hirai 1991)	12
Table 1.2	Development of Al_2TiO_5 crystal structure lattice parameters	17
Table 1.3	Previous experimental studies on TiO_2 (rutile) crystal structure after 1960	20
Table 1.4	Differences between the models of Kisi et al. (1998) and Jeitschko and Nowotny (1967) for Ti_3SiC_2	23
Table 1.5	Mechanical properties of 99.9% pure α -alumina. (Schneider, 1994)	27
Table 1.6	Thermal expansion coefficients of Al_2TiO_5 along the three crystal axes (from room temperature to 1200°C)	27
Table 1.7	Thermo-mechanical properties of Al_2TiO_5 -based ceramics. (The Encyclopedia of Advanced Materials 1994)	28
Table 1.8	Physical and mechanical properties of rutile (TiO_2). (Yan et al. 1981)	29
Table 1.9	Examples of processing methods used for the fabrication of ceramic composites.	34
Table 1.10	Comparison of the kinetics decomposition in six MAX-phase samples.	45
Table 1.11	Comparison of the Avrami decomposition kinetics in MAX phases. (Low and Pang 2013)	48
Table 5.1	Figures-of-merit from Rietveld refinement with ND data for isothermal stability of Al_2TiO_5 in air at 1100°C .	113
Table 5.2	Figures-of-merit from Rietveld refinement with ND data for isothermal stability of Al_2TiO_5 in argon at 1100°C	115
Table 5.3	Figures-of-merit from Rietveld refinement of ND data for Al_2TiO_5 in air from room temperature to 1400°C	118
Table 5.4	Figures-of-merit from Rietveld refinement with ND (MRPD) data for Al_2TiO_5 at 1100°C in the atmosphere of 50% oxygen and 50% argon from 1 h to 16 h	121

Table 5.5	Figures-of-merit from Rietveld refinement of ND data for reformation of Al_2TiO_5 from 20°C to 1500°C	125
Table 5.6	Relative phase abundances from Rietveld refinement with ND (MRPD) for the self-recovery in Al_2TiO_5 from room temperature to 1500°C	126
Table 5.7	Relative phase abundances determined by Rietveld analysis for XRD data: Composition depth profiles of vacuum-annealed Ti_3SiC_2	131
Table 5.8	Figures-of-merit for Rietveld refinements based on XRD depth-profiling data for thermal stability of Ti_3SiC_2	132
Table 5.9	Figures-of-merit from Rietveld refinement with ND (MRPD) data for Ti_3SiC_2 annealed in argon from room temperature to 1400°C	137
Table 5.10	Relative phase abundances determined from Rietveld refinement using MRPD data for Ti_3SiC_2 annealed in argon from 20°C to 1400°C	138
Table 5.11	Relative phase abundances determined from Rietveld refinement using MRPD, in-situ ND results for Ti_3SiC_2 oxidized in air from room temperature to 1350°C and from 1350°C to room temperature on cooling	141
Table 5.12	Figures-of-merit from Rietveld refinement with ND (MRPD) data for Ti_3SiC_2 oxidized in air from room temperature to 1350°C	142
Table 5.13	Relative phase abundance determined from Rietveld analysis refinement using ND results for Ti_3SiC_2 (Maxthal 312) oxidized in air from 23°C to 1400°C and cooled from 1400°C to 23°C	147
Table 5.14	Figures-of-merit from Rietveld refinement with ND data for Ti_3SiC_2 (Maxthal 312) oxidized in air from room temperature to 1400°C	148
Table 5.15	Relative phase compositions determined from Rietveld refinement with XRD data for depth-profiling of phase abundances in Ti_3SiC_2 oxidized at 1300°C for 20 min in air	152
Table 5.16	Figures-of-merit from Rietveld refinement with XRD data for Ti_3SiC_2 oxidized at 1300°C for 20 min in air	152
Table 5.17	List of structure models, ICSD numbers and authors used for the Rietveld Analysis	161

Table 5.18	(a), (b) and (c) Operational conditions when using in POLARIS	165
Table 5.19	Operational conditions when using XRD	167
Table 5.20	Operational condition when using DTA/TGA	172
Table 5.21	Operational conditions when using MRPD to analyze Al_2TiO_5	175
Table 5.22	Operational conditions when using MRPD to analyze Ti_3SiC_2	176

LIST OF ABBREVIATIONS

ANBF	Australian National Beamline Facility
ANSTO	Australian Nuclear Science and Technology Organisation
CVD	Chemical Vapor Deposition
DTA	Differential Thermal Analysis
FGM	Functionally-Graded Material
GISRD	Grazing-Incidence Synchrotron Radiation Diffraction
HIP	Hot-Isostatic-Pressing
ICSD	International Crystal Structure Database
ICSD-PDF	International Centre for Diffraction Data-Powder Diffraction File
LGM	Layer-Graded Materials
MRPD	Medium Resolution Powder Diffraction
ND	Neutron Diffraction
PVD	Physical Vapor Deposition
SEM	Scanning Electronic Microscopy
SIMS	Secondary Ions Mass Spectrometry
SRD	Synchrotron Radiation Diffraction
TGA	Thermo-Gravimetric Analysis

TABLE OF CONTENTS

TITLE PAGE

DECLARATION

DEDICATION

ABSTRACT **i**

ACKNOWLEDGEMENTS **iii**

LIST OF PUBLICATIONS INCLUDED AS PART OF THE THESIS **v**

STATEMENT OF CONTRIBUTION OF OTHERS **vi**

**LIST OF PUBLICATIONS BY THE CANDIDATE RELEVANT TO THE
THESIS BUT NOT FORMING PART OF IT** **vii**

LIST OF BOOK CHAPTERS **ix**

LIST OF FIGURES **x**

LIST OF TABLES **xiv**

LIST OF ABBREVIATIONS	xvii
------------------------------	-------------

TABLE OF CONTENTS	xviii
--------------------------	--------------

1	INTRODUCTION AND OVERVIEW	1
1.1	Introduction	1
1.1.1	Aims and Significance	4
1.1.2	Research Methodology	5
1.2	Background	10
1.2.1	Functionally-Graded Materials (FGMs)	10
1.2.1.1	Processing Method	11
1.2.2	Crystal Structure	13
1.2.2.1	Alumina (Al_2O_3)	13
1.2.2.2	Aluminum Titanate (Al_2TiO_5)	14
1.2.2.3	Titanium Oxide (TiO_2)	18
1.2.2.4	Titanium Silicon Carbide (Ti_3SiC_2)	21
1.2.2.5	Titanium Carbide (TiC)	25
1.2.3	Physical and Mechanical Properties	26
1.2.3.1	Alumina (Al_2O_3)	26
1.2.3.2	Aluminium Titanate (Al_2TiO_5)	26
1.2.3.3	Titanium Oxide (TiO_2)	28
1.2.3.4	Titanium Silicon Carbide (Ti_3SiC_2)	30

1.2.3.5	Titanium Carbide (TiC)	32
1.2.4	Ceramic Systems containing Al_2O_3 - Al_2TiO_5	32
1.2.5	Decomposition Behavior of Al_2TiO_5	35
1.2.6	Thermal Decomposition Behavior of MAX Phases	38
1.2.7	Oxidation Behavior of Ti_3SiC_2	49
1.3	Bibliography: List of all references cited in the Introduction and Overview	53
2	PUBLICATIONS FORMING PART OF THE THESIS	72
2.1	Effect of Atmospheres on the Thermal Stability of Aluminium Titanate	73
2.2	In Situ Diffraction study of Self-Recovery in Aluminium Titanate	77
2.3	Reformation of Phase Composition in Decomposed Aluminium Titanate	81
2.4	Diffraction Studies of a Novel Ti_3SiC_2 -TiC System with Graded Interfaces	86
2.5	Effect of Vacuum Annealing on the Phase Stability of Ti_3SiC_2	92
2.6	Dynamic Study of the Thermal Stability of Impure Ti_3SiC_2 in Argon and Air by Neutron Diffraction	98
3	CONCLUSIONS	102
4	RECOMMENDATIONS FOR FURTHER WORK	105
5	APPENDIX 1: SUPPLEMENTARY INFORMATION FOR PUBLICATIONS	109
5.1	Appendix I-A: Supplementary Information for “Effect of Atmospheres on the Thermal Stability of Aluminium Titanate”	110

	Appendix I-B: Supplementary Information for “In Situ Diffraction study of Self-Recovery in Aluminium Titanate”	122
	Appendix I-C: Supplementary Information for “Reformation of Phase Composition in Decomposed Aluminium Titanate”	122
	Appendix I-D: Supplementary Information for (i) “Effect of Vacuum Annealing on the Phase Stability of Ti_3SiC_2 ” (ii) “Diffraction Studies of a Novel Ti_3SiC_2 -TiC System with Graded Interfaces”	128
	Appendix I-E: Supplementary Information for “Dynamic Study of the Thermal Stability of Impure Ti_3SiC_2 in Argon and Air by Neutron Diffraction”	133
5.2	Appendix I-F: Supplementary Information for “All Publications Used as Parts of Thesis”	154
5.2.1	Rietveld Data Analysis	155
5.3	Appendix I-G: Supplementary Information for (i) “Effect of Vacuum Annealing on the Phase Stability of Ti_3SiC_2 ” (ii) “Diffraction Studies of a Novel Ti_3SiC_2 -TiC System with Graded Interfaces”	162
5.3.1	POLARIS Medium-Resolution, High Intensity Powder Diffractometer	163
5.3.2	X Ray Diffraction (XRD)	166
5.4	Appendix I-H: Supplementary Information for (i) “Effect of Vacuum Annealing on the Phase Stability of Ti_3SiC_2 ”, (ii) “Dynamic Study of the Thermal Stability of Impure Ti_3SiC_2 in Argon and Air by Neutron Diffraction”	168
5.4.1	Secondary Ion Mass Spectroscopy (SIMS)	169
5.5	Appendix I-I: Supplementary Information for “Reformation of Phase Composition in Decomposed Aluminium Titanate”	171
5.5.1	Differential Thermal Analysis (DTA)/Thermo-gravimetric Analysis (TGA)	172

5.5.2	Scanning Electronic Microscopy (SEM)	173
5.6	Appendix I-J (i) Supplementary Information for “Effect of Atmospheres on the Thermal Stability of Aluminium Titanate.”, (ii) “Reformation of Phase Composition in Decomposed Aluminium Titanate”, (iii) “In Situ Diffraction study of Self-Recovery in Aluminium Titanate” and (iv) “Dynamic Study of the Thermal Stability of Impure Ti_3SiC_2 in Argon and Air by Neutron Diffraction”	174
5.6.1	MRPD-Medium Resolution Powder Diffraction (Neutron Diffraction)	175
5.7	Appendix I-K: ICSD Crystal Structure Data	177
6	APPENDIX II: STATEMENT OF CONTRIBUTIONS OF OTHERS	187
6.1	Appendix II-A: “Statement of Contribution of Others” for “LOW, I.M., OO, Z. & O’CONNOR. B.H. 2006. Effect of Atmospheres on the Thermal Stability of Aluminium Titanate. <i>Physica B</i> , 385-386, 502-504”.	188
6.2	Appendix II-B: “Statement of Contribution of Others” for “LOW, I.M. and OO, Z. 2008. In Situ Diffraction study of Self-Recovery in Aluminum Titanate. <i>Journal of the American Ceramic Society</i> , 91, 3, 1027-1029”.	192
6.3	Appendix II-C: “Statement of Contribution of Others” for “LOW, I.M. and OO, Z. 2008. Reformation of Phase Composition in Decomposed Aluminium Titanate. <i>Materials Chemistry and Physics</i> , 111, 9-12”.	194
6.4	Appendix II-D: “Statement of Contribution of Others” for “LOW, I.M. and OO, Z. 2002. Diffraction Studies of a Novel Ti_3SiC_2 -TiC system with Graded Interfaces. <i>Journal of the Australian Ceramic Society</i> , 38, 2, 2002, 112-116”.	196
6.5	Appendix II-E: “Statement of Contribution of Others” for “LOW, I.M., OO, Z. & PRINCE, K.E. 2007. Effect of Vacuum Annealing on the Phase Stability of Ti_3SiC_2 . <i>Journal of the American Ceramic Society</i> , 90, 2610-2614”	198

6.6	Appendix II-F: “Statement of Contribution of Others” for “OO, Z., LOW, I.M. & O’ CONNOR, B.H. 2006. “Dynamic Study of the Thermal Stability of Impure Ti ₃ SiC ₂ in Argon and Air by Neutron Diffraction. <i>Physica B</i> , 385-386, 499-501”.	202
7	APPENDIX III: COPYRIGHT FORMS	205
7.1	Appendix III-A: Elsevier Journal Articles	206
7.2	Appendix III-B: Wiley Inter-Science Articles	208
7.3	Appendix III-C: Journal of Australasian Ceramic Society Articles	210
8	BIBLIOGRAPHY (REFERENCES CITED IN THE APPENDICES SECTION)	212

1. INTRODUCTION AND OVERVIEW

1.1 Introduction

Currently, a new class of ceramics called “advanced ceramics” has come to the scene as materials systems become more refined, and special compounds and processes are developed for structural and electronic applications. These advanced ceramics are distinguished by their high chemical purity, careful processing and high values of useful properties. In general, oxide ceramics are hard, brittle and high melting point materials with low electrical and thermal conductivity, low thermal expansion, good chemical and thermal stability, good creep resistance, high elastic modulus and high compressive strength.

About ninety percent of the advanced ceramics that are used for electronics or related applications are called electro-ceramics (Moulson and Herbert, 2003). The remaining ten percent constitute “structural ceramics” in which the mechanical properties such as strength, elastic modulus, plastic deformation, toughness, wear resistance, hardness, etc. are of primary interest. Due to their high modulus and hardness, low density and resistance to high temperature and corrosive environment, there is a great interest in using ceramics in demanding structural applications such as heat engines, turbines and automotive components, where their use would result in long life, operation at high temperatures and weight saving (Barsoum, 1997).

Amongst the oxide ceramics, alumina (Al_2O_3) is a commonly used ceramic which has an enormous range of technological and industrial applications due to its properties such as high thermal conductivity, high hardness, and resistance to many corrosive media, abrasion resistance, low density, and high electrical resistivity. In addition, due to its strong demand in diverse applications, alumina is frequently incorporated with other materials to obtain more advanced or specific properties and microstructures.

For instance, layer-graded alumina/aluminium titanate ($\text{Al}_2\text{O}_3/\text{Al}_2\text{TiO}_5$) and alumina-zirconia /aluminium titanate ($\text{Al}_2\text{O}_3\text{-ZrO}_2/\text{Al}_2\text{TiO}_5$) systems were synthesized using TiCl_4 or $\text{Ti}(\text{OC}_2\text{H}_5)_4$ as an infiltrant (Skala, 2000; Low et al. 1996). Layer-graded

materials (LGMs) display superior mechanical properties such as mechanical strength, fracture and thermal shock resistance. These LGMs were designed as multifunctional new generation layer-composites with a top hard layer for wear resistance and under-layer for damage tolerance.

In 1980, functionally-graded materials (FGMs) were introduced as multi-functional materials which contain various compositions for specific applications (Mortensen & Suresh, 1997). To achieve the highest possible mechanical properties of FGMs, tailored designs of functionally-graded $\text{Al}_2\text{TiO}_5\text{-Al}_2\text{O}_3$ were developed (Pratapa, 1997; Pratapa and Low, 1998; Skala, 2000). Aluminum titanate (Al_2TiO_5), is widely used as a refractory material and as a thermal insulator in engine components by virtue of its low thermal expansion coefficient ($1 \times 10^{-6}\text{C}^{-1}$), high melting point (1860°C), low thermal conductivity, and excellent thermal shock resistance (Cleveland et al. 1978; Buscaglia et al. 1997). However, the full potential of Al_2TiO_5 has been limited by its low fracture toughness, low mechanical strength and poor high-temperature stability.

Amongst the non-oxide ceramics, ternary carbides or $\text{M}_{n+1}\text{AX}_n$ phases (where M is an early transition metal, A is a group A element and X is either carbon or nitrogen, $n = 1, 2, 3$), such as Ti_3SiC_2 , Ti_3GeC_2 and Ti_3AlC_2 are novel structural and functional materials that combine the merits of both ceramics and metals.

MAX phases are remarkable materials that exhibit a unique combination of characteristics of both ceramics and metals with unusual mechanical, electrical and thermal properties (Barsoum 2000; Barsoum and El-Raghy 1996; 2001; Low 1998). Similar to most other ceramics, they possess low density, low thermal expansion coefficient, high modulus and high strength, and good high-temperature oxidation resistance. Like metals, they are good electrical and thermal conductors, readily machinable, tolerant to damage, and resistant to thermal shock. The unique combination of these interesting properties enables these ceramics to be promising candidate materials for use in diverse fields which include automobile engine components, heating

elements, rocket engine nozzles, aircraft brakes, racing car brake pads and low-density armour.

Ti₃SiC₂ was first synthesized by Wolfgang Jeitschko and Hans Nowotny in 1967 via a chemical reaction between TiH₂, Si and graphite at 2273 K (Jeitschko & Nowotny, 1967). Dense polycrystalline samples of pure Ti₃SiC₂ were fabricated by Barsoum and co-workers (Barsoum et al. 1996; 1997a, b; 1999a) via reactive hot pressing of Ti, graphite and SiC powders at 1600°C. This material has a hexagonal structure with planar Si layers linked together by TiC octahedral to form a deformable basal slip plane. Micro-lamellae of 3-4 μm thickness exist within each grain and Ti₃SiC₂ displays a unique combination of mechanical, electrical and physical properties (Goto et al. 1987; Barsoum, 2000; Low et al. 1998; 2001). For instance, its electrical and thermal conductivities are higher than those of pure Ti, its thermal shock resistance is comparable to those of metals, and its machinability is similar to that of graphite.

However, Ti₃SiC₂ is relatively soft, not wear resistant, and has a relatively low thermal stability (<1700°C). Barsoum and co-workers (Barsoum et al. 1998) have improved the surface hardness and oxidation resistance of Ti₃SiC₂ by using both carburization and silicidation to form surface layers of TiC and SiC. Similarly, Low and colleagues (Low et al. 2001) have shown that it is possible to form surface layers of TiC on Ti₃SiC₂ by employing a high temperature vacuum heat-treatment, where the thickness of TiC coating formed can range from nanometers to micrometers, depending on the duration and temperature of heat-treatment.

Recent developments in layered ceramics have provided a strategy for designing laminates with increased strength and toughness. These structures have an outermost homogeneous layer to provide strength or wear resistance, and an underlying heterogeneous layer to provide toughness (Low et al. 1998). Unlike more traditional layered structures which promote toughness by interlayer crack deflection or strength by incorporating macroscopic compressive residual stresses, the new approach deliberately seeks to produce strong interlayer bonding to eliminate residual macroscopic stresses. In

this project, the main objectives were: studying the parameters that control the thermal stability in functionally- graded aluminium titanate (Al_2TiO_5) and titanium silicon carbide (Ti_3SiC_2) based ceramics and evaluating the oxidation properties of Ti_3SiC_2 at elevated temperatures.

1.1.1 Aims and Significance

This study is aimed at designing and characterizing functionally-graded Al_2TiO_5 - and Ti_3SiC_2 -based composites with improved properties for advanced engineering applications.

The general objectives were:

- to synthesize functionally-graded Al_2TiO_5 - and Ti_3SiC_2 -based systems by using a new approach: die-pressing followed by vacuum heat treatment.
- to study the parameters that control the thermal stability of functionally-graded Al_2TiO_5 - Al_2O_3 and Ti_3SiC_2 -TiC systems produced by vacuum heat treatment.
- to analyze the characteristics of functionally-graded Al_2TiO_5 - Al_2O_3 and Ti_3SiC_2 -TiC phase developments by X-ray diffraction (XRD), neutron diffraction (ND), synchrotron radiation diffraction (SRD), scanning electron microscopy (SEM).
- to conduct diffraction studies on the thermal stability of Al_2TiO_5 - Al_2O_3 composites and the oxidation behavior of Ti_3SiC_2 -TiC composites.

This study draws its significance from the following points:

- Al_2TiO_5 -based ceramics by neutron diffraction (medium resolution powder diffractometer - MRPD) is used to monitor the decomposition of Al_2TiO_5 to form Al_2O_3 and TiO_2 in temperatures ranging from 20°-1400°C.
- Al_2TiO_5 -based ceramics exhibit thermal stability at 1100°C in different atmospheres, oxygen partial pressure, and rate of change in temperature.
- Al_2TiO_5 -based ceramics show the process of decomposition in Al_2TiO_5 is reversible and that self-recovery can occur readily when decomposed Al_2TiO_5 is re-heated above 1300°C.

- Ti_3SiC_2 -based ceramics results in the formation of TiC when using high temperature vacuum heat-treatment.
- Ti_3SiC_2 -based ceramics represent an important role in the thermal stability of Ti_3SiC_2 which depends on the controlled atmosphere of vacuum and argon.
- The characteristic of the oxidation of Ti_3SiC_2 in the temperatures ranging from 20°C to 1400°C, was investigated by in-situ ND and secondary ion mass spectroscopy (SIMS).
- Understanding the structure-property relationships and the factors controlling thermal stability will enable the unique multi-functional properties of Al_2TiO_5 and Ti_3SiC_2 to be fully utilized in a wide range of applications.

1.1.2 Research Methodology

In order to achieve the objectives, this thesis specifies three major aspects of interactive materials research and development: processing, characterization, and properties evaluation. A series of experiments (see Figures 1.1, 1.2 (a) and (b)) was conducted to achieve the goals. The research methodologies were as follows:

(i) Processing of Al_2TiO_5 - and Ti_3SiC_2 -based systems

Vacuum heat treatment of reaction-synthesized Al_2TiO_5 -based and Ti_3SiC_2 -based ceramics

The raw materials used in the synthesis of Al_2TiO_5 -based ceramics consisted of high purity commercial powders of Al_2O_3 (99.9%) and TiO_2 (99.5%). These dry powders were mixed in the ratio of 1:1 by mortar and pestle. Ethanol was added during mixing to produce slurry which was then dried in a ventilated oven at 100°C for 24h. Cylindrical bars of length 20 mm and diameter 12 mm were uniformly made by pressing in a steel die at 150 MPa, followed by sintering at 1500°C in air for 2 h.

Similarly, for Ti_3SiC_2 - based ceramics, vacuum heat-treatment of Ti_3SiC_2 samples was conducted at 1400–1600°C for 1- 4 h at 10^{-5} torr to convert the near surface layer into TiC with graded interfaces.

(ii) Characterization:

1. The thermal stability of Al_2TiO_5 -based ceramics in different atmospheres and temperatures was analyzed by ND and SEM.
2. The reformations of phase composition of Al_2TiO_5 - based ceramics were analyzed by ND.
3. The thermal stability and phase transition of vacuum-annealed Ti_3SiC_2 from the 23°C to 1500°C were analyzed by ND and SRD.
4. Depth-profiling of near-surface composition in vacuum-treated Ti_3SiC_2 at 1500°C was analyzed by XRD and SIMS.
5. The oxidation characteristics, phase abundances and phase transition of Ti_3SiC_2 from 23°C to a high temperature of 1350°C were analyzed using in-situ neutron diffraction (ND), XRD, differential thermal analysis (DTA), thermo-gravimetric analysis (TGA) and SIMS.

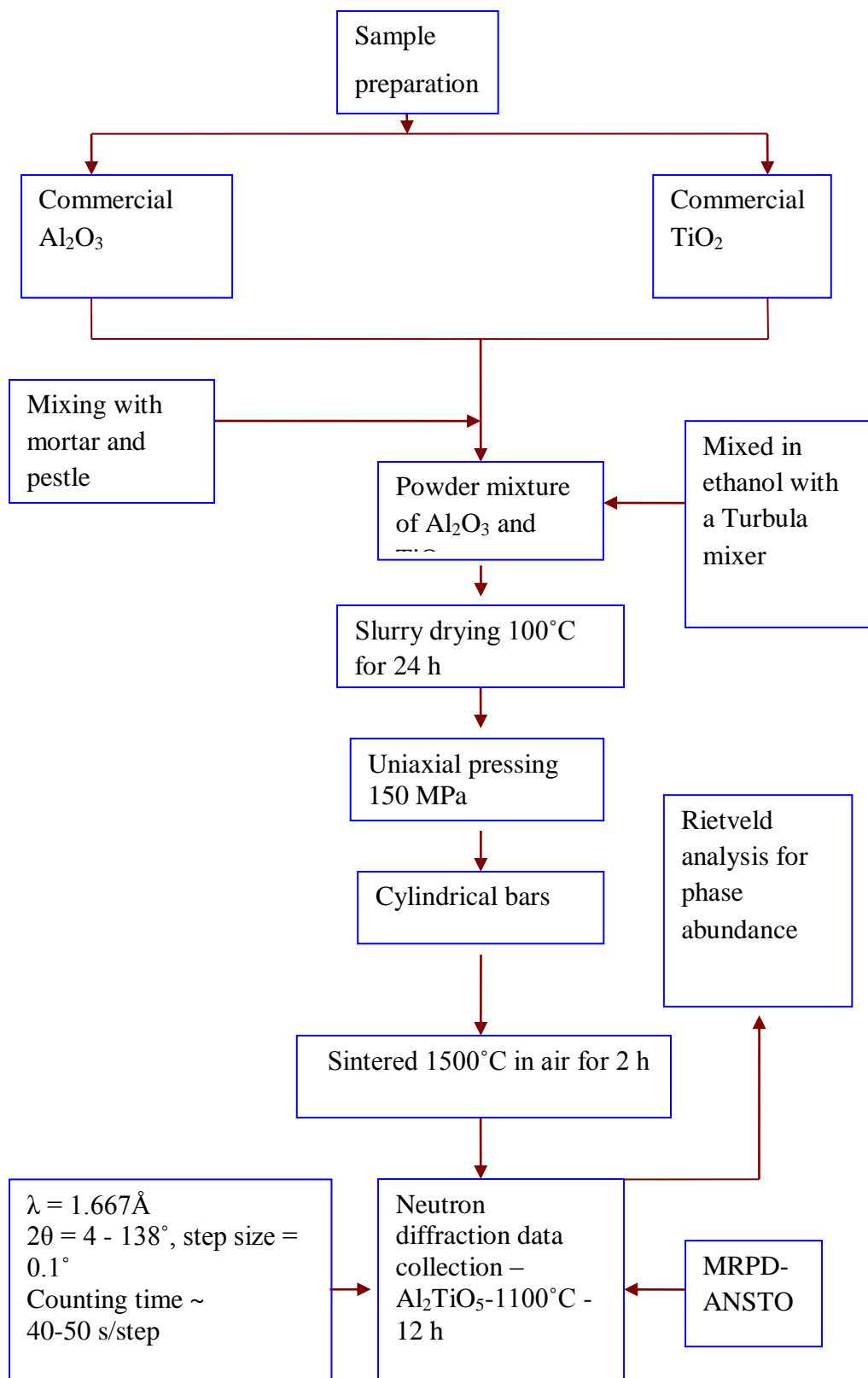


Figure 1.1: Flowchart of experimental design for characterization of Al_2TiO_5 .

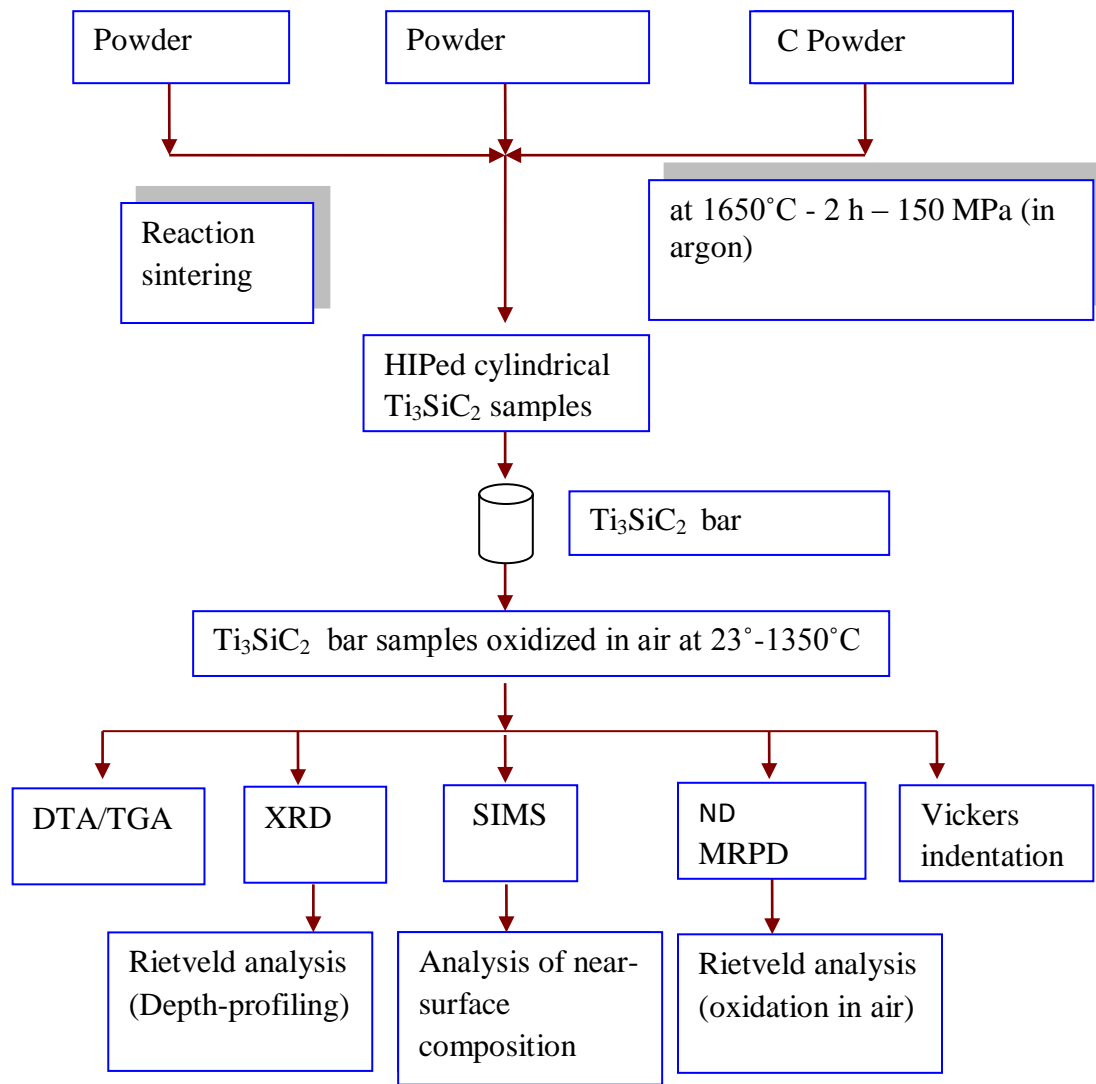


Figure 1.2: (a) Flowchart of experimental design for characterization of oxidized Ti_3SiC_2 .

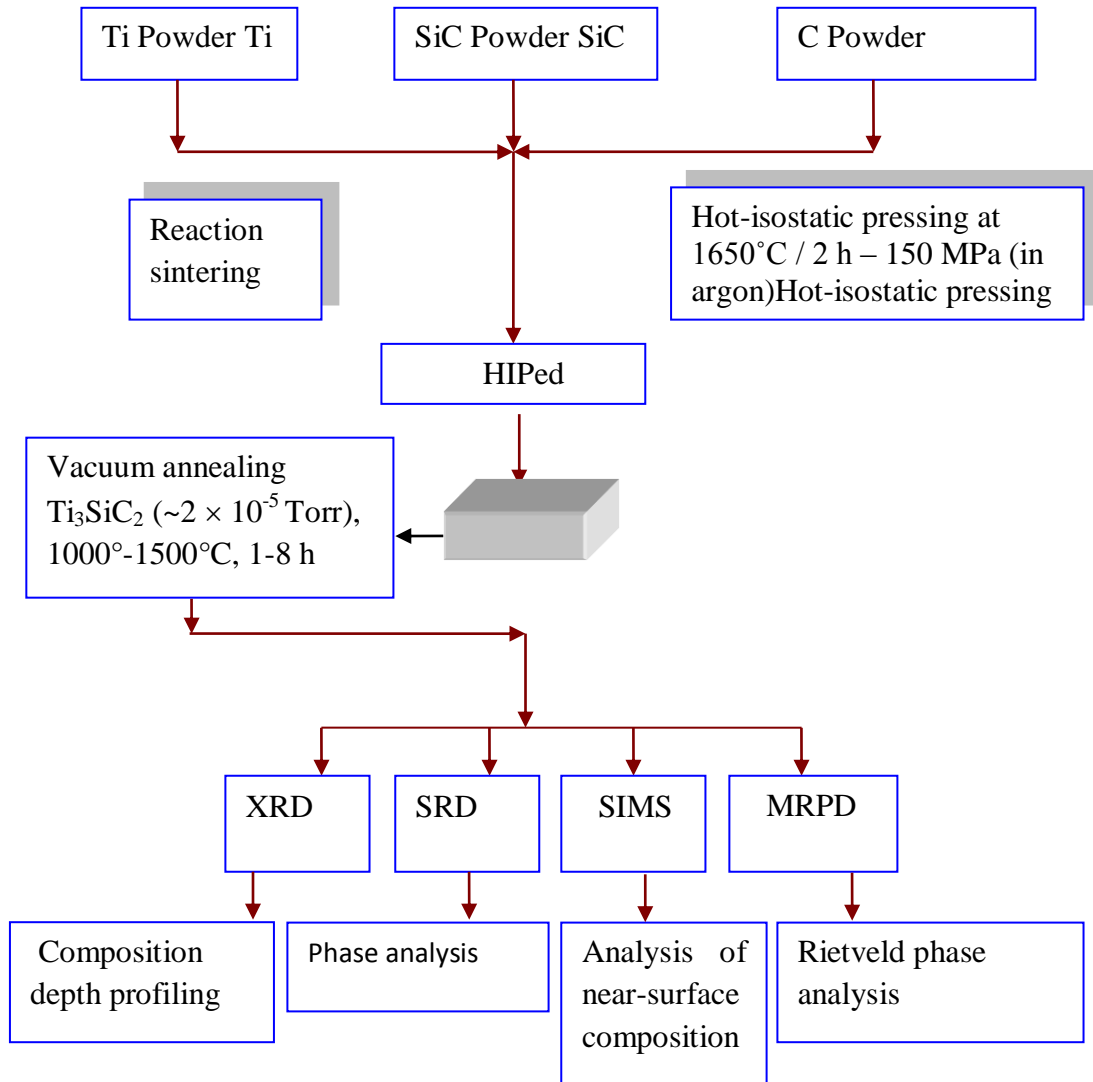


Figure 1.2: (b) Flowchart of experimental design for characterization techniques of vacuum-annealed Ti_3SiC_2 .

1.2 Background

1.2.1 Functionally-Graded Materials (FGMs)

A functionally-graded material (FGM) is defined as a two-component composite characterized by a compositional gradient from one component to the other. Since significant proportions of an FGM contain the pure form of each component, the properties of both components can be fully utilized. For example, the toughness of a metal can be mated with the refractoriness of a ceramic, without any compromise in the toughness of the metal or the refractoriness of the ceramic.

The concept of FGMs was first proposed by Shen and Bever (1972). Later, Niino and co-workers from Japan (Hirai, 1996; Holt et al. 1993) conducted research on the production methods. Their research was based on the demand for thermal barriers materials that led to the development of high performance heat resistant materials.

Neubrand and Rodel (1997) classified the number of possibilities of the graded materials according to the classes of materials which can be combined, for example, metal/ceramic, polymer/ceramic, metal/metal, ceramic/ceramic, etc. In functionally-graded coatings and joints, the gradient extends only over a part of the component close to its interface or in the interior. However, in functionally-graded bulk materials, the gradients comprise the entire part.

FGMs produce a gradual improvement of properties in ceramic compositions, which depend on the method of the creation of the layers. The FGMs exhibit a progressive change in composition, structure, and properties as a function of position within the material (Koizumi, 1997; Hirai, 1996). The significant characteristics of ceramic-metal FGMs are:

- (i) higher fracture resistance resulting in increased toughness due to crack bridging in a graded volume fraction and,
- (ii) high temperature resistance by controlling of thermal stresses in elements exposed to high temperatures (up to 1600°C) (Bahr et al. 2003).

1.2.1.1 Processing Methods

FGMs can be designed at micro-structural levels to tailor a material for a specific functional and performance requirement of an application. They can be fabricated in various ways to produce several types of continuous component changes (Hirai, 1996). In type one, they exhibit a continuous change in state, where the material has a very dense surface on one side and a porous surface on the other side (Figures 1.3 and 1.4) (Koizumi, 1997). In type two, they exhibit continuous change in concentration with phase abundance, density and depth dependent shrinkage varying in every layer. Generally, most FGMs show this behavior. The third type shows a continuous change in morphology, where one side consists of spherical particles and the other side consists of fiber-like particles. The fourth type has a continuous change in crystallinity which represents the different behavior in terms of crystalline and amorphousness.

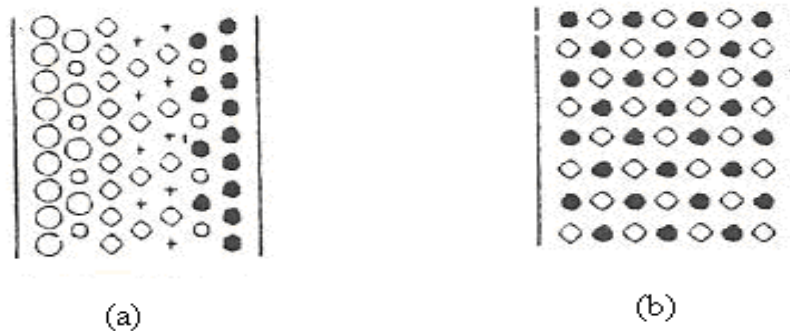


Figure 1.3: (a) Structure of FGM showing composition variations, and (b) Structure of non-FGM showing composition uniformity.

Legend: Ceramics (O), metal (●), fiber (◇ +) and micropore (○). (Koizumi and Niino, 1995)

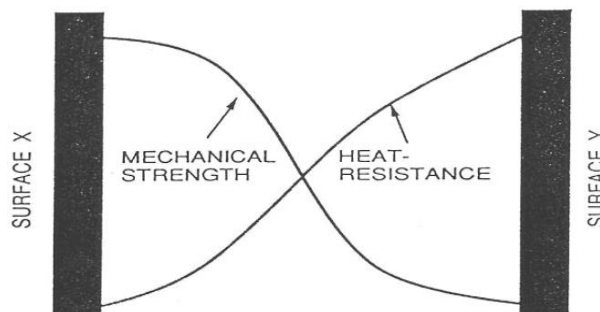


Figure 1.4: Variations in properties of a functionally-graded material (FGM). (Koizumi and Niino, 1995)

FGMs can be fabricated by a variety of methods which are listed in Table 1.1 (Sakai and Hirai, 1991). Since 1993, new methods have been developed for synthesizing FGMs. These include slip casting (Sanchez-Herencia, 1997), powder metallurgy (Kimura et al. 1993, Watanabe et al. 1995), laser alloying and cladding (Abboud et al. 1994), dynamic ion-mixing (Nakashima et al. 1994), and sputtering (Jiang et al. 1995).

Table 1.1: Different types of FGM (Sakai and Hirai 1991)

Phase	Method	Examples of FGMs
Gas	CVD	SiC/C, SiC/TiC, TiC/C, C/C-C
	Ion Plating	TiN/Ti, TiC/Ti, ZrO ₂ /Cu, C/Cr
	Plasma Spraying	YSZ/NiCrAlY, YSZ/ NiCr
Liquid (melt)	Electro-deposition	Ni/Cu
	Plasma spraying	YSZ, NiCrAlY, YSZ/NiCr
	Eutectic Reaction	Si/ZrSi ₂
Solid	Self-propagating high temperature synthesis	TiB ₂ /Cu, TiB/Ni, TiC/Ni ZrO ₂ /Ni, PTZ/Ni, PZT/Nb
	Smearing	YSZ/SUS, YSZ/Mo, Si ₃ N ₄ /Ni
	Sintering	Ni/Al
	Diffusion	

In addition, coating (Tsuchida et al, 1998), thermal spray, powder processing (Tomsia et al. 1998), chemical vapor deposition (CVD) (Takanori et al. 1999), novel jet vapor deposition (JVD) (Wadley, Hsiung and Lankey, 1995), physical vapor deposition (PVD), self-propagating high temperature synthesis, diffusion treatment and sedimentation have been developed. Moreover, Travitzky and Shlayan (1998) have reported on the liquid metal penetration, graded processing of metal matrix composites and fabrication of Al₂O₃/Cu-O composites.

Pratapa and co-workers (1998) proposed an infiltration process where the secondary phases are dispersed in a graded composition within the primary matrix that displays synergistic performance in hardness, toughness and high damage tolerance (Pratapa, Low, and O'Connor, 1997). Manurung (2001) reported a design of functionally graded alumina-zirconia/aluminium titanate which has damage tolerance and exhibits graded mechanical properties. It was designed using an infiltration method accompanied by permeation of liquid precursors into a porous preform and then sintered to form in-situ phases.

In this research, FGMs were designed through the thermal annealing process, in which a primary material is thermally decomposed in vacuum, air and argon.

1.2.2 Crystal Structure

1.2.2.1 Alumina (Al_2O_3)

The most commonly used material for structure ceramics component is α -alumina. The structure model of alpha-alumina ($\alpha\text{-Al}_2\text{O}_3$) was first introduced by Bragg and Bragg (1916), followed by Pauling and Hendricks (1930). Newham and DeHaan (1962) published a refined structure model for $\alpha\text{-Al}_2\text{O}_3$. Subsequently, Lewis, Schwarzenbach and Flack (1982) reported that the crystal structure of $\alpha\text{-Al}_2\text{O}_3$ is rhombohedral, belonging to the space group $R\bar{3}c$ with unit cell parameters $a = 4.7602 \text{ \AA}$ and $c = 12.9933 \text{ \AA}$. To get more improved structural parameters, the crystal structure has to consist of hexagonal close-packed layers of oxygen atoms with two thirds of the octahedral sites occupied by aluminum atoms in a regular way. The distance between mean aluminum and oxygen in the octahedral is 1.92 \AA , with the bonding between the atoms being predominately covalent (Skala, 2000). In 1993, Maslen et al. (1993) refined the $\alpha\text{-Al}_2\text{O}_3$ crystal structure model using a synchrotron radiation X-ray study of the electron density in $\alpha\text{-Al}_2\text{O}_3$ diffraction data. Maslen et al. (1993) stated that the lattice parameters of crystal structure of $\alpha\text{-Al}_2\text{O}_3$ are $a = b = 4.754 (1) \text{ \AA}$, $c = 12.982(1) \text{ \AA}$, space group $R\bar{3}cH$, belong to the hexagonal cell which contains six formula units cell for hexagonal unit cell. In this thesis, the International Crystallography Structure Database (ICSD) collection code number 73725 (Maslen, 1993) is used. The crystal

structure of $\alpha\text{-Al}_2\text{O}_3$ consists of oxygen two negative (O^{2-}) ions in the $A\text{-}B\text{-}A\text{-}B$ sequence and aluminum three positive (Al^{3+}) ions in a $P\text{-}Q\text{-}R\text{-}P\text{-}Q\text{-}R$ sequence. Therefore, a hexagonal crystallographic structure for the $\alpha\text{-Al}_2\text{O}_3$ has hexagonal stacking closed packed $A\text{-}P\text{-}B\text{-}Q\text{-}A\text{-}R\text{-}B\text{-}P$ (Munro, 1997), and this gives $\alpha\text{-Al}_2\text{O}_3$ good mechanical and thermal properties. Figure 1.5 shows the crystallographic $\alpha\text{-Al}_2\text{O}_3$ structure constructed using Powder cell software package (Kraus and Nolze, 1999) by Manurung, 2001. The ionic radii are proportional to 0.55 Å for Al^{3+} (red) and 1.35 Å for O^{2-} (blue). The unit cell of $\alpha\text{-Al}_2\text{O}_3$ is an acute rhombohedral of side length 5.2 Å and phase angle of approximately 55°.

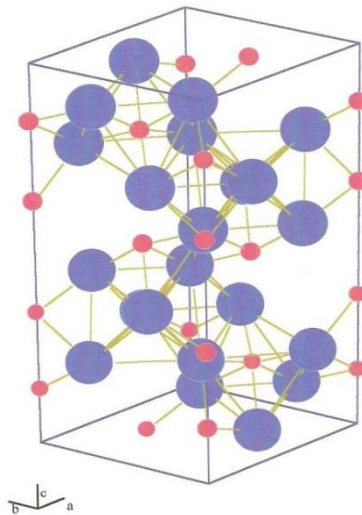
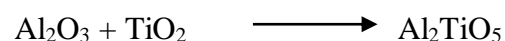


Figure 1.5: Crystal structure of α -alumina. The parameters are based on Model ICSD #73725. (Maslen et al. 1993)

Legend: Al^{3+} (red) and O^{2-} (blue) (Kraus and Nolze, 1999)

1.2.2.2 Aluminum Titanate (Al_2TiO_5)

Aluminum titanate, (Al_2TiO_5) is synthesized by solid state reaction between alumina (Al_2O_3) and titanium oxide (TiO_2) at a temperature above the eutectoid temperature of 1280°C:



α - Al_2TiO_5 is stable up to a temperature of $\sim 1820^\circ\text{C}$ and β - Al_2TiO_5 is only stable up to a temperature of $\sim 1400^\circ\text{C}$ (Sekar and Patil, 1994). According to Epicier's model (Epicier et al. 1991) (Figure 1.6), Al_2TiO_5 has as an orthorhombic unit cell crystal structure with the lattice lengths and angles of $a = 3.591 \text{ \AA}$, $b = 9.429 \text{ \AA}$, $c = 9.636 \text{ \AA}$ and $\alpha = \beta = \gamma = 90^\circ$ respectively. The chosen point positions in space group cm cm are $(4c)$ for one set of titanium (Ti1) atom, $(8f)$ for another one set of for titanium (Ti2) atom, $(4c)$ for one set of aluminum (Al1), $(8f)$ for another one set of aluminum (Al2), $(4c)$ for one set of oxygen atoms, and $(8f)$ for two sets of eight oxygen atoms.

In this thesis, β - Al_2TiO_5 is used because it is one of several materials which are isomorphous with the mineral pseudobrookite (Fe_2TiO_5) (Austin and Schwatz, 1953; Morosin and Lynch, 1972). In this crystal structure, each Al^{3+} or Ti^{4+} cation is surrounded by six oxygen ions forming distorted oxygen octahedra. These AlO_6 or TiO_6 octahedra form (001) oriented double chains and are weakly bonded by shared edges. This structural feature is responsible for the strong thermal expansion anisotropy which generates localized internal stresses to cause severe microcracking. Although this microcracking weakens the material, it imparts a desirable low thermal expansion coefficient and excellent thermal shock resistance.

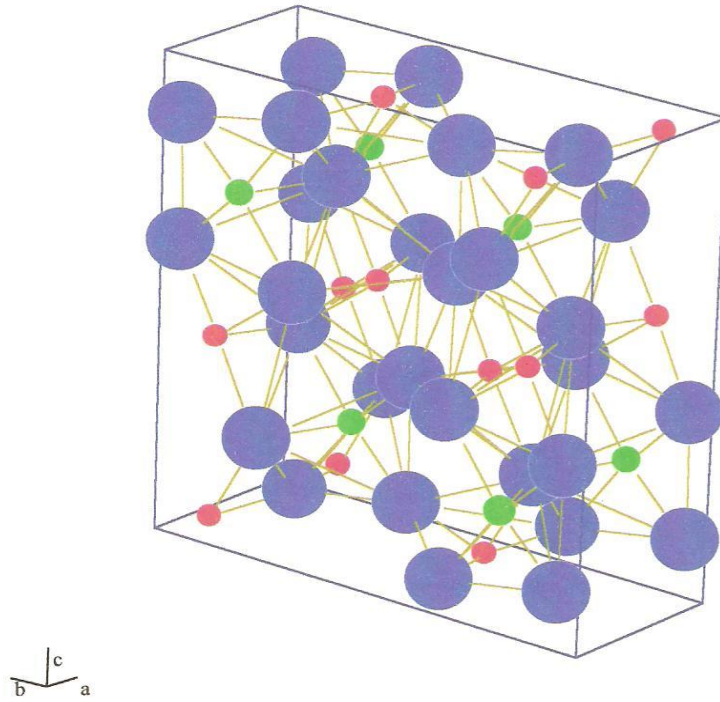


Figure 1.6: Orthorhombic crystal structure of aluminium titanate (Al_2TiO_5) based on the model of Epicier et al. (1991).

Legend: red is Al, blue is O and green is Ti. (Kraus and Nolze, 1999)

Based on the observations in Table 1.2, Austin and Schwartz (1953) presented the pseudobrookite-type $\beta\text{-Al}_2\text{TiO}_5$ crystal structure (Pauling and Hendricks, 1930), as shown in Figure 1.7. Norberg and colleagues (2005) observed that the translational period of a chain in $\beta\text{-Al}_2\text{TiO}_5$ can be divided into two basic units which are repeated in an *M1 M2 M1 M2* fashion along *c* axis. Norberg et al. (2005) re-determined the preferential occupation of octahedral sites for Al and Ti. The larger Ti^{4+} ion prefers more regular *4c* octahedral site to some extent.

Table 1.2: Development of Al₂TiO₅ crystal structure lattice parameters

*HRTEM = High Resolution Transmission Electron Microscopy

Description		Space group	Lattice lengths			Reference
			<i>a</i> (Å)	<i>b</i> (Å)	<i>c</i> (Å)	
Crystal Structure	Ortho-rhombic	CMCM	3.557(2)	9.436(5)	9.648(5)	Austin & Schwartz (1953)
Temperature and duration	1600°C for 6 hours	CMCM	9.360(30)	3.560(20)	9.680 (50)	Hamelin (1958)
	23°C-600°C	BBMM	9.429(2)	9.636(2)	3.591(1)	Morosin & Lynch (1972)
Techniques	XRD	CMCM	3.591(1)	9.429(2)	9.636(2)	Holcombe & Coffey (1973)
	HRTEM*	CMCM	3.591	9.429	9.636	Epicier et al. (1991)

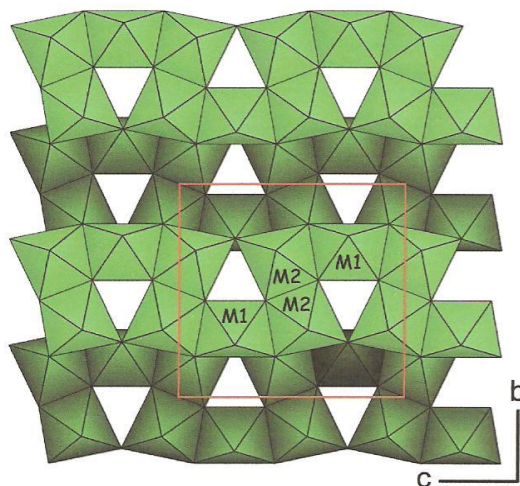


Figure 1.7: A polyhedral representation of the pseudobrookite-type β - Al_2TiO_5 crystal structure (Austin & Schwartz, 1953).

1.2.2.3 Titanium Oxide (TiO_2)

Titanium oxide (TiO_2), a multifaceted compound, is the ingredient that makes toothpaste white and paint opaque. It has been studied for its interesting qualities, such as electronic properties (Yan and Rhode, 1981; Reintjes and Schultz, 1968), optical properties (Mo and Ching, 1995), magnetic properties (Battle et al. 1983) and catalytic properties (Tauster et al. 1978). TiO_2 has been very widely used in catalysis as sensors.

TiO_2 has been studied extensively (Hanaor et al. 2012; Hanaor and Sorrell, 2011; Valencia et al. 2010) because most crystal-growth techniques basically yield TiO_2 in the rutile phase in the simplest structure. The most common form is rutile TiO_2 which is also the most stable. Anatase and brookite both convert to rutile upon heating. Rutile, anatase and brookite contain six-coordinated titanium with the same composition, TiO_2 , but possess different crystal structures. Both rutile and anatase have tetragonal crystal structures while brookite has an orthorhombic crystal structure (Greenwood et al. 1999).

Generally, the rutile structure is defined by three crystallographic parameters: two lattice parameters a , c and the oxygen fractional coordinate. Anatase and rutile have the

same crystal structure, tetragonal. But they have different space group, for rutile, $42/m n m$, and for anatase, $41/amd$. The first investigation of the crystal structures of anatase and rutile was reported in 1916 by using Bragg's ionization method (Vegard, 1916). Greenwood (1924) reported Vegard's results for rutile confirmation in 1924. Huggins (1926) verified the results for both anatase and rutile again. However, these crystal structures were not sufficiently precise to permit a detailed study of minor differences between the anatase and rutile. In 1954, Cromer and Herrington (1955) revised the acceptable crystal structures of rutile by using X-ray Diffraction. Their cell parameters for rutile were, $a = 4.5929 \pm 0.0005 \text{ \AA}$ and $c = 2.9591 \pm 0.0003 \text{ \AA}$ and the oxygen parameter for rutile was $0.3056 \pm 0.0006 \text{ \AA}$. The unit cell structure of TiO_2 (rutile) and TiO_2 (anatase) are shown in Figure 1.9. In rutile, there are four Ti-O distances of $1.946 \pm 0.003 \text{ \AA}$, and two Ti-O distances of $1.984 \pm 0.004 \text{ \AA}$. In anatase, there are four Ti-O distances of $1.937 \pm 0.003 \text{ \AA}$ and two Ti – O distances of $1.964 \pm 0.009 \text{ \AA}$.

Shintani et al. (1975) reported that the rutile crystal structure is tetragonal, with bond angles $\alpha = \beta = \gamma = 90^\circ$ as parameters. In this thesis, the TiO_2 model has been chosen because it is very common for further investigations of the properties of defects, impurities, thin films, surfaces and interfaces. Burdett et al. (1986) examined the electronic structure of anatase and rutile by using the Rietveld analysis of time of flight pulsed neutron diffraction of powders: it showed a nearly isotropic shrinkage of the structures of rutile, as illustrated in Table 1.3. The rutile structure is more stable than the anatase structure and it is less dense (Lazzeri et al. 2001). The developments of TiO_2 crystal structure after 1960 are summarized below.

Table 1.3: Previous experimental studies on TiO₂ (rutile) crystal structure after 1960.

Year	Reference	Space group	Lattice Parameters			Remark
			a (Å)	b (Å)	c (Å)	
1975	Shintani et al.	P42/mnm	4.584(0)	4.584(0)	2.943(0)	ED ⁺
1986	Burdett et al.	P42/mnm	4.593(0)	4.593(0)	2.958(8)	ND*
1994	Shang et al.	P42/mnm	4.593(6)	4.593(6)	2.595(8)	

*ND (Neutron Diffraction), ⁺ED (Electron Diffraction)

By using a qualitative analysis of both structures, Adil et al. (1993) verified that distortions relative to regular crystal lattices are made of undistorted octahedra.

Figure 1.8 (a) shows that rutile crystal structure has titanium ions (4⁺) at the center of octahedra of six O²⁻ ions. Each oxygen atom has three titanium neighbors and therefore belongs to three different octahedra. Similarly, for the anatase structure (as shown in Fig 1.8 (b)), three parameters are involved: the two Ti-O bond lengths and the angle 2θ (the largest Ti-O-Ti angle; the smallest O-Ti-O angle which concerns one apical and one equatorial Ti-O bond).

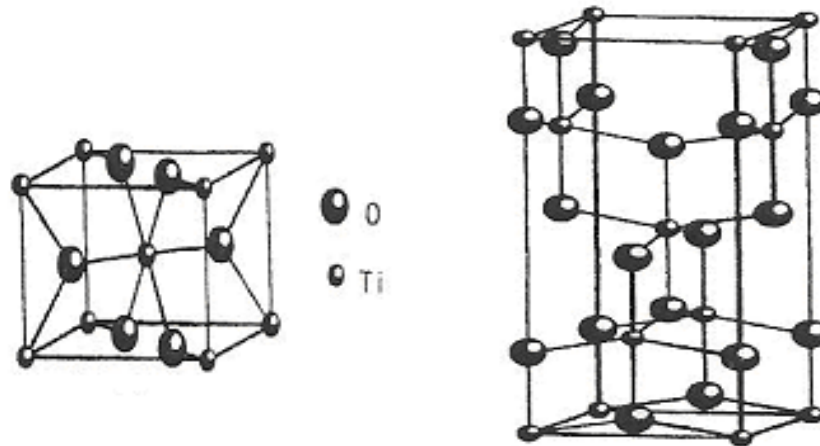


Fig 1.8 (a)

Fig 1.8 (b)

Figure 1.8: The basic unit cell crystal structures of TiO_2 (a) rutile (b) anatase.
(Cromer and Harrington, 1954)

1.2.2.4 Titanium Silicon Carbide (Ti_3SiC_2)

Titanium silicon carbide (Ti_3SiC_2) is unique in that it has desirable properties of both metals and ceramics. Ti_3SiC_2 was first synthesized over 30 years ago via a chemical reaction between TiH_2 , Si and graphite at 2000°C (Jeitschko and Nowotny, 1967). It has a hexagonal structure with weakly bonded silicon planes linked to TiC octahedral layers in Ti_3SiC_2 (Jeitschko and Nowotny, 1967; Goto et al. 1987). Jeitschko and his co-workers (1967) made first attempts on the exploration of layered ternary carbides and nitrides, and they identified a large number of ternary compounds in 1960. Unfortunately, these layered ternary carbides and nitrides were ignored for many years after the early discovery. In 1990, Barsoum published a detailed review of a new class of solids called MAX phases, or $\text{M}_{n+1}\text{AX}_n$ where: 'M' is an early transition metal element, 'A' represents a group "IIIA" and "IVA" element, and 'X' represents either "C" or "N" and $n = 1, 2, 3, \dots$ (Barsoum et al. 2000). Since 1990, the remarkable material Ti_3SiC_2 has been shown to combine the strength, hardness, and heat resistance of a ceramic with the machinability and ductility of a metal (Barsoum et al. 1996; 1997a, b, c; 1999; Low 1998; Low et al. 1998, Wang and Zhou 2002, Hong and Lin 2010, Sun 2011).

In 1998, Kisi and co-workers (Kisi et al. 1998) reported that the structure of Ti_3SiC_2 , is hexagonal in space group $P63/mmc$ and space group number (194) with unit cell dimension $a = b = 0.30575(1)$ nm and $c = 1.762349(30)$ nm. The Ti occupies (2a) and (4f) sites, Si a (2b) site and C a (4f) site. Individual thermal parameters for Kisi's model are 0.04(6) for Ti, 0.08(4) for Ti again, 0.39(4) for Si and 0.06(2) for C. As shown in Figure 1.9, this phase consists of a layered structure with lattice parameters of $a = 3.0665 \text{ \AA}$ and $c = 17.67 \text{ \AA}$ and a stacking sequence consisting of alternating double Ti-C blocks and Si layers, each made up of two edge-sharing CTi_6 octahedra. The CTi_6 octahedra are edge-sharing and are identical to the NaCl-type structure of the corresponding binary carbides. A square-planar Si sheet separates the double Ti-C blocks. The in-plane Si-Si distance is 0.30575 nm, and the out-plane Si-Ti distance is 0.2681 nm (Kisi et al. 1998). In this thesis, Kisi's model has been used to discuss the structure and crystal chemistry of Ti_3SiC_2 using the Rietveld analysis method. This model can explain electrical and mechanical properties and the oxidation resistance characteristics of Ti_3SiC_2 (Kisi et al. 1998). Table 1.4 shows the list of differences between Kisi's model (1998) and Jeitschko's model (1967).

Table 1.4: Differences between the models of Kisi et al. (1998) and Jeitschko and Nowotny (1967) for Ti_3SiC_2

Item	Kisi (1998) ICSD 86213	Jeitschko and Nowotny (1967) ICSD 25762
Unit cell	x = 3.0575(1) Å y = 3.0575(1) Å z = 17.62349(30) Å	x = 3.068(2) Å y = 3.068(2) Å z = 17.669(6) Å
Volume	144.03 m ³	142.68 m ³
Space group	P63/mmc	P63/mmc
Crystal structure	Hexagonal	Hexagonal
Atom Ti (4f)	X = 0.6667 Å Y = 0.3333 Å Z = 0.1355 (1) Å	X = 0.3333 Å Y = 0.6667 Å Z = 0.1357(15) Å
Atom Ti (2a)	X = 0.0000 Å Y = 0.0000 Å Z = 0.0000 Å	X = 0.0000 Å Y = 0.0000 Å Z = 0.0000 Å
Atom Si (2b)	X = 0.0000 Å Y = 0.0000 Å Z = 0.75 Å	X = 0.0000 Å Y = 0.0000 Å Z = 0.2500 Å
Atom C (4f)	X = 0.3333 Å Y = 0.6667 Å Z = 0.0722 (1) Å	X = 0.3333 Å Y = 0.6667 Å Z = 0.570(4) Å

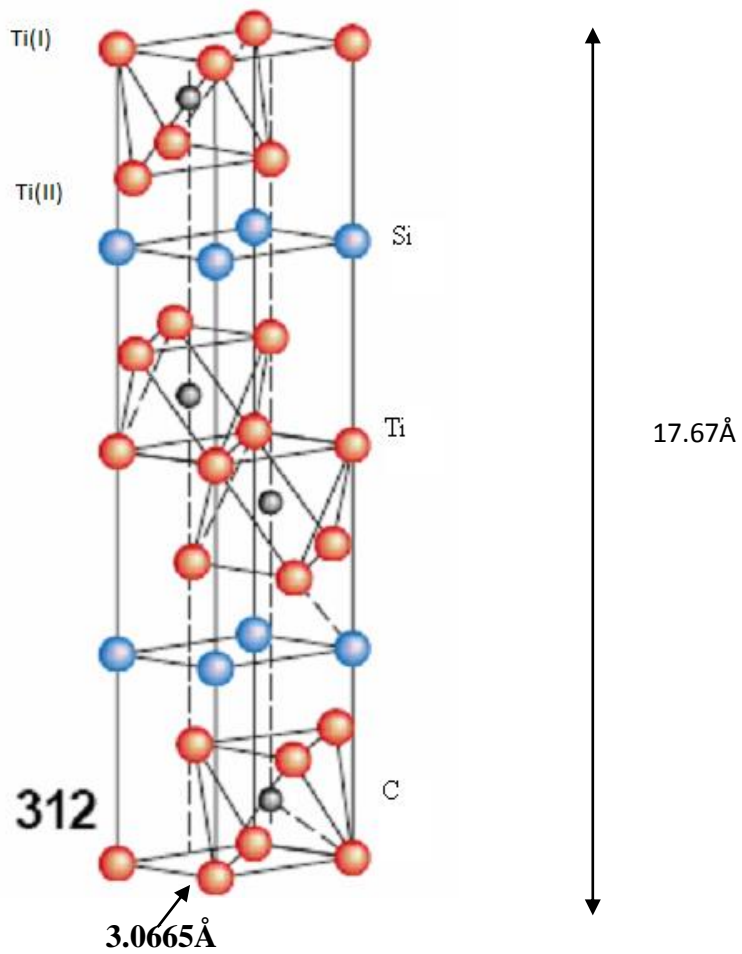


Fig. 1.9: Unit cell of Ti_3SiC_2 crystal structure.

Legend: Blue is Si, red is Ti and black is C. (Barsoum et al. 2000)

Sun (2011) reviewed recent researches on synthesis and characterization of MAX phases (e.g. Ti_3SiC_2 , Ti_3AlC_2 , Ti_2AlC , Ti_2GeC , Ti_4SiC_3 , and Ta_4AlC_3) in bulk, film and powder forms. Johari and co-workers (Johari et al. 2012) presented the effects of excess Si in the reactant mixture of Ti/Si/C powders on the formation of Ti_3SiC_2 by using the arc melting method. Vishnyakov and co-workers (Vishnyakov et al. 2013) reported the formation of Ti_3SiC_2 using magnetron sputtering on multilayered deposits of Ti-Si-C at 650°C . Ti_3SiC_2 has been shown to be a promising candidate for high temperature applications (Barsoum et al. 1996).

1.2.2.5 Titanium Carbide (TiC)

As one of the most promising high-temperature structural materials, titanium carbide has been under active development for demanding elevated temperature applications, because of its unique combination of a high melting point (3160°C), good thermal stability and erosion resistance (Wei et al. 1984, Cho et al. 1996, Wang et al. 2004).

TiC binary compounds usually act as impurities in Ti_3SiC_2 products. For this reason, microstructure and crystal structure of TiC have been studied to understand clearly the reaction mechanism between elements within the Ti-Si-C systems. In order to be able to design Ti-Si-C composites, an understanding of the phase composition and its variation with process parameters (such as temperature) is required (Barsoum, 2000). At elevated temperatures, typically 1200°-1400°C for bulk materials, the Ti-Si-C system forms the ternary compound Ti_3SiC_2 , in equilibrium with TiC (Barsoum, 2000).

In TiC, C atoms occupy the octahedral void (see Figure 1.10). Referring to TiC octahedral layers sandwiched between Si layers in Ti_3SiC_2 , the C atomic sites are relaxed towards the Si interlayer thereby shortening the $Ti_{(II)}$ -C bond relative to the $Ti_{(I)}$ -C bond and resulting in a distortion of the Ti_6C octaherda (Kisi et al. 1998). Riley (2003) reported TiC crystal structure as follows:

- Space group $O_h^s - FM\bar{3}$ (225)
- Lattice parameters : $a = 4.3280 \text{ \AA}$
- Crystallographic sites : Ti - 4(a) ; C - 4(b)
- Atomic positions :

	X	Y	Z
Ti	0	0	0
C	½	½	½

The crystal structure of TiC is a face-centred-cubic structure. In this thesis, the Christensen (1978) model has been selected to analyze to the TiC crystal structure. Its unit cell lattice length and angle are 4.328 (2) Å and 90° respectively.

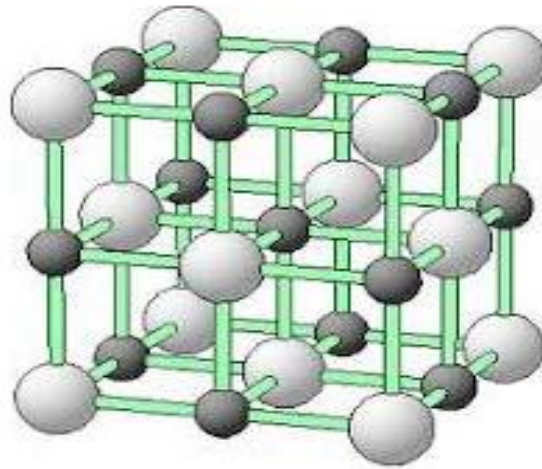


Figure 1.10: The crystal structure of TiC. (Li et al. 2008)

1.2.3 Physical and Mechanical Properties

1.2.3.1 Alumina (Al_2O_3)

Alumina (Al_2O_3) is one of the most versatile of refractory ceramic oxides. Its excellent hardness makes it suitable for use as an abrasive and as a cutting tool material. Thus, alumina is the most cost effective and widely used material in the ceramics family. The key properties are excellent wear resistance, excellent thermal conductivity, excellent capability to change size and shape, high strength and stiffness, and high temperature resistance (Runyan, 1991). Hardness of α -alumina can be varied by starting alumina grade as well as processing procedures. The mechanical properties of 99.9% pure α -alumina (Schneider, 1994) are shown in Table 1.5.

1.2.3.2 Aluminium Titanate (Al_2TiO_5)

The thermo-mechanical properties can be tailored by varying the composition and processing method. Al_2TiO_5 is highly anisotropic in thermal expansion. As a result, thermal stress builds up in the material resulting in inter-granular cracks observable in the microstructure. The inter-granular micro-cracking is responsible for the outstanding thermal shock resistance and the low mechanical strength of Al_2TiO_5 .

According to the bonding system of Al_2TiO_5 , it has a mixture of ionic and covalent characters with a theoretical density of $3700 \text{ kg}\cdot\text{m}^{-3}$. The thermal expansion coefficients are given in Table 1.6.

Table 1.5: Mechanical properties of 99.9% pure α -alumina. (Schneider, 1994)

Mechanical property	Value
Porosity (%)	0
Flexural strength (MPa)	345
Elastic modulus (GPa)	300
Shear modulus (GPa)	124
Bulk modulus (GPa)	172
Poisson's ratio	0.22
Compressive strength (MPa)	2600
Vickers hardness (GPa)	18-23
Tensile strength (MPa)	220
Elastic modulus (GPa)	375
Fracture toughness ($\text{MPa}\sqrt{\text{m}}$)	2.7-4.2
Coefficient of thermal expansion ($25^\circ - 1000^\circ\text{C}$) (K)	8.1×10^{-6}

Table 1.6: Thermal expansion coefficients of Al_2TiO_5 along the three crystal axes (from room temperature to 1200°C).

Source	$a(10^{-6} \text{ K}^{-1})$	$b(10^{-6} \text{ K}^{-1})$	$c(10^{-6} \text{ K}^{-1})$
Bayer (1971)	-3.0	11.8	21.8
Skala (2000)	-2.4	12.0	20.8

The mechanical properties of Al_2TiO_5 have a very strong microstructural dependence which is directly related to the degree of micro-cracking present and stress redistribution in the matrix. Some disadvantages of Al_2TiO_5 are as follows:

- the existence of many micro-cracks at room temperature
- the blockage of micro-cracks at 300°C .
- the adhesion of micro-cracks and recombination of micro-cracking at 700°C (Wohlfrohm et al. 1991).

Typical values for thermo-mechanical properties of Al_2TiO_5 are given in Table 1.7. Crack healing with rising temperature results in increased strength and Young's modulus (Ohya et al. 1988). As crack healing on heating and re-cracking on cooling occur at different temperatures, thermal cycling gives rise to hysteresis effects, which may be accompanied by aging.

Table 1.7: Thermo-mechanical properties of Al_2TiO_5 -based ceramics.

(The Encyclopedia of Advanced Materials 1994)

Property	Value
Young's modulus (GPa)	5-30
Bend strength (room temperature) (MPa)	10-50
Thermal conductivity ($\text{Wm}^{-1}\text{K}^{-1}$)	2

Liu and Perera (1998) studied the high-temperature mechanical properties and thermal stability of sintered Al_2TiO_5 ceramics containing magnesium and iron. Both materials were found to exhibit a pronounced inelastic stress – strain behavior caused by extensive micro-cracks.

1.2.3.3 Titanium Oxide (TiO_2)

Pure titanium oxide (TiO_2) does not occur in nature. It is derived from ilmenite (Chris 1992) or leucocene ores (Deer et al. 1996). The physical and mechanical properties of sintered rutile are summarized in Table 1.8.

Table 1.8: Physical and mechanical properties of rutile (TiO₂). (Yan et al. 1981)

Property	Value
Density (g.cm ⁻³)	4
Porosity (%)	0
Modulus of Rupture (MPa)	140
Compressive Strength (MPa)	680
Poisson's Ratio	0.27
Fracture Toughness (MPa.m ^{1/2})	3.2
Shear Modulus (GPa)	90
Modulus of Elasticity (GPa)	230
Microhardness (HV0.5)	880
Resistivity (25°C) (ohm.cm)	10 ¹²
Resistivity (700°C) (ohm.cm)	2.5×10 ⁴
Dielectric Constant (1MHz)	85
Dielectric strength (kVmm ⁻¹)	4
Thermal expansion (RT-1000°C) (K ⁻¹)	9 × 10 ⁻⁶
Thermal Conductivity (25°C) (Wm ⁻¹ K ⁻¹)	11.7

1.2.3.4 Titanium Silicon Carbide (Ti_3SiC_2)

Ti_3SiC_2 behaves like a soft ceramic compound making it easily machinable (Barsoum, 1997). Goto and Hirai (1987) reported the Ti_3SiC_2 hardness value of 6 GPa. Pampuch et al. (1989) tested samples containing 10-20 vol% TiC, and reported Young's modulus and shear modulus of ~326 GPa and ~135 GPa respectively. Lis et al. (1995) found the hardness of Ti_3SiC_2 -TiC composites as a function of TiC content and estimated that the hardness of pure, polycrystalline Ti_3SiC_2 to be ~ 4 GPa. Okano and co-workers (1995) studied bulk, 95% dense samples that contained some secondary phases (TiC_x and titanium silicates), and they reported a flexural strength of 580 MPa and a fracture toughness of $6.9 \text{ MPa}\cdot\text{m}^{1/2}$ at ambient temperatures. Okano and co-workers (1995) reported large plastic deformations in samples tested at 1200°C , which they attributed to the presence of a grain-boundary phase. Rudnik and Lis (1997) fabricated hot-pressed Ti_3SiC_2 -TiC composites with ~15 vol% TiC and reported compressive and three-point bend strengths of 1120 ± 270 and 350 ± 63 MPa respectively.

In summary, these previous researchers above have investigated the mechanical properties of Ti_3SiC_2 including machinable process, elastic and shear modulus, hardness, bending strength, high fracture toughness and high flexural strength from ambient temperature to high temperature. However, the characterizations of thermal stability of Ti_3SiC_2 in air and argon and oxidation resistance of Ti_3SiC_2 at elevated temperatures have not been investigated. Hence, this current study focused on these characterizations.

In addition, Ti_3SiC_2 is thermal shock resistant compared to most ceramics (Barsoum and El-Raghy, 1996) though fine-grained samples have shown a of Ti_3SiC_2 decrease in strength when quenched from temperatures above 750°C (El-Raghy, 1999c). A plausible explanation for this behaviour is the gradual change of Ti_3SiC_2 from brittle condition at room temperature to plastic condition at temperatures above 1200°C (Barsoum and El-Raghy, 1996, 1997b, 1999a). Macro-grained samples of (3-4 mm) have also been shown to deform plastically at room temperature (Barsoum and El-Raghy, 1999).

Coarse-grained Ti_3SiC_2 samples exhibit the failure characteristics in the stress-strain curves which show a sharp drop in plastic deformation after the yield stress (Barsoum et al. 2000., Tzenov and Barsoum 2000). The ultimate tensile, compressive and flexural strengths of coarse-grained Ti_3SiC_2 at room temperature are 180 MPa, 720 MPa and 350 MPa respectively (Radovic et al. 2002., El-Raghy et al. 1999., Gilbert et al. 2000), while the ultimate tensile, compressive and flexural strengths of fine-grained Ti_3SiC_2 samples at room temperature are 298 MPa, 1050 MPa and 600 MPa respectively. The fracture toughness of coarse-grained and fine-grained samples are ($8\text{-}9.5 \text{ MPa}\cdot\text{m}^{1/2}$) and ($8.5\text{-}16 \text{ MPa}\cdot\text{m}^{1/2}$) respectively (Radovic et al. 2002., El-Raghy et al. 1999., Gilbert et al. 2000). In conclusion, the mechanical properties such as, ultimate tensile, compressive and flexural strengths are dependent on grain size; coarse-grained solids are weaker than their fine-grained counterparts (Barsoum and Radovic, 2011).

Ti_3SiC_2 samples were tested to undergo brittle to plastic transition (BPT) (Barsoum et al. 2000., El-Raghy et al. 1999) mechanism at higher temperature (1300°C). It is important to understand the high-temperature response of the Ti_3SiC_2 samples and the brittle to plastic transition (BPT) caused by increasing decohesion between the grains and/or increasing delamination between the layers as the temperature increases (Barsoum and Radovic, 2011). As more cyclic hardening was done, the number of loops increased until finally a linear elastic region appeared. In summary, stress-strain behaviour of Ti_3SiC_2 can be sensitive to the strain rate, particularly at elevated temperature. A significant increase in the strain rate generally increases strength but reduces the ductility of Ti_3SiC_2 . However, the strain rate effect can be small at room temperature.

The electrical and mechanical properties of bulk MAX phases were studied in detail by Barsoum and Radovic (2011). The mechanical properties of MAX phases are remarkable because they have high specific stiffness together with high machinability, such as 343 GPa for Ti_3SiC_2 and 340 GPa for Ti_3GeC_2 (Barsoum and Radovic 2011). Barsoum and Radovic (2011) also pointed out that, Ti_3SiC_2 has a low coefficient of

friction ($\mu_s = 2-5 \times 10^{-3}$). The deformation mechanism dominant in Ti_3SiC_2 depends on the level of porosity, temperature range and kink boundaries formation.

1.2.3.5 Titanium Carbide (TiC)

A particularly interesting feature of transition metals is that they form a host of different compounds when paired with other elements. One such family of compounds is transition-metal carbides (TMCs), which have many industrially important uses. For instance, TiC is an extremely hard and light refractory material with high thermal shock and is abrasion resistant. Transition metal carbides such as TiC have a unique combination of properties, such as chemical stability, excellent hardness, high melting point and excellent electrical and thermal conductivity, making them highly suitable for many technological applications. The effect of the addition of TiC to Ti_3SiC_2 -TiC composites could be improved hardness, fracture toughness and flexural strength. The in-situ addition of TiC particles to Ti_3SiC_2 matrix can prevent evidently the coalescence of Ti_3SiC_2 grains. Furthermore, with the addition of TiC from 0 – 30 vol%, the Vickers hardness and fracture toughness of the composites increase compared to those of Ti_3SiC_2 matrix (Zhang et al. 2008).

Koc and Folmer (1997) described an industrial method for the production of crystalline TiC powders, which used a carbon-thermal reduction of TiO_2 in a temperature range from 1900° to 2700°C and was associated with the following reaction (Equation 1.1).



1.2.4 Ceramic Systems Containing Al_2O_3 - Al_2TiO_5

Ceramics are known for being inherently brittle. However this can be alleviated slightly by a process known as grain bridging. Grain bridging is the process of introducing an increase of microstructural heterogeneity (Bartolome et al. 1996) following weak grain of boundaries, large grain size, and high internal residual stresses. Heterogeneously toughened by grain bridging or otherwise, ceramics are also susceptible to contact fatigue. When an indentation or contact is applied, the material will deform by

distributing micro damage (short cracks) under the shear zone instead of cone fracture. This has the effect of preventing long cracks propagating from the shear zone but with repetitive contact, a severe strength loss and accelerated material removal can occur. However, this can be minimized by effective control of powder characteristics during material preparation to prevent low as-fired densities (<90% theoretical) and abnormal grain growth (Runyan & Bennison, 1989).

Alumina is widely used for conventional structural applications because of its high melting point, high wear and corrosion resistance, electrical insulation, and good high-temperature strength. However, it has a limitation in advanced structural applications because of its low fracture toughness. It is well known that incorporation of a second phase with a high aspect ratio (whiskers, fibers, and platelets) into alumina can improve the fracture toughness by promoting toughening mechanisms such as crack deflection and crack-bridging. However, a major drawback of this approach is that the composites are difficult to sinter to high density without the use of hot pressing or hot-isostatic pressing. Residual stress can be enhanced by the inclusion of a secondary phase whose coefficient of thermal expansion shows a desired degree of mismatch with that of the matrix (Bartolome et al. 1996). This improves the flaw tolerance characteristic of the primary phase by up to approximately one order of magnitude if the primary phase is Al_2O_3 and the secondary phase is Al_2TiO_5 . This process has a greater improvement rate compared to grain growth scaling.

Al_2TiO_5 is widely used as a refractory material and as a thermal insulator in engine components due to its low thermal expansion coefficient ($1 \times 10^{-6} \text{ }^\circ\text{C}^{-1}$), high melting point (1860°C), low thermal conductivity, and excellent thermal shock resistance. The reaction between Al_2O_3 and TiO_2 to form Al_2TiO_5 is reversible and occurs at $\sim 1300^\circ \text{C}$. In 1952, Lang and colleagues reported that Al_2TiO_5 is thermodynamically stable from $\sim 1280^\circ \text{C}$ to the melting temperature, 1860°C. Buscaglia and Nanni (1998) found that the decomposition rate of Al_2TiO_5 is very slow, below $\sim 800^\circ \text{C}$. The full potential of Al_2TiO_5 has therefore been limited by its low fracture toughness, low mechanical strength and poor high-temperature stability below 1280°C. Through the addition of

stabilizers such as SiO_2 , Fe_2O_3 and MgO , the thermal and mechanical performance of Al_2TiO_5 can be greatly enhanced. Table 1.9 lists several processing methods used to fabricate ceramic composites.

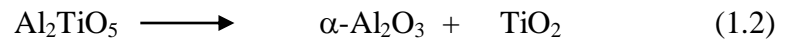
Table 1.9: Examples of processing methods used for the fabrication of ceramic composites.

Material	Method	Reference
$\text{Al}_2\text{O}_3/\text{ZrO}_2$ composites	Tape casting	Boch, Chartier and Huttepain, 1986
Trilaminate composites	Lamination	Harmer, Chan and Miller, 1992
Alumina/calcium-hexaluminate composites	Lamination	An et al. 1996
Alumina/ Al_2TiO_5 composites	Reaction sintering	Hasselmann et al. 1993
Alumina/ Al_2TiO_5 composites $\text{Al}_2\text{O}_3/\text{Al}_2\text{O}_3$	Duplex-bimodal composites	Bueno et al. 2005; Runyan and Bennison, 1991; Padture, Bennison and Chan, 1993; Braun, Bennison and Lawn 1992
Alumina/ Al_2TiO_5 and alumina-zirconia/ Al_2TiO_5 composites	Infiltration	Skala, 2000; Low et al. 1996a
Alumina-mullite, Al_2O_3 -AT and Al_2O_3 - $\text{CaAl}_{12}\text{O}_{19}$ composites	Infiltration	Marple and Green, 1991; Skala, 2000; Asmi et al. 1999

1.2.5 Decomposition Behavior of Al₂TiO₅

Due to several promising properties such as an excellent refractoriness, thermal shock resistance, low thermal expansion coefficient and high melting point, good compatibility with non-ferrous metals etc. Al₂TiO₅ has found many applications as an engineering ceramics material.

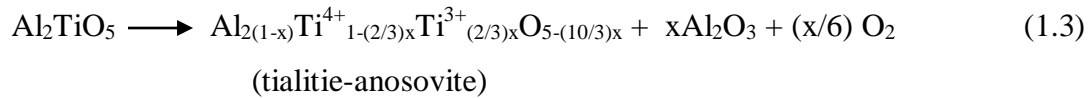
Al₂TiO₅ in pure form melts at 1860°C and it is thermodynamically stable only above, 1280°C and within the temperature range of 900°-1200°C, (Kato et al. 1979; 1980; Buscaglia and Nanni, 1998) at other temperatures it becomes unstable and decomposes into Al₂O₃ and TiO₂ with an overall decomposition process as follows (Lang et al. 1952) (Equation 1.2):



For pure Al₂TiO₅, the rate-controlling step in the decomposition is the transport to Al³⁺ ions through the TiO₂-rutile phase, the growth rate of decomposition products is constant and the decomposition mechanism is likely to be controlled by an unidentified interfacial process.

Studies have also been carried out on the decomposition kinetics of pure Al₂TiO₅ in oxidizing atmospheres (oxygen, argon or air) (Kameyama and Yamaguchi, 1976; Kato et al. 1979; Thomas et al. 1989). The decomposition rate of Al₂TiO₅ at 1100°C is significantly enhanced by vacuum (10⁻⁴ torr) or argon where > 95% of Al₂TiO₅ decomposed in 5h of soaking when compared to less than 30% decomposition in atmospheric air (Low et al. 2002, Manurung, 2002). Below 900°C, the decomposition rate of Al₂TiO₅ is usually very low, even after a long annealing time; the material can be stable from a kinetic point of view (Buscaglia et al. 1996). Hennicke and Lingenberg (1986) have attempted to explain the decomposition of Al₂TiO₅ by the formation of intermediate metastable Al₂TiO₅-Ti₃O₅ (tialite-anosovite) solid solutions. They observed that the as-sintered samples were likely to be the consequence of incomplete reaction rather than of decomposition.

Navrotsky (1975) proposed that, the decomposition of Al_2TiO_5 could be possible at high temperatures because of the contribution of entropy resulting from disordered distribution of atomic structure in cationic sub-lattice; this is caused by the radius difference between Al^{3+} (0.050 nm) and Ti^{4+} (0.068 nm) and the presence of small number of Al^{3+} ions. Furthermore, the decomposition of Al_2TiO_5 is expected to be very sensitive to the ageing annealing atmosphere, because Ti^{4+} is progressively reduced to Ti^{3+} if the oxygen partial pressure is decreased. Sperisen and Mocellin (1991) attempted to explain the decomposition of Al_2TiO_5 by the formation of intermediate metastable $\text{Al}_2\text{TiO}_5\text{-Ti}_3\text{O}_5$ (tialitie-anosovite) solid solutions. Duran et al. (1994) studied the beginning of decomposition of Al_2TiO_5 -based materials at 975°C under a nitrogen gas/oxygen gas mixed atmosphere using spectroscopic techniques. The decomposition detection of Al_2TiO_5 solid solution is explained in Equation 1.3



The decomposition kinetics of Al_2TiO_5 is as follows (Buscaglia and Nanni, 1998):

- The maximum decomposition rate is in the range of $1100^\circ - 1150^\circ\text{C}$.
- Half transformation times from 2 to 25 h have been observed in the temperature range of $1100^\circ\text{-}1150^\circ\text{C}$, depending on sintering temperatures, density, grain size, and annealing above the decomposition temperature.
- Decomposition kinetics can be described by the Johnson-Mehl-Avrami (JMA) equation and probably follows a nucleation and growth mechanism (Buscaglia and Nanni, 1998). No microstructure observations have been conducted to support nucleation mechanism.
- Decomposition is affected by the microstructure and stresses related to the thermal expansion anisotropy of the individual Al_2TiO_5 grains.

In view of the decomposition behavior of Al_2TiO_5 discussed above, significant effort has been directed towards improving the thermal stability of Al_2TiO_5 through substitution of stabilizers such as Fe_2O_3 , MgO , etc. (Rezaie et al. 2009).

The decomposition of Al_2TiO_5 treated with TiO_2 has been reported by Hwang, Nakagawa and Hamano (1993). The presence of TiO_2 was found to accelerate the decomposition, but the residual thermal stresses decreased. Decomposition of Al_2TiO_5 was accompanied by the formation of the rutile grains and pores at the interfaces with Al_2O_3 .

Mechanical properties strongly depend on the microstructures of Al_2TiO_5 . Buscaglia and Nanni (1998) observed the microstructure of partially decomposed samples which showed the presence of a limited number of nodules. The shape of the nodules is approximately spherical or ellipsoidal. For pure Al_2TiO_5 , the formation of a TiO_2 layer around aggregates of crystals can be observed at the beginning of the decomposition process (Figure 1.11 (a)) and as the reaction proceeds further, this core-shell microstructure is gradually destroyed with the formation of a random mixture of aggregates of elongated Al_2O_3 and rutile (Figure 1.11 (b) and (c)).

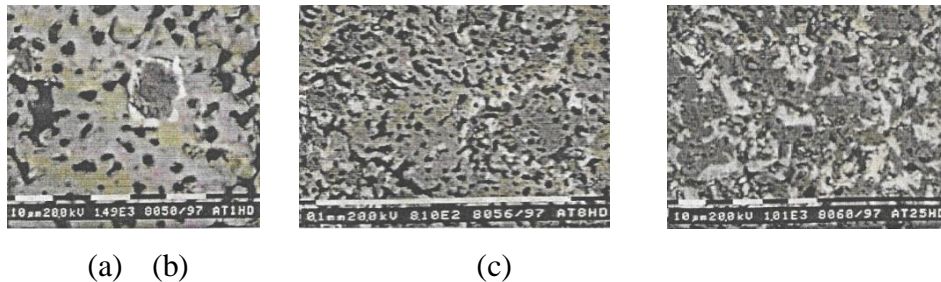


Figure 1.11: Microstructures (BS-SEM) of Al_2TiO_5 after (a) 1h, (b) 8h, and (c) 25h annealing at 1100°C . (Legend: TiO_2 , rutile is white, Al_2TiO_5 is light gray, Al_2O_3 is dark gray and black are pores and cracks). (Buscaglia and Nanni, 1998)

Microstructures of Al_2TiO_5 evolution with different annealing times at constant temperature of 1100°C is also one of the reasons for the initial nucleation stage. The decomposition occurs mainly through the growth of the nodules of the reaction products initially formed.

Buscaglia and Nanni (1998) explained that nodules formed with an Al_2O_3 core and a TiO_2 shell, grow at the maximum rate in comparison to other morphological features,

because the slow diffusion of titanium is avoided. Another factor is that the plastic deformation of TiO_2 occurs at lower temperatures than in Al_2O_3 at 1000°C (Hirthe and Brittain, 1963).

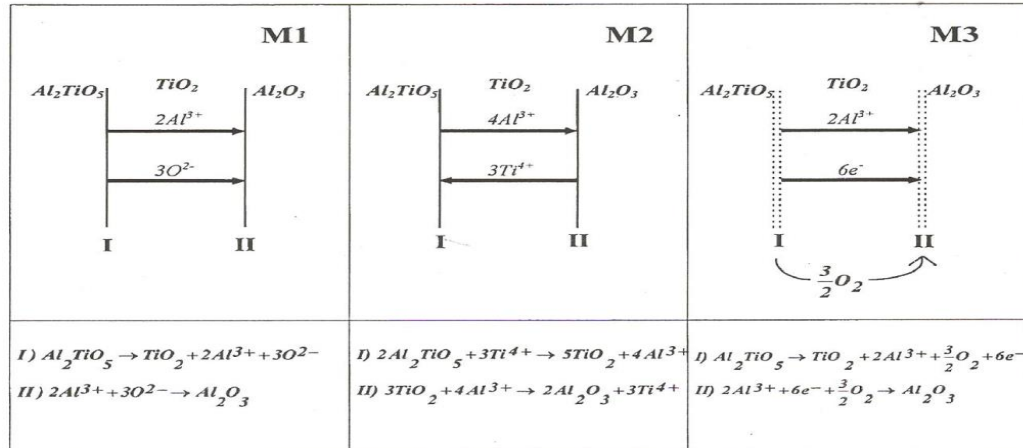


Figure 1.12: Schematic diagram showing the possible decomposition mechanisms of Al_2TiO_5 (Buscaglia and Nanni, 1998).

The mechanism by which Al_2TiO_5 decomposes is shown in Figure 1.12. In the case M1, growth of the Al_2O_3 layer occurs by unidirectional diffusion of Al^{3+} and O^{2-} ions through the TiO_2 shell. In the case M2, the Al^{3+} flux is coupled with a countercurrent of Ti^{4+} cations. In the case M3, molecular oxygen is transported through the gas phase and local electro-neutrality is maintained by means of electronic conduction in the TiO_2 layer.

1.2.6 Thermal Decomposition Behavior of MAX Phases

The high-temperature thermochemical stability in MAX phases has hitherto generated much controversy among researchers. For instance, several researchers have reported that Ti_3SiC_2 became unstable at temperatures greater than 1400°C in an inert atmosphere (e.g. vacuum or nitrogen), by dissociating into Si, TiC_x and/or $\text{Ti}_5\text{Si}_3\text{C}_x$ (Low 2004; Low and Pang 2011). A similar phenomenon has also been observed for Ti_3AlC_2 whereby it decomposes in vacuum to form TiC and Ti_2AlC (Pang et al. 2010; Pang and Low 2009; Low et al. 2011).

In other studies, Zhang et al. (2008) reported Ti_3SiC_2 to be thermally stable up to 1300°C in nitrogen, but above this temperature drastic degradation and damage occurred due to surface decomposition. Feng et al. (1999) annealed the Ti_3SiC_2 -based bulk samples at 1600°C for 2h and 2000°C for 0.5 h in vacuum (10^{-2} Pa) and found that TiC_x was the only phase remaining on the surface. According to Gao et al. (2002) the propensity of decomposition of Ti_3SiC_2 to TiC_x was related to the vapour pressure of Si, i.e., the atmosphere where the Ti_3SiC_2 exists. They believed that the partial pressure of Si plays an important role in maintaining the stability of Ti_3SiC_2 whereby it has a high propensity to decompose in N_2 , O_2 or CO atmosphere at temperatures above 1400°C . This process of surface-initiated phase decomposition was even observed to commence at temperatures as low as $1000\text{--}1200^\circ\text{C}$ in Ti_3SiC_2 thin films during vacuum annealing (Emmerlich et al. 2007). The large difference in observed decomposition temperatures between bulk and thin-film Ti_3SiC_2 has been attributed to the difference in diffusion length scales involved and measurement sensitivity employed in the respective studies. In addition, Ti_3SiC_2 has also been observed to react readily with molten Al, Cu, Ni and cryolite (Na_3AlF_6) at high temperatures.

In contrast, Barsoum and co-workers (1996) have shown that Ti_3SiC_2 was thermodynamically stable up to at least 1600°C in vacuum for 24 h and in argon atmosphere for 4 h. They further argued that the reduced temperature at which Ti_3SiC_2 decomposed as observed by others was due to the presence of impurity phases (e.g. Fe or V) in the starting powders which interfered with the reaction synthesis of Ti_3SiC_2 and thus destabilized it following prolonged annealing in an inert environment (Tzenov et al. 2000). However, mixed results have been reported by Radhakrishnan et al. (1999). In their investigation, Ti_3SiC_2 was shown to be stable in a tungsten-heated furnace for 10 h at 1600°C and 1800°C in an argon atmosphere, but dissociated to TiC_x under the same conditions when using a graphite heater.

These conflicting results suggest that the thermochemical stability of MAX phases is still poorly understood although it has been established that its susceptibility to thermal decomposition is strongly influenced by factors such as purity of powders and sintered

materials, temperature, vapour pressure, atmosphere, and the type of heating elements used. In general, the onset temperature of decomposition depends on the quality of vacuum present in the furnace. At a medium vacuum of 10^{-5} torr, most MAX phases will tend to become unstable at 1400°C and begin to decompose (Figure 1.13).

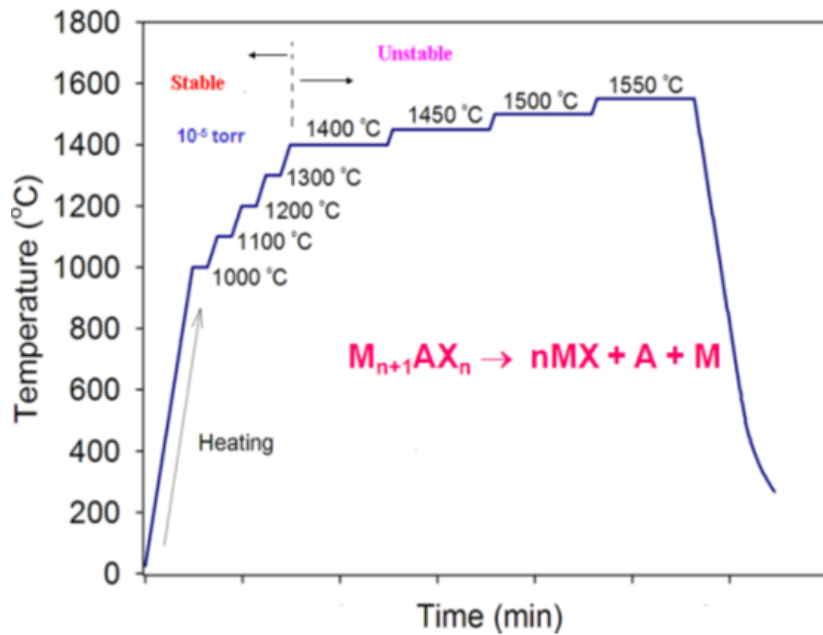


Figure 1.13: A schematic showing the thermal stability of MAX phases at elevated temperature in vacuum (Low and Pang 2013).

When the vapour pressure is lower than 10^{-5} torr, MAX phases will decompose below 1400°C . In addition, the nature of microstructure of the decomposed surface layer formed during annealing remains controversial, especially in relation to the role of pore sizes in the decomposition kinetics at the near surface. Pang and Low (2010) conducted a comparative study to elucidate the role of pore microstructures on the decomposition kinetics of several MAX phases during vacuum annealing in the temperature range $1000\text{--}1800^{\circ}\text{C}$. The effect of pore-size on the activation energy of decomposition was evaluated using the Arrhenius equation. The kinetics of phase decomposition was modelled using a modified Avrami equation (Pang 2010).

The phase transitions in the MAX phases investigated and their relative phase abundances at various temperatures as revealed by in-situ neutron diffraction was shown in Figure 1.14. A weight loss of ~4% was observed for decomposed Ti_3SiC_2 which may be attributed to the release of gaseous Si by sublimation during the decomposition process. For Ti_3AlC_2 , its decomposition into TiC and Ti_2AlC as lower order or intermediate phase was observed at $\geq 1400^\circ\text{C}$. However, at higher temperatures, when compared to TiC, a smaller growth rate for Ti_2AlC may indicate that Ti_2AlC experienced further decomposition into TiC via the sublimation of Al, similar to decomposition of Ti_3SiC_2 . In contrast to Ti_3AlC_2 , no intermediate or lower order phase was observed for the decomposition of Ti_3SiC_2 , Ti_2AlC or Ti_2AlN . This difference can be attributed to the fact that Ti_3SiC_2 is the only stable ternary phase in Ti-Si-C system and Ti_2AlC is the lowest order phase in the Ti-Al-C system. The same applies to Ti_2AlN where it is the lowest order phase in the Ti-Al-N system. Fig. 1.14 (e) shows the excellent stability of Ti_2AlN at 1500°C for up to 350 minutes. The inferior thermal stability of Ti_4AlN_3 is shown in Fig. 1.14(f) where it decomposed by more than 60% when annealed in vacuum at 1500°C for 500 minutes.

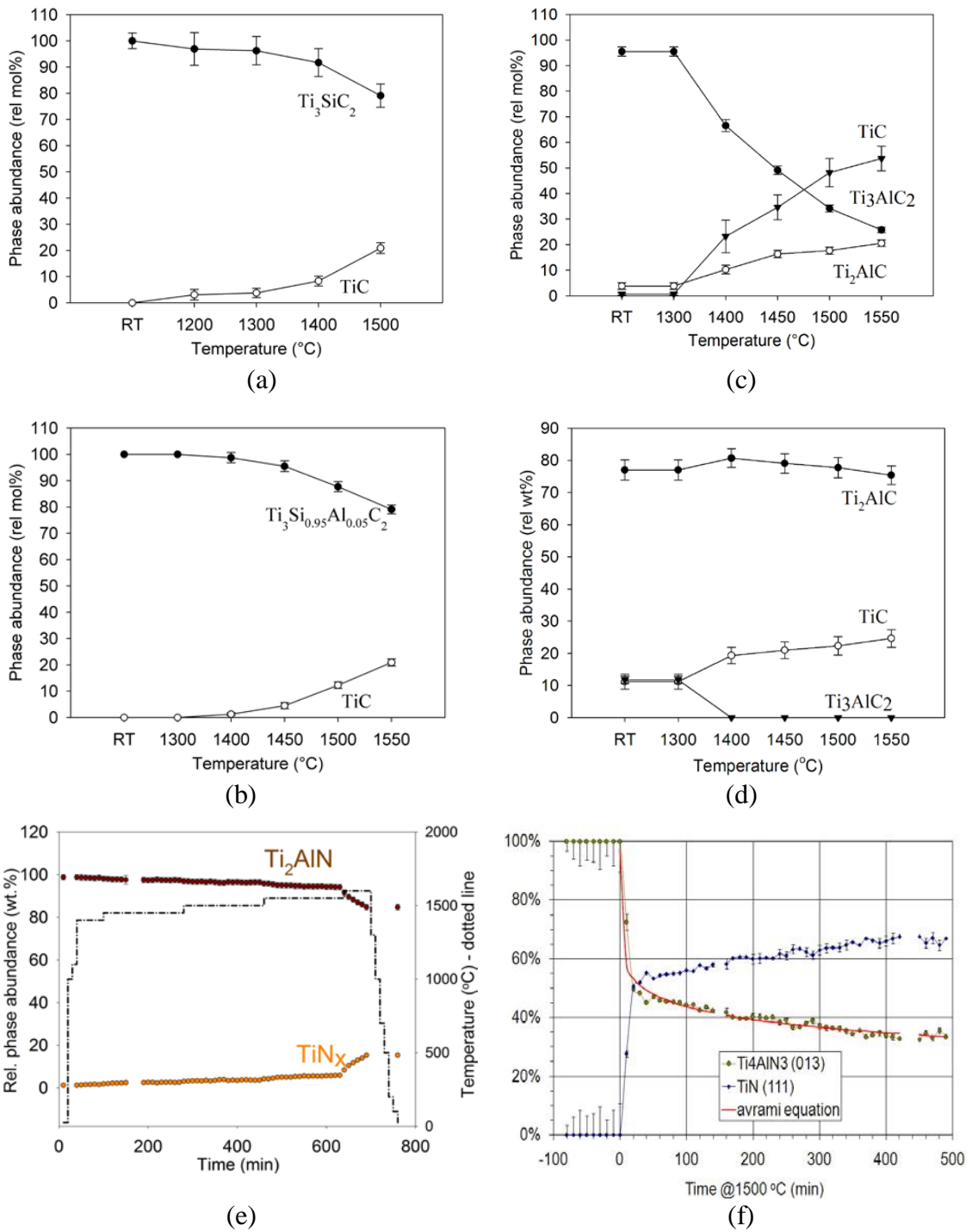


Figure 1.14: Phase abundance as a function of temperature for the decomposition of (a) Ti_3SiC_2 , (b) $\text{Ti}_3\text{Si}_{0.95}\text{Al}_{0.05}\text{C}_2$, (c) Ti_3AlC_2 , (d) Ti_2AlC_2 , (e) Ti_2AlN and (f) Ti_4AlN_3 in vacuum (Low and Pang 2013).

In general, a weight loss of up to 20% was observed as a result of decomposition for MAX phases can be attributed to the release of gaseous A element by sublimation during the decomposition process because the vapour pressures of the A elements exceed the ambient pressure of the furnace (i.e. $\leq 5 \times 10^{-5}$ torr) at $\geq 1500^\circ\text{C}$. Since the vapor pressure of a substance increases non-linearly with temperature according to the Clausius-Clapeyron relation (Callen 1985), the volatility of A elements will increase with any incremental rise in temperature. Figure 1.15 shows the weight loss as a function of temperature for Ti_2AlN and Ti_4AlN_3 which shows that Ti_2AlN has a superior resistance to thermal decomposition.

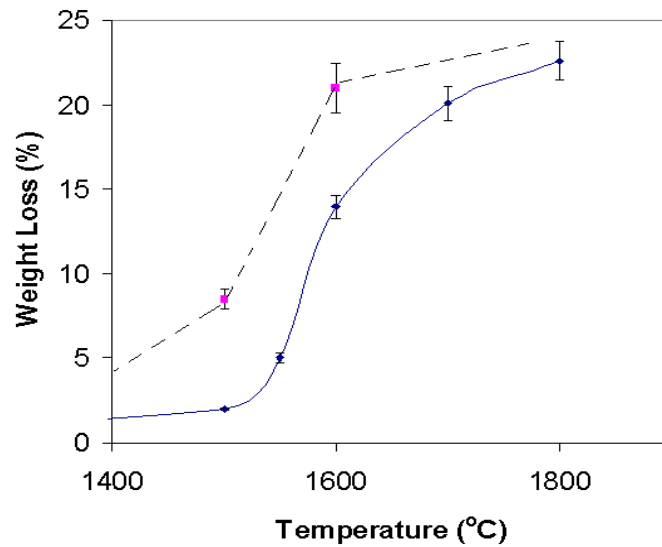
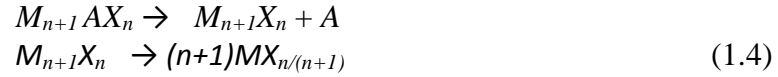


Figure 1.15: Variation of weight loss as a function of temperature for Ti_4AlN_3 (■) and Ti_2AlN (◆) (Low and Pang 2013).

It is well known that A elements such as Si and Al have high vapour pressure and become volatile at elevated temperature (Low and Pang 2013). Thus, at the temperature of well over 1500°C used in this study, both Al and Si should become volatile and sublime readily and continuously in a dynamic environment of high vacuum. When the vapor pressure becomes sufficient to overcome ambient pressure in the vacuum furnace, bubbles will form inside the bulk of the substance which eventually appears as voids on the surface of decomposed MAX phase. Since Si has a lower vapour pressure than Al (Low and Pang 2013), it helps to explain why Ti_3SiC_2 is more resistant to decomposition than Ti_3AlC_2 or Ti_2AlN (Pang et al. 2010) In all cases, the kinetics of

decomposition process is driven mainly by a highly restricted out-diffusion and sublimation of high vapour pressure *A* element (e.g. Al, Si) from the bulk to the surface of the sample and into the vacuum, i.e.,



As previously shown in Figure 1.14, the weight losses of up to 11.6% and over 20% in decomposed Ti_4AlN_3 and Ti_2AlN (Pang et al. 2010) respectively can be attributed to the release of gaseous Al (and possibly Ti) by sublimation during the decomposition process because the vapor pressures of both Al and Ti exceed the ambient pressure of the furnace (i.e. $\leq 5 \times 10^{-5}$ torr) at $\geq 1500^\circ C$ (Low and Pang 2013). Figure 1.16 shows the vapour pressures of various elements at elevated temperature, and at a vapour pressure of 5×10^{-2} torr in the vacuum furnace, both Al and Ti become volatile as the temperature approaches 1200° and $1700^\circ C$ respectively. Thus, at the temperature of well over $500^\circ C$ used in this study, both Al and a small amount of Ti should become volatile and sublime readily and continuously in a dynamic environment of high vacuum. When the vapor pressure becomes sufficient to overcome ambient pressure in the vacuum furnace, bubbles will form inside the bulk of the substance which eventually appears as voids on the surface of decomposed *MAX* phase (Pang and Low 2009; Pang et al. 2010; Low et al. 2011). A closer look of Figure 1.16 may further explain why Ti_3SiC_2 is more resistant to decomposition than Ti_3AlC_2 or Ti_4AlN_3 because Si has a lower vapour pressure than Al.

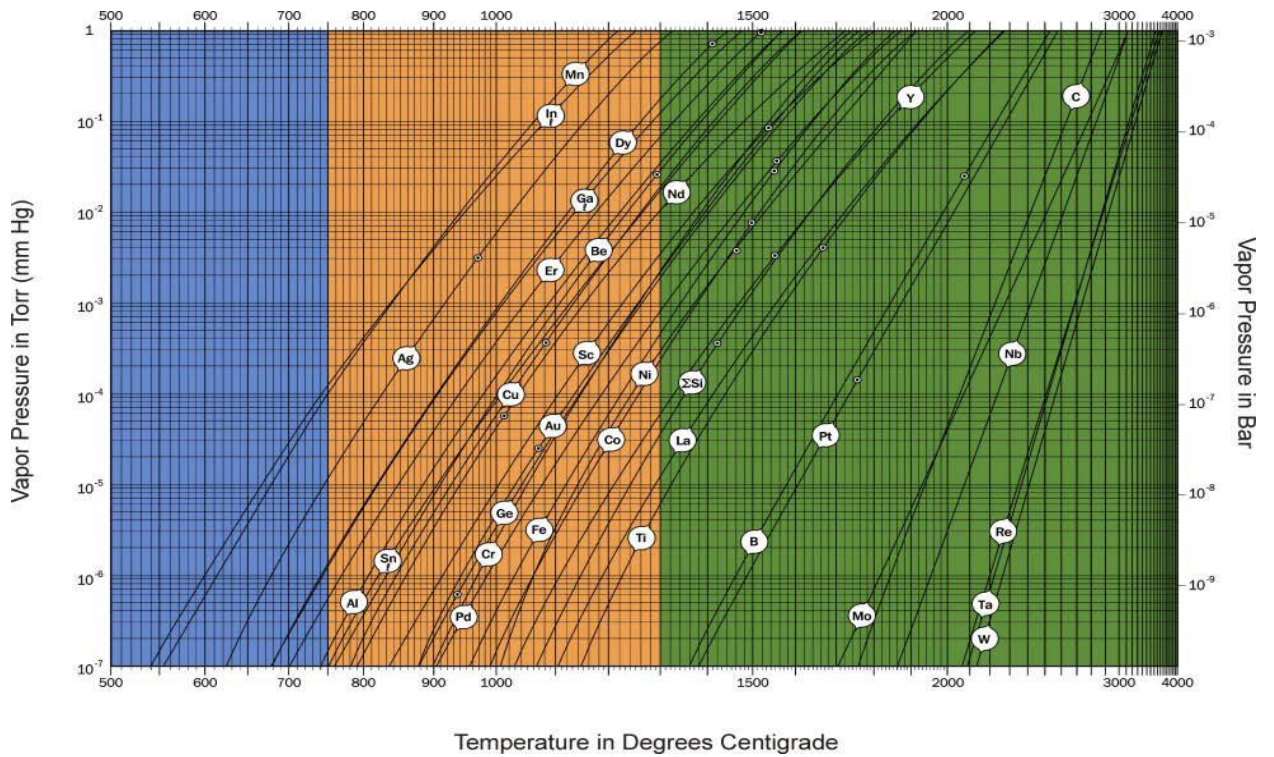


Figure 1.16: Vapour pressure of selected elements at various temperature (www.veeco.com/library/Learning_Centre/Growth_Information/Vapor_Pressure_Data_For_Selected_Elements/Index.aspx).

Table 1.10: Comparison of the kinetics of decomposition in six MAX-phase samples.

MAX phase	Activation energy (KJ mol ⁻¹)	Pore size (μm)	Proposed reaction
Ti ₃ SiC ₂	169.6	1.0-3.0	Ti ₃ SiC ₂ → 3TiC _{0.67} + Si ↑
Ti ₃ Si _{0.95} Al _{0.05} C ₂	76.7	2.0-10.0	Ti ₃ Si _{0.95} Al _{0.05} C ₂ → 3TiC _{0.67} + 0.95Si ↑ + 0.05 Al ↑
Ti ₃ AlC ₂ (bulk)	-71.9	0.5-0.8	Ti ₃ AlC ₂ → 3TiC _{0.67} + Al ↑
Ti ₃ AlC ₂ (powder)	71.9	>1.0	Ti ₃ AlC ₂ → 3TiC _{0.67} + Al ↑
Ti ₂ AlC	85.7	2.0-10.0	Ti ₂ AlC → 2TiC _{0.5} + Al ↑
Ti ₂ AlN	573.8	2.0-8.0	Ti ₃ AlN → 3TiN _{0.5} + Al ↑
Ti ₄ AlN ₃	410.8	1.8-3.0	Ti ₄ AlN ₃ → 4TiN _{0.75} + Al ↑

Based on the role of pore microstructures on decomposition kinetics, the activation energies calculated from the Arrhenius equation for five *MAX* phases and the proposed reactions are summarized and listed in Table 1.10 (Low and Pang 2013).

All the calculated activation energies are positive except for bulk Ti_3AlC_2 . However, when powder of Ti_3AlC_2 was used a positive activation energy was obtained which implies the importance of pore microstructures in the decomposition kinetics (Low and Pang 2013). A negative activation energy indicates that the rate of decomposition in Ti_3AlC_2 decreased with increasing temperature due to the dense TiC surface layer with very fine pores ($<1.0 \mu\text{m}$), which exert an increasing resistance to the sublimation process as the temperature increases (see Figure 1.17d) (Low and Pang 2012). In contrast, a more porous decomposed layer with coarser pores ($>2.0 \mu\text{m}$) formed in other *MAX* phases and in powdered Ti_3AlC_2 which enabled the sublimation of Al or Si to progress with minimum resistance, and resulting in an increasing rate of decomposition with temperature (Low and Pang 2012). In summary, the pore sizes play a critical role in determining the value of activation energy and the rate of decomposition. Hence, the ability to manipulate the pore microstructure either through densification to reduce pore-size or engineering of pore-free microstructure will allow the process of decomposition in *MAX* phases to be minimized or arrested.

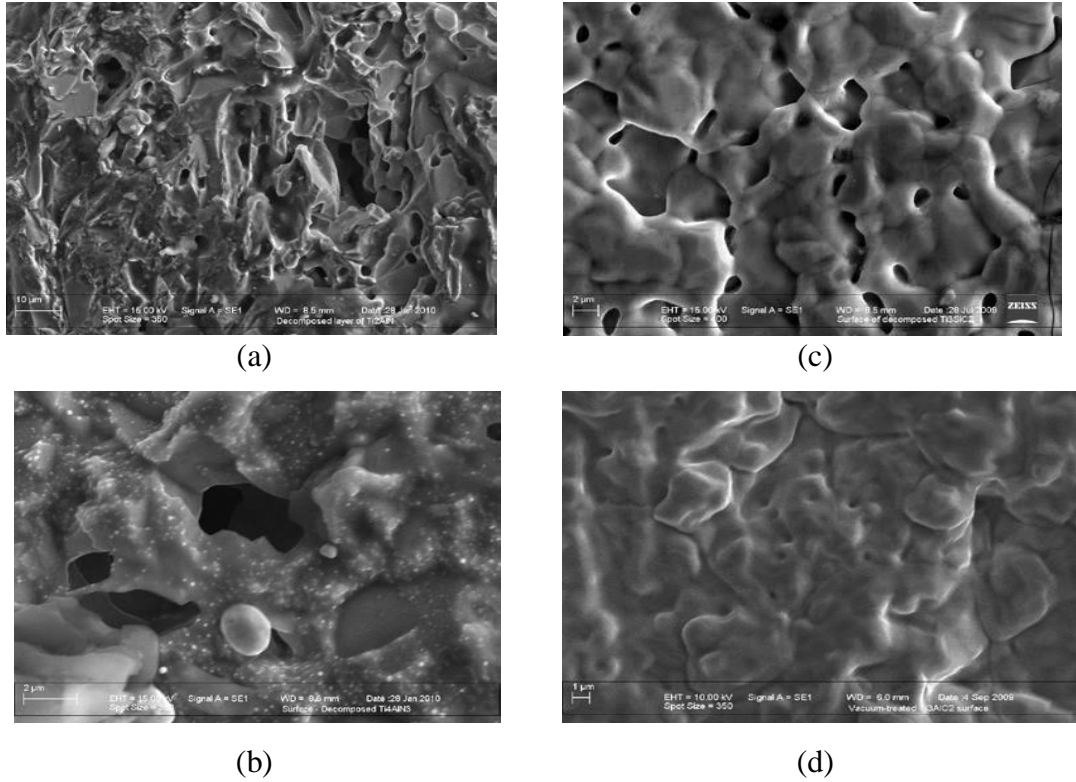


Figure 1.17: Scanning electron micrographs of the surface microstructures of vacuum-decomposed MAX phases; (a) Ti_2AlN , (b) Ti_4AlN_3 , (c) Ti_3SiC_2 , and (d) Ti_3AlC_2 (Low and Pang 2013).

During the isothermal decomposition of MAX phases at between 1200-1500°C, the Avrami kinetics of decomposition was modeled using Equation (1.5)

$$y = \exp(-kt^n) \quad (1.5)$$

where k and n are time –independent constants for the particular reaction, and the Avrami constants were evaluated. The Avrami fits of isothermal decomposition of Ti_2AlN and Ti_3SiC_2 are shown in Figure 1.18. The calculated Avrami exponent (n) and Avrami constant (k) for the MAX phases are summarized in Table 1.11.

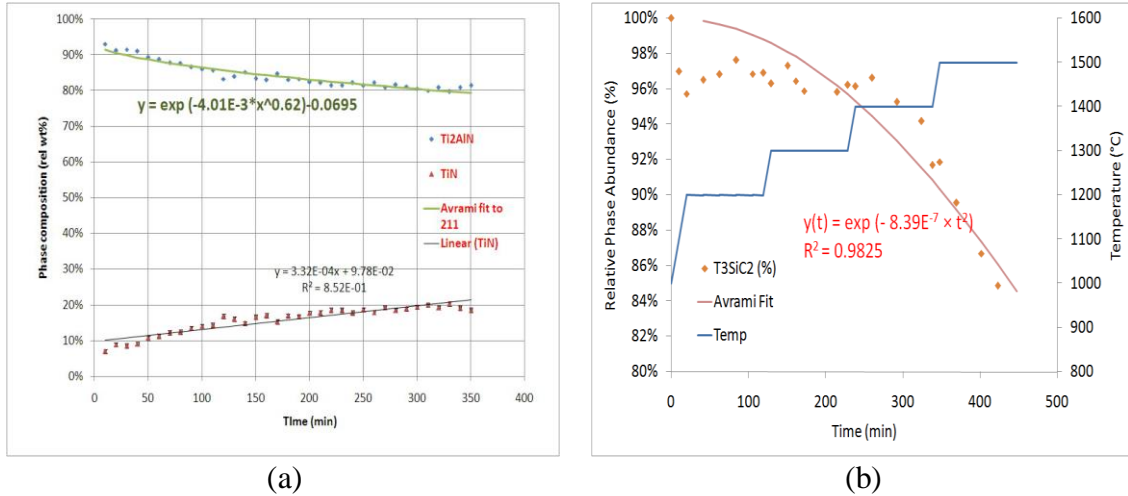


Figure 1.18: Time-dependent phase abundance and Avrami fit isothermal decomposition of (a) Ti_2AlN , (b) Ti_3SiC_2 at $1550^\circ C$ in vacuum (Low and Pang 2013).

Table 1.11: Comparison of the Avrami decomposition kinetics in MAX phases. (Low and Pang 2013).

MAX phase	Avrami exponent (n)	Avrami constant (k) mol% (min) ⁻ⁿ
Ti_4AlN_3	0.18	0.37
Ti_2AlN	0.62	0.004
Ti_3AlC_2	0.0023	0.93
Ti_2AlC	0.11	0.608
Ti_3SiC_2	8.93×10^{-7}	2

Moreover, above $1400^\circ C$, MAX phases decomposed to binary carbide (e.g. TiC_x) or binary nitride (e.g. TiN_x), primarily through the sublimation of A-elements such as Al or Si, which results in a porous surface layer of MX_x being formed. Positive activation energies were determined for the decomposition of MAX phases except for Ti_3AlC_2 where negative activation energy of 71.9 kJ mol^{-1} was obtained due to formation of fine pores on TiC_x . The kinetics of isothermal phase decomposition at $1550^\circ C$ modelled with the Avrami equation suggests a highly restricted diffusion of Al or Si between the channels of M_6X octahedral. This is indicated by the display of low Avrami exponent (n) values (i.e. <1.0) in these materials. The pore microstructure of decomposed MAX

phase has been shown to play a vital role in the kinetics of decomposition with coarse-pores facilitating the decomposition process but the fine-pores hindering it.

1.2.7 Oxidation Behavior of Ti_3SiC_2

Oxidation behavior is necessary to investigate the materials at high temperatures. Ti_3SiC_2 is a promising structural material for high temperature because of its unique combination of metal-like properties.

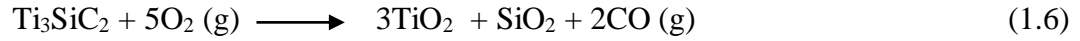
The oxidation of Ti_3SiC_2 was reported by Recault et al. (1994) to commence at temperature as low as 400°C through the formation of an anatase-like TiO_2 film that eventually transformed to rutile at $\sim 1050^\circ\text{C}$. Between 650° and 850°C both rutile and anatase were observed to co-exist, rapidly becoming protecting films and giving rise to the slow formation of SiO_2 and more TiO_2 . By increasing the temperature, both oxidation processes (i.e. direct reaction and diffusion through oxide layers) were activated and an almost total oxidation was achieved at 1050° - 1250°C , resulting in titania (rutile) and silica (cristobalite). In addition, the oxidation resistance of Ti_3SiC_2 was reported by Tong et al. (1995) and Zhou et al. (2004; 2009) to be excellent at temperature below 1100°C due to the formation of protective SiO_2 surface layers.

Barsoum et al. (1997) studied the oxidation of polycrystalline samples of Ti_3SiC_2 in the air in the temperature range of 900° - 1400°C . It was found that oxidation was parabolic with parabolic rate constants (k_p) that increase as the temperature increases from 900° to 1400°C . The outer layer was pure TiO_2 (rutile), and the inner layer consisted of a mixture of SiO_2 and TiO_2 . The results are consistent with the model in which growth of the oxide layer occurs by the inward diffusion of oxygen and the simultaneous outward diffusion of titanium and carbon.

Sun and colleagues (2001) reported that the oxidation of Ti_3SiC_2 from 900°C to 1300°C follows a parabolic process, as observed in the marker experiment diffusion process under isothermal oxidation conditions at 1200°C for 100h. During the oxidation process, the inward diffusion of oxygen and outward diffusion of titanium and carbon

occur simultaneously (Sun et al. 2001, 2004 and Barsoum et al 1997), thereby making internal oxidation predominant.

The oxidation process of Ti_3SiC_2 is expressed below in Equations 1.6 and 1.7:

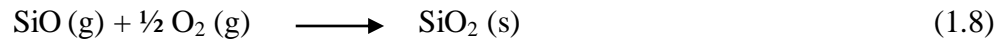


or



Sun and colleagues (2001) also explained the formation of the SiO_2 layer within the outer TiO_2 . The oxidation at 1100-1200°C formed a two-layer scale after a short oxidation time; an outer layer of coarse grained TiO_2 and an inner layer of a mixture of fine grained TiO_2 and SiO_2 . The oxygen pressure of the inner layer was much lower than that of the outer layer, resulting in the formation of SiO . This process is expressed in Equation 1.7.

The evolved SiO gas transformed to solid SiO_2 when the oxygen pressure was sufficiently high to support the process, as expressed in Equation 1.8:



Therefore SiO_2 precipitated in the outer TiO_2 layer as the oxygen pressure in the outer TiO_2 was much higher than that in the inner mixture layer.

However, if the diffusion of SiO had occurred, it would allow for large channels such as cracks. More cracks or defects produced at 1200°C could have changed the lattice diffusion to below 1100°C. But when the oxidation temperature was above 1200°C, the concentration gradient of oxygen pressure in the scale was not steep. Oxidation at the scale/matrix interface occurred according to Equation 1.6 to form SiO_2 , instead of SiO (Sun et al. 2001).

Zhou et al. (2004) reported the oxidation resistance behavior of Ti_3SiC_2 by heating a $\text{Ti}_3\text{Si}_{0.9}\text{Al}_{0.1}\text{C}_2$ solid solution at 1000-1350°C for 20h in air. At 1000-1100°C, the oxidation resistance of $\text{Ti}_3\text{Si}_{0.9}\text{Al}_{0.1}\text{C}_2$ was significantly improved because of the formation of a scale consisting of a continuous $\alpha\text{-Al}_2\text{O}_3$ inner layer and a discontinuous TiO_2 (rutile) outer layer. At 1200-1300°C, the continuous inner layer was $\alpha\text{-Al}_2\text{O}_3$ and outer layer was a mixture of TiO_2 (rutile) and Al_2TiO_5 . However, the oxidation resistance of $\text{Ti}_3\text{Si}_{0.9}\text{Al}_{0.1}\text{C}_2$ deteriorated at 1350°C because of the depletion of $\alpha\text{-Al}_2\text{O}_3$. This depletion was caused by the extensive reaction between TiO_2 (rutile) and $\alpha\text{-Al}_2\text{O}_3$ to form Al_2TiO_5 .

Zhou et al. (2006) investigated the reaction path to synthesize Ti_3SiC_2 doped with Al through in situ hot pressing/solid-liquid reaction. In this process, the beneficial effect of Al dopant on the oxidation resistance of Ti_3SiC_2 was presented. The influence of Al content on the preparation of $\text{Ti}_3\text{Si}(\text{Al})\text{C}_2$ was also examined. Al doping improves the oxidation resistance of Ti_3SiC_2 by generating a continuous inner layer of $\alpha\text{-Al}_2\text{O}_3$ and a discontinuous outer layer of TiO_2 (rutile) at 1000-1100°C. At 1200-1300°C, the oxidized layers consist of a continuous inner layer of $\alpha\text{-Al}_2\text{O}_3$ and two discontinuous outer layers of TiO_2 (rutile) and Al_2TiO_5 . Zhou et al. (2006) described the oxidation behavior of Ti_3SiC_2 at 1400°C and 1500°C respectively. At 1400°C, TiC_x acts as a “real initial material” and “effective TiC_x ” but at 1500°C, TiC_x presents “invalid TiC_x ”. The addition of a small amount of Al, the amount of effective TiC_x is increased and relatively decreased that of “invalid TiC_x ”. In summary, the impurity phase of TiC_x is removed from Ti_3SiC_2 by the addition of significant amount of Al. The results show that the substitution of Si with small amount of Al strongly improved the oxidation resistance of Ti_3SiC_2 . In the case of Ti_3SiC_2 and $\text{Ti}_3\text{Si}(\text{Al})\text{C}_2$ samples, the high-temperature oxidation resistance has a close relationship with the weak covalent bonding interactions between the Ti and Si or Al atomic layers. This is due to the fact that the degrees of covalent bonding of Ti-Si or Ti-Al bonds are weaker than those of Ti-C bonds. Subsequently, the Si or Al atoms are able to escape outward easily to form the protective oxide scale SiO_2 or Al_2O_3 . Therefore, the high activity and diffusion of Al and the low solubility of oxygen in the solid solutions are the main key factors for the

formation of the continuous α -Al₂O₃ layer during the high-temperature oxidation (Zhou et al. 2004).

Zheng et al. (2011) stated that improved high-temperature oxidation resistance behavior of Ti₃Si(Al)C₂ solid solution could be achieved by Nb (niobium) doping. The oxidation kinetics of (TiNb)₃(SiAl)C₂ at 1000-1300°C obeyed the parabolic law and the oxidation process of (TiNb)₃(SiAl)C₂ at 1000-1300°C was diffusion controlled. However, the oxidation process of Ti₃(SiAl)C₂ was diffusion controlled only at 1000°C. Moreover, Zheng et al. (2011) compared the values of oxide layer thickness (Δx) (where Δx is the change in thickness of oxide layer formed with respect to the temperature), for (TiNb)₃(SiAl)C₂ and Ti₃(SiAl)C₂ in the temperature range of 1000-1300°C in air for 20 h. The results indicated that the oxide layer formed on (TiNb)₃(SiAl)C₂ was thinner and smaller in grain size than that formed in Ti₃(SiAl)C₂.

Zheng et al. (2011) also presented the phase composition of oxide scales formed in (TiNb)₃(SiAl)C₂ and Ti₃(SiAl)C₂ during oxidation at 1000-1300°C in air for 20 h. The common oxide scales of rutile (TiO₂), α -Al₂O₃ and cristobalite (SiO₂) were identified during the oxidation of (TiNb)₃(SiAl)C₂ and Ti₃(SiAl)C₂ at 1000° and 1100°C respectively. Ti₃(SiAl)C₂ oxidized to form an outer layer of rutile (TiO₂) and Al₂TiO₅ at 1300°C whereas (TiNb)₃(SiAl)C₂ oxidized to form a duplex structure with an outer thin layer of TiO₂ and an inner mixed layer of rutile (TiO₂) and amorphous SiO₂. Zheng et al. (2011) found that with increasing temperature, the thickness of the oxide scales increased. Nb doping of Ti₃(SiAl)C₂ increases its resistance to oxidation by reducing the concentration of oxygen vacancies and Ti interstitials at 1300°C (Zheng et al. (2011)).

1.3 Bibliography: List of all references cited in the Introduction and Overview

- ABBOUD, J. H., RAWLINGS, R. D. & WEST, D. R. F. 1994. Functionally-Graded Layers of TiAl-Based Alloys Produced by Laser Alloying and Cladding, *Materials Science and Technology*, 10, 414-419.
- ADIL, F. & CHRISTIAN, M. 1993. Theoretical Analysis of the Structures Titanium Dioxide Crystals, *Physical Review B* 47, 11717-11724.
- ANDRADE, J., VILLAFUERTE-CASTREJON, M. E., VALENZUELA, R., & WEST, A. R. 1986. Rutile Solid Solution Containing $M^+(Li)$, $M^{2+}(Zn, Mg)$, $M^{3+}(Al)$ and $M^{5+}(Nb, Ta, Sb)$ ions, *Journal of Materials Science Letters*, 5, 147-149.
- AN, L., CHAN, H. M., PADTURE, N. P. & LAWN, B. R. 1996. Damage-Resistance Alumina-Based Layer Composites. *Journal of Materials Research*, 11, 204-207.
- ASMI, D., LOW, I. M., KENNEDY, S. & DAY, R. A. 1999. Characteristics of a Layered and Graded Alumina/calcium-Hexaluminate Composite, *Materials Letters*, 40, 96-102.
- AUSTIN, A. E. & SCHWARTZ, C. M. 1953. The Crystal Structure of Aluminium Titanate. *Acta Crystallographica*, 6, 812-813.
- BAHR, H.-A., BALKE, H., FETT, T., HOFINGER, I., KIRCHHOFF, G., MUNCHZ, D., NEUBRAND, A., SEMENOV, A. S., WEISS, H.-J. & YAND, Y. Y. 2003. Cracks in Functionally Graded Materials, *Materials Science and Engineering, A* 362, 2-16.
- BARSOUM, M.W. & EL-RAGHY, T. 1996. Synthesis and Characterization of a Remarkable Ceramic: Ti_3SiC_2 , *Journal of the American Ceramic Society*, 79, 1953-1956.
- BARSOUM, M.W. 1997. *Fundamentals of Ceramics*. McGraw-Hill Series in Materials Science and Engineering, ISBN 0-07-005522-X (SM).
- BARSOUM, M.W., EL-RAGHY, T. & OGBUJI, L. 1997a. Oxidation of Ti_3SiC_2 in Air, *Journal of the Electrochemical Society*, 144, 2508-2516.
- BARSOUM, M. W. & EL-RAGHY, T. 1997. A Progress Report Ti_3SiC_2 , Ti_3GeC_2 , and the H-Phases, M_2BX , *Journal of Materials Synthesis and Processing*, 5, 197-216.

- BARSOUM, M. W., BRODKIN, D. & EL-RAGHY, T. 1997c. Layered Machinable Ceramics for High Temperature Applications, *Scripta Materialia*, 36, 535-541.
- BARSOUM, M. W. & EL-RAGHY, T. 1999. Room Temperature Ductile Carbides, *Metallurgical and Materials Transactions*. 30A, 363-369.
- BARSOUM, M. W., EL-RAGHY, T., RAWN. C. J., PORTER. W. D., WANG, H., PAYZANT, E. A. & HUBBARD, C. R. 1999. Thermal Properties of Ti_3SiC_2 , *Journal of Physics and Chemistry of Solids*, 60, 429-439.
- BARSOUM, M. W. 2000. The $M_{N+1}AX_N$ Phases: A New Class of Solids: Thermodynamically Stable Nanolaminates, *Progress in Solid State Chemistry*, 28, 201-281.
- BARSOUM, M. W., ALI, M & EL. RAGHY, T. 2000. Processing and Characterization of Ti_2AlC , Ti_2AlN and $Ti_2AlC_{0.5}N_{0.5}$. *Metallurgical and Materials Transactions A: Physical Metallurgy and Materials Science*, 31 A: 1857-1865.
- BARSOUM, M. W. & EL-RAGHY, T. 2001. The MAX Phases: Unique New Carbide and Nitride Materials, *American Scientist* 89, 336-343.
- BARSOUM, M. W., RADOVIC, M., FINKEL, P. & EL-RAGHY, T. 2001. Ti_3SiC_2 and Ice, *Applied Physics Letter*, 79, 479-481.
- BARSOUM, M. W. & RADOVIC, M. 2011. Elastic and Mechanical Properties of the MAX Phases, *Annual Review Materials Research*, 41, 195-227.
- BARTOLOME, J.F., REQUENA, J., MOYA, J.S., LI, M. & GUIU, F. 1996. Cyclic Fatigue Crack Growth Resistance of $Al_2O_3-Al_2TiO_5$ composites, *Acta Materialia*, 44, (4), 1361-1370.
- BATTLE, P. D., GOODENOUGH, J. B., & PRICE, R. 1983. The Crystal Structures and Magnetic Properties of Be_2LaRuO_6 and Ca_2LaRuO_6 , *Journal of Solid State Chemistry*, 46, 2, 234-244.
- BECHER, P. F. 1991. Microstructural Design of Toughened Ceramic, *Journal of the American Ceramic Society*, 74(2), 255-269.
- BOCH, P., CHATIER, T. & HUTTEPAIN, M. 1986. Tape Casting of Al_2O_3/ZrO_2 Laminated Composites, *Journal of the American Ceramic Society*, 69(8), 191-202.

- BRAGG, W. H. & BRAGG, W. L. 1916. *X-rays and Crystal Structure*. Bell and Sons, London.
- BRAUN, L.M., BENNISON, S.J. & LAWN, B.R. 1992. Objective Evaluation of Short-Crack Toughness Curves Using Indentation Flaws; Case Study on Alumina Based Ceramics, *Journal of the American Ceramic Society*, 75, 3049-3054.
- BUENO, S., MORENO, R. & BAUDIN, C. 2005. Design and Processing of Al_2O_3 - Al_2TiO_5 Layered Structures, *Journal of the European Ceramic Society*, 25(6), 847-856.
- BURDETT, J. K., HUGHBANKS, T., MILLER, G. J., JR RICHARDSON W. & SMITH, J.V. 1986. Structural-Electronic Relationships in Inorganic Solids: Powder Neutron Diffraction Studies of the Rutile and Anatase Polymorphs of Titanium Dioxide at 15 and 295 K, *Journal of the American Ceramic Society*, 109, 3639-3646
- BUSCAGLIA, V., CARACCILO, F. & LEONI, M., NANNI, P., VIVIANI, M. & LEMATRE, J. 1997. Synthesis, Sintering and Expansion of $\text{Al}_{0.8}\text{Mg}_{0.6}\text{Ti}_{1.6}\text{O}_5$: a Low-Thermal-Expansion Material Resistant to Thermal Decomposition, *Journal of Materials Science*, 32, 6525-6531.
- BUSCAGLIA, V., NANNI, P., BATTILANA, G., ALIPRANDI, G. & CARRY, C. 1994. Reaction Sintering of Aluminium Titanate: I- Effect of MgO Addition, *Journal of the European Ceramic Society*, 13, 411-417.
- BUSCAGLIA, V. & NANNI, P. 1998. Decomposition of Al_2TiO_5 and $\text{Al}_{2(1-x)}\text{Mg}_x\text{Ti}_{(1+x)}\text{O}_5$ Ceramics, *Journal of the American Ceramic Society*, 81, 2645-2653.
- CAGLOTI, G., PAOLETTI, A. & RICCI, F. P. 1958. Choice of Collimator for a Crystal Spectrometer for Neutron Diffraction, *Nuclear Instrumentation Methods*, 3, 223-228.
- CALLEN, H. B. 1985. *Thermodynamics and an Introduction to Thermostatistics*. Wiley. ISBN: 978-0-471-86256-7.
- CLEVELAND, J. J. & BRADT, R. C. 1978. Grain Size/Microcracking Relations for Pseudobrookite Oxides, *Journal of the American Ceramic Society*, 61, 478-481.

- CHEN, J., ZHOU, Y. C., ZHANG, H. B., WAN, D. T. & LIU, M. Y. 2007. Thermal Stability of Ti_3AlC/Al_2O_3 Composites in High Vacuum, *Materials Chemistry and Physics*, 104, 109-112.
- CHEN, H. C., LIU, Z. Y. and CHUANG, Y. C., (1993). Degradation of Plasma Sprayed Alumina and Zirconia Coatings on Stainless Steel during Thermal Cycling and Hot Corrosion, *Thin Solid Films*, 223, 1, 56-64.
- CHO, K. S., KIM, Y. W., CHOI, H. J. & LEE, J. G. 1996. In Situ-Toughened Silicon Carbide-Titanium Carbide Composites, *Journal of the American Ceramic Society*, 79, 1711-1713.
- CHRIS PELLANT. 1992. Rocks and Minerals, Dorling Kindersley Hand Books, Dorling Kindersley Limited, London, 79-80.
- CHRISTENSEN, A. N. 1978. The Temperature Factor Parameters of Some Transition Metal Carbides and Nitrides by Single Crystal X-Ray and Neutron Diffraction, *Acta Chemica Scandinavica, Series A*. 32, 89-90.
- CROMER D. T. & HARRINGTON K. 1955. The Structure of Anatase and Rutile, *Journal of the American Ceramic Society*, 77, 4708-4709.
- CHU, J., ISHIBASHI, H., HAYASHI, K., TAKEBE, H. & MORINAGA, K. 1993. Slip Casting of FGM, *Journal of the Ceramic Society, Japan*, 101, 841.
- DAHLQVIST, M., ALLING, B., ABRIKSOV, I. A. & ROSÉN, J. 2010. Phase Stability of Ti_2AlC upon Oxygen Incorporation: A First-Principles Investigation, *Physical Review B*, 81, 024111-1-024111-8.
- DEER, W. A., HOWIE, R. A. & ZUSSMAN, J. 1996. *An Introduction to the Rock-Forming Minerals*, 2nd Edition. Prentice Hall, 303, 544, 546.
- DURAN, A., WOHLFROMM, H. & PENA, P, 1994. Study of the Behavior of Al_2TiO_5 Material in Reducing Atmosphere by Spectroscopic Techniques, *Journal of the European Ceramic Society*, 13, 73-80.
- DU, Y. L., SUN, Z. M & HASHIMOTO, H. 2010. First-Principles Study on Phase Stability and Compression Behavior of Ti_2SC and Ti_2AlC , *Physica B: Condensed Matter*, 405, 720-723.

- EKLUND, P., BECKERS, M., JANSSON, U., HÖGBERG, H. & HULTMAN, L. 2010, The Mn+1AX_n Phases: Materials Science and Thin Film Processing, *Thin Solid Films*, 518, 1851-1878.
- EL-RAGHY, T., ZAVALIANGOS, A., BARSOUM, M. W. & KALIDINDI, S. R. 1997. Damage Mechanisms around Hardness Indentation in Ti₃SiC₂, *Journal of the American Ceramic Society*, 80, 513-516.
- EL-RAGHY, T. & BARSOUM, M. W. 1998. Diffusion Kinetics of the Carburization and Silicidation of Ti₃SiC₂, *Journal of Applied Physics*, 83, 112-119.
- EL-RAGHY, T. & BARSOUM, M. W. 1999b. Processing and Mechanical Properties of Ti₃SiC₂. Part 1. Reaction Path and Microstructure Evolution, *Journal of the American Ceramic Society*, 82, 2849-2854.
- EL-RAGHY, T. & BARSOUM, M. W., ZAVALIANGOS, A. & KALIDINDI, S. R. 1999a. Processing and Mechanical Properties of Ti₃SiC₂: II, Effects of Grain Size and Deformation Temperature, *Journal of the American Ceramic Society*, 82, 2855-2860.
- EMMERLICH, J., DENIS, M., PER, E., OLA, W., ULF, J., JOCHEN, M. S., HANS, H. & LARS, H. 2007. Thermal Stability of Ti₃SiC₂ Thin Films, *Acta Materialia*, 55, 1479-1488.
- EPICIER, T., THOMAS, G., WOHLFROMM, H. & MOYA, J. S. 1991. High Resolution Electron Microscopy Study of the Cationic Disorder in Al₂TiO₅, *Journal of Materials Research*, 6, 138-145.
- FINKEL, P., BARSOUM, M. W. & EL-RAGHY, T. 2000. Low Temperature Dependencies of the Elastic Properties of Ti₄AlN₃ and Ti₃Al_{1.1}C_{1.8} and Ti₃SiC₂. *Journal of Applied Physics*, 87, 1701-1703.
- GOTO, T. & HIRAI, T. 1987. Chemically Vapour Deposited Ti₃SiC₂. *Materials Research Bulletin*, 22, 1195-1201.
- GREENWOOD, G. 1924. The Crystal Structure of Cuprite and Rutile, *Philosophical Magazine*, 6, 48, 654-663.
- GREENWOOD, R. & KENDALL, K. J. 1999. Selection of Suitable Dispersants for Aqueous Suspensions of Zirconia and Titania Powders using Acoustophoresis, *Journal of the European Ceramic Society*, 19, 479-488.

- GREEN, D. J., HANNINK, R. H. J. & SWAIN, M. V. 1989. *Transformation Toughening of Ceramics*, CRC Press, Boca Raton, Florida.
- HAMELIN, M. 1958. Structure du Compose $TiO_2 \cdot Al_2O_3$ Comparaison Avec La Pseudo-Brookite, *Bulletin de la Societe Chimique de France*, 1559-1566.
- HANAOR, D. A. H., KOSHY, P. & SORRELL, C. C. 2012. Phase Stability and Transformations in TiO_2 , In J. Low (ed), *Rutile: Properties, Synthesis and Applications*, Nova Science Publishers, Hauppauge, NY, 11-28.
- HANAOR, D. A. H. & SORRELL, C. C. 2011. Review of the Anatase to Rutile Phase Transformation, *Journal of Materials Science*, 46, 855-874.
- HARMER, M. P., CHAN, H. & MILLER, G. A. 1992. Unique Opportunities for Microstructural Engineering with Duplex and Laminar Ceramic Composites, *Journal of the American Ceramic Society*, 75, 1715-1728.
- HASSELMAN, D. P. H., DONALDSON, K. Y., ANDERSON, E. M. & JHONSON, T. A. 1993. Effect of Thermal History on the Thermal Diffusivity and Thermal Expansion of Alumina-Aluminium Titanate Composite, *Journal of the American Ceramic Society*, 76, 2180-2184.
- HENNICKE, H. W. & LINGENBERG, W. 1986. Dependence of Microstructure and Physical Properties of Materials on the Basis of Aluminium Titanate. In *Proceedings of the Second International Symposium on Ceramic Materials and Components for Engines*, Ed. W. Bunk and H. Hausner. DKG, Bad Honnef, Germany, 619-623.
- HENNICKE, H. W. & LINGENBERG, W. 1986. The Formation and Decomposition of Aluminium Titanate. II. The Decomposition Reaction of Aluminium Titanate, *Ber. Dtsch. Keram. Ges*, 63, 100-106.
- HILL, R.J., HOWARD, C. J. & Hunter, B.A Barwell, 1995. Computer Program for Rietveld Analysis of Fixed Wavelength X-ray and Neutron Powder Diffraction Patterns. Australian Atomic Energy Commission (now ANSTO) Report No. M112, Lucas Heights Research Laboratories, New South Wales, Australia.
- HILL, R. J. & Howard, C. J. 1987. Quantitative Phase Analysis from Neutron Powder Diffraction Data using the Rietveld Method, *Journal of Applied Crystallography*, 20, 467-474.

- HIRAI, T. 1996., Chapter 20, "Functionally Gradient Materials" Materials Science and Technology, vol 17B, Chan, R. W., Haasen, P and Kramer, E. J (eds), VCH Verlagsgesellschaft mbH Publishers, Weinheim, Germany, 293-341.
- HIRTHER, W. M. & BRITTAIN, J. O. 1963. High-Temperature Steady-State Creep in Rutile, *Journal of the American Ceramic Society*. 46. 411-417.
- HOLT, J. B., KOIZUMI, M., HIRAI, T. & MUNIR, Z. A. 1993. Ceramic Transaction: Functionally Graded Materials, *The American Ceramic Society*, Westerville, OH, Vol. 34, 11-20.
- HOLCOMBE JR, C. E. & COFFEY JR, A. L. 1973. Calculated X-Ray Powder Diffraction Data for Beta Al_2TiO_5 , *Journal of the American Ceramic Society*, 56, 220-221.
- HONG, F. Y & LIN, L. L. 2010. Effect of Processing Condition on the Microstructure and Mechanical Properties of $\text{Ti}_3\text{SiC}_2/\text{SiC}$ Composites, *Materials Science Forum*, 8, 32-38.
- HU, C., LI, F., ZHANG, J., WANG, J. & ZHOU, Y. 2007. Nb_4AlC_3 : A New Compound Belonging to the MAX Phases. *Scripta Materialia*, 57, 893-896.
- HU, C., ZHANG, J., BAO, Y., WANG, J., LI, M. & ZHOU, Y. 2008. In-Situ Reaction Synthesis and Decomposition of Ta_2AlC . *International Journal of Materials Research (Z. Metallkd.)* 99, 8-13.
- HUGGINS, M. L. 1926. The Crystal Structure of Anatase and Rutile, the Tetragonal Forms of TiO_2 , *Physical Review B*. 27, 637-644.
- HULL, S., SMITH, R. I., DAVID, W., HANNON, A., MAYERS, J. & CYWINSKI, R. 1992. The POLARIS Powder Diffractometer at ISIS, *Physica B*, 180-181, 1000-1002.
- HUNTER, B. A. & HOWARD, C. J. 1998. A Computer Program for Rietveld Analysis of Fixed Wavelength X-Ray and Neutron Powder Diffraction Patterns. Australian Atomic Energy Commission (now ANSTO) Report No. M112, Lucas Heights Research Laboratories, New South Wales, Australia.
- HWANG, C. S., NAKAGAWA, Z. & HAMANO, K. 1993. Microstructures and Mechanical Properties of TiO_2 -Doped Alumina Ceramics Owing to

- Decomposition of Formed Al_2TiO_5 , *Journal of the Ceramic Society, Japan*, 102, 253-306.
- ISHITSUKA, M., SATO, T., ENDO, T. & SHIMADA, M. 1987. Synthesis and Thermal Stability of Aluminium Titanate Solid Solutions, *Journal of the American Ceramic Society*, 70, 69-71.
- JIANG, E. Y. & LIU, M. S., 1995. Thin Film Prepared by Facing Targeted Sputtering, *Journal of Physics: D - Applied Physics*. 28, 4-6.
- JEITSCHKO, W. & NOWOTNY, H. 1967. Die Kristallstruktur von Ti_3SiC_2 -Ein Neuer Komplexcarbidge-Typ. *Monatsh. Chemistry*. 98, 329-337.
- JOHARI ABU, M., JULIE J. M. & ZAINAL A. A. 2012. Effect of Excess Silicon on the Formation of Ti_3SiC_2 Using Free Ti/Si/C Powders Synthesized via Arc Melting, *International Scholarship Research Network*, ISRN Ceramics, 2012, Article ID 341285, DOI: 10.5402/2012/341285, 1-10.
- KAMEYAMA, T. & YAMAGUCHI, T. 1976. Kinetics Studies on the Eutectoid Decomposition of Al_2TiO_5 , *Journal of the Ceramic Society of Japan*. 84, 589-593.
- KATO, E., DAIMON, K. & KOBAYASHI, Y. 1979. Decomposition Kinetics of Aluminium Titanate (Al_2TiO_5) in Powdered State, *Journal of the Ceramic Society of Japan*, 87, 81-85.
- KATO, E., DAIMON, K. & TAKAHASHI, J. 1980. Decomposition Temperature of beta- Al_2TiO_5 , *Journal of the American Ceramic Society*, 63, 355-356.
- KIM, I. J., ZOGRAFOU, C. & KROENERT, W. 1993. Synthesis and Characterization of Submicrometer Monosized Ceramic Powders of Aluminium Titanate-Mullite Composite by Sol-Gel Process, *International Journal of Materials, Product and Technology*, 8, 440-451.
- KIM, I. K. & CAO, G. 2002. Low Thermal Expansion Behavior and Thermal Durability of ZrTiO_4 - Al_2TiO_5 - Fe_2O_3 Ceramics between 750 and 1400°C, *Journal of the European Ceramics Society* 22, 2627-2632.
- KIM, I. J., KWEON, O. S., KO, Y. S. & ZOGRAFOU, C. 1996. Effect of Grain Size on Thermomechanical Properties of Al_2TiO_5 Ceramics, *Korean Journal of Ceramics*, 2, 246-250.

- KIMURA, H. & KOBAYASHI, S. 1993. Fabrication of a FGM of TiAl/PSZ System via Pulse Electric Discharge Consolidation with Temperature Slope Control Using a Stepped Die, *Journal of the Japan Institute of Metals*, 57, 1346-1351.
- KISI, E. H. 1994. Rietveld Analysis of Powder Diffraction Patterns, *Materials Forum*, 18, 135-153.
- KISI, E. H., CROSSLEY, J. A. A., MYHRA, S. & BAROSUM, M. W. 1998. Structure and Crystal Chemistry of Ti_3SiC_2 , *Journal of Physics and Chemistry of Solids*, 59, (9), 1437-1443.
- KOC, R. & FOLMER, J. S. 1997. Carbothermal Synthesis of Titanium Carbide using Ultrafine Titania Powders, *Journal of Materials Science*, 32, 3101-3111.
- KOIZUMI, M. 1997. FGM Activities in Japan, *Composites Part B*, 28B, 1-4.
- KOIZUMI, M. & NIINO, M. 1995. Overview of FGM Research in Japan, *Materials Research Society Bulletin*, 19-21.
- KRAUS, W. & NOLZE, G. 1999. PowderCell for Windows Version 2.3.
- LANG, S. M., FILMORE, C.L. & MAXWELL, L. H. 1952. The System Beryllia-Alumina-Titania: Phase Relations and General Physical Properties of Three-Component Porcelains, *Journal of Research of the National Bureau of Standards*, 48, 298-312.
- LANGENSIEPEN, R. A., TRESSLER, R. E. & HOWELL, P. R. 1983. A Preliminary Study of Precipitation in Ti^{4+} -Doped Polycrystalline Alumina, *Journal of Materials Science*, 18, 2771-2776.
- LAZZERI, M., VITTADINI, A. & SELLONI, A. 2001. Structure and Energetics of Stoichiometric TiO_2 Anatase Surfaces, *Physical Review B*, 63, 155409-1-155409-0.
- LEWIS, J., SCHWARZENBACH, D. & FLACK, H. D. 1982. Electric Field Gradients and Charge Density in Corundum, $\alpha-Al_2O_3$, *Acta Crystallographica*, A 38, 733-739.
- LIS, J., MIYAMOTO, Y., PAMPUCH, R. & TANIHATA, K. 1995. Ti_3SiC_2 -Based Materials by HIP-SHS Techniques, *Materials Letters*, 22, 163-168.

- LIU, T. S. & PERERA, D. S. 1998. Long Term Thermal Stability and Mechanical Properties of Aluminium Titanate at 1000-1200°C, *Journal of Materials Science*, 33, 995-1001.
- LOW, I. M., SKALA, R. D. & ZHOU, D. 1996. Synthesis of Functionally-Graded Aluminium Titanate/Alumina Composites, *Journal of Materials Science Letters*, 15, 345-347.
- LOW, I. M., LEE, S. K., LAWN, B. R. & BARSOUM, M. W. 1998. Contact Damage Accumulation in Ti_3SiC_2 , *Journal of the American Ceramic Society*, 81, 225-228.
- LOW, I. M. 1998. Vickers Contact Damage of Micro-Layered Ti_3SiC_2 , *Journal of the European Ceramic Society*, 18, 709-713.
- LOW, I. M. 1998a. Processing of an In-Situ Layered and Graded Alumina-Aluminium Titanate Composites, *Materials Research Bulletin*, 33, 1475-1482.
- LOW, I. M. 1998b. Synthesis and Properties of In-Situ Layered and Graded Aluminium Titanate/Alumina Composites, *Journal of the Australian Ceramic Society*, 34, 250-255.
- LOW, I. M., SINGH, M., MANURUNG, P., WREN, E., SHEPPARD, D. P. & BARSOUM, M. W. 2002. Depth-Profiling of Phase Composition and Texture in Layered-Graded Al_2O_3 - & Ti_3SiC_2 - Based Systems Using X-Ray and Synchrotron Radiation Diffraction, *Key Engineering Materials*, 224-226, 505-510.
- LOW, I. M., MANURUNG, P., SMITH, R. I. & LAWRENCE, D. 2002. A Novel Processing Method for the Microstructural Design of Functionally-Graded Ceramic Composites, *Key Engineering Materials*, 224-226, 465-470.
- LOW, I. M. & WREN, E. 2003. Characterisation of Phase Relations in Air-Oxidised Titanium Silicon Carbide (Ti_3SiC_2), *Journal of the Australian Ceramic Society*, 39, 103-107.
- LOW, I. M. 2004. Depth-Profiling of Phase Composition in a Novel Ti_3SiC_2 -TiC System with Graded Interfaces, *Materials Letters*, 58, 927-930.

- LOW, I. M., LAWRENCE, D. & SMITH, R. I. 2005. Factors Controlling the Thermal Stability of Aluminium Titanate in Vacuum, *Journal of the American Ceramic Society*, 88, 2957-2961.
- LOW, I. M. & PANG, W. K. 2011. Kinetics of Decomposition in MAX Phases at Elevated Temperature, *Materials Australia*, 45 (2), 33-35.
- LOW, I. M. & PANG, W. K. 2012. A Comparative Study of Decomposition Kinetics in MAX Phases at Elevated Temperature, in *Advanced Ceramic Coatings and Materials for Extreme Environments II* (D. Zhu, H.-T. Lin, Y. Zhou, T. Hwang, M. Halbig and S. Mathur (Eds)), John Wiley & Sons, Inc., Hoboken, NJ, USA. Doi: 10.1002/9781118217474, 179-186.
- LOW, I. M., & PANG, W. K. 2013. Decomposition Kinetics of MAX Phases in Extreme Environments, Chapter 2 in *MAX Phases and Ultra-High Temperature for Extreme Environments* (I. M. Low, Y. Sakka., and C. F. Hu (Eds)), IGI Global, Hershey PA, USA, 34-48.
- LUO, Y., LI, S., CHEN, J., WANG, R., LI, J. & PAN, W. 2002. Preparation and Characterization of $\text{Al}_2\text{O}_3\text{-Ti}_3\text{SiC}_2$ Composites and its Functionally Graded Materials. *Materials Research Bulletin*, 38, 69-78.
- LU, Q., HU, J., TANG, K., DENG, B., QIAN, Y., ZHOU, G. & LIU, X. 1999. The Co-Reduction route to TiC Nanocrystallites at Low Temperature, *Chemical Physics Letters*, 314, 37-39.
- MANURUNG, P. 2001. Microstructural Design and Characterisation of Alumina/Aluminium Titanate Composites, *PhD Thesis*, Curtin University of Technology.
- MARPLE, B. R. & GREEN, D. J. 1991. Mullite/Alumina Particulate Composites by Infiltration: III, Mechanical properties, *Journal of the American Ceramic Society*, 74, 2453-2459.
- MASLEN, E. N, STRELTSOV, V. A., STRELTSOVA, N. R., ISHIZAWA, N. & SATOW, Y. 1993. Synchrotron X-Ray Study of the Electron Density in Alpha- Al_2O_3 , *Acta Crystallographica*, B49, 973-980.

- MOCELLIN, A. & FREUDENBERG, B. 1987. Aluminium Titanate Formation by Solid-State Reaction of Fine Al_2O_3 and TiO_2 Powders, *Journal of the American Ceramic Society*, 70, 1259-1262.
- MOROSIN, B. & LYNCH, R. W. 1972. Structure Studies on Al_2TiO_5 at Room Temperature and 600°C , *Acta Crystallographica*, B 28, 1040-1046.
- MOULSON, A. J & HERBERT, J. M. 2003. Electroceramics, Materials-Properties-Application, Second edition, *John Wiley & Sons Ltd*. Chichester, England. 5-547.
- MO, S.D. & CHING, W. Y. 1995. Electronic and Optical Properties of Three Phases of Titanium Dioxide: Rutile, Anatase, and Brookite, *Physical Review B*, 51, 13023-13032.
- MUNRO, R. G. 1997. Evaluated Material Properties for a Sintered α -Alumina, *Journal of the American Ceramic Society*, 80, 1919-1928.
- NAKASHIMA, S., ARIKAWA, H., CHIGASAKI, M. & KOJIMA, Y. 1994. ZrO_2 and Cu Functionally Gradient Materials Prepared by a Dynamic Ion Mixing Process, *Surface and Coatings Technology*, 66, 330-333.
- NATHAN, J., BRYAN, H. & DWIGHT, M. 2013. Oxidation Transitions for SiC Part 1. Active-to-Passive Transitions, *Journal of American Ceramic Society*, 96, 838-844.
- NAVROTSKY, A. 1975. Thermodynamics of Formation of Some Compounds with the Pseudobrookite Structure and of the FeTi_2O_5 - Ti_3O_5 Solid Solution Series, *American Mineralogist*, 60, 249-256.
- NEUBRAND, A. & RODEL, J. 1997. Gradient Materials: an Overview of a Novel Concept. *Z Metallk.* 88, 548-371.
- NEWNHAM, R. E. & DE. HANN, Y. M. 1962. Refinement of the α - Al_2O_3 , Ti_2O_3 , V_2O_3 and Cr_2O_3 Structures. *Zeitschrift fuer Kristallographie*, 117, 235-237.
- NORBERG, S. T., NOBOU, I., HOFFMANN, S. & MASAHIRO, Y. 2005. Re-Determination of β - Al_2TiO_5 Obtained by Melt Casting, *Acta Crystallographica, E* 61, i160-i162.
- O'CONNOR, B. H. & LI, D. Y. 2000. Influence of Refinement Strategies on Rietveld Phase Composition Determinations. *Advances in X-ray Analysis*, 42, 204-211.

- OHYA, Y., NAKAGAWA, Z. & HAMANO, K. 1987. Grain Boundary Microcracking Due to Thermal Expansion Anisotropy in Aluminium Titanate Ceramics, *Journal of the American Ceramic Society*, 70, C184-C186.
- OHYA, Y., NAKAGAWA, Z. & HAMANO, K. 1988. Crack Healing and Bending Strength of Aluminium Titanate Ceramics at High Temperature, *Journal of the American Ceramic Society*, 71, C23-C33.
- OKANO, T., YANO, T. & ISEKI, T. 1993. Synthesis and Mechanical Properties of Ti_3SiC_2 Ceramics, *Transactions of the Material Research Society Japan*, 14A, 597-600.
- PADTURE, N. P., BENNISON, S. J. & CHAN., H. M. 1993. Flaw-Tolerance and Crack-Resistance Properties of Alumina-Aluminium Titanate Composites with Tailored Microstructures, *Journal of the American Ceramic Society*, 76, 2312-2320.
- PAMPUCH, R., LIS, J., STOBIERSKI, L. & TYMKIEWICZ, M. 1989. Solid Combustion Synthesis of Ti_3SiC_2 , *Journal of the European Ceramic Society*, 5, 283-287.
- PANG, W. K. & LOW, I. M. 2009. Diffraction Study of Thermal Dissociation in the Ternary Ti-Al-C System, *Journal of the Australian Ceramic Society*, 45, 39-43.
- PANG, W. K., LOW, I. M., O'CONNOR, B. H., STUDER, A. J., PETERSON, V. K., SUN, Z. M. & PALMQUIST, J-P. 2010. Comparison of Thermal Stability in MAX 211 and 312 Phases, *Journal of Physics: Conference Series* 251, 012025.
- PANG, W. K., LOW, I. M., O'CONNOR, B. H., PETERSON, V. K., STUDER, A. J., & PALMQUIST, J-P. 2011. *In-Situ* Diffraction Study of Thermal Dissociation of Maxthal Ti_2AlC , *Journal of Alloys & Compounds*, 509, 172-176.
- PANG, W. K. 2010. Thermal and Phase Stability of Novel Layered Ceramics $M_{n+1}AX_n$ Phases, *PhD Thesis*, Curtin University, Australia.
- PANG, W. K., LOW, I. M., O'CONNOR, B. H., SUN, Z. M. & PRINCE, K. E. 2009. Oxidation Characteristics of Ti_3AlC_2 Over the Temperature Range 500-900°C, *Materials Chemistry and Physics*, 117, 384-389.
- PANG, W. K., LOW, I. M. & HANNA, J. V. 2010. Characterisation of Amorphous Silica in Air-oxidised Ti_3SiC_2 at 500-1000°C using Secondary-Ion Mass

- Spectrometry, Nuclear Magnetic Resonance and Transmission Electron Microscopy. *Materials Chemistry and Physics*, 121, 453-458.
- PANG, W. K., LOW, I. M. & SUN, Z. M. 2009. *In-Situ* High-temperature Diffraction Study of Thermal Dissociation of Ti_3AlC_2 in Vacuum. *Journal of the American Ceramic Society*, 93, 2871-2876.
- PANG, W. K., LOW, I. M., O'CONNOR, B. H., STUDER, A. J., PETERSON, V. K., & PALMQUIST, J-P. 2009. Effect of Vacuum Annealing on the Thermal Stability of $Ti_3SiC_2/TiC/TiSi_2$ Composites. *Journal of the Australian Ceramic Society*, 45, 72-77.
- PANG, W. K., LOW, I. M., KENNEDY, S. J. & SMITH, R. I. 2010. *In-Situ* Diffraction Study on Decomposition of Ti_2AlN at 1500-1800°C in Vacuum, *Materials Science & Engineering A*, 528, 137-142.
- PAULING, L. & HENDRICKS, S. B. 1925. The Crystal Structures of Hematite and Corundum, *Journal of the American Ceramic Society*, 47, 781-790.
- PRATAPA, S. 1997. Synthesis and Characterization of Functionally-graded Aluminium Titanate/ZTA System Ceramics, *MSc Thesis*, Curtin University of Technology, Perth, WA.
- PRATAPA, S., LOW, I. M. & O'CONNOR, B. H. 1997. Infiltration-Processed, Functionally Graded Aluminium Titanate/Zirconia-Alumina Composite: I. Microstructural Characterisation and Physical Properties, *Journal of Materials Science*, 33, 3037-3045.
- PRATAPA, S. & LOW, I. M. 1998. Infiltration-Processed, Functionally Graded Aluminium Titanate/ Zirconia-Alumina Composite: II. Mechanical Properties, *Journal of Materials Science*, 33, 3047-3053.
- RESTREPO, G., VALENCIA, S. & MARIN, J. M. 2010. Study of the Bandgap of Synthesized Titanium Dioxide Using the Sol-Gel Method and a Hydrothermal Treatment, *The Open Materials Science Journal*, 4, 9-14.
- REZAIIE, H. R., NADER, G., SHOKUHFAR, A., NAGHIZADEH, R. & ATASHGAR, S. 2009. The Effect of Talc on the Reaction Sintering, Microstructure and Physical Properties of Al_2TiO_5 Based Ceramics, *Journal of Ceramic Processing Research*, 10, 1, 16-20.

- RACAULT, C., LANGLAIS, F. & NASLAIN, R. 1994. Solid State Synthesis and Characterization of the Ternary Phase Ti_3SiC_2 , *Journal of Materials Science*, 29, 3384-3392.
- RADHAKRISHNAN, R., WILLIAMS, J. J. & AKINC, M. 1999. Synthesis and High Temperature Stability of Ti_3SiC_2 , *Journal of Alloys and Compounds*, 285, 85-88.
- RADOVIC, M. & BARSOUM, M. W. 2013, MAX Phases: Bridging the Gap Between Metals and Ceramics, *The Bulletin of the American Ceramic Society*, 92, 3, April, 20-27.
- RADOVIC, M., BARSOUM, M. W., EL-RAGHY T., SEIDENSTICKER, J. & WIEDERHORN, S. 2000. Tensile Properties of Ti_3SiC_2 in the 25-1300°C Temperature Range, *Acta Materialia*, 48, 453-459.
- REINTJES, J. & SCHULTZ, M. B. 1968. Photoelastic Constants of Selected Ultrasonic Delay-Line Crystals, *Journal of Applied Physics*, 39, 5254-5258.
- RIETVELD, H. M. 1967. Line Profiles of Neutron Powder-Diffraction Peaks for Structure Refinement, *Acta Crystallographica*. 22, 151-152.
- RIETVELD, H. M. 1969. A Profile Refinement Method for Nuclear and Magnetic Structures, *Journal of Applied Crystallography*, 2, 65-71.
- RILEY, D. P. 2003. In-Situ Neutron Diffraction Analysis of Titanium Silicon Carbide (Ti_3SiC_2) during Self-Propagating High-Temperature Synthesis, *PhD Thesis*, The University of Newcastle, Australia.
- RUDNIK, T. & LIS, J. 1997. The Ti_3SiC_2 -Based Structural Ceramics, *Journal of Archives of Metallurgy*, 42, 59-66.
- RUNYAN, J. L. & BENNISON, S. J. 1991. Fabrication of Flaw-Tolerant Aluminium Titanate-Reinforced Alumina, *Journal of the European Ceramic Society*, 74, 93-96.
- SAKAI, M. & HIRAI, T. 1991. Fabrication and Properties of FGMs, *Journal of the Ceramic Society, Japan*, 99, 1002-1013.
- SANCHEZ-HERENCIA, A. J., MORINAGA, K. & MOYA, J. S. 1997. Al_2O_3/Y -TZP Continuous Functionally Graded Ceramics by Filtration-Sedimentation, *Journal of the European Ceramic Society*, 17, 1551-1554.

- SCHNEIDER, S. J. 1994. *Engineered Materials Handbook*. 4, ASM International. New York, USA.
- SHEN, M. & BEVER, M. B. 1972. Gradients in Polymeric Materials, *Journal of Materials Science*, 7, 741-746.
- SEKAR, M. M. A. & PATIL, K. C. 1994. Synthesis and Properties of Tialite, β - Al_2TiO_5 , *British Ceramic Transactions*, 93(4), 146-149.
- SHINTANI, H., SATO, S. & SAITO, Y. 1975. Electron-Density Distribution in Rutile Crystals, *Acta Crystallographica*. B24, 31, 1981-1982.
- SKALA, R. D. 2000. Development of a Functionally-Graded Aluminium Titanate/Alumina Composite, *PhD Thesis*, Curtin University of Technology, Perth, Australia.
- SPERISEN, T. & MOCELLIN, A. 1991. On Structures of Mixed Titanium Aluminium Oxides, *Journal of Materials Science Letters*, 10, 831-833.
- SUN, Z. M. 2011. Progress in Research and Development on MAX Phases: A Family of Layered Ternary Compounds, *International Materials Reviews*, 56, 3, 143-166.
- SUN, Z. M., ZHOU, Y. C. & LI, M. S. 2001. High Temperature Oxidation Behavior of Ti_3SiC_2 -Based Material in Air, *Acta Materialia*, 49, 4347-4353.
- SUN, Z. M. & ZHOU, Y. C. 1999a. Synthesis of Ti_3SiC_2 Powders by a Solid-Liquid Method, *Scripta Materialia*, 41, 61-66.
- SUN, Z. M. & ZHOU, Y. C. 1999b. Fluctuation and Characterization of Fiber-Like Ti_3SiC_2 Powders, *Materials Research Innovations*, 2, 227-231.
- SURESH, S. & MORTENSEN, A. 1997. Functionally Graded Metals and Metal-Ceramics Composites: Part 2 Thermomechanical Behavior, *International Materials Reviews*, 42, 85-116.
- TAKANORI, W., SHIN-ICHIRO, S., TOSHIO, T. & YASUO, I. 1999. Reactive Infiltration of Magnesium Vapor into Alumina Powder Compacts, *Journal of the European Ceramic Society*, 19, 1889-1893.
- TAUSTER, S. J., FUNG, S. C. & GARTEN, R. L. 1978. Strong Metal-Support Interactions. Group 8 Nobel Metals Supported on Titanium Dioxide, *Journal of the American Chemical Society*, 100, 170-175.

- THOMAS, H. A. J. & STEVENS, R. 1989. Aluminium Titanate – A Literature Review, *British Ceramics Transaction and Journal*, 88, 144-151.
- TOMSIA, A. P., SAIZ, E., ISHIBASHI, H., DIAZ, M., REQUENA, J. & MOYA, J. S. 1998. Powder Processing of Mullite/Mo Functionally Graded Materials, *Journal of the European Ceramic Society*, 18, 1365-1371.
- TONG, X., OKANO, T., ISEKI, T. & YANO, T. 1995. Synthesis and High Temperature Mechanical Properties of Ti_3SiC_2/SiC Composites, *Journal of Materials Science*, 30, 3087-3090.
- TRAVITZKY, N. A. & SHLAYEN, A. 1998. Microstructure and Mechanical Properties of Alumina/Cu-O, *Materials Science and Engineering*, A 224, 154-160.
- TSUCHIDA, Y., KIRIHARA, S., TOMOTA, Y. & TSUJIMOTO, T. 1998. Ti/ Ti_3Sn Functionally Graded Coating by Reaction Diffusion and Eutectic Reaction, *Japan Institute of Metals*, 62, 992-998.
- TZENOV, N., BARSOUM, M. W. & EL-RAGHY, T. 2000. Influence of Small Amounts of Fe and V on the Synthesis and Stability of Ti_3SiC_2 , *Journal of the European Ceramic Society*, 20, 801-806.
- VEGARD, L. 1916. Results of Crystal Analysis, *Philosophical Magazine*, 32, 505-515.
- VISHNYAKOV, V., LU, J., EKLUND, P., HULTMAN, L. & COLLIGON, J. 2013. Ti_3SiC_2 -Formation during Ti-C-Si Multilayer Deposition by Magnetron Sputtering at 650°C, *Vacuum*, 93, 56-59.
- WADLEY, H. N. G., HSIUNG, L. M. & LANKEY, R. L. 1995. Artificially Layered Nanocomposites Fabricated by Jet Vapor Deposition, *Composites Engineering*, 5, 935-940.
- WANG, X. H & ZHOU, Y. C. 2002. Oxidation Behavior of Ti_3AlC_2 Powders in Flowing Air, *Journal of Materials Chemistry*, 12, 2781-2788.
- WANG, X. H. & ZHOU, Y. C. 2003b, Oxidation Behavior of Ti_3AlC_2 at 1000-1400°C in Air, *Corrosion Science*, 45, 891-907.
- WANG, J., ZHOU, Y., LIAO, T., ZHANG, J & LIN, Z. 2008. A First-Principles Investigation of the Phase Stability of Ti_2AlC with Al Vacancies, *Scripta Materialia*, 58, 227-230.

- WANG, L. J., JIANG, W., BAI, S. Q., WANG, G. & CHEN, L. D. 2004. Rapid Fabrication of Nano-structured Ti_5Si_3 -TiC Composites by Spark Plasma Sintering, *Journal of Inorganic Materials*, 19, 1436-1440.
- WANG, L. J., JIANG, W., BAI, S. Q. & CHEN, L. D. 2004. Rapid Reactive Synthesis and Sintering of Submicron TiC/SiC Composites through Spark Plasma Sintering, *Journal of the American Ceramic Society*, 87, 1157-1160.
- WARREN, B. E. 1969. X-Ray Diffraction, Addison-Wesley, Massachusetts, USA.
- WATANABE, R. 1995. Powder Processing of Functionally Gradient Materials, *MRS Bulletin*, 29, 32-34.
- WEI, G. C. & BECHER, P. F. 1984. Improvements in Mechanical Properties in SiC by the Addition of TiC Particles, *Journal of the American Ceramic Society*, 67, 571-574.
- WOHLFROMM, H., EPICIER, T., MOYA, J. S., PENA, P. & THOMAS, G. 1991. Microstructural Characterization of Aluminium Titanate-Based Composite Materials, *Journal of the European Ceramic Society*, 7, 385-396.
- WU, E. D., KISI, E. H., KENNEDY, S. J. & STUDER, A. J. 2001. In-Situ Neutron Powder Diffraction Study of Ti_3SiC_2 Synthesis, *Journal of the American Ceramic Society*, 84, 2281-2288.
- YAN, M. F. & RHODE, W. W. 1981. Effect of Cations Contaminants in Conductive TiO_2 Ceramics, *Journal of Applied Physics*, 53, 8809-8818.
- YANG, S. L., SUN, Z. M., HASHIMOTO, H. & ABE, T. 2003. Formation of Ti_3SiC_2 from Ti-Si-TiC powders by the Pulse Discharge sintering (PDS) Technique, *Material Research Innovations*, 7, 225-230.
- YANG, S., SUN, Z. M. & HASHIMOTO, H. 2004. Reaction in Ti_3SiC_2 Powder Synthesis from a Ti-Si-TiC Powder Mixture, *Journal of Alloys and Compounds*, 368, 312-317.
- YOUNG, R. A. (Ed). 1993. *The Rietveld Method*. International Union of Crystallography, Oxford University Press, Great Britain.
- ZHANG, J., WANG, L., JIANG, W. & CHEN, L. 2008. Effect of TiC content on the Microstructure and Properties of Ti_3SiC_2 -TiC Composites In-Situ Fabricated by Spark Plasma Sintering, *Materials Science and Engineering A*, 487, 137-143.

- ZHENG, L. L., SUN, L. C., LI, M. S. & ZHOU, Y. C. 2011. Improving the High-Temperature Oxidation Resistance of $\text{Ti}_3(\text{SiAl})\text{C}_2$ by Nb-Doping, *Journal of the American Ceramic Society*, 94, 3599-3586.
- ZHOU, Y. C., ZHANG, H. B., BAO, Y. W. & LI, M. S. 2004. Improving the Oxidation Resistance of Ti_3SiC_2 by forming a $\text{Ti}_3\text{Si}_{0.9}\text{Al}_{0.1}\text{C}_2$ Solid Solution, *Acta Materialia*, 52, 3631-3637.
- ZHOU, Y. C., WAN, D. T., BAO, Y. W. & YAN, C. K. 2006. In Situ Reaction Synthesis and Characterization of $\text{Ti}_3\text{Si}(\text{Al})\text{C}_2/\text{SiC}$ Composites, *Ceramics International*, 32, 883-890.
- ZHOU, Y. C., ZHANG, H. B., BAO, Y. W., LI, M. S. & WANG, J. Y. 2006. Intermediate Phases in Synthesis of Ti_3SiC_2 and $\text{Ti}_3\text{Si}(\text{Al})\text{C}_2$ Solid Solutions from Elemental Powders, *Journal of the European Ceramic Society*, 26, 2373-2380.
- ZHOU, Y. C., BAO, Y. W. & ZHANG, H. B. 2009. Current Status in Layered Ternary Carbide Ti_3SiC_2 , a Review, *Journal of Materials Science & Technology*, 25, 1-38.
- ZOU, Y., SUN, Z. M., TADA, S. & HASHIMOTO, H. 2008. Synthesis Reactions for Ti_3SiC_2 Through Pulse Discharge Sintering $\text{TiH}_2/\text{Si}/\text{TiC}$ Powder Mixture, *Materials Research Bulletin* 43, 968-975.

2. PUBLICATIONS FORMING PART OF THESIS

2.1 Effect of Atmospheres on the Thermal Stability of Aluminium Titanate

LOW, I. M., OO. Z. & O'CONNOR, B. H. 2006. Effect of Atmospheres on the Thermal Stability of Aluminium Titanate, *Physica B*, 385-386, 502-504.



Effect of atmospheres on the thermal stability of aluminium titanate

I.M. Low*, Z. Oo, B.H. O'Connor

Department of Applied Physics, Curtin University of Technology, GPO box U1987, Perth, WA 6845, Australia

Abstract

Aluminium titanate (Al_2TiO_5) is a promising engineering material because of its low thermal expansion coefficient, excellent thermal shock resistance, good refractoriness and non-wetting with most metals. However, it is susceptible to thermal dissociation in the temperature range ~ 1100 – 1300 °C which degrades its desirable properties. In this work, the effect of atmospheres (i.e., air, argon, 50% oxygen/50% argon) on the isothermal stability at 1100 °C as well as the thermal instability of Al_2TiO_5 in the temperature range 20 – 1400 °C has been characterized by neutron diffraction to study the temperature- and time-dependence microstructural changes in real time. Results show that the thermal stability of Al_2TiO_5 is strongly influenced by both temperature and atmosphere, but the temperature range of thermal instability is not dependent on the ageing atmosphere.

Crown Copyright © 2006 Published by Elsevier B.V. All rights reserved.

Keywords: Thermal stability; Oxygen partial pressure; Aluminium titanate; Atmospheres

1. Introduction

Aluminium titanate (Al_2TiO_5) is an excellent refractory and thermal shock resistant material due to its relatively low thermal expansion coefficient ($\sim 1 \times 10^{-6}$ °C $^{-1}$) and high melting point (1860 °C). It is one of several materials which is isomorphous with the mineral pseudobrookite (Fe_2TiO_5) [1,2]. In this structure, each Al^{3+} or Ti^{4+} cation is surrounded by six oxygen ions forming distorted oxygen octahedra. These AlO_6 or TiO_6 octahedra form (001) oriented double chains weakly bonded by shared edges. This structural feature is responsible for the strong thermal expansion anisotropy which generates localised internal stresses to cause severe microcracking. Although this microcracking weakens the material, it imparts a desirable low thermal expansion coefficient and an excellent thermal shock resistance.

In addition, Al_2TiO_5 is only thermodynamically stable above 1280 °C and undergoes a eutectoid-like decomposition to α - Al_2O_3 and TiO_2 (rutile) within the temperature range 900 – 1280 °C [3–7]. This undesirable decomposition has limited its wider application. Hitherto, the mechanisms of decomposition are poorly understood but experimental

evidences suggest a nucleation and growth-controlled process. It is generally agreed that the decomposition rate peaks at 1100 °C and that residual alumina particles might act as preferred nucleation sites for the decomposition [3]. The impact of this thermal instability can be improved through the use of various stabilisers such as MgO , Fe_2O_3 and SiO_2 .

In recent studies by Low and co-workers [8–11], the ageing environment or atmosphere has been observed to have a profound influence on the thermal stability of Al_2TiO_5 . For instance, the decomposition rate of Al_2TiO_5 at 1100 °C is significantly enhanced in vacuum (10^{-4} Torr) where $>90\%$ of Al_2TiO_5 decomposed after only 4 h soaking when compared to less than 10% in atmospheric air [8]. This suggests that the process of decomposition of Al_2TiO_5 is susceptible to environmental attack or sensitive to the variations in the oxygen partial pressure during ageing. The stark contrast in the mechanism of phase decomposition is believed to arise from the vast differences in the oxygen partial pressure that exists between air and vacuum. In addition, it is still unclear whether the variation of oxygen partial pressure has any influence on the range and onset of decomposition temperature of Al_2TiO_5 .

In this paper, we present results on the effect of atmospheres on the isothermal stability of Al_2TiO_5 at 1100 °C as well as its decomposition behaviour in the

*Corresponding author. Tel.: +61 8 92667544; fax: +61 8 92662377.
E-mail address: rlowim@curtin.edu.au (I.M. Low).

temperature range 20–1400 °C. The temperature-dependent thermal stability and isothermal decomposition of Al_2TiO_5 have been dynamically monitored and characterized using neutron diffraction to study the structural changes occurring during phase decomposition in real time.

2. Experimental procedure

The starting powders used for the synthesis of Al_2TiO_5 (AT) consisted of high-purity commercial alumina (99.9% Al_2O_3) and rutile (99.5% TiO_2). One mole of alumina powder and one mole of rutile powder were initially mixed using a mortar and pestle. The powder mixture was then wet mixed in ethanol using a Turbula mixer for 1 h. The slurry was then dried in a ventilated oven at 100 °C for 24 h. The dried powder was uniaxially pressed in a steel die at 150 MPa to form cylindrical bars of length 20 mm and diameter 12 mm, followed by sintering at 1500 °C in air for 2 h.

The collection of neutron diffraction data of isothermal phase stability of Al_2TiO_5 at 1100 °C for up to 12 h in different atmospheres, namely air, argon (99.99% purity) and 50% argon–50% oxygen, was performed using a medium resolution powder diffractometer (MRPD) located at the Australian Nuclear Science and Technology Organisation (ANSTO) in Lucas Heights, NSW. The operation conditions were $\lambda = 1.667 \text{ \AA}$, 2θ range = 4–138°, step size = 0.1°, counting time ~ 40 –50 s/step, monochromator of 8 Ge crystals (115 reflection), and 32 ^3He detectors 4° apart. The relative abundance of phases present was computed using the Rietveld method. The models used to calculate the phase abundance for MRPD were Maslen et al. [12] for alumina, Epicier et al. [13] for Al_2TiO_5 , and Howard et al. [14] for rutile. The software used to analyse the data was Rietica 1.7.7.

3. Results and discussion

Fig. 1 shows the isothermal stability of Al_2TiO_5 at 1100 °C in air for a duration of 12 h. The sample remained fairly stable with no apparent phase decomposition for up to 5 h. Further ageing caused only $\sim 5\%$ decomposition. In contrast, substantial phase decomposition was observed when Al_2TiO_5 was aged in an argon atmosphere (Fig. 2) where more than 98% of the sample decomposed to form corundum (Al_2O_3) and rutile (TiO_2) after only 5 h of ageing. When the ageing atmosphere was changed to 50% argon and 50% oxygen (Fig. 3), the decomposition rate was considerably reduced compared with the rate for 100% argon but more substantial than the rate for air.

A closer look at the results in Figs. 1–3 suggests that the rate of phase decomposition of Al_2TiO_5 is dependent on the atmosphere or oxygen partial pressure during isothermal ageing. This implies that the oxygen partial pressure in the atmosphere plays a key role in triggering the thermal instability via oxygen nonstoichiometry changes and/or disordering of cations in Al_2TiO_5 [6]. Indeed, nitrogen

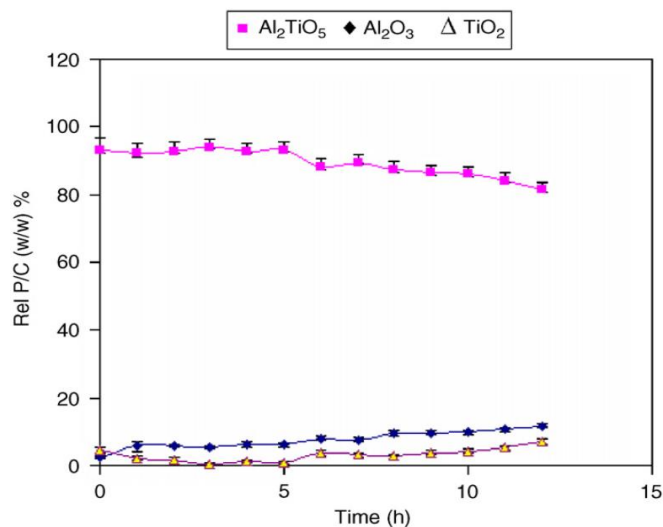


Fig. 1. Isothermal stability of Al_2TiO_5 at 1100 °C in air. Error bars indicate two estimated standard deviations $\pm 2\sigma$. Legend: \blacksquare = Al_2TiO_5 ; \blacklozenge = Al_2O_3 ; \triangle = TiO_2 .

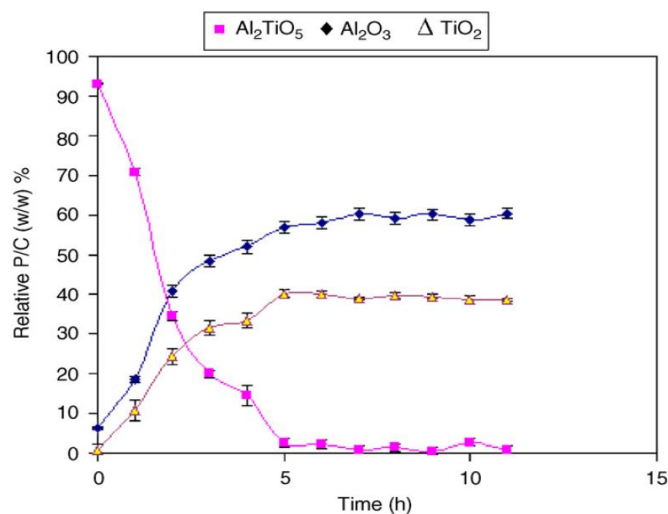


Fig. 2. Isothermal stability of Al_2TiO_5 at 1100 °C in argon atmosphere. Error bars indicate two estimated standard deviations $\pm 2\sigma$. Legend: \blacksquare = Al_2TiO_5 ; \blacklozenge = Al_2O_3 ; \triangle = TiO_2 .

atmosphere has also been observed to cause enhanced thermal instability in Al_2TiO_5 [15]. Similar observations have also been observed for the enhanced dissociation of Ti_3SiC_2 in vacuum and argon which can also be attributed to the role of oxygen partial pressures [16,17].

It is postulated that in the presence of very low oxygen partial pressure, the titanium ions in TiO_2 are very susceptible to non-stoichiometry, thus triggering the release of oxygen atoms and the concomitant decomposition process. However, the exact mechanism of enhanced phase

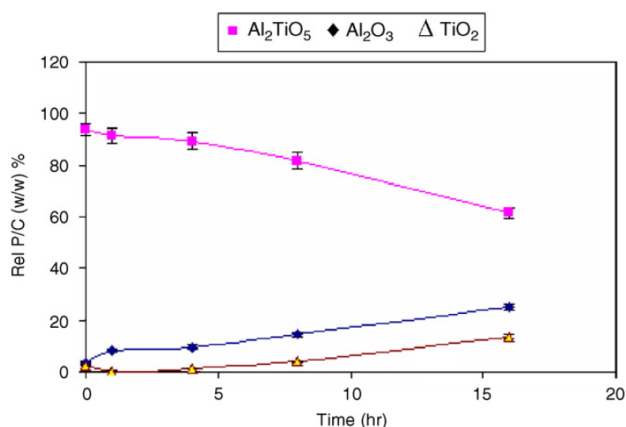


Fig. 3. Isothermal stability of Al_2TiO_5 at 1100°C in the atmosphere of 50% oxygen and 50% argon. Errors bars indicate two estimated standard deviations $\pm 2\sigma$. Legend: \blacksquare = Al_2TiO_5 ; \blacklozenge = Al_2O_3 ; \blacktriangle = TiO_2 .

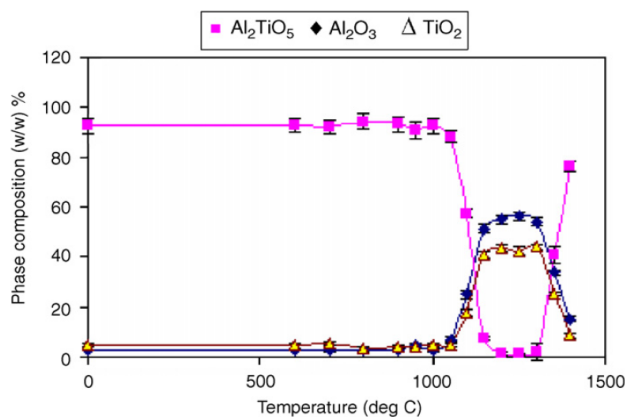


Fig. 4. Thermal stability of Al_2TiO_5 in air over the temperature range 20 – 1400°C . Note the display of pronounced thermal decomposition at ~ 1150 – 1300°C . Errors bars indicate two estimated standard deviations $\pm 2\sigma$. Legend: \blacksquare = Al_2TiO_5 ; \blacklozenge = Al_2O_3 ; \blacktriangle = TiO_2 .

decomposition in argon or inert atmosphere remains unclear, especially in relation to the role of oxygen partial pressures in reducing the free energy change for thermal decomposition of Al_2TiO_5 . If the oxygen partial pressure is the cause, then the decomposition rate of Al_2TiO_5 should depend on the variation of the oxygen partial pressure as indicated in Fig. 3. It follows that an increase in the oxygen partial pressure should reduce the rate of decomposition and vice-versa. This further implies that the thermal

stability of Al_2TiO_5 will be improved in an atmosphere of 100% oxygen when compared to ageing in air.

The thermal stability of Al_2TiO_5 in the temperature range 20 – 1400°C in air is shown in Fig. 4. Clearly, Al_2TiO_5 was stable up to $\sim 1100^\circ\text{C}$ and became unstable at between ~ 1150 and 1300°C . Beyond 1300°C , the thermal decomposition was arrested and the phase stability was restored. This suggests that the process of thermal decomposition is reversible or recoverable provided the restricted temperature range of between ~ 1150 – 1300°C is not transgressed. Interestingly, the use of either argon or oxygen atmosphere did not appear to alter or affect the temperature range of thermal decomposition. To the best of our knowledge, this is the first time that the in situ display of the temperature range for thermal decomposition of Al_2TiO_5 during ageing as shown in Fig. 4 has been reported in the literature.

Acknowledgements

This work was supported by the Australian Institute of Nuclear Science and Engineering (AINSE Award no. 04/207). We thank Mr. M. Prior of the Bragg Institute of ANSTO for experimental assistance in the collection of MRPD data.

References

- [1] A.E. Austin, C.M. Schwartz, *Acta Crystallogr.* 6 (1953) 812.
- [2] B. Morosin, R.W. Lynch, *Acta Crystallogr.* B28 (1972) 1040.
- [3] H.A.J. Thomas, R. Stevens, *Br. Ceram. Trans.* J. 88 (1989) 144.
- [4] G. Tilloca, *J. Mater. Sci.* 26 (1991) 2809.
- [5] E. Kato, K. Daimon, Y. Kobayashi, *J. Am. Ceram. Soc.* 63 (1980) 355.
- [6] R.W. Grimes, J. Pilling, *J. Mater. Sci.* 29 (1994) 2245.
- [7] M. Ishitsuka, et al., *J. Ceram. Soc. Jap.* 70 (1987) 69.
- [8] I.M. Low, D. Lawrence, R.I. Smith, *J. Am. Ceram. Soc.*, in press.
- [9] I.M. Low, P. Manurung, R.I. Smith, D. Lawrence, *Key Eng. Mater.* 224–226 (2002) 465–470.
- [10] P. Manurung, Ph.D. Thesis, Department of Applied Physics, Curtin University, 2002.
- [11] I.M. Low, R.I. Smith, in: I.M. Low, D.N. Phillips (Eds.), *Proceedings of AUSTCERAM 2002*, 30 September–4 October, 2002, Perth, WA, pp.175–176.
- [12] E.N. Maslen, V.A. Streltsov, N.R. Streltsova, N. Ishizawa, Y. Satow, *Acta Crystallogr.* B49 (1993) 937.
- [13] T. Epicier, G. Thomas, H. Wohlfromm, J.S. Moya, *J. Mater. Res.* 6 (1991) 138.
- [14] C.J. Howard, T.M. Sabine, F. Dickson, *Acta Crystallogr.* B47 (1991) 462.
- [15] D.S. Perera, M.E. Bowden, *J. Mater. Sci.* 26 (1991) 1585–1587.
- [16] I.M. Low, in: I.M. Low, D.N. Phillips (Eds.), *Proceedings of AUSTCERAM 2002*, 30 September–4 October, 2002, Perth, WA, pp. 191–192.
- [17] Z. Oo, I.M. Low, B.H. O'Connor, *Physica B*, in press.

2.2 In Situ Diffraction Study of Self-Recovery in Aluminium Titanate

LOW, I. M. & OO, Z. 2008. In Situ Diffraction Study of Self-Recovery in Aluminium Titanate, *Journal of the American Ceramic Society*, 90, 1027-1029.

In Situ Diffraction Study of Self-Recovery in Aluminum Titanate

It-Meng Low[†] and Zeya Oo

Materials Research Group, Department of Applied Physics, Curtin University of Technology, Western Australia 6845, Australia

Aluminum titanate (Al_2TiO_5) is an excellent refractory and thermal shock resistant material due to its relatively low-thermal expansion coefficient and high melting point. However, Al_2TiO_5 is only thermodynamically stable above 1280°C and undergoes a eutectoid decomposition to $\alpha\text{-Al}_2\text{O}_3$ and TiO_2 (rutile) in the temperature range of 900°C – 1280°C . In this paper, we describe the use of high-temperature neutron diffraction to study the properties of self-recovery in Al_2TiO_5 when it is annealed at $\geq 1300^\circ\text{C}$ in air. It is shown that the process of decomposition in Al_2TiO_5 is reversible and that self-recovery occurs readily when decomposed Al_2TiO_5 is reheated above 1300°C . It is further shown that the existence of a temperature range (900°C – 1280°C) in which Al_2TiO_5 is prone to decomposition can be explained by the competing dominance of self-recovery at $\geq 1280^\circ\text{C}$ and decomposition at $\leq 1280^\circ\text{C}$.

I. Introduction

ALUMINUM TITANATE (Al_2TiO_5) is an excellent refractory and thermal shock-resistant material due to its relatively low thermal expansion coefficient ($\sim 1 \times 10^{-6} \text{ }^\circ\text{C}^{-1}$) and high melting point (1860°C). It is one of the several materials which is isomorphous with the mineral pseudobrookite (Fe_2TiO_5).^{1–4} In this structure, each Al^{3+} or Ti^{4+} cation is surrounded by six oxygen ions forming distorted oxygen octahedra. These AlO_6 or TiO_6 octahedra form (001) oriented double chains weakly bonded by shared edges. This structural feature is responsible for the strong thermal expansion anisotropy which generates localized internal stresses to cause severe microcracking. Although this microcracking weakens the material, it imparts a desirable low thermal expansion coefficient and an excellent thermal shock resistance.

In addition, Al_2TiO_5 is only thermodynamically stable above 1280°C and undergoes a eutectoid decomposition to $\alpha\text{-Al}_2\text{O}_3$ and TiO_2 (rutile) within the temperature range of 900°C – 1280°C .^{5–9} This undesirable decomposition has limited its wider application. Hitherto, the mechanisms of decomposition are poorly understood but experimental evidence suggests a nucleation and growth-controlled process. It is generally agreed that the decomposition rate peaks at 1100°C and that residual alumina particles might act as preferred nucleation sites for the decomposition.⁵ The impact of this thermal instability can be improved through the use of various stabilizers such as MgO , Fe_2O_3 , and SiO_2 .^{5,10–12}

Hitherto, the reason or underlying cause for the existence of a temperature range (900°C – 1280°C) in which Al_2TiO_5 is prone to decomposition remains an enigma. In addition, the kinetics of decomposition are poorly understood and it is still unclear

whether the process of phase decomposition is a reversible or irreversible process. If the process is reversible, it may be possible for the decomposed Al_2TiO_5 to undergo self-recovery or “self-healing” when it is reheated to elevated temperatures (i.e., $> 1300^\circ\text{C}$).

In this paper, we present *in-situ* neutron diffraction (ND) results to confirm the capability of previously decomposed Al_2TiO_5 to undergo full self-recovery when it is reheated to a temperature above 1300°C in air. It is further shown that the existence of a temperature range (900°C – 1280°C) in which Al_2TiO_5 is sensitive to decomposition can be explained by the formation of Al_2TiO_5 in a metastable state. A novel “top-down” approach has been successfully used to study the dynamics of isothermal decomposition in high-purity Al_2TiO_5 .

II. Experimental Procedure

(1) Sample Preparation

The starting powders used for the synthesis of Al_2TiO_5 samples consisted of high-purity commercial alumina (99.9% Al_2O_3) and rutile (99.5% TiO_2). One mole of alumina powder and one mole of rutile powder were initially mixed using a mortar and pestle. The powder mixture was then wet mixed in ethanol using a Turbula mixer for 1 h. The slurry was then dried in a ventilated oven at 100°C for 24 h. The dried powder was uniaxially pressed in a steel die at 150 MPa to form cylindrical bars of length 20 mm and diameter 12 mm, followed by pressureless sintering at 1500°C in an air-ventilated furnace for 2 h and then furnace-cooled to room temperature. The heating and cooling rates were $3.0^\circ\text{C}/\text{min}$.

(2) ND

A medium resolution powder diffractometer (MRPD) located at the Australian Nuclear Science and Technology Organization (ANSTO) in Lucas Heights, NSW was used for ND study of thermal decomposition and self-recovery in Al_2TiO_5 in air at the elevated temperature. Two approaches were used to study the dynamics of thermal decomposition in Al_2TiO_5 at 1100°C in air atmosphere for up to 12 h. In the first approach (i.e., bottom-up), the samples were heated up to 1100°C from room temperature and held at this temperature for up to 24 h to monitor the complete decomposition of Al_2TiO_5 . In the second approach (i.e., top-down), the previously decomposed samples from the bottom-up approach were reused to study the capability of this material to self-recover when heated again to elevated temperature. Here the samples were heated up to 1450°C for 2 h before the temperature was lowered to 1100°C and held at this temperature for up to 12 h to monitor the dynamics of phase decomposition in self-recovered Al_2TiO_5 . Figure 1 shows the schematic representation of the two approaches.

Finally, a new set of samples were heated from room temperature to 1400°C in order to study the “forbidden” temperature range in which Al_2TiO_5 becomes susceptible to thermal decomposition. Diffraction patterns were collected over 1 h for every 50°C rise from 600° to 1400°C . This allows the

E. Kisi—contributing editor

Manuscript No. 23339. Received June 14, 2007; approved October 16, 2007.

[†]Author to whom correspondence should be addressed. e-mail: rlowim@cc.curtin.edu.au

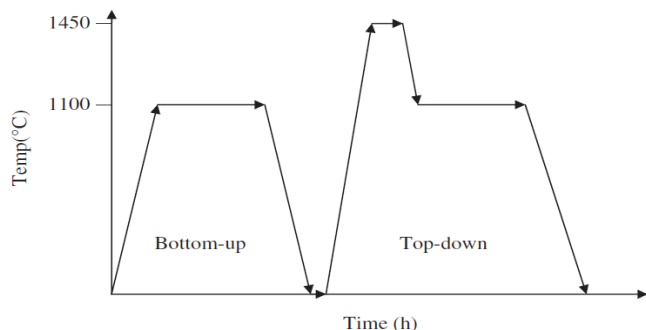


Fig. 1. Schematic representation of the bottom-up and top-down approaches for the study of isothermal decomposition in Al_2TiO_5 at 1100°C .

temperatures for the onset of decomposition and self-recovery to be determined.

The operation conditions of the MRPD were $\lambda = 1.667 \text{ \AA}$, 2θ range = 4° – 138° , step size = 0.1° , counting time ~ 40 – 50 s/step, monochromator of 8 Ge crystals (115 reflection), and 32 ^3He detectors 4° apart. The relative abundance of phases present was computed using the Rietveld method. The models used to calculate the phase abundance for MRPD were Maslen *et al.*¹³ for alumina, Epicier *et al.*³ for Al_2TiO_5 , and Howard *et al.*¹⁴ for rutile. The software used to analyze the data was Rietica 1.7.7. During Rietveld analysis, constraints such as background B0 B1 B2 B3 and B5 were used but no restraints were used. A typical difference plot showing the quality of fit is shown in Fig. 2 together with the corresponding values for the agreement indices such as R_{wp} , χ^2 , and R_B .

III. Results and Discussion

(1) Temperature Range of Thermal Decomposition

The thermal stability of Al_2TiO_5 in the temperature range 20° – 1400°C in air as revealed by ND is shown in Fig. 3. Clearly, Al_2TiO_5 was relatively stable to just below 1100°C and became visibly unstable, decomposing to form corundum and rutile at between 1100° – 1280°C . Beyond 1300°C , the thermal decomposition was arrested and the phase stability was restored. This implies that the process of thermal decomposition is reversible and will self-recover according to Eq (1) provided the restricted temperature range of between 1100° – 1280°C is not traversed. Hitherto, there has been no hypothesis to explain the existence of this temperature range.

It is proposed here that the existence of a temperature range (1100° – 1280°C) as shown in Fig. 3 wherein Al_2TiO_5 is prone to decomposition can be explained in terms of the vital role of the temperature-dependent atomic diffusion rates and the competing dominance between self-recovery and decomposition. At temperatures below $\sim 1000^\circ\text{C}$, the decomposition of the mate-

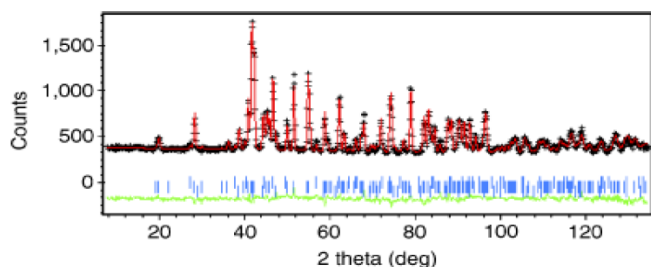


Fig. 2. A typical difference plot from Rietveld analysis showing the quality of fit for as-sintered Al_2TiO_5 at room temperature. $R_{\text{wp}} = 4.32$; χ^2 (GoF) = 3.68; R_B (corundum) = 2.59; R_B (Al_2TiO_5) = 3.05; R_B (rutile) = 1.99.

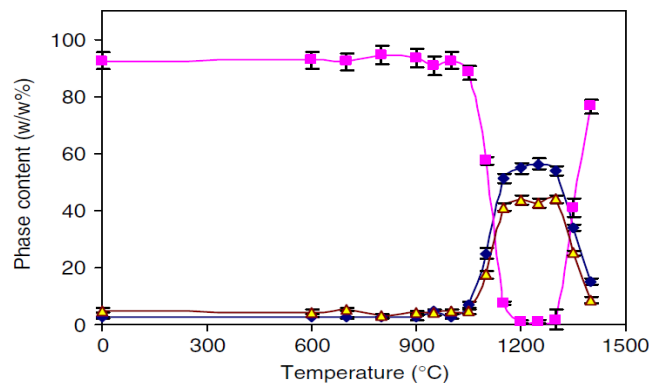


Fig. 3. Thermal stability of Al_2TiO_5 in air over the temperature range 20° – 1400°C . Note the display of pronounced thermal decomposition at $\sim 1100^\circ$ – 1300°C . Errors bars indicate two estimated standard deviations $\pm 2\sigma$. ■, Al_2TiO_5 ; ◆, Al_2O_3 ; △, TiO_2 .

rial is insignificant because the rates of atomic diffusion are too low. As the temperature rises above $\sim 1000^\circ\text{C}$ the diffusion rates become high enough for a significant decomposition to take place. However, as the temperature rises beyond 1280°C , self-recovery dominates and occurs rapidly to form Al_2TiO_5 because of very high atomic diffusion rates. It is this competing dominance between self-recovery and decomposition that gives rise to the observed decomposition range.

(2) Phase Decomposition and Self-Recovery

Figure 4 shows the isothermal decomposition of Al_2TiO_5 at 1100°C in air for up to 24 h using the bottom-up approach. The sample commenced to decompose very rapidly within the first 4 h where more than 80% of the sample had decomposed to form corundum (Al_2O_3) and rutile (TiO_2) in the first 2 h. This rapid process of phase decomposition in Al_2TiO_5 has also been observed in vacuum or argon atmosphere.^{15,16} The presence of residual corundum and rutile in the starting sample was due to the unavoidable spontaneous decomposition of Al_2TiO_5 when the samples were furnace cooled to room temperature. It would be necessary to rapidly quench the samples from 1500°C to overcome or minimize the spontaneous decomposition, but this would weaken the samples considerably due to severe microcracking.

However, when this previously decomposed Al_2TiO_5 sample was reheated from room temperature to 1450°C for 2 h, self-recovery took place through the rapid reaction of corundum and

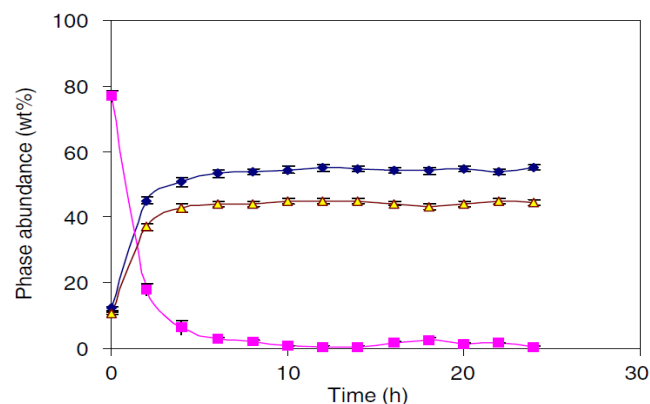


Fig. 4. Isothermal decomposition of sintered Al_2TiO_5 at 1100°C in air according to the bottom-up approach. Errors bars indicate two estimated standard deviations $\pm 2\sigma$. ■, Al_2TiO_5 ; ◆, Al_2O_3 ; △, TiO_2 .

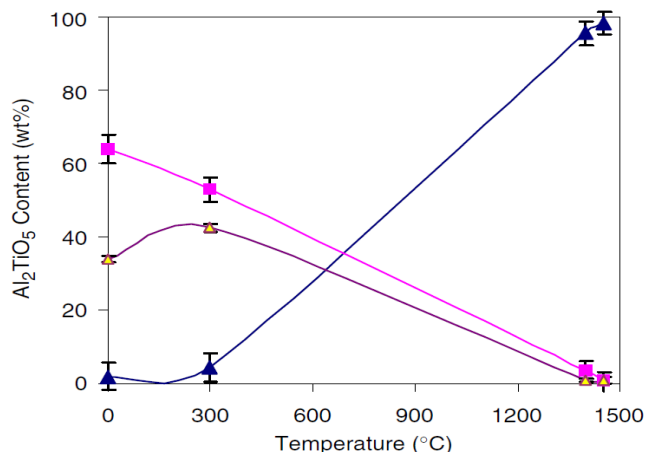


Fig. 5. Formation of Al_2TiO_5 through self-recovery in the previously decomposed sample by reheating it to 1450°C and dwelling for 2h. \blacktriangle , Al_2TiO_5 ; \blacksquare , Al_2O_3 ; \triangle , TiO_2 .

rutile to form Al_2TiO_5 with >98 wt% phase purity as shown in Fig. 5 as compared with only ~ 80 wt% phase purity in sintered samples (Fig. 4). This capability of self-recovery further suggests that the process of decomposition is spontaneous and reversible as follows:



This high phase purity would be lost in the sample if it was cooled down to room temperature due to the tyranny of spontaneous decomposition as described in Eq. (1). In order to maintain the high phase purity in the sample, the temperature in the furnace was lowered from 1450° to 1100°C (i.e., the top-down approach), and the dynamics of decomposition in self-recovered Al_2TiO_5 was analyzed over a period of 12 h as shown in Fig. 6. In both approaches, the samples were almost completely decomposed within a period of 10–12 h. When compared with the sample decomposed using the bottom-up approach, the decomposition in self-recovered Al_2TiO_5 using the top-down approach appeared less rapid probably due to its higher Al_2TiO_5 content (>98 wt%). However, if a correction is made for the bottom-up approach sample (~ 80 wt% Al_2TiO_5), the rate of decomposition is almost similar in both approaches.

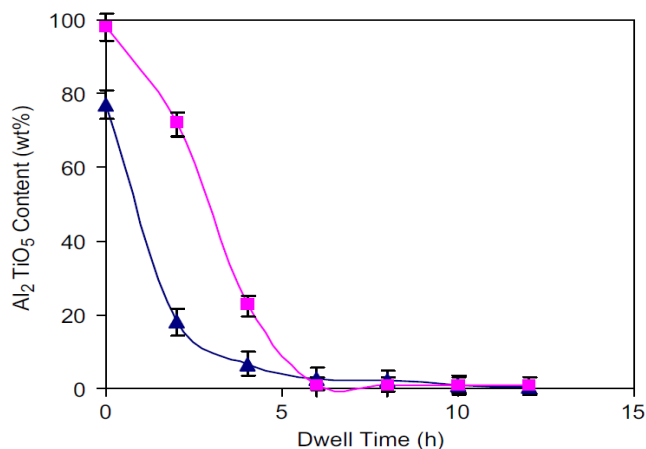


Fig. 6. Comparison of isothermal decomposition of Al_2TiO_5 at 1100°C in air between the bottom-up and top-down approaches. \blacksquare , top-down; \blacklozenge , bottom-up.

Hitherto, it is unknown at this stage what will be the likely effect of self-recovery on the physical, thermal and mechanical properties of Al_2TiO_5 . Further research is necessary to elucidate this phenomenon. Nevertheless, the implication of this phenomenon is far-reaching whereby it may just be possible to restore any previously decomposed Al_2TiO_5 to its original condition by thermal annealing in air at $>1400^\circ\text{C}$ through self-recovery and perhaps self-healing of the microcracks formed.^{17,18} The ability of Al_2TiO_5 to be recycled will allow a much longer service life of this material. In addition, high-purity Al_2TiO_5 may be produced as a refractory material without the use of stabilizers that may alter its intrinsic thermal and physical properties because at the service temperature it will adopt the desired phase.

IV. Conclusions

The use of high-temperature ND has shown that the process of decomposition in Al_2TiO_5 is reversible and that self-recovery can occur readily when decomposed Al_2TiO_5 is reheated above 1300°C . It is further shown that the existence of a decomposition temperature range in Al_2TiO_5 can be explained by the competition in the dominance of self-recovery at $\geq 1280^\circ\text{C}$ and decomposition at $\leq 1280^\circ\text{C}$.

Acknowledgments

This work was supported by the Australian Institute of Nuclear Science and Engineering (AINSE Awards 04/207 & 05/206). We are grateful to our colleague, E/Prof. B. O'Connor, for advice on Rietveld analysis of ND data. We thank Dr. Maxim Avdeev of the Bragg Institute of ANSTO for experimental assistance in the collection of MRPD data.

References

- A. E. Austin and C. M. Schwartz, "The Crystal Structure of Aluminium Titanate," *Acta Cryst.*, **6**, 812–3 (1953).
- B. Morosin and R. W. Lynch, "Structure Studies on Al_2TiO_5 at Room Temperature and at 600°C ," *Acta Cryst. B*, **28**, 1040–6 (1972).
- T. Epicier, G. Thomas, H. Wohlfromm, and J. S. Moya, "High Resolution Electron Microscopy Study of the Cationic Disorder in Al_2TiO_5 ," *J. Mater. Res.*, **6**, 138–45 (1991).
- R. W. Grimes and J. Pilling, "Defect Formation in $\beta\text{-Al}_2\text{TiO}_5$ and its Influence on Structure Stability," *J. Mater. Sci.*, **29**, 2245–9 (1994).
- H. A. J. Thomas and R. Stevens, "Aluminum Titanate—A Literature Review. Part 1: Microcracking Phenomena," *Br. Ceram. Trans. J.*, **88**, 144–90 (1989).
- H. A. J. Thomas and R. Stevens, "Aluminum Titanate—A Literature Review. Part 2: Engineering Properties and Thermal Stability," *Br. Ceram. Trans. J.*, **88**, 184–90 (1989).
- E. Kato, K. Daimon, and Y. Kobayashi, "Factors Affecting Decomposition Temperature of $\beta\text{-Al}_2\text{TiO}_5$," *J. Am. Ceram. Soc.*, **63**, 355–6 (1980).
- B. Freudenberg and A. Mocellin, "Aluminum Titanate Formation by Solid-State Reaction of Coarse Al_2O_3 and TiO_2 Powders," *J. Am. Ceram. Soc.*, **71**, 22–28 (1988).
- B. Freudenberg and A. Mocellin, "Aluminum Titanate Formation by Solid State Reaction of Al_2O_3 and TiO_2 Single Crystals," *J. Mater. Sci.*, **25**, 3701–8 (1990).
- G. Tilloca, "Thermal Stabilization of Aluminum Titanate and Properties of Aluminum Titanate Solid Solutions," *J. Mater. Sci.*, **26**, 2809–14 (1991).
- V. Buscaglia, P. Nanni, G. Battilana, G. Aliprandi, and C. Carry, "Reaction Sintering of Aluminum Titanate: 1-Effect of MgO Addition," *J. Eur. Ceram. Soc.*, **13**, 411–7 (1994).
- A. Tsetsekou, "A Comparison Study of Tialite Ceramics Doped with Various Oxide Materials and Tialite-Mullite Composites: Microstructural, Thermal and Mechanical Properties," *J. Eur. Ceram. Soc.*, **25**, 335–48 (2005).
- E. N. Maslen, V. A. Streltsov, N. R. Streltsova, N. Ishizawa, and Y. Satow, "Synchrotron X-Ray Study of the Electron Density in Alpha Al_2O_3 ," *Acta Crystallogr.*, **B49**, 937–80 (1993).
- C. J. Howard, T. M. Sabine, and F. Dickson, "Structural and Thermal Parameters for Rutile and Anatase," *Acta Cryst. B*, **47**, 462–8 (1991).
- I. M. Low, D. Lawrence, and R. I. Smith, "Factors Controlling the Thermal Stability of Aluminium Titanate in Vacuum," *J. Am. Ceram. Soc.*, **88**, 2957–61 (2005).
- I. M. Low, Z. Oo, and B. H. O'Connor, "Effect of Atmospheres on the Thermal Stability of Aluminium Titanate," *Phys. B: Condens. Matter*, **385–386**, 502–4 (2006).
- Y. Ohya, Z. Nakagawa, and K. Hamano, "Crack Healing and Bending Strength of Aluminium Titanate Ceramics at High Temperature," *J. Am. Ceram. Soc.*, **71**, C23–33 (1988).
- T. S. Liu and D. S. Perera, "Long-Term Thermal Stability and Mechanical Properties of Aluminium Titanate at $1000\text{--}1200^\circ\text{C}$," *J. Mater. Sci.*, **33**, 995–1001 (1998). □

2.3 Reformation of Phase Composition in Decomposed Aluminium Titanate

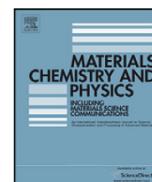
LOW, I. M. & OO, Z. 2008. Reformation of Phase Composition in Decomposed Aluminium Titanate, *Materials Chemistry and Physics*, 11, 1, 9-12.



ELSEVIER

Contents lists available at ScienceDirect

Materials Chemistry and Physics

journal homepage: www.elsevier.com/locate/matchemphys

Materials science communication

Reformation of phase composition in decomposed aluminium titanate

I.M. Low*, Z. Oo

Materials Research Group, Department of Applied Physics, Curtin University of Technology, GPO Box U1987, WA 6845 Australia

ARTICLE INFO

Article history:

Received 24 December 2007

Received in revised form 13 March 2008

Accepted 20 March 2008

Keywords:

Reformation

Decomposition

Al₂TiO₅

Neutron diffraction

Differential thermal analysis

ABSTRACT

The ability of decomposed Al₂TiO₅ to undergo reformation in phase composition has been characterised by neutron diffraction at elevated temperature and verified by differential thermal analysis. It is shown that the process of phase decomposition in metastable Al₂TiO₅ is reversible and that reformation occurs readily when decomposed Al₂TiO₅ is re-heated above 1300 °C. Subsequent decomposition of reformed Al₂TiO₅ during cooling below ~1200 °C is governed by the temperature-dependent atomic diffusion rates.

Crown Copyright © 2008 Published by Elsevier B.V. All rights reserved.

1. Introduction

In the Al₂O₃–TiO₂ system, aluminium titanate (Al₂TiO₅) is the only thermodynamically stable compound above 1280 °C, up to its melting point. It is one of several materials that is isomorphous with the mineral pseudobrookite (Fe₂TiO₅) [1–4]. It is both an excellent thermal shock resistant material and refractory with a relatively low thermal expansion coefficient ($\sim 1 \times 10^{-6} \text{ °C}^{-1}$) and a melting point of 1860 °C. Below 1280 °C, metastable Al₂TiO₅ undergoes a eutectoid decomposition to α -Al₂O₃ and TiO₂ (rutile) within the temperature range 900–1280 °C [5–9]. It is generally agreed that the decomposition rate peaks at 1100 °C. This undesirable decomposition has limited its wider applications as an engineering material.

Hitherto, the kinetics of decomposition is poorly understood and it is still unclear whether the process of phase decomposition is a reversible or irreversible process. If the process is reversible, it may be possible for the decomposed Al₂TiO₅ to undergo self-recovery or “reformation” when it is reheated to elevated temperature (i.e. >1300 °C). Although “self-healing” of cracks in Al₂TiO₅ has been observed at elevated temperature [10–12], recovery in decomposed Al₂TiO₅ by “reformation” has hitherto remained a mystery. In this paper, we present results from neutron diffraction and differential thermal analysis to confirm the capability of previously decomposed Al₂TiO₅ to undergo reformation in phase composition when it is re-heated to a temperature above 1300 °C in air.

2. Experimental procedure

2.1. Sample preparation

The starting powders used for the synthesis of Al₂TiO₅ samples consisted of high purity commercial alumina (99.9% Al₂O₃) and rutile (99.5% TiO₂). One mole of alumina powder and one mole of rutile powder were initially mixed using a mortar and pestle. The powder mixture was then wet mixed in ethanol using a Turbula mixer for 1 h. The slurry was then dried in a ventilated oven at 100 °C for 24 h. The dried powder was uniaxially pressed in a steel die at 150 MPa to form cylindrical bars of length 20 mm and diameter 12 mm, followed by pressureless sintering at 1600 °C in an air-ventilated furnace for 4 h and then furnace-cooled to room temperature. The heating and cooling rates were 3.0 °C min⁻¹.

2.2. Neutron diffraction

A medium resolution powder diffractometer (MRPD) located at the Australian Nuclear Science and Technology Organisation (ANSTO) in Lucas Heights, NSW was used for neutron diffraction study of phase decomposition and reformation in Al₂TiO₅ in air at elevated temperatures. In order to achieve full phase decomposition, the cylindrical bar sample was heated from room temperature to 1100 °C and held at this temperature for up to 22 h. The same decomposed sample was then re-used to study the capability of this material to self-recover when heated again to elevated temperatures. Here the sample was heated up to 1450 °C and held for 2 h, followed by controlled cooling to room temperature. The dynamics of phase self-recovery during re-heating and phase decomposition during cooling were monitored in real time. The use of neutron diffraction is the most suitable technique for the work proposed here as it allows the bulk information on the thermal decomposition process to be obtained because of the bulk sampling and penetrating nature of neutrons. In contrast, X-ray diffraction only provides surface information which may not be representative of the sample. In addition, neutron diffraction allows measurements under non-ambient conditions and environments to be conducted with ease.

The operation conditions of the MRPD were $\lambda = 1.665 \text{ \AA}$, 2θ range = 4–138°, step size = 0.1°, counting time $\sim 40\text{--}50 \text{ s step}^{-1}$, monochromator of 8 Ge crystals (115 reflection), and 32 ³He detectors 4° apart. The relative abundance of phases present was computed using the Rietveld method. The models used to calculate the phase abundance for MRPD were Maslen et al. [13] for alumina, Epicier et al. [3] for Al₂TiO₅,

* Corresponding author. Tel.: +61 8 9266 7544; fax: +61 8 9266 7544.
E-mail address: rlowim@cc.curtin.edu.au (I.M. Low).

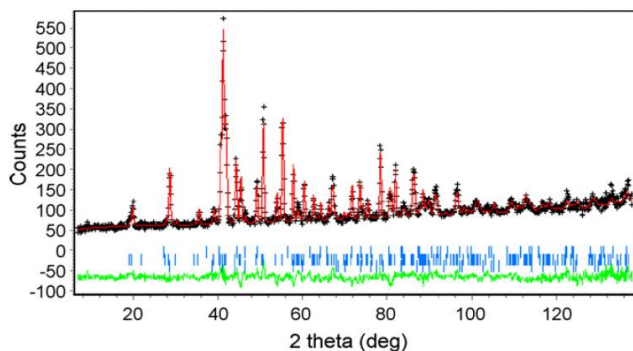


Fig. 1. A typical neutron diffraction profile plot of reformed Al_2TiO_5 at 1450°C after Rietveld refinement. Measured pattern indicated by crosses, calculated pattern indicated by solid line. Intensity differences between the two patterns are shown along the bottom of the plot. The three rows of vertical bars represent the allowable peak positions for each of three phases (top, $\alpha\text{-Al}_2\text{O}_3$; middle, Al_2TiO_5 ; lower, rutile- TiO_2). The corresponding phase abundances (wt%) are: $\alpha\text{-Al}_2\text{O}_3 = 0.6$; $\text{Al}_2\text{TiO}_5 = 98.3$; rutile = 1.1. Quality of fit: $R_p = 5.8$; χ^2 (GoF) = 2.18; R_B (corundum) = 2.59; R_B (Al_2TiO_5) = 3.05; R_B (rutile) = 1.99.

and Howard et al. [14] for rutile. The software used to analyse the data was Rietica 1.7.7. During Rietveld analysis, constraints such as background B0, B1, B2, B3 and B5 were used but no restraints were used. A typical difference plot showing the quality of fit is shown in Fig. 1 together with the corresponding values for the agreement indices such as R_p , χ^2 and R_B .

2.3. Differential thermal and gravimetric analysis (DTA/TGA)

The DTA/TGA measurement of decomposed Al_2TiO_5 powder was carried in flowing air on a SETARAM instrument. This was done in order to monitor the thermochemical reactions that occurred during the chemical reaction of reformation in decomposed Al_2TiO_5 . Specimen weighing 10 mg were placed in a platinum crucible and heated to a maximum temperature of 1450°C at a heating rate of $10^\circ\text{C min}^{-1}$ with an empty reference.

3. Results and discussion

The microstructure of as-sintered Al_2TiO_5 sample is shown in Fig. 2(a) where relatively large and smooth grains of $10\text{--}20\ \mu\text{m}$ formed with occasional appearance of microcracks in certain large grains. When this sample was isothermally decomposed at 1100°C for 22 h, finer grains of rutile (white) and $\alpha\text{-Al}_2\text{O}_3$ (light gray) can be seen to form in situ within the original Al_2TiO_5 grain as shown in Fig. 2(b). This physical separation or decomposition of Al_2TiO_5 into finer grains of alumina and rutile has not resulted in observable shrinkage or disintegration of the decomposed sample. In fact, the decomposed sample appears to be harder and stronger due to the presence of alumina and rutile in the microstructure. However, development of secondary intragranular porosity can be seen in the decomposed microstructure which concurs with the work of Hennicke and Lingenberg [15]. The formation of fine grains of alumina and rutile during decomposition may also aid in the reformation of Al_2TiO_5 by virtue of enhanced atomic diffusion and shorter diffusion paths when the decomposed sample was re-heated to above 1300°C .

Fig. 3(a) shows the diffraction pattern of Al_2TiO_5 that was isothermally decomposed at 1100°C in air for 22 h. The sample almost decomposed completely forming $\sim 55\ \text{wt}\%$ corundum ($\alpha\text{-Al}_2\text{O}_3$) and $\sim 45\ \text{wt}\%$ rutile (TiO_2). This rapid process of phase decomposition in Al_2TiO_5 has also been observed in vacuum or argon atmosphere [16,17]. However, when this previously decomposed Al_2TiO_5 sample was re-heated from room temperature to 1450°C for 2 h, self-recovery took place through the rapid reaction of corundum and rutile to form Al_2TiO_5 with $>98\ \text{wt}\%$ phase

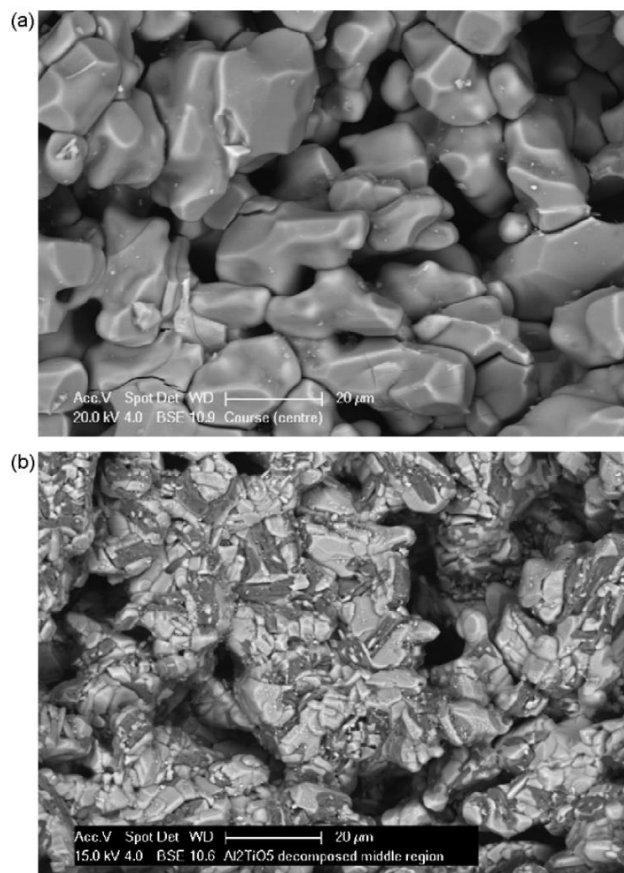


Fig. 2. Back-scattered electron micrographs showing the microstructure of (a) as-sintered Al_2TiO_5 and (b) isothermally decomposed Al_2TiO_5 at 1100°C for 22 h. (White phase is rutile (TiO_2), light gray is Al_2TiO_5 , dark gray is $\alpha\text{-Al}_2\text{O}_3$ and black are pores and cracks.)

purity as shown in Fig. 3(b). This capability of reformation is verified by differential thermal analysis that showed a sharp endotherm at 1362°C (Fig. 4) which can be attributed to the formation of Al_2TiO_5 through solid state reaction between corundum and rutile [8,9]. This further suggests that the process of decomposition is spontaneous and reversible as follows:



Fig. 5 shows the in situ neutron diffraction results of (a) reformation when previously decomposed Al_2TiO_5 was re-heated continuously from room temperature to 1450°C at a heating rate of $\sim 20^\circ\text{C min}^{-1}$, and (b) the subsequent decomposition of reformed Al_2TiO_5 during controlled cooling to room temperature at $\sim 10^\circ\text{C min}^{-1}$. It is evident that reformation or recovery in phase composition occurred when decomposed Al_2TiO_5 was re-heated to 1450°C , where more than 98 wt% Al_2TiO_5 self-recovered. During cooling from 1450 to 1200°C , the sample remained quite stable without any visible phase degradation. However, on further cooling from 1200 to 1000°C , rapid decomposition of Al_2TiO_5 commenced with $\sim 20\%$ of the sample decomposed at 1000°C . When compared to isothermal decomposition at 1100°C [16,17], the rate of non-isothermal decomposition observed here is much slower. Further cooling to 600°C and room temperature did not cause any further degradation of the sample. It is postulated that at temperatures below $\sim 1000^\circ\text{C}$, the decompo-

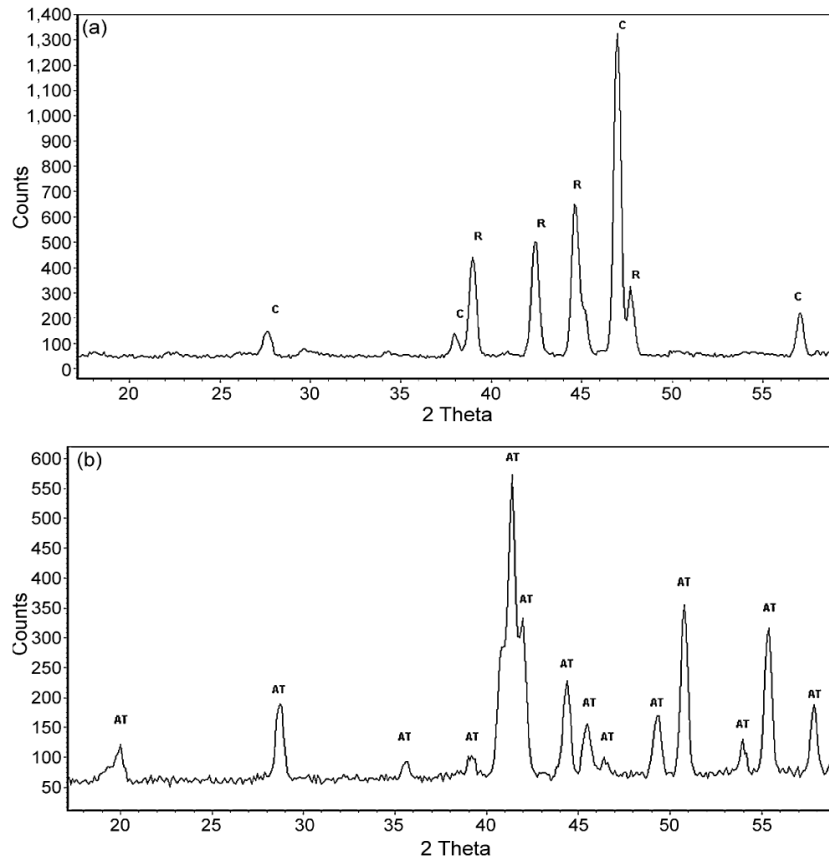


Fig. 3. Diffraction patterns showing (a) the formation of corundum (C) and rutile (R) in Al₂TiO₅ sample that was isothermally decomposed at 1100 °C for 22 h and (b) self-healing of the same sample in (a) after re-heating to 1450 °C for 2 h (legend: AT, Al₂TiO₅).

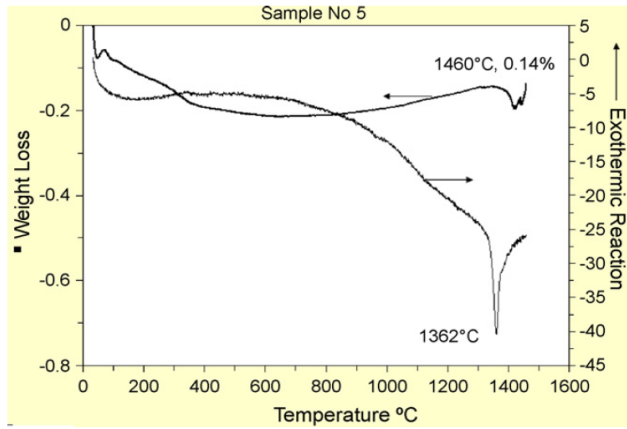


Fig. 4. A plot of DTA–TGA for decomposed Al₂TiO₅ showing a sharp endotherm at 1362 °C, which can be attributed to self-healing and re-formation of Al₂TiO₅.

sition of metastable Al₂TiO₅ is insignificant because the rates of atomic diffusion are too low. As the temperature rises above ~1000 °C the diffusion rates become high enough for a significant decomposition to take place. However, as the temperature rises beyond 1300 °C, reformation or recovery dominates and occurs rapidly to form Al₂TiO₅ because of very high atomic diffusion rates.

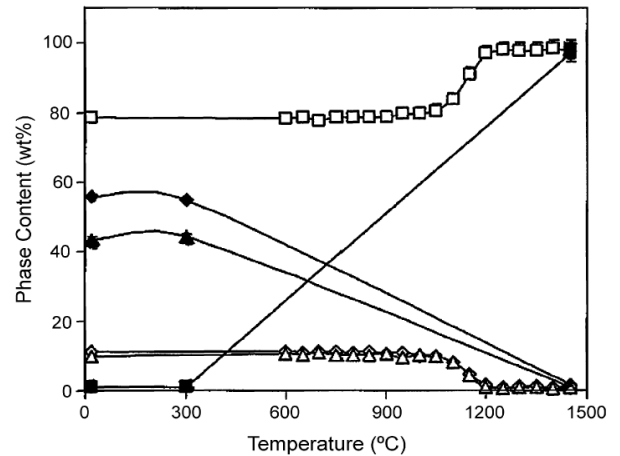


Fig. 5. In situ neutron diffraction results showing the variations of phase content of previously decomposed Al₂TiO₅ during (a) re-heating from room temperature to 1450 °C (legend: ■ Al₂TiO₅; ♦ Al₂O₃; ▲ TiO₂) and (b) controlled cooling to room temperature from 1450 °C (legend: □ Al₂TiO₅; ◇ Al₂O₃; △ TiO₂).

4. Conclusions

The use of high-temperature neutron diffraction and differential thermal analysis has shown that the process of decomposition in metastable Al₂TiO₅ is reversible and that reformation can occur readily when decomposed Al₂TiO₅ is re-heated above 1300 °C. It is

further shown that decomposition of Al_2TiO_5 during cooling below $\sim 1200^\circ\text{C}$ is governed by the temperature-dependent atomic diffusion rates.

Acknowledgments

This work was supported by the Australian Institute of Nuclear Science and Engineering (AINSE Awards 04/207 & 05/206). We are grateful to our colleague, E/Prof. B. O'Connor, for advice on Rietveld analysis of ND data. We thank Dr. Maxim Avdeev of the Bragg Institute of ANSTO for experimental assistance in the collection of MRPD data.

References

- [1] A.E. Austin, C.M. Schwartz, *Acta Cryst.* 6 (1953) 812.
- [2] B. Morosin, R.W. Lynch, *Acta Cryst.* B 28 (1972) 1040.
- [3] T. Epicier, G. Thomas, H. Wohlfromm, J.S. Moya, *J. Mater. Res.* 6 (1991) 138.
- [4] R.W. Grimes, J. Pilling, *J. Mater. Sci.* 29 (1994) 2245.
- [5] H.A.J. Thomas, R. Stevens, *Br. Ceram. Trans. J.* 88 (1989) 144.
- [6] H.A.J. Thomas, R. Stevens, *Br. Ceram. Trans. J.* 88 (1989) 184.
- [7] E. Kato, K. Daimon, Y. Kobayashi, *J. Am. Ceram. Soc.* 63 (1980) 355.
- [8] B. Freudenberg, A. Mocellin, *J. Am. Ceram. Soc.* 71 (1988) 22.
- [9] B. Freudenberg, A. Mocellin, *J. Mater. Sci.* 25 (1990) 3701.
- [10] H.C. Kim, K.S. Lee, O.S. Kweon, C.G. Aneziris, I.J. Kim, *J. Eur. Ceram. Soc.* 27 (2007) 1431.
- [11] Y. Ohya, Z. Nakagawa, K. Hamano, *J. Am. Ceram. Soc.* 71 (1988) C23.
- [12] T.S. Liu, D.S. Perera, *J. Mater. Sci.* 33 (1998) 995.
- [13] E.N. Maslen, V.A. Streltsov, N.R. Streltsova, N. Ishizawa, Y. Satow, *Acta Crystallogr. B* 49 (1993) 937.
- [14] C.J. Howard, T.M. Sabine, F. Dickson, *Acta Crystallogr. B* 47 (1991) 462.
- [15] H.W. Hennicke, W. Lingenberg, *Ber. Dtsch. Keram. Ges.* 63 (1986) 100–106.
- [16] I.M. Low, D. Lawrence, R.I. Smith, *J. Am. Ceram. Soc.* 88 (2005) 2957.
- [17] I.M. Low, Z. Oo, B.H. O'Connor, *Physica B: Condens. Mat.* 385–386 (2006) 502.

2.4 Diffraction Studies of a Novel Ti₃SiC₂-TiC System with Graded Interfaces.

LOW, I. M. & OO, Z. 2002. Diffraction Studies of a Novel Ti₃SiC₂-TiC System with Graded Interfaces, *Journal of the Australasian Ceramic Society*, 38, 112-116.

DIFFRACTION STUDIES OF A NOVEL Ti_3SiC_2 -TiC SYSTEM WITH GRADED INTERFACES

I.M. LOW¹, Z. OO²

¹*Materials Research Group, Department of Applied Physics, Curtin University of Technology, GPO Box U1987, WA. 6845 Australia*

²*School of Engineering and Science, Curtin University of Technology, Sarawak Campus Malaysia, CDT 250, 98009 Miri, Sarawak, Malaysia*
Email: j.low@curtin.edu.au

SUMMARY

A high-temperature vacuum heat-treatment process has been proposed for the designing of Ti_3SiC_2 -TiC composites with graded interfaces. The phase evolution and the graded nature of this system have been characterised by x-ray diffraction (XRD), synchrotron radiation diffraction (SRD) and neutron diffraction (ND). Results of SRD and ND in the temperature range 1000-1500°C show that the TiC layer commenced to form near the surface at 1200°C and grew rapidly in thickness with rising temperature. Depth-profiling of the TiC layer by XRD and SRD has revealed a distinct gradation in phase composition.

KEYWORDS

TiC, Ti_3SiC_2 , x-ray diffraction, neutron diffraction, synchrotron radiation diffraction

INTRODUCTION

Ti_3SiC_2 displays a unique combination of mechanical, electrical, thermal and physical properties [1-7]. For instance, its electrical and thermal conductivities are higher than those of pure Ti, its thermal shock resistance is comparable to those of metals, and its machinability is similar to that of graphite. It is also relatively light (4.5 g/cm³), oxidation resistant, exhibits a ultra-low friction coefficient ($\mu = 3 \times 10^{-3}$), and is elastically rigid. However, with a Vickers hardness (H_v) of only 4 GPa and a Young's modulus (E) of 320 GPa, the low value of H_v/E suggests a mechanical behaviour of Ti_3SiC_2 somewhat similar to that of ductile metals.

However, unlike traditional binary carbides (eg. WC, SiC and TiC), which are among some of the hardest (> 25 GPa), stiffest, and most refractory (~2000°C) materials known, the ternary carbide Ti_3SiC_2 is relatively soft, not wear resistant, and has lower thermal stability (~1700°C). To counteract this, Barsoum and co-workers improved the surface hardness and oxidation resistance of Ti_3SiC_2 by using both

carburization and silicidation to form surface layers of TiC and SiC [8].

Here, we propose an alternative method for the formation of TiC layer on Ti_3SiC_2 . This approach involves the controlled heat-treatment of Ti_3SiC_2 in vacuum at high temperature. It has been proposed that the very low partial pressure of oxygen in the vacuum treatment may facilitate the surface formation of TiC via the following thermal dissociation reaction [9]. By interfacing Ti_3SiC_2 and TiC it is hoped that the combination of the hard-wearing surface layer of TiC and the tough under-layer of Ti_3SiC_2 will produce a composite that is stronger and more resistant to fatigue, wear and damage.

In this paper, we present results on the evolution of phase composition of vacuum heat-treated Ti_3SiC_2 at elevated temperatures. The development of TiC in the temperature range 1000-1500°C was monitored dynamically using neutron diffraction. Depth-profiling of the near-surface composition of TiC layer has been conducted by x-ray diffraction and grazing incidence synchrotron radiation diffraction.

EXPERIMENTAL METHOD

Sample Preparation

Ti_3SiC_2 samples were fabricated by reaction-sintering and hot-isostatic-pressing of Ti, SiC and C powders. The powder compacts were initially prepared by mixing in the proper molar ratio, cold pressed, followed by reaction-sintered in a vacuum furnace (~10⁻⁵ torr) at 1500°C for 1 h, and finally hot-isostatically-pressed (HIPed) in argon at 1650°C for 2 h with a pressure of 150 MPa. Figure 1a shows a typical XRD plot of an as-HIPed Ti_3SiC_2 sample. In order to study the temperature range of thermal dissociation of Ti_3SiC_2 in vacuum to form TiC by x-ray and synchrotron radiation diffraction, thin slices (~2 mm) of HIPed samples were heated-treated in an Elatec™ vacuum furnace (~2 × 10⁻⁵ torr) at 900 - 1500°C for 1 - 8 h. Figure 1b shows a typical XRD plot of a vacuum heat-treated Ti_3SiC_2 sample.

Samples were accurately weighed before and after the vacuum-treatment to monitor mass change due to thermal dissociation of Ti_3SiC_2 to form TiC at various temperatures.

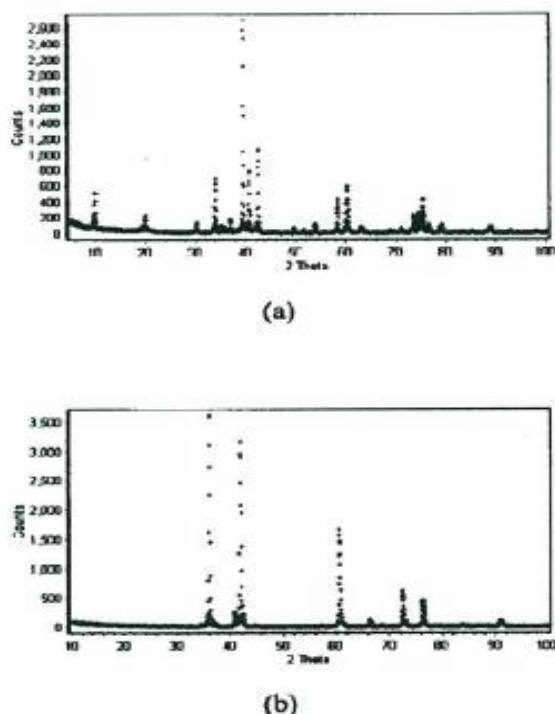


Fig. 1: Typical XRD plots of HIPed Ti_3SiC_2 (a) before and (b) after vacuum heat-treatment at 1500°C for 8h.

X-ray Diffraction (XRD)

Laboratory XRD patterns of vacuum-treated Ti_3SiC_2 samples were obtained with an automated Siemens D500 Bragg-Brentano instrument using $\text{CuK}\alpha$ radiation ($\lambda = 0.15418$ nm), produced at 40 kV and 30 mA over the 2θ range $5^\circ - 130^\circ$, step size 0.04 and counting time 2.4 s/step. Samples were mounted onto aluminium sample holders using a viscous adhesive and adjusted to the correct height with a glass slide. To obtain the graded composition profiles, the vacuum-treated samples were lightly polished with an emery paper to reach the desired depth. The relative phase abundance of Ti_3SiC_2 and TiC formed was computed using the Rietveld refinement method.

Synchrotron Radiation Diffraction (SRD)

The purpose of these experiments was to conduct in-situ depth-profiling of the near-

surface phase composition of Ti_3SiC_2 heat-treated in vacuum at various temperatures and dwelling times. Synchrotron radiation diffraction (SRD) patterns of vacuum-treated samples were collected using the BIGDIFF diffractometer at the Australian National Beamline Facility in Tsukuba, Japan. Imaging plates were used to record the patterns over 2θ of $10-100^\circ$. The diffractometer was operated in Debye-Scherrer mode under vacuum with wavelength of 0.8 \AA and grazing incidence angles of $0.1, 0.3, 0.5, 1.0, 3.0, 5.0$ and 10° . An incident beam of height 10 mm and width $100 \mu\text{m}$ and an exposure time of 20 min were used for each run. For the purpose of comparison, multi-wavelength SRD patterns ($\lambda \approx 0.8-1.54 \text{ \AA}$) were also collected. The relative phase abundance of TiC formed was estimated using the relative peak intensity ratio of (111) for TiC, and (102) for Ti_3SiC_2 .

Neutron Diffraction (ND)

High temperature time-of-flight neutron diffraction was used to monitor the real time structural evolution of phase development of HIPed Ti_3SiC_2 in vacuum from 20 to 1500°C . Neutron diffraction data were collected using the Polaris medium resolution, high intensity powder diffractometer at the UK pulsed spallation neutron source ISIS, Rutherford Appleton Laboratory. Two diffraction patterns were collected at 17°C and at every 100°C between 1000 and 1500°C with a rate of $20^\circ\text{C}/\text{min}$. A total of 6 patterns were collected at 1500°C . The data acquisition times were 1 h ($\sim 200 \mu\text{Ah}$) for the room temperature diffraction pattern, and 15 min ($\sim 50 \mu\text{Ah}$) for each of the diffraction patterns collected at elevated temperatures. The relative phase abundance of TiC formed was estimated using the relative peak intensity ratio of (111) for TiC, and (102) for Ti_3SiC_2 .

RESULTS AND DISCUSSION

Evolution of Phase Development

Figure 2 shows the relative abundance of TiC formed at various temperatures in vacuum. There is clearly no apparent dissociation of Ti_3SiC_2 to form TiC at temperatures below 1100°C . It dissociates initially slowly at $1100-1200^\circ\text{C}$ but the process becomes quite rapid from 1250 to 1500°C . However, in addition to TiC, a transient phase of $\text{Ti}_2\text{Si}_3\text{C}$ is also observed [10]. This phase is believed to form at the initial dissociation stage of Ti_3SiC_2 and it eventually converts to the stable TiC at elevated temperature. Figure 3 shows the in-situ

neutron diffraction of Ti_3SiC_2 heat-treated in vacuum from 17-1500°C with a dwelling time 3 h at 1500°C. Below 1500°C, Ti_3SiC_2 is relatively stable and it commences to dissociate rapidly to form TiC only when the temperature approaches 1500°C. The relative abundance of TiC formed increases very rapidly with dwelling time of 1 to 3 h.

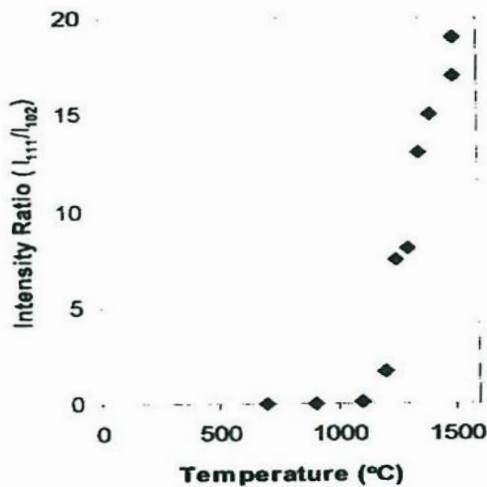


Figure 2: The relative abundance of TiC formed at various temperatures in vacuum as revealed by synchrotron radiation diffraction.

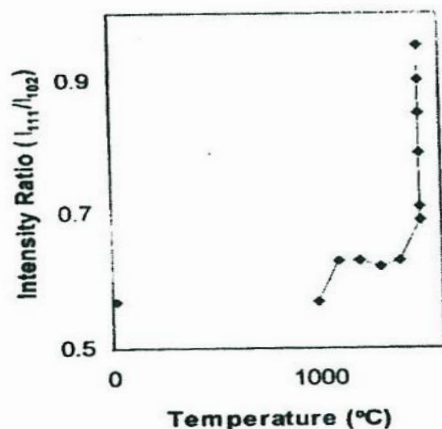
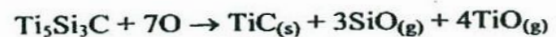


Fig. 3: The relative abundance of TiC formed at various temperatures and dwelling time (0-3 h) at 1500°C in vacuum as revealed by in-situ neutron diffraction.

The apparent discrepancy in the commencement temperature for rapid Ti_3SiC_2 dissociation to form TiC as revealed by SRD and ND can be attributed to the difference in depths of information provided by both techniques. The former provides the near-surface information while the latter gives the average or bulk information which results in a much lower averaged phase content. This discrepancy also implies that the mechanism of Ti_3SiC_2 dissociation is *surface-initiated* rather than a *bulk* process. This suggests that a *diffusion-controlled* process may be responsible for the observed dissociation which starts at the surface and progresses slowly into the bulk. This further implies that the initially formed TiC surface layer may be of only a few nanometres at ~1100°C which can only be detected by SRD due to its high brightness and excellent sensitivity. The initial TiC surface layer formed will increase rapidly in thickness with rising temperature. With a dwelling time of 3 h at 1500°C, it may reach a thickness of ~100 μm which can be readily detected by ND. This hypothesis of surface-initiated dissociation in vacuum-treated Ti_3SiC_2 is corroborated by the depth-profiling results to be presented in the next section.

The effect of prolonged dwelling time during vacuum heat-treatment at 1500°C has been observed to increase the abundance and thickness of the TiC layer formed, indicating a time-dependent dissociation process [9]. A dwelling time of more than 10 h would be necessary to form a sufficiently thick layer of pure-TiC on Ti_3SiC_2 .

The exact surface chemistry of this TiC formation in vacuum remains unclear. It is proposed here that in the presence of a very low oxygen partial pressure as in vacuum, the surface of Ti_3SiC_2 may undergo a high temperature thermal dissociation process to form TiC and $\text{Ti}_5\text{Si}_3\text{C}$ in two stages as follows:



According to the above equations, the mass of samples following the heat-treatment should decrease as the temperature increases due to an increased volatility of CO, SiO and TiO. This hypothesis is corroborated by the observation of an increase in mass loss in vacuum as the heat-treatment temperature increases (Fig. 4)

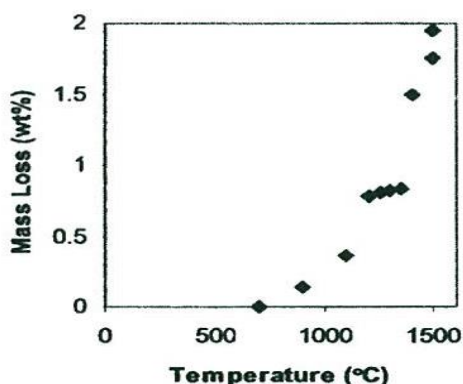


Fig. 4: Variation of mass loss as a function of temperature during vacuum heat-treatment.

Depth-Profiling of Phase Composition

The presence of graded composition in vacuum-treated Ti_3SiC_2 has previously been revealed by XRD [9]. Before polishing with an emery paper, the as-treated surface contained >98% TiC. The content of TiC decreased rapidly the surface to the bulk. Table 1 shows the depth-dependent variation of phase abundances of a Ti_3SiC_2 sample vacuum-treated at 1500°C for 1 h as revealed by XRD. The results clearly show that the near-surface TiC layer has a graded composition with the top surface very rich in TiC and its content decreases rapidly with an increase in depth.

Table 1: Depth-profiling of relative phase abundance of a Ti_3SiC_2 sample vacuum-treated at 1500°C for 1 h

Depth (µm)	TiC (wt%)	Ti_3SiC_2 (wt%)
0	85.8	14.2
~10	79.9	20.1
~50	4.8	95.2
~150	3.0	97.0

The graded nature of the near-surface composition of vacuum-treated Ti_3SiC_2 has also been verified by the variation of phase composition at different wavelengths [11,12]. The composition is a minimum on the surface ($\lambda = 1.54 \text{ \AA}$) and increases as the depth

increases, reaching a maximum for $\lambda = 1.0 \text{ \AA}$. This display of composition gradation at the near-surface is more pronounced when the grazing incident angle increased from 0.5 to 5.0°. These results support the above-mentioned hypothesis of a surface-initiated process for the formation of TiC. It is further proposed here that the dissociation to form TiC occurs initially on the surface by a nucleation and growth mechanism. As the dissociation progresses, this mechanism propagates into the bulk of the sample through a diffusion process.

CONCLUSIONS

The feasibility of using the high-temperature vacuum heat-treatment to deposit a graded layer of TiC on Ti_3SiC_2 through a controlled dissociation process has been verified in this study. The graded nature of this system has been confirmed by x-ray diffraction and synchrotron radiation diffraction. Much work is still needed to examine the microstructure and to measure the microhardness and wear-resistance of the TiC layer. However, the nanostructure of this layer may pose considerable challenges both in microstructural and mechanical properties evaluation.

For this system to exhibit superior wear properties, the TiC layer needs to have a dense and fine grained microstructure. In addition, the TiC formed must be an equilibrium or stoichiometric phase with a cubic and not a hexagonal structure. Non-stoichiometric TiC_x and/or hexagonal TiC is known to be very much softer than its cubic and stoichiometric counterpart. Hence, a rigorous crystallographic work based on the Rietveld refinement method would be necessary to fully ascertain the structure and composition of the TiC formed. Complementary analytical tools such as x-ray fluorescence, high resolution electron transmission electron, and electron microprobe should also be used to unravel the true nature and property of the TiC phase formed following the high-temperature thermal dissociation of Ti_3SiC_2 in vacuum.

Hitherto, it is unclear how the surface dissociation process would affect the quality of the TiC layer formed. It is quite likely that the evaporation of CO, TiO and SiO during the thermal dissociation of Ti_3SiC_2 may cause the formation of a porous TiC layer. In addition, it remains unknown whether the similar high-temperature dissociation will occur in an inert atmosphere such as argon or nitrogen where a low oxygen partial pressure may exist as in vacuum. Under these circumstances, new

strategies will need to be sought which require a full understanding of the surface chemistry and chemical processes involved during the thermal dissociation to form TiC.

ACKNOWLEDGMENTS

This work was supported by funding from AINSE (Project 02/075), ISIS (Proposal RB13248) and the Australian Synchrotron Research Program (ANBF proposal 01/02-AB-36). We thank Dr D. Perera of ANSTO, Dr. R. Smith of ISIS and Dr. J. Hester of ANBF for experimental assistance in the HIPing of samples and the collection of ND and SRD data respectively.

REFERENCES

1. Barsoum, M.W. & El-Raghy, T. "Synthesis and Characterisation of a Remarkable Ceramic: Ti_3SiC_2 ." *J. Am. Ceram. Soc.* Vol. 79 (1996) 1953.
2. Barsoum, M.W., Brodtkin, D. & El-Raghy, T. "Machineable Layered Ceramics for High Temperature Applications." *Scr. Met. et. Mater.* Vol. 36 (1997) 535.
3. Low, I.M., Lee, S.K., Barsoum, M.W. & Lawn, B.R. "Contact Hertzian Response of Ti_3SiC_2 Ceramics." *J. Am. Ceram. Soc.* Vol. 81 (1998) 225.
4. Low, I.M. "Vickers Contact Damage of Micro-layered Ti_3SiC_2 ." *J. Europ. Ceram. Soc.* Vol. 18 (1998) 709.
5. Barsoum, M.W. and El-Raghy, T. "Room Temperature Ductile Carbides." *Metall. Mater. Trans.*, Vol. 30A, (1999) 363.
6. El-Raghy, T., Zavaliangos, A., Barsoum, M.W. & Kalidindi, S.R. "Damage Mechanisms Around Hardness Indentations in Ti_3SiC_2 ." *J. Am. Ceram. Soc.*, Vol. 80 (1997) 513.
7. Barsoum, M.W., Zhen, T., Kalidindi, S.R., Radovic, M. & Murugaiah, A. "Fully Reversible Dislocation-based Compressive Deformation of to 1 GPa." *Nature Materials*. Vol. 2 (2003) 107.
8. El-Raghy, T. Barsoum, M. W. "Diffusion Kinetics of the Carburisation and Silicidation of Ti_3SiC_2 ." *J. Appl. Phys.* Vol. 83 (1998) 112.
9. Low, I.M., Manurung, P., Smith, R.I. & Lawrence, D. "A Novel Processing Method for the Microstructural Design of Functionally Graded Ceramic Composites." *Key Engineering Materials* Vol. 224-226 (2002) 465.
10. Low, I.M. "Characterisation of Vacuum and Argon Heat-Treated Ti_3SiC_2 ." pp.191-192 in *Proc. of AUSTCERAM 2002* (Eds. I.M. Low & D.N. Phillips), 30 Sept – 4 Oct. 2002, Perth, WA.
11. Low, I.M., Singh, M., Manurung, P., Wren, E., Sheppard, D.P. & Barsoum, M.W. "Depth Profiling of Phase Composition and Texture in Layered-Graded Al_2O_3 - & Ti_3SiC_2 -Based Systems using X-ray and Synchrotron Radiation Diffraction." *Key Engineering Materials* Vol. 224-226 (2002) pp. 505-510.
12. Sheppard D.P & Low, I.M. "Characterisation of Phase Composition Character in High-Temperature Vacuum Treated Ti_3SiC_2 ." pp.162-171 in *Proc. 2001 Joint AXAA/ WASEM Conference* (Eds. M. Saunders et al.) 21-23 Sept. 2001, Mandurah, WA.

2.5 Effect of Vacuum Annealing on the Phase Stability of Ti_3SiC_2

LOW, I. M., OO, Z. & PRINCE, K. E. 2007. Effect of Vacuum Annealing on the Phase Stability of Ti_3SiC_2 , *Journal of the American Ceramic Society*, 90, 2610-2614.

Effect of Vacuum Annealing on the Phase Stability of Ti_3SiC_2

It Meng Low[†] and Zeya Oo

Department of Applied Physics, Centre for Materials Research, Curtin University of Technology, Perth, Western Australia, Australia

Kathryn E. Prince

Australian Nuclear Science and Technology Organisation (ANSTO), PMB 1, Menai, New South Wales 2234, Australia

The effect of vacuum annealing on the thermal stability and phase transition of Ti_3SiC_2 has been investigated by X-ray diffraction (XRD), neutron diffraction, synchrotron radiation diffraction, and secondary ion mass spectroscopy (SIMS). In the presence of vacuum or a controlled atmosphere of low oxygen partial pressure, Ti_3SiC_2 undergoes a surface dissociation to form nonstoichiometric TiC and/or $\text{Ti}_5\text{Si}_3\text{C}_x$ that commences at $\sim 1200^\circ\text{C}$ and becomes very pronounced at $\geq 1500^\circ\text{C}$. Composition depth profiling at the near surface of vacuum-annealed Ti_3SiC_2 by XRD and SIMS revealed a distinct gradation in the phase distribution of TiC and $\text{Ti}_5\text{Si}_3\text{C}_x$ with depth.

I. Introduction

HIGH-temperature thermochemical stability in bulk and thin-film Ti_3SiC_2 has hitherto generated considerable controversy among researchers. For instance, several researchers have reported that Ti_3SiC_2 becomes unstable at temperatures $> 1400^\circ\text{C}$ in an inert atmosphere (e.g., vacuum, argon, or nitrogen), by dissociating into Si, TiC_x, and/or $\text{Ti}_5\text{Si}_3\text{C}_x$.^{1–5} Feng *et al.*⁶ annealed Ti_3SiC_2 -based bulk samples at 1600°C for 2 h and 2000°C for 0.5 h in vacuum (10^{-2} Pa) and found that TiC_x was the only phase remaining on the surface. According to Gao *et al.*,⁷ the propensity of decomposition of Ti_3SiC_2 to TiC_x was related to the vapor pressure of Si, i.e., the atmosphere where the Ti_3SiC_2 exists. They believed that the partial pressure of Si plays an important role in maintaining the stability of Ti_3SiC_2 , whereby it has a high propensity to decompose in a N₂, O₂, or CO atmosphere at temperatures above 1400°C . This process of surface-initiated phase decomposition was even observed to commence at a temperature as low as 1000°C – 1200°C in Ti_3SiC_2 thin films during vacuum annealing.^{8,9} The large difference in the observed decomposition temperatures between bulk and thin-film Ti_3SiC_2 has been attributed to the difference in diffusion length scales involved and measurement sensitivity used in the respective studies. In addition, Ti_3SiC_2 has also been observed to react readily with molten Al, Cu, Ni, and cryolite (Na_3AlF_6) at high temperatures.^{10–12}

In contrast, Barsoum and colleagues^{13–15} have shown that Ti_3SiC_2 was thermodynamically stable up to at least 1600°C in vacuum for 24 h and in an argon atmosphere for 4 h. They further argued that the reduced temperature at which Ti_3SiC_2 decomposed as observed by others was due to the presence of

impurity phases (e.g., Fe or V) in the starting powders, which interfered with the reaction synthesis of Ti_3SiC_2 , and thus destabilized it following prolonged annealing in an inert environment.¹⁶ However, mixed results have been reported by Radakrishnan *et al.*¹⁷ In their investigation, Ti_3SiC_2 was shown to be stable in a tungsten-heated furnace for 10 h at 1600° and 1800°C in an argon atmosphere, but dissociated to TiC_x under the same conditions when using a graphite heater. These conflicting results suggest that the thermochemical stability of Ti_3SiC_2 is still poorly understood, although its susceptibility to thermal decomposition is strongly influenced by factors such as the purity of the powders and sintered materials, temperature, vapor pressure, atmosphere, and the type of heating elements used. In addition, the nature and composition of the decomposed surface layer formed during annealing remain controversial, especially in relation to the presence of $\text{Ti}_5\text{Si}_3\text{C}_x$ and the composition variation at the near surface.

In this paper, the effect of vacuum annealing on the thermal stability of Ti_3SiC_2 has been investigated by X-ray diffraction (XRD), synchrotron radiation diffraction (SRD), and neutron diffraction (ND) in the temperature range 1000° – 1500°C . The roles of controlled atmosphere with low oxygen partial pressures in the complex surface chemistry of thermal dissociation of Ti_3SiC_2 are discussed.

II. Experimental Procedure

(1) Sample Preparation

Ti_3SiC_2 samples were fabricated using a procedure described elsewhere.¹⁸ Essentially, powders of Ti, SiC, and C were mixed in the proper molar ratio, cold pressed, and then hot isostatically pressed at 1600°C for 4 h at a pressure of 40 MPa to produce dense Ti_3SiC_2 samples with a grain size in the range of 10–30 μm and with ~ 3 wt% TiC as an impurity (Fig. 1(a)). Thin flat plates of ~ 3 -mm thick were cut from the HIPed Ti_3SiC_2 sample using a diamond blade. One of the plates was used as a control and the remaining plates were each annealed in vacuum ($\sim 2 \times 10^{-5}$ torr) at 1000° – 1500°C for 1.0–8.0 h. Vacuum annealing was conducted in an Elatec[™] vacuum furnace (Wilmington, MA) fitted with graphite heating elements at a heating rate and cooling rate of $5.0^\circ\text{C}/\text{min}$. Figure 1(b) shows the pronounced formation of TiC_x on a vacuum-annealed sample at 1500°C for 8 h.

(2) XRD

Laboratory XRD patterns of vacuum-annealed Ti_3SiC_2 samples were obtained with an automated Siemens D500 Bragg-Brentano instrument (Eindhoven, the Netherlands) using $\text{CuK}\alpha$ radiation ($\lambda = 0.15418$ nm), produced at 40 kV and 30 mA over the 2θ range 5° – 130° , step size 0.04, and counting time 2.4 s/step. Samples were mounted onto aluminum sample holders using a viscous adhesive and adjusted to the correct height with a glass slide. To obtain graded composition profiles, the vacuum-treated samples were lightly polished with an emery paper to

R. Riedel—contributing editor

Manuscript No. 22707. Received January 20, 2007; approved March 27, 2007.

This work formed part of a much broader project on the thermal stability of ternary carbides, which is funded by an ARC Discovery-Project grant (DP0664586) and an ARC Linkage-International grant (LX0774743) for one of us (I. M. L.). The collection of SRD, ND, and SIMS data for this work were conducted at the Photon Factory, Rutherford-Appleton Laboratory, and ANSTO with financial support from ASRP (05/06-AB-24 & 06/07-ABPP-09), ISIS (RB13248), and AINSE (05/106).

[†]Author to whom correspondence should be addressed. e-mail: j.low@curtin.edu.au

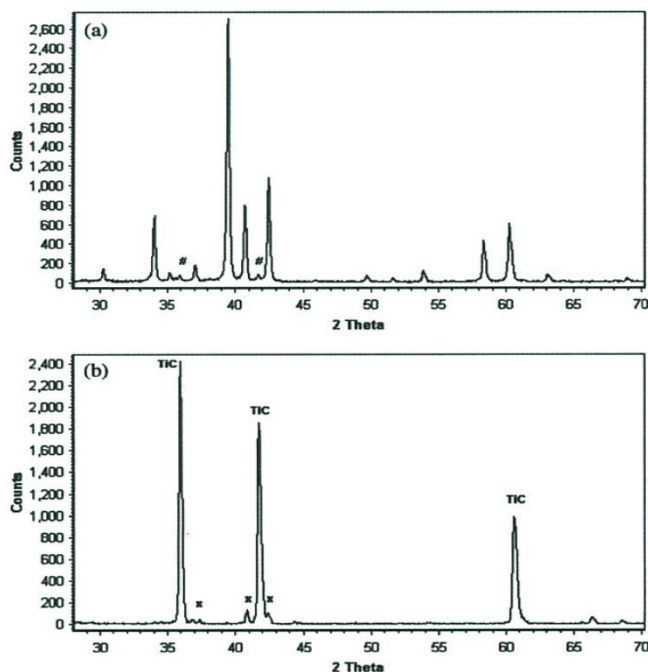


Fig. 1. (a) Phase compositions of as-prepared Ti_3SiC_2 as determined by X-ray diffraction. The presence of a minor TiC phase (#) is evident; (b) dissociated Ti_3SiC_2 after vacuum annealing at $1500^\circ C$ for 8 h. Note the pronounced formation of TiC due to vacuum annealing. The presence of residual Ti_3SiC_2 (x) is also evident.

attain the desired depth. A precision digital micrometer was used to measure the change in thickness after each abrasion. The relative abundances of the phases formed were computed using the Rietveld refinement method.¹⁹ The models of Kisi *et al.* (ICSD #86213) for Ti_3SiC_2 , Christensen *et al.* (ICSD #1546) for TiC, and Nowotny *et al.* (ICSD #44386) for $Ti_5Si_3C_x$ were used for the Rietveld analysis.

(3) SRD

Flat plates of vacuum-annealed Ti_3SiC_2 in the temperature range 1000° – $1500^\circ C$ were analyzed at the Photon Factory using the BIGDIFF diffractometer (Clayton, Australia). Imaging plates were used to record the patterns over the 2θ range of 5° – 90° . The diffractometer was operated in the Debye–Scherrer mode under vacuum with a wavelength of 0.8 Å and at an incidence angle of 1° .

(4) ND

High-temperature time-of-flight ND in a vacuum furnace ($\sim 10^{-4}$ torr) fitted with tantalum elements was used to monitor the structural evolution of phase decomposition in Ti_3SiC_2 from 20° to $1500^\circ C$ in real time. A dense rectangular bar sample of Ti_3SiC_2 with dimensions 10 mm \times 10 mm \times 40 mm and ~ 10 wt% TiC as an impurity was used for the study. ND data were collected using the Polaris medium-resolution, high-intensity powder diffractometer at the U.K. pulsed spallation neutron source ISIS, Rutherford Appleton Laboratory.²⁰ The diffraction patterns were collected at $20^\circ C$ and at every $100^\circ C$ between 1100° and $1500^\circ C$ at a rate of $20^\circ C/min$. The data acquisition times were 1 h ($\sim 200 \mu A \cdot h$) for the room-temperature diffraction pattern, and 15 min ($\sim 50 \mu A \cdot h$) for each of the diffraction patterns collected at elevated temperatures. Normalized data collected in the highest resolution, backscattering detector bank over the d -spacing range of ~ 0.4 – 3.2 Å were analyzed by the Rietveld method using the General Structure Analysis System²¹

to compute the changes in the phase content of Ti_3SiC_2 and TiC during vacuum annealing at elevated temperatures.

(5) Secondary Ion Mass Spectroscopy (SIMS)

SIMS is an analysis technique for gathering compositional information about the surface and near-surface regions of solid materials, and is particularly suited to the measurement of concentration profiles. It uses a beam of primary ions to eject secondary ions from near-surface regions of the target. The secondary ions are collected and focused through a mass spectrometer, and then directed into a detector. Because a sample will be gradually eroded with time, a depth profile can be obtained by recording the detector signal as a function of time. A profilometer was also used to measure the depth of the crater formed—at the end of each SIMS run—and this allowed the thickness of the TiC_x layer to be determined directly from a depth versus time calibration curve. The depth profiling of vacuum-treated Ti_3SiC_2 samples was conducted through the elemental imaging of titanium, carbon, silicon, and oxygen on the near surface. The enhanced elemental sensitivity of SIMS allows the detection of oxygen (if present) within the structure of the near-surface layer.

The facility used in this work is the Cameca ims-5f SIMS of the Australian Nuclear Science and Technology Organisation (ANSTO). Positive secondary ion depth profiles were taken using 150 nA primary Cs^+ ion current at 3 keV impact energy, rastered over a $250 \mu m \times 250 \mu m$ area. The ion count rates in all mass channels were normalized to Cs^+ secondary ion counts rate to minimize the effect of variations in the primary ion beam current.

III. Results and Discussion

(1) Thermochemical Stability of Ti_3SiC_2 at Elevated Temperature

The phases present and their relative abundance after Ti_3SiC_2 samples were vacuum treated at 1000° , 1200° , 1400° , and $1500^\circ C$ as revealed by SRD, and are listed in Table I. There was no apparent dissociation of Ti_3SiC_2 to form TiC at temperatures below $1200^\circ C$. It dissociated initially slowly at 1200° – $1300^\circ C$ but the process became quite rapid from 1400° to $1500^\circ C$. The formation of $Ti_5Si_3C_x$ was also observed at $1400^\circ C$. This transient phase is believed to convert eventually into stable TiC_x at an elevated temperature. The detection of phase dissociation at $\sim 1200^\circ C$ in this study is consistent with the observations of Eklund *et al.*⁸ and Emmerlich *et al.*,⁹ where decomposition of epitaxial Ti_3SiC_2 thin films was found to occur at $1000^\circ C$ in vacuum ($\sim 1 \times 10^{-10}$ torr) by synchrotron radiation photoemission and at 1100° – $1200^\circ C$ by *in situ* XRD. This detection of a much lower decomposition temperature when compared with the typical temperature of 1400° – $1600^\circ C$ reported in the literature^{1–7} can be attributed to the use of much intense and higher sensitivity of synchrotron radiation as well as the very short diffusion length scales involved. In addition, the use of a much higher vacuum ($\sim 1 \times 10^{-10}$ torr) may also have provided a reduced chemical potential for the breakdown of Ti_3SiC_2

Table I. Relative Peak Intensity of the Phases Present in Ti_3SiC_2 Vacuum Annealed at Elevated Temperatures as Revealed by SRD

Temperature ($^\circ C$)	Ti_3SiC_2	TiC	Ti_5Si_3C
25	vs	w	—
1000	vs	w	—
1200	vs	m	—
1400	s	m	w
1500	w	s	m

vs, very strong; s, strong; m, medium; w, weak; t, trace; SRD, synchrotron radiation diffraction.

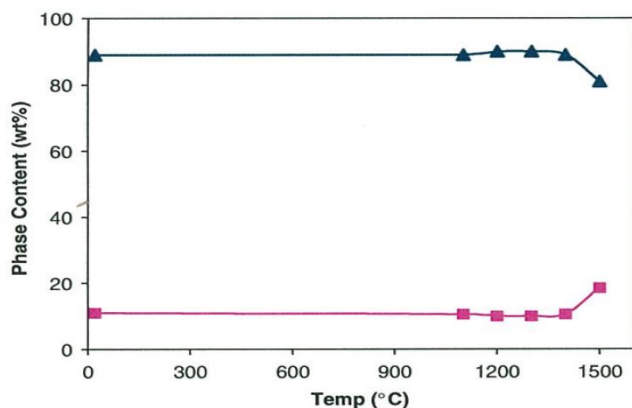


Fig. 2. Thermal stability of Ti_3SiC_2 under vacuum: effect of temperature on the weight percentage of Ti_3SiC_2 (\blacktriangle) and TiC (\blacksquare), as determined by neutron diffraction.

through deintercalation of Si and the concomitant formation of TiC_x .⁸

To the best of our knowledge, the *in situ* study of the thermal dissociation of Ti_3SiC_2 in vacuum by ND has not been reported previously. Figure 2 shows the dynamic structural changes of Ti_3SiC_2 during thermal dissociation into TiC_x in vacuum in the temperature range 20°–1500°C as revealed by ND. From room temperature to 1400°C, the phase concentration of Ti_3SiC_2 and initial TiC_x remained quite stable and constant. At $\sim 1500^\circ\text{C}$, Ti_3SiC_2 dissociated quite rapidly to form TiC_x . The detection of a higher decomposition temperature here can be attributed to the lower intensity and sensitivity of neutrons when compared with synchrotron radiations. In addition, the high penetration of neutrons provides the average composition of the *bulk*, whereas the average composition at the *near surface* several micrometers in depth is provided by the photons. It is worth mentioning here that the existence of $\text{Ti}_5\text{Si}_3\text{C}_x$ as a transient phase was not detected by ND in this study, although it was detected by SRD shown in Table I as well as when Ti_3SiC_2 was annealed in argon.⁴ This observation may be due to the very small amount of this phase formed, which was below the detection limit of the neutrons. It is also interesting to note that this phenomenon of pronounced thermal instability at an elevated temperature is strikingly similar to that of aluminum titanate when it is annealed in vacuum²² or argon.²³ It should also be noted that the observed phenomena concerning the decomposition of Ti_3SiC_2 are similar to those of Si_3N_4 , wherein the powders decompose at 1300°–1400°C while bulk materials decompose at temperatures higher than 1700°C.

(2) Composition Depth Profiles at the Near Surface

Figure 3 shows the depth-dependent variation of phase abundances of a Ti_3SiC_2 sample vacuum treated at 1500°C for 8 h as revealed by XRD. The results clearly show that the near-surface TiC layer has a graded composition, with the top surface being very rich in TiC_x (i.e., >90 wt%), and its content decreases rapidly with an increase in depth. Note the presence of a small amount of $\text{Ti}_5\text{Si}_3\text{C}_x$ on the surface but its content increases to a maximum value of over 60 wt% at a depth of $\sim 30\ \mu\text{m}$. The existence of $\text{Ti}_5\text{Si}_3\text{C}_x$ is not unexpected as this phase has also been reported previously.^{4–7,15,16,24–26} It is very likely that Ti_3SiC_2 may have dissociated initially into $\text{Ti}_5\text{Si}_3\text{C}_x$ as an *intermediate* phase before its final dissociation into TiC_x . The formation of a surface layer of TiC_x has the potential to impart high hardness and wear resistance to the otherwise soft but damage-resistant Ti_3SiC_2 ^{18,27,28} if the TiC_x layer formed has a nonporous cubic or NaCl structure.²⁹

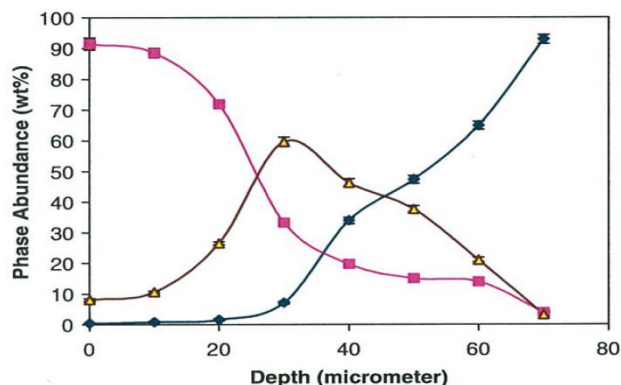


Fig. 3. X-ray diffraction depth profiling of phase abundances in vacuum-annealed Ti_3SiC_2 at 1500°C for 8 h. \blacklozenge , Ti_3SiC_2 ; \blacksquare , TiC ; \blacktriangle , $\text{Ti}_5\text{Si}_3\text{C}_x$.

The high sensitivity of SIMS has provided further evidence of a graded composition within the dissociated TiC_x layer in the near surface. As would be expected, the control sample shows no variations in the elemental compositions of Ti, Si, and O with depth. In contrast, the sample vacuum treated for 4 h shows an initial decline in the concentration of Si before leveling off after 1000 s. Its concentration then increases again after 5000 s (Fig. 4). This implies that the near surface of the sample is covered mainly ($\sim 90\ \text{wt}\%$) with a thin layer of TiC_x ($\sim 5\ \mu\text{m}$) following vacuum annealing. The presence of a graded composition at the Ti_3SiC_2 – TiC_x interface has been verified. The apparently high level of the H element in Fig. 4 is probably due to the H_2 present in the sample chamber atmosphere of the SIMS equipment during measurement.

More complex results are observed for the sample vacuum treated at 8 h (Fig. 5). High concentrations of Ti, Si, C, and O are present at the near surface (0–3000 s), which indicates that in addition to TiC_x , a second phase coexists, i.e. $\text{Ti}_5\text{Si}_3\text{C}_x$ with dissolved O_2 . This phase is believed to have caused the color of Ti_3SiC_2 to turn brownish following a prolonged vacuum treatment at 1500°C. The $\text{Ti}_5\text{Si}_3\text{C}_x$ (with dissolved O_2) phase acts as an intermediate or precursor phase for the eventual formation of TiO_2 and SiO_2 . This further suggests that $\text{Ti}_5\text{Si}_3\text{C}_x$ can act as a

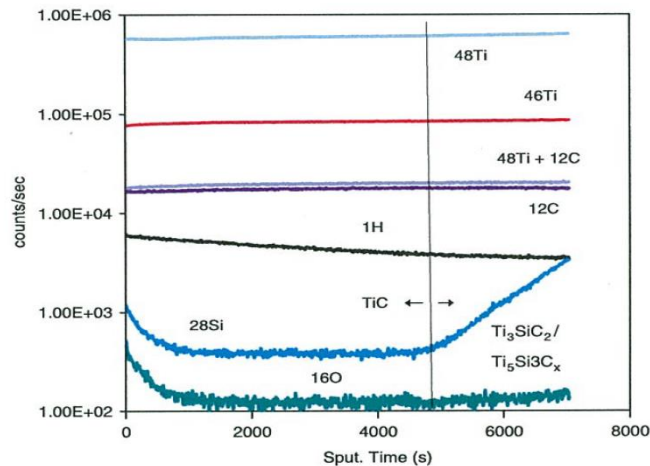


Fig. 4. Elemental composition versus time/depth in Ti_3SiC_2 vacuum treated at 1500°C for 4 h, as determined by secondary ion mass spectroscopy. Note the rapid increase in Si content after 5000 s.

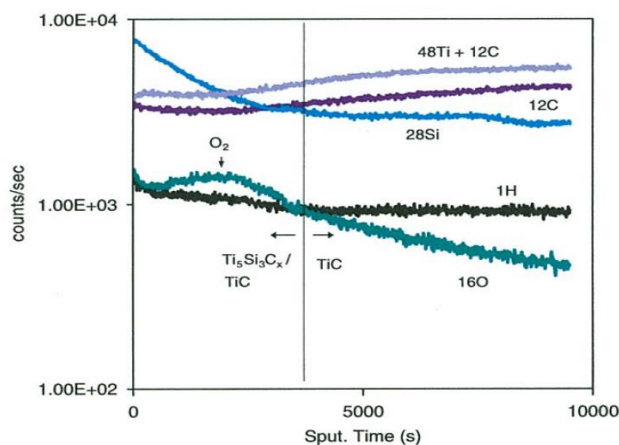


Fig. 5. Elemental composition versus time/depth in Ti_3SiC_2 vacuum treated at $1500^\circ C$ for 8 h, as determined by secondary ion mass spectroscopy. Note the large O_2 peak (see arrow) at 2000 s.

“sponge” to soak up oxygen and when a supersaturated state is reached as in during air oxidation, the $Ti_5Si_3C_x$ (with supersaturated O_2) will segregate out to form TiO_2 (anatase or rutile) and SiO_2 (tridymite or cristobalite) with the concomitant release of CO.

(3) Chemistry of Thermochemical Dissociation

From this study, it is quite obvious that Ti_3SiC_2 becomes thermally unstable in vacuum at an elevated temperature (i.e., $\geq 1200^\circ C$) and dissociates to form TiC_x and $Ti_5Si_3C_x$. According to Wu *et al.*,⁵ the initial dissociation of Ti_3SiC_2 to $Ti_5Si_3C_x$ is more favorable to TiC_x because silicon has a low diffusion rate in TiC-related systems. Thus, the $Ti_5Si_3C_x$ phase is more likely to nucleate on Ti_3SiC_2 because this mechanism would not contain any long-range diffusion of Si atoms. In view of this, it is proposed that the pathways for the thermal dissociation of Ti_3SiC_2 in the presence of a low oxygen partial pressure to form TiC and $Ti_5Si_3C_x$ occur in two steps



The release of a highly reducing CO gas in step 1 would invariably result in enhancement of further decomposition of Ti_3SiC_2 in step 2 with the concomitant release of SiO vapor.

The proposed volatility of gaseous CO and SiO released is consistent with the observed results of an increasing mass loss when Ti_3SiC_2 is annealed in vacuum at elevated temperatures.³ In addition, the highly reducing effect of CO vapor in the decomposition process may help to explain why there is a much greater propensity for Ti_3SiC_2 to undergo thermal dissociation when annealed in a graphite-element furnace than in a tungsten-element furnace.¹⁷ The use of a furnace with graphite elements would release additional CO vapor which may exacerbate the kinetics of dissociation through the evaporation of Si from Ti_3SiC_2 . This process of structural breakdown that involves deintercalation of Si from Ti_3SiC_2 with the concomitant formation of TiC is consistent with the models proposed previously by Barsoum³⁰ and Zhou and Sun.³¹ According to Barsoum, the decomposition process occurs through the removal of Si from the structure with the concomitant detwinning of the Ti_3SiC_2 layers to form TiC_x .

It should be pointed out that carbon nonstoichiometry exists in both TiC_x and $Ti_5Si_3C_x$ and its defect concentration is sensitive to the variation in the oxygen partial pressure and

temperature.^{5,32,33} In the case of TiC_x , the value of x has an astonishing range from 0.5 to 0.97, without a change in crystal structure.²⁹ However, recent photoemission studies by Eklund *et al.*⁸ using synchrotron radiation have detected the presence of graphitic carbon in TiC_x formed when Ti_3SiC_2 thin films were annealed in vacuum at $1000^\circ C$. This implies that the dissociated TiC_x layer formed in this study and others may also have graphitic carbon, which, together with high porosity, are undesirable for imparting high hardness and wear resistance. The ease of removal of the TiC_x layer even by emery paper as described above for the XRD depth-profiling work is a good indication of poor wear resistance and thus low hardness by virtue of high porosity in the dissociated TiC_x microstructure.³⁴

The presence of Ti ions in Ti_3SiC_2 having an unstable oxidation state is believed to enhance carbon content variations with a concomitant susceptibility to surface dissociation. Changes in the oxidation state of titanium from 4^+ to 3^+ at low oxygen partial pressure give rise to carbon vacancy formation. The change in defect concentrations in TiC_x and $Ti_5Si_3C_x$ with atmosphere may be attributed to the variation in charge-compensation mechanisms to form carbon vacancies and other defects. Indeed, nonstoichiometry in TiC_x has been ascribed to the existence of defects such as stacking faults and Si solid solution.³³ A thorough study of the defect chemistry is essential to gain a complete understanding of the nonstoichiometry and defects associated with the thermal dissociation of Ti_3SiC_2 in a controlled atmosphere of varying oxygen partial pressure.

IV. Conclusion

The phase stability and transition of Ti_3SiC_2 at elevated temperature are strongly dependent on the oxygen partial pressure of the annealing atmosphere within the furnace. In the presence of vacuum or low oxygen partial pressure, it dissociates slowly to nonstoichiometric TiC_x and $Ti_5Si_3C_x$ at $\sim 1200^\circ C$ but becomes quite rapid at $\geq 1500^\circ C$. The use of a vacuum furnace with graphite elements may accelerate the thermochemical process of Ti_3SiC_2 dissociation during annealing due to the release of highly reducing CO gas. Composition depth profiling at the near surface of vacuum-annealed Ti_3SiC_2 by XRD and SIMS has revealed a distinct gradation in the phase distribution of TiC_x and $Ti_5Si_3C_x$ with depth.

Acknowledgments

Rietveld analysis of ND by Dr. D. Li is gratefully acknowledged. We thank Mr. D. Sheppard, Dr. J. Hester, and Dr. R. Smith for technical assistance in the collection of XRD, SRD, and ND data. We also thank our colleague E/Prof. B. O'Connor for advice on the Rietveld analysis of XRD data. We thank Prof. Michel Barsoum of Drexel University for providing Ti_3SiC_2 samples for the initial study.

References

1. T. Okano, T. Yano, and T. Iseki, "Synthesis and Mechanical Properties of Ti_3SiC_2 ," *Trans. Met. Soc. Jpn.*, **14A**, 597 (1993).
2. C. Racault, F. Langlais, and R. Naslain, "Solid State Synthesis and Characterization of the Ternary Phase Ti_3SiC_2 ," *J. Mater. Sci.*, **29**, 3384–92 (1994).
3. I. M. Low, "Depth-Profiling of Phase Composition in a Novel Ti_3SiC_2/TiC System With Graded Interfaces," *Mater. Lett.*, **58**, 927 (2004).
4. Z. Oo, I. M. Low, and B. H. O'Connor, "Dynamic Study of the Thermal Stability of Impure Ti_3SiC_2 in Argon and Air by Neutron Diffraction," *Physica B*, **385–386**, 499–501 (2006).
5. E. Wu, E. H. Kisi, S. J. Kennedy, and A. J. Studer, "In Situ Neutron Powder Diffraction Study of Ti_3SiC_2 Synthesis," *J. Am. Ceram. Soc.*, **84**, 2281–8 (2001).
6. A. Feng, T. Orling, and Z. A. Munnir, "Field-Activated Pressure-Assisted Combustion Synthesis of Polycrystalline Ti_3SiC_2 ," *J. Mater. Res.*, **14**, 925–39 (1999).
7. N. F. Gao, Y. Miyamoto, and D. Zhang, "On Physical and Thermochemical Properties of High-Purity Ti_3SiC_2 ," *Mater. Lett.*, **55**, 61–6 (2002).
8. P. Eklund, C. Virojanadara, J. Emmerlich, L. I. Johansson, H. Höglberg, and L. Hultman, "Photoemission Studies of Ti_3SiC_2 and Nanocrystalline-TiC/Amorphous Nanocomposite Thin Films," *Phys. Rev. B*, **74**, (2006), Art. No. 045417.

- ⁹J. Emmerlich, D. Music, P. Eklund, O. Wilhelmsson, U. Jansson, J. M. Schneider, H. Högberg, and L. Hultman, "Thermal Stability of Ti_3SiC_2 Thin Films," *Acta Mater.*, **55**, 1479–88 (2007).
- ¹⁰T. El-Raghy, M. W. Barsoum, and M. Sika, "Reaction of Al With Ti_3SiC_2 in the 800–1000°C Temperature Range," *Mater. Sci. Eng. A*, **298**, 174–8 (2001).
- ¹¹M. W. Barsoum, T. El-Raghy, L. Farber, M. Amer, R. Christini, and A. Adams, "The Topotactic Transformation of $TiSiC$ into a Partially Ordered Cubic $Ti(CSi)$ Phase by the Diffusion of Si into Molten Cryolite," *J. Electrochem. Soc.*, **146**, 3919 (1999).
- ¹²W. L. Gu, C. K. Yan, and Y. C. Zhou, "Reactions Between Al and Ti_3SiC_2 in Temperature Range of 600–650°C," *Scripta Mater.*, **49**, 1075–80 (2003).
- ¹³M. W. Barsoum and T. El-Raghy, "Synthesis and Characterization of Remarkable Ceramic: Ti_3SiC_2 ," *J. Am. Ceram. Soc.*, **79**, 1953–6 (1996).
- ¹⁴M. W. Barsoum and T. El-Raghy, "A Progress Report on Ti_3SiC_2 , Ti_3GeC_2 , and H-Phases, M_2BX ," *J. Mater. Synth. Process.*, **5**, 197 (1997).
- ¹⁵T. El-Raghy and M. W. Barsoum, "Processing and Mechanical Properties of Ti_3SiC_2 : I, Reaction Path and Microstructure Evolution," *J. Am. Ceram. Soc.*, **82**, 2849–54 (1999).
- ¹⁶N. Tzenov, M. W. Barsoum, and T. El-Raghy, "Influence of Small Amounts of Fe and V on the Synthesis and Stability of Ti_3SiC_2 ," *J. Eur. Ceram. Soc.*, **20**, 801–6 (2000).
- ¹⁷R. Radakrishnan, J. J. Williams, and M. Akinc, "Synthesis and High-Temperature Stability of Ti_3SiC_2 ," *J. Alloys Compd.*, **285**, 85–8 (1999).
- ¹⁸M. W. Barsoum and T. El-Raghy, "Synthesis and Characterization of a Remarkable Ceramic: Ti_3SiC_2 ," *J. Am. Ceram. Soc.*, **79**, 1953 (1996).
- ¹⁹R. J. Hill and C. J. Howard, "Quantitative Phase Analysis from Neutron Powder Diffraction Data Using the Rietveld Method," *J. Appl. Crystallogr.*, **20**, 467 (1987).
- ²⁰S. Hull, R. I. Smith, W. David, A. Hannon, J. Mayers, and R. Cywinski, "The POLARIS Powder Diffractometer at ISIS," *Physica B*, **180–181**, 1000–2 (1992).
- ²¹A. C. Larson and R. B. Von Dreele, "General Structure Analysis System GSAS"; *Report LAUR 86-748*, Los Alamos National Laboratory, 1984.
- ²²I. M. Low, D. Lawrence, and R. I. Smith, "Factors Controlling the Thermal Stability of Aluminium Titanate in Vacuum," *J. Am. Ceram. Soc.*, **88**, 2957 (2005).
- ²³I. M. Low, Z. Oo, and B. H. O'Connor, "Effect of Atmospheres on the Thermal Stability of Aluminium Titanate," *Physica B*, **385–386**, 502–4 (2006).
- ²⁴I. M. Low, Z. Oo, B. H. O'Connor, and K. E. Prince, "Effect of Oxygen Partial Pressure on the Phase Stability of Ti_3SiC_2 ," *Ceram. Eng. Sci. Proc.*, **26**, 323–30 (2005).
- ²⁵D. P. Riley, D. J. O'Connor, P. Dastoor, N. Brack, and P. J. Pigram, "Comparative Analysis of Ti_3SiC_2 and Associated Compounds Using X-Ray Diffraction and X-Ray Photoelectron Spectroscopy," *J. Phys. D*, **35**, 1603–11 (2002).
- ²⁶M. Naka, H. Sakai, M. Maeda, and H. Mori, "Formation and Thermal Stability of Amorphous Ti–Si–C Alloys," *Mater. Sci. Eng. A*, **226–228**, 774 (1997).
- ²⁷I. M. Low, "Vickers Contact Damage of Micro-Layered Ti_3SiC_2 ," *J. Eur. Ceram. Soc.*, **18**, 709 (1998).
- ²⁸I. M. Low, S. K. Lee, M. W. Barsoum, and B. Lawn, "Contact Hertzian Response of Ti_3SiC_2 Ceramics," *J. Am. Ceram. Soc.*, **81**, 225 (1998).
- ²⁹S. Williams, "Transition-Metal Carbides," *Prog. Solid State Chem.*, **6**, 57–118 (1971).
- ³⁰M. W. Barsoum, "MAX Phases: A New Class of Solids; Thermodynamically Stable Nanolaminates," *Prog. Solid State Chem.*, **28**, 201 (2000).
- ³¹Y. Zhou and Z. Sun, "Crystallographic Relations Between Ti_3SiC_2 and TiC ," *Mater. Res. Innovations*, **3**, 286–91 (2000).
- ³²W. S. Williams, "Physics of Transition Metal Carbides," *Mater. Sci. Eng. A*, **105/106**, 1–10 (1988).
- ³³M. W. Barsoum, "Comment on Reaction Layers Around SiC Particles in Ti: An Electron Microscopy Study," *Scripta Mater.*, **43**, 285–6 (2000).
- ³⁴T. El-Raghy and M. W. Barsoum, "Diffusion Kinetics of the Carburization and Silicidation of Ti_3SiC_2 ," *J. Appl. Phys.*, **83**, 112–9 (1998). □

2.6 Dynamic Study of the Thermal Stability of Impure Ti_3SiC_2 in Argon and Air by Neutron Diffraction.

OO, Z., LOW, I. M. & O' CONNOR, B. H. 2006. Dynamic Study of the Thermal Stability of Impure Ti_3SiC_2 in Argon and Air by Neutron Diffraction, *Physica B*, 385-386, 499-501.



Dynamic study of the thermal stability of impure Ti_3SiC_2 in argon and air by neutron diffraction

Z. Oo^{a,*}, I.M Low^a, B.H. O'Connor^b

^a*School of Engineering and Science, Curtin University of Technology, Sarawak Campus, CDT 250, 98009 Miri, Sarawak, Malaysia*

^b*Materials Research Group, Department of Applied Physics, Curtin University of Technology, GPO Box U1987, WA 6845, Australia*

Abstract

The dynamic thermal stability and topotactic phase transition of impure Ti_3SiC_2 in air and argon have been investigated by neutron diffraction (ND). In the presence of a low oxygen partial pressure as in argon, Ti_3SiC_2 underwent a surface dissociation and TiC and/or $\text{Ti}_5\text{Si}_3\text{C}$ were detected at 1200 °C. In contrast, oxide layers of rutile (TiO_2), TiO and cristobalite (SiO_2) were detected at ~1000, 1250 and 1300 °C respectively when exposed to an oxygen-rich environment. Near-surface depth profiling of Ti_3SiC_2 oxidized in air at 1200 °C by secondary ion mass spectroscopy (SIMS) has revealed a distinct gradation in phase composition at the interface of homogeneous rutile and heterogeneous cristobalite–rutile layers.

© 2006 Elsevier B.V. All rights reserved.

Keywords: Ti_3SiC_2 ; TiC; Neutron diffraction; Oxidation; Thermal stability; Rutile; Cristobalite

1. Introduction

Titanium silicon carbide (Ti_3SiC_2) exhibits a unique combination of mechanical, electrical, thermal and physical properties such as good high-temperature strength, and excellent corrosion and damage resistance [1–5]. This remarkable ceramic has electrical and thermal conductivities greater than that of titanium and machinability similar to graphite. However, Ti_3SiC_2 is thermally stable in air only up to ~1700 °C. Recently, we have observed the dissociation of Ti_3SiC_2 in vacuum to form TiC at a temperature well below 1700 °C [6–10]. In atmospheres of low oxygen partial pressure, the formation of TiC as a surface layer commenced at ~1200 °C and it grew rapidly in thickness with rising temperature. In contrast, it oxidizes to rutile (TiO_2) and cristobalite (SiO_2) at elevated temperature in the presence of high oxygen partial pressure such as air [10,11].

In this paper, the in situ thermal stability of impure Ti_3SiC_2 in argon and air has been investigated by neutron diffraction (ND) in the temperature range 23–1400 °C and analysed using the Rietveld method. The role of the oxygen

partial pressure on the chemistry of thermal dissociation in argon and diffusion-controlled oxidation in air is discussed.

2. Experimental procedures

Samples of Ti_3SiC_2 were fabricated by mixing the proper molar ratio of Ti, SiC and C powders in Tubular mixer for at least 1 h. The powder mixture was then placed in a steel mould, uniaxially pressed at 150 MPa and then reaction sintered in an Eletec vacuum furnace (~ 10^{-5} Torr) at 1500 °C for 1 h, followed by hot-isostatic pressing in argon for 2 h at 1650 °C at a pressure of 150 MPa. The HIPed cylindrical samples were 15 mm in diameter, 20 mm in height and contained ~30% open pores.

The in situ ND of HIPed Ti_3SiC_2 in air and argon was performed using a medium-resolution powder diffractometer (MRPD) [12] located at the Australian Nuclear Science and Technology Organization (ANSTO), Lucas Heights, NSW. The MRPD was used to monitor the bulk evolution of dissociation-induced phase changes within the cylindrical bars of HIPed Ti_3SiC_2 from 23 to 1350 °C in air and from 23 to 1400 °C in argon, using a wavelength of 1.665 Å. The holding time at each temperature was 2 h and the angle range 2θ was 10–135°. The relative abundances of

*Corresponding author.

E-mail address: zeyaa.oo@curtin.edu.my (Z. Oo).

the phases formed were computed using the Rietveld refinement method. The models of Kisi et al. (ICSD #86213) for Ti_3SiC_2 , Christensen et al. (ICSD #1546) for TiC, Shintani et al. (ICSD #64987) for TiO_2 -rutile, Liu et al. (ICSD #44094) for SiO_2 -Cristobalite, Fleming et al. (ICSD #43801) for SiO_2 -Tridymite and Loehman et al. (ICSD #60483) for TiO were used for the Rietveld analysis.

A Cameca ims-5f SIMS was used for the depth profiling of air-oxidized Ti_3SiC_2 samples through the elemental imaging of titanium, carbon, silicon and oxygen on the near-surface. The enhanced elemental sensitivity of SIMS allows the detection of oxygen within the structure of the surface oxide layers. Positive secondary ion depth profiles were taken using 150 nA primary Cs^+ ion current at 3 keV impact energy, rastered over a $250 \times 250 \mu\text{m}^2$ area. The ion count rates in all mass channels were normalized to Cs^+ secondary ion counts rate to minimize the effect of variations in the primary ion beam current.

3. Results and discussion

Fig. 1 shows the temperature dependence of the relative phase abundances during the dissociation of Ti_3SiC_2 in argon. From room temperature to 1000°C , the phase concentrations of Ti_3SiC_2 and TiC remain quite stable and constant. At 1100°C , Ti_3SiC_2 commences to dissociate to form TiC. Below 1200°C , the thermal-dissociation process is slow but the process becomes quite rapid from 1250 to 1400°C . In addition, a small amount of $\text{Ti}_5\text{Si}_3\text{C}$ is observed as a transient phase from 20 to 1400°C . This phase is believed to form during the initial decomposition stage of Ti_3SiC_2 and converts to the stable TiC at elevated temperature. Rutile (TiO_2) is also observed to have formed

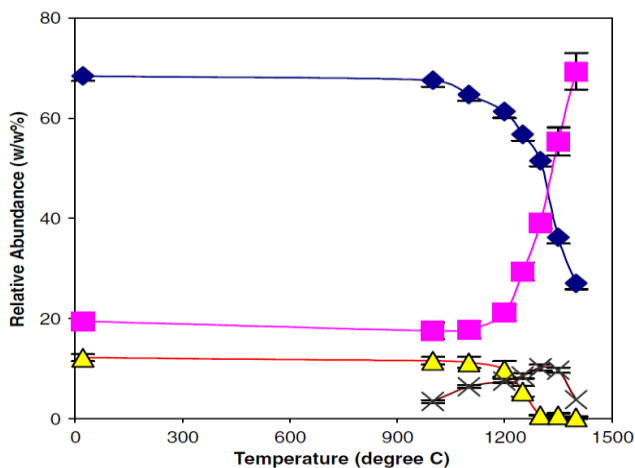
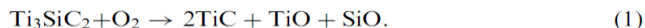


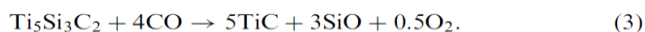
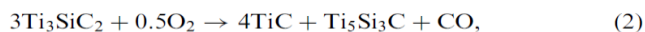
Fig. 1. Relative phase abundances of TiC (■), $\text{Ti}_5\text{Si}_3\text{C}$ (Δ), Ti_3SiC_2 (◆) and TiO_2 (×) present during the heat treatment of Ti_3SiC_2 in argon from room temperature to 1400°C . Error bars indicate two estimated standard deviations $\pm 2\sigma$.

with an initial content of $\sim 3.4\text{wt}\%$ at 1000°C due to partial oxidation. Its content increases to $\sim 10.1\text{wt}\%$ at 1300°C but decreases again to $3.7\text{wt}\%$ at 1400°C .

From this study, the sintered Ti_3SiC_2 appeared to be thermally unstable in argon from 1100°C and above. A small amount of TiO_2 also formed as a result of partial oxidation due to the fact that the alumina tube used to deliver the argon became porous at elevated temperatures. The intermediate phase $\text{Ti}_5\text{Si}_3\text{C}$ slowly disappeared at around 1400°C but significant amounts of Ti_3SiC_2 and TiC remained. In the presence of a very low oxygen partial pressure, it was previously postulated that the surface of Ti_3SiC_2 might undergo a high-temperature thermal-dissociation process to form TiC as follows [8]:



However, this chemical reaction is inconsistent with the above observations and it does not explain the existence of $\text{Ti}_5\text{Si}_3\text{C}$. According to Wu et al. [13] the growth of Ti_3SiC_2 upon crystallites of $\text{Ti}_5\text{Si}_3\text{C}$ occurs during the synthesis of Ti_3SiC_2 . It follows that the reverse reaction will prevail during the thermal dissociation of Ti_3SiC_2 . The dissociation of Ti_3SiC_2 – $\text{Ti}_5\text{Si}_3\text{C}$ is deemed more favourable to TiC because silicon has a low diffusion rate in TiC-related systems. Thus the $\text{Ti}_5\text{Si}_3\text{C}$ phase is more likely to nucleate on Ti_3SiC_2 because this mechanism would not contain any long-range diffusion of Si atoms. In view of this, it is proposed that the pathways for the topotactic thermal dissociation of Ti_3SiC_2 in the presence of low oxygen partial pressure together with the release of reducing gas CO to form TiC and $\text{Ti}_5\text{Si}_3\text{C}$ are as follows:



The proposed volatility of CO, SiO and O_2 released is consistent with the observed results of reduced Ti_3SiC_2

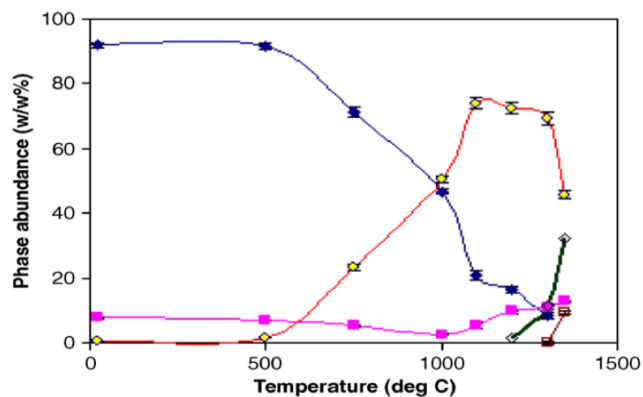


Fig. 2. Relative phase abundances of TiC (■), TiO_2 (◇), Ti_3SiC_2 (◆) TiO (◇) and SiO_2 (□) during the oxidation of Ti_3SiC_2 in air from room temperature to 1350°C . Error bars indicate two estimated standard deviations $\pm 2\sigma$.

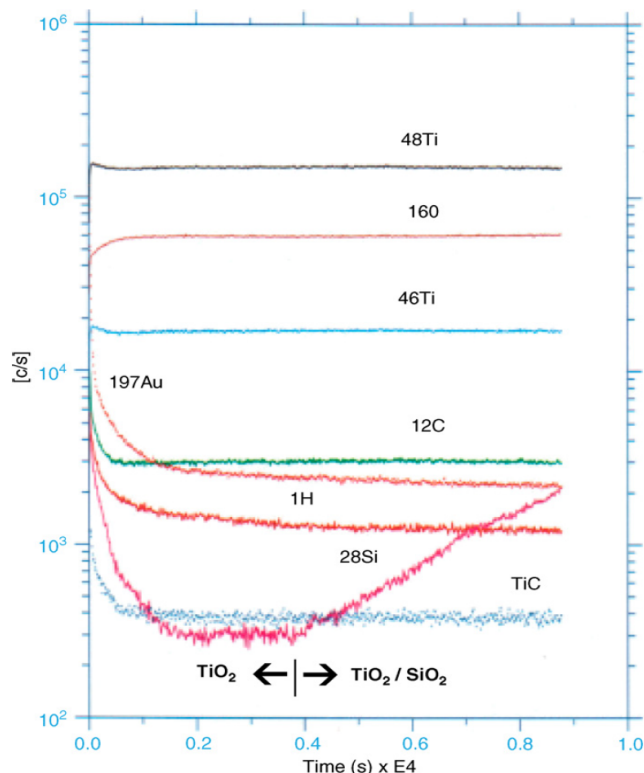


Fig. 3. Elemental composition versus time/depth in air-oxidized Ti_3SiC_2 at 1200°C for 15 min. Note the rapid rise in the Si content at time $>4000\text{s}$.

mass following the heat treatment in vacuum or argon [8,9]. The release of O_2 in reaction (3) may also contribute to the partial oxidation of Ti_3SiC_2 as observed in Fig. 1.

Fig. 2 shows the phase evolution of Ti_3SiC_2 during oxidation and relative abundance of oxidized phases formed at various temperatures as revealed by in situ ND. Before oxidation, the phases present in sample were mainly Ti_3SiC_2 with TiC as a minor phase. At $\sim 750^\circ\text{C}$, a portion of Ti_3SiC_2 commenced to oxidize to form rutile (TiO_2) which reached a maximum content of $\sim 75\text{wt}\%$ at 1100°C before it started to become unstable and decomposed to form TiO. It is interesting to note that the increase in content of TiO from 1100 to 1350°C is commensurate with a decrease in the content of TiO_2 . This suggests that a zone of low oxygen partial pressure existed within the

sample during oxidation which facilitated the reduction process as follows:



Since the process of oxidation is diffusion controlled by the ingress of oxygen, a zone deficient in oxygen can exist within the bulk of sample during oxidation. As previously mentioned, the reduction reaction of TiO_2 to form TiO is highly possible when an atmosphere of low oxygen partial pressure exists, as indicated by Reactions (1)–(3). This hypothesis is further corroborated by the observation of an increasing TiC content at the same temperature range when TiO is formed (see Fig. 1).

Fig. 3 shows the existence of an outer surface layer of TiO_2 on Ti_3SiC_2 that was oxidized at 1200°C for 15 min as revealed by SIMS. Interestingly, an inner layer of duplex $\text{TiO}_2/\text{SiO}_2$ is also evident which serves to suggest the formation of a glassy phase prior to its devitrification to form cristobalite at 1350°C .

Acknowledgements

IML is grateful to AINSE (99/030, 00/90P, 01/091, 02/075 and 05/106P) to provide fundings for the HIPing of Ti_3SiC_2 samples and the collection of MRPD and SIMS. We thank Drs. D. Perera, A. Studer, K. Prince and Mr. A. Atanacio of ANSTO for experimental assistance in HIPing and the collection of MRPD and SIMS data, respectively.

References

- [1] M.W. Barsoum, T. El-Raghy, *J. Am. Ceram. Soc.* 79 (1996) 1953.
- [2] M.W. Barsoum, D. Brodtkin, T. El-Raghy, *Scr. Metall. et Mater.* 36 (1997) 535.
- [3] M.W. Barsoum, T. El-Raghy, *Metall. Mater. Trans.* 30A (1999) 363.
- [4] I.M. Low, *J. Eur. Ceram. Soc.* 18 (1998) 709.
- [5] I.M. Low, S.K. Lee, M. Barsoum, B. Lawn, *J. Am. Ceram. Soc.* 81 (1998) 225.
- [6] I.M. Low, P. Manurung, R.I. Smith, D. Lawrence, *Key Eng. Mater.* 224–226 (2002) 465.
- [7] I.M. Low, M. Singh, P. Manurung, E. Wren, D.P. Sheppard, M.W. Barsoum, *Key Eng. Mater.* 224–226 (2002) 505.
- [8] I.M. Low, Z. Oo, *J. Aust. Ceram. Soc.* 38 (2002) 112.
- [9] I.M. Low, *Mater. Lett.* 58 (2004) 927.
- [10] I.M. Low, Z. Oo, B.H. O'Connor, K.E. Prince, in: D. Zhu, W.M. Kriven (Eds.), *Ceramic Engineering and Science Proceedings*, vol. 26, issue 3 and 4, 2005, pp. 323–330.
- [11] I.M. Low, E. Wren, *J. Aust. Ceram. Soc.* 39 (2003) 103.
- [12] S.J. Kennedy, *Adv. X-ray Anal.* 38 (1994) 35.
- [13] E. Wu, E.H. Kisi, S.J. Kennedy, A. Studer, *J. Am. Ceram. Soc.* 88 (2001) 81.

3. CONCLUSIONS

The effect of atmosphere and annealing time on the thermal stability of Al_2TiO_5 -based functionally-graded ceramics was investigated. The effect of atmospheres (i.e., 100% air, 100% argon, and the combination of 50% oxygen and 50% argon) on the isothermal stability of Al_2TiO_5 at 1100°C was analysed.

The major conclusions are as follows:

1. Al_2TiO_5 was stable with no apparent phase decomposition for up to 5 h at 1100°C in air. Further ageing caused only about 5% of decomposition.
2. Significant phase decomposition was observed when Al_2TiO_5 was aged at 1100°C for 5 h in an argon atmosphere. More than 98 wt% of the Al_2TiO_5 was decomposed to form corundum (Al_2O_3) and rutile (TiO_2).
3. There was a marked difference in the effect of atmosphere on the isothermal stability of Al_2TiO_5 at 1100°C. In an atmosphere of 50% argon and 50% oxygen, the decomposition rate was considerably reduced as compared to 100% argon, but Al_2TiO_5 was fairly stable with no decomposition in air for up to 5 h dwell. It was found that the rate of phase decomposition of Al_2TiO_5 is dependent on the atmosphere or oxygen partial pressure during isothermal ageing. The oxygen partial pressure in the atmosphere played a key role in triggering the thermal instability of Al_2TiO_5 .

The effect of temperature and annealing time, on the thermal stability of Al_2TiO_5 in the temperature range of 20–1400°C, was also studied.

The major conclusions are as follows:

1. Below 1100°C in air, Al_2TiO_5 was relatively stable but became visibly unstable at between 1100–1280°C, decomposing to ~55 wt% corundum (Al_2O_3) and ~45 wt% rutile (TiO_2). Beyond 1300°C, the thermal decomposition was arrested and the phase stability was restored.

2. When the previously decomposed Al_2TiO_5 sample was re-heated from room temperature to 1450°C for 2 h, self-recovery took place through the rapid reaction of corundum (Al_2O_3) and rutile (TiO_2) to form Al_2TiO_5 with greater than ~ 98 wt% phase purity.
3. During cooling from 1450°C to room temperature, it was found that Al_2TiO_5 was quite stable up to 1200°C , without any visible phase degradation.
4. Upon further cooling from 1200 to 1000°C , rapid decomposition of Al_2TiO_5 commenced with ~ 20 wt% of sample decomposed at 1000°C . At temperatures below 1000°C , the decomposition of Al_2TiO_5 was insignificant.
5. Al_2TiO_5 exhibited a slower rate of decomposition in non-isothermal than in isothermal conditions. The process of decomposition was reversible and self-recovery occurred readily when decomposed Al_2TiO_5 was re-heated above 1300°C . It was further shown that the existence of a temperature range in the decomposition of Al_2TiO_5 could be explained by the differences in the self-recovery rates at $\geq 1280^\circ\text{C}$ and in decomposition at $\leq 1280^\circ\text{C}$.

The effect of atmosphere on the phase stability of Ti_3SiC_2 in vacuum in the temperature range of $1000^\circ\text{-}1500^\circ\text{C}$ was investigated.

The major conclusions are as follows:

1. There was no apparent dissociation of Ti_3SiC_2 to form TiC at temperatures below 1100°C . However, at 1100°C onwards, Ti_3SiC_2 commenced to dissociate to form TiC at a slow rate initially, but the process became quite rapid from 1400°C to 1500°C .
2. Phases of TiC (~ 90 wt%), $\text{Ti}_5\text{Si}_3\text{C}_x$ (~ 9 wt%) and Ti_3SiC_2 (~ 1 wt%) were observed on the existence of the graded composition at the near top surface (~ 5 μm) of Ti_3SiC_2 vacuum-annealed at 1500°C for 8 h. The TiC content decreased rapidly

with an increase in depth. The amount of $\text{Ti}_5\text{Si}_3\text{C}$ increased to a maximum value of over 60 wt% at a depth of $\sim 30 \mu\text{m}$.

The phase stability of Ti_3SiC_2 in argon for temperatures ranging from 23°C (room temperature) to 1400°C was studied.

The major conclusions are as follows:

1. In-situ neutron diffraction study of the thermal dissociation of Ti_3SiC_2 in argon showed that Ti_3SiC_2 was thermally unstable at 1200°C and it commenced to dissociate to form TiC. Below 1200°C , the thermal-dissociation process was slow but from 1250°C to 1400°C , the process became quite rapid.
2. The intermediate phase of $\text{Ti}_5\text{Si}_3\text{C}$ was observed in the temperature range of 23°C to 1400°C . The phase abundance of $\text{Ti}_5\text{Si}_3\text{C}$ slowly decreased between 1200°C and 1300°C and finally disappeared at 1400°C . This transient phase was believed to convert eventually into stable TiC at 1500°C .

The oxidation behavior of Ti_3SiC_2 in air, for temperatures ranging from 1000°C to 1500°C was also studied.

The major conclusions were as follows:

1. In air, Ti_3SiC_2 oxidized readily to rutile (TiO_2) and cristobalite (SiO_2). During the oxidation of Ti_3SiC_2 , at $\sim 600^\circ\text{C}$, formation of amorphous-like anatase (TiO_2) commenced and at 750°C , rutile (TiO_2) formed. The maximum content of ~ 75 wt % of rutile (TiO_2) was formed on the outer surface at 1100°C and ~ 30 wt% of cristobalite (SiO_2) was observed at 1350°C .
2. At the temperature range of 1100 to 1350°C , the TiO content increased whereas the content of rutile (TiO_2) decreased. This implies the presence of a zone of low oxygen partial pressure during oxidation.

3. Below 1000°C, a duplex layer of TiO₂ and SiO₂ initially formed as a glassy phase in the inner layer before it crystallized to cristobalite at temperatures greater than 1300°C. Between 1300°C and 1350°C, the crystallization of cristobalite was observed. However, this glassy phase can readily devitrify to form tridymite when it is cooled from 1100°C to room temperature.

4. RECOMMENDATIONS FOR FURTHER WORK

The effects of atmosphere, isothermal annealing and oxygen partial pressure on the thermal stability of Al₂TiO₅ have been studied for high-temperature applications. The grain-size has been shown to affect the propensity of thermal degradation in Al₂TiO₅. Coarse-grained Al₂TiO₅ exhibited the slowest rate of thermal decomposition, when compared to medium and fine-grained counterparts. The thermal stability of Al₂TiO₅ increases as the grain-size increases. However, the effect of grain sizes on the kinetics of thermal stability is still not fully understood yet.

Suggestions for further work on Al₂TiO₅-based ceramics:

- In order to better understand, how thermal stability is critical in the development of low thermal expansion materials, the effect of different grain-sizes (coarse, medium, and fine) of Al₂TiO₅ on thermal stability should be further investigated.
- The inter-relationship between the microcracking phenomenon of Al₂TiO₅ and increasing grain sizes needs to be analyzed.
- The choice of method for doping Al₂TiO₅-based composites with sintering aid should be investigated in order to find out its effect on the resulting properties such as low thermal expansion, high thermal shock resistance, unique mechanical, thermal stability properties, and good insulating property as required for materials in efficient engine parts (such as catalytic converters, and diesel engine components) in the automobile, aircraft and other related industries.

A high-temperature vacuum annealing process was proposed for the designing of Ti_3SiC_2 -TiC composites with graded interfaces. In the presence of vacuum or controlled atmosphere of low oxygen partial pressure, it was found that Ti_3SiC_2 decomposed to form a surface layer of nonstoichiometric TiC_x and/or $\text{Ti}_5\text{Si}_3\text{C}_x$ at temperatures above 1200°C . Also, the composition depth profiling at the near surface of vacuum-annealed Ti_3SiC_2 by XRD and SIMS, revealed composition gradation in the phase distribution of TiC_x and $\text{Ti}_5\text{Si}_3\text{C}_x$. Results showed that the phase stability and transition of Ti_3SiC_2 at elevated temperatures were strongly dependent on the oxygen partial pressure of the annealing atmosphere of the furnace.

There remain several unresolved issues which relate to the thermal and phase stability of Ti_3SiC_2 :

- understanding of phase stability of ternary carbides in vacuum and inert atmosphere.
- purity of samples
- vapour pressure of A elements
- surface chemistry and kinetics of dissociation process.
- temperature range and annealing time.
- heating elements used.

Suggestions for further work on Ti_3SiC_2 -based ceramics are as follows:

- An important future research direction for MAX phases is the systematic experimental studies of phase stability property.
- On the synthesis side, research directions that should be pursued further include low temperature deposition of MAX phases (for thin-films), where novel approaches to reduce the deposition temperature below 400°C would be important for widespread thin-film applications, such as low friction surfaces, electrical contacts, sensors, and tunable damping films for micro-electromechanical systems.

- All the results from current research further underline the main point that the decomposition temperature depends strongly on the controlled atmosphere and impurities. The vacuum annealing experiments showed that the chemical potential of Si in the various environments will determine the stability of Ti_3SiC_2 . This reasoning is generally applicable to all MAX phases.
- For better understanding, theoretical prediction of thermal stability of the high temperature resistance material Ti_3SiC_2 , will be required. The phase stability of MAX phases is still needed to be fully understood. The vapour pressure of element “A” is critical to the phase stability of MAX phases. If the vapour pressure of element “A” is high, the more susceptible the MAX phase is to phase dissociation at higher temperature.

The oxidation behavior of Ti_3SiC_2 , and its composition profile and phase transition have been studied in the temperature range of 20°-1400°C by ND and XRD. The results show that, anatase formed at 600°C and TiO_2 (rutile) formed at temperatures of 750°C and above; at 1350°C, slow formation of SiO_2 (cristobalite) was observed. SIMS analysis of the oxidation results showed a gradation in phase composition at the interface of the homogeneous rutile and heterogeneous cristobalite –rutle layers.

Suggestions for further work on oxidation behavior of Ti_3SiC_2 material are as follows:

Ti_3SiC_2 is considered a material suitable for applications at high temperatures, where the growth rates of the oxide layer formation, with respect to time and temperature, are found to be small, indicating that Ti_3SiC_2 has good oxidation resistance (Barsoum et al. 1997). Other MAX phase materials could be similarly investigated to determine their respective temperature ranges for good oxidation resistance. This would help to identify materials suitable for application at high temperatures, such as $\text{Ti}_3(\text{SiAl})\text{C}_2$, whose oxidation resistance may be improved by doping with Nb, Hf or Zr (Zheng et al. 2011).

Since SiC is thermodynamically stable with Ti_3SiC_2 and SiC has excellent oxidation resistance (Sun, 2011), Ti_3SiC_2 -SiC was the earliest MAX based composite synthesized and investigated (Tong et al. 1995). The oxidation growth rates and the weight change per unit area as a function of time and temperature of advanced Ti_3SiC_2 composites should be investigated to seek further improvement of their oxidation resistance. This Ti_3SiC_2 -SiC composite model should be developed for better understanding of the enhanced mechanisms of oxidation resistance.

More experimental investigations on the oxidation properties of Ti_3SiC_2 are needed to improve its oxidation resistance, for example, monitoring the phase composition of oxide scales and the thickness of oxide layer of $\text{Ti}_3(\text{SiAl})\text{C}_2$ at 1600°C by using Zr, Hf, or Nb doping. Doping would cause the slow-down of oxygen diffusion through the surface and bulk of Ti_3SiC_2 at high temperatures and thus the formation of thinner oxide layers and smaller grain sizes (Zheng et al. 2011). It is suggested that further analysis of phase compositions of oxide scales for Ti_3SiC_2 could be carried out by using scanning electron microscopy/energy dispersive spectroscopy (SEM/EDS).

5. APPENDIX 1: SUPPLEMENTRY INFORMATION ON PUBLICATIONS

Appendix 1-A: Supplementary Information on “Effect of Atmospheres on the Thermal Stability of Aluminium Titanate”

LOW, I.M. OO. Z. & O’CONNOR, B.H. 2006. Effect of Atmospheres on the Thermal Stability of Aluminium Titanate. *Physica B*, 385-386, 502-504.

Supporting Information

The isothermal stability of Al_2TiO_5 at 1100°C in air, argon and a combination of air and argon has been discussed in this thesis. Further calculations, figures and tables have been used to support the data analysis as follows:

(a) Isothermal stability of Al_2TiO_5 at 1100°C in air

Neutron diffraction (ND) data collection was performed at the Australian Nuclear Science and Technology Organization (ANSTO) using the medium resolution powder diffraction (MRPD) and the Rietveld analysis method (Hill, Howard, and Hunter, 1995) to calculate the relative phase abundances.

The model of Epicier et al. (1991) for Al_2TiO_5 gave the most suitable and acceptable results. The refinement parameters were the background profile parameters (B's), 2θ -zero, scale factor (s), profile broadening parameters (U, V, W), lattice parameters (a, b, c), preferred orientation factor (PO), asymmetry factor (As), mixing parameter (γ) and atom isotropic thermal parameters (T). The atom coordinates (x, y, z) were not refined. The data sets of M22115 to M22127 were used to analyze isothermal stability of Al_2TiO_5 in air at 1100°C for 12 h. The neutron diffraction difference plots for Al_2TiO_5 in air at a temperature of 1100°C for 2 h is shown in Figure 5.1, and the figures-of-merit for samples obtained by Rietveld analysis are shown in Table 5.1.

For the quality of refinement, the R_B factors for the individual phases in each refinement with ND are 3 ~ 4% for Al_2O_3 , 2 ~ 7% for Al_2TiO_5 and 2 ~ 4% for TiO_2 . The goodness of fit (GOF) for ND is 3.6 from the refined results and the R_{exp} value is 4.9, which indicate that the qualities of refinements are acceptable. In Figures 5.1 and 5.2, the observed data are shown by a (+) sign, and the calculated data are indicated by a solid line (red). The vertical blue bars represent the Bragg peak positions for Al_2O_3 , Al_2TiO_5 , and TiO_2 from the top to the bottom respectively. The difference plot between observation and calculation is shown by the green line. The wavelength for ND is 1.665 \AA .

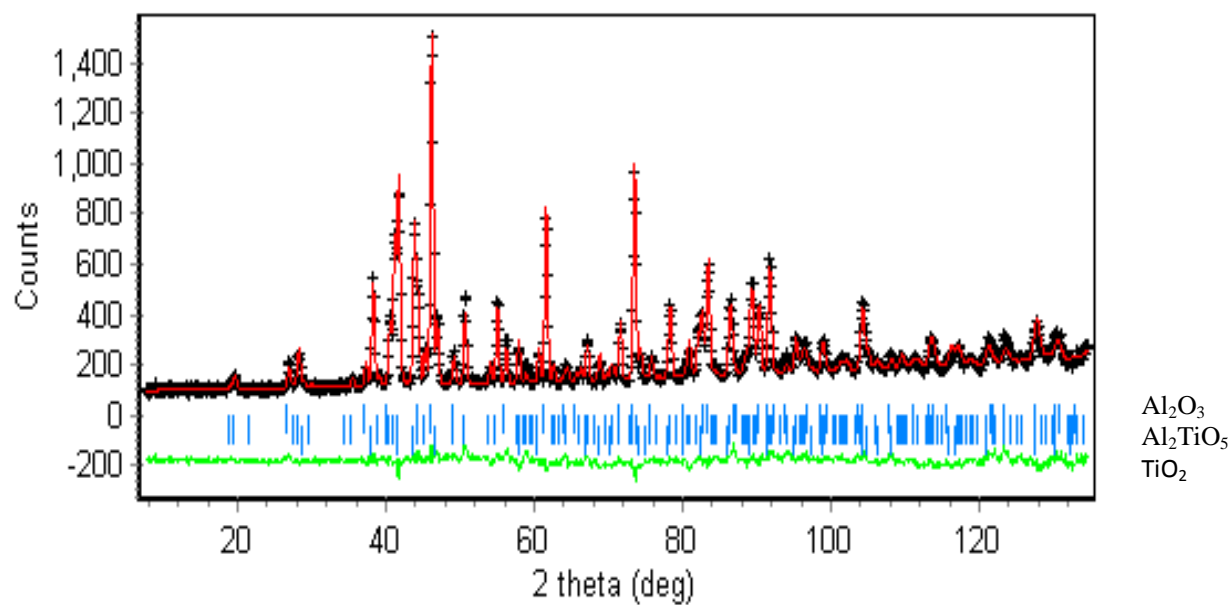


Figure 5.1: Neutron diffraction (MRPD) Rietveld difference plot for Al₂TiO₅ in air at 1100°C for 2 h.

Table 5.1 Figures-of-merit from Rietveld refinement with ND data for isothermal stability of Al_2TiO_5 in air at 1100°C .

Run number	Time (h)	R_{wp}	R_{exp}	GOF	R_{B} Al_2O_3	R_{B} Al_2TiO_5	R_{B} TiO_2
M22115	0	9.4	4.9	3.6	5.0	5.0	5.4
M22116	1	9.5	5.0	3.6	7.7	5.4	6.7
M22117	2	8.4	5.0	2.8	5.7	4.9	3.1
M22118	3	7.2	4.9	2.1	2.9	4.7	4.0
M22119	4	7.3	4.9	2.5	4.5	5.1	4.0
M22120	5	7.6	4.9	2.5	5.0	5.1	2.0
M22121	6	7.8	4.9	3.0	4.6	5.5	4.3
M22122	7	7.1	4.9	2.0	2.7	4.1	5.3
M22123	8	7.2	5.0	3.2	4.3	5.6	4.6
M22124	9	7.0	4.9	1.9	2.8	4.6	2.3
M22125	10	7.1	4.9	2.0	3.4	4.4	3.1
M22126	11	7.0	4.9	1.9	3.2	4.5	2.7
M22127	12	7.0	4.9	1.9	3.1	4.3	2.2

(b) Isothermal stability of Al_2TiO_5 at 1100°C in argon

The figures-of-merit for M22131-M22143 runs obtained by Rietveld analysis with the ND data are presented in Table 5.2. The R_B factors for the individual phases in each composition obtained from ND are approximately 2 to 7%. The GOF values range from 2.0 to 2.5, which indicate that the qualities of refinements are acceptable.

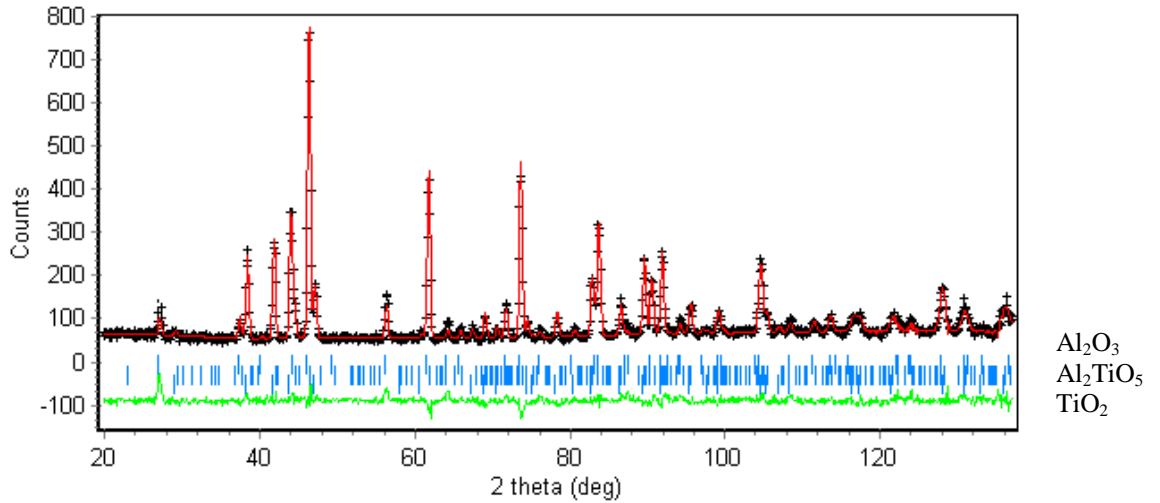


Figure 5.2: Neutron diffraction (MRPD) Rietveld difference plot for Al_2TiO_5 in argon at 1100°C for 2 h.

Table 5.2: Figures-of-merit from Rietveld refinement with ND data for isothermal stability of Al_2TiO_5 in argon at 1100°C .

Run number	Time (h)	R_{wp}	R_{exp}	R_{B} Al_2O_3	R_{B} Al_2TiO_5	R_{B} TiO_2	GOF
M22131	0	7.5	4.9	3.9	3.7	3.9	2.3
M22133	1	7.1	4.9	3.4	3.3	2.2	2.0
M22134	2	7.3	4.9	3.5	3.4	2.4	2.2
M22135	3	7.3	5.0	3.9	2.7	2.6	2.1
M22136	4	7.5	5.0	3.5	2.8	2.6	2.2
M22137	5	7.7	5.0	4.1	7.0	3.0	2.4
M22138	6	8.0	5.0	4.4	4.8	3.0	2.5
M22139	7	7.8	5.0	4.5	5.6	3.0	2.4
M22140	8	7.7	5.0	4.6	4.6	2.5	2.4
M22141	9	7.7	5.0	4.6	6.7	2.7	2.3
M22142	10	7.6	5.0	4.2	5.2	3.1	2.4
M22143	11	7.7	5.0	4.7	3.4	3.0	2.4

(c) Thermal instability of Al_2TiO_5 in the temperature range of 20-1400°C in air

The results of neutron diffraction studies on the thermal stability of Al_2TiO_5 in the temperature range 20–1400°C in air are shown in Figures 5.3 and 5.4. In addition, Figures 5.3 and 5.4 show the observed and calculated pattern, indicated by black crosses (+) sign, and solid line (red) respectively. Vertical blue bars represent the Bragg peak positions for Al_2O_3 , Al_2TiO_5 , and TiO_2 from the top to the bottom respectively. The difference plot between observation and calculation is shown by the green line. The wavelength for ND is 1.665Å.

Al_2TiO_5 was relatively stable at below 1100°C and became visibly unstable, decomposing to form corundum and rutile at between 1100°C -1280°C. Beyond 1300°C, the thermal decomposition was arrested and the phase stability was restored.

The success of refinement results, such as R_B values for Al_2O_3 , Al_2TiO_5 , TiO_2 , R_{wp} , R_{exp} and GOF, are shown in Table 5.3 with acceptable results ranging 1.3 to 1.7.

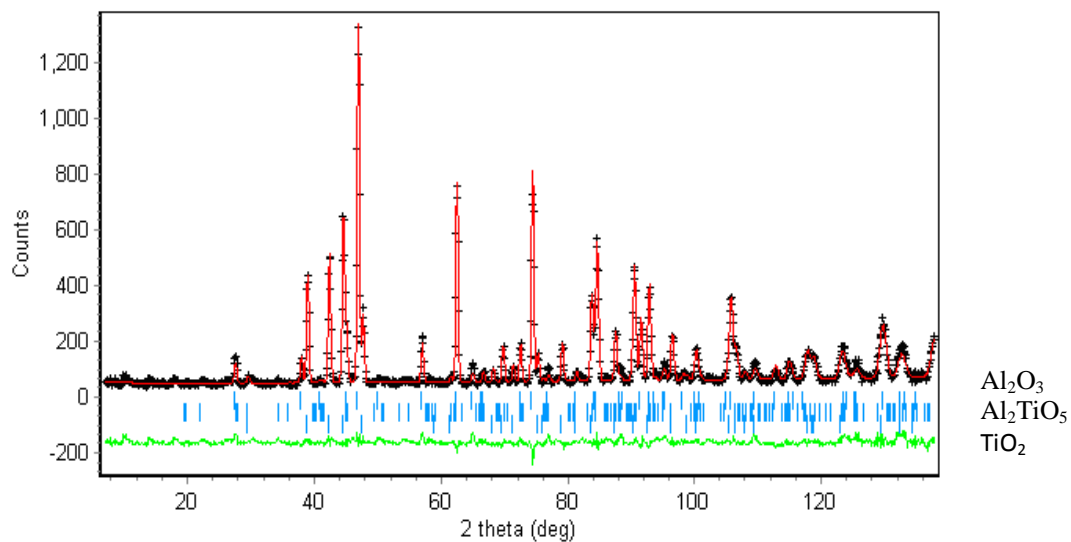


Figure 5.3: Neutron diffraction Rietveld difference plot for Al_2TiO_5 in air at room temperature.

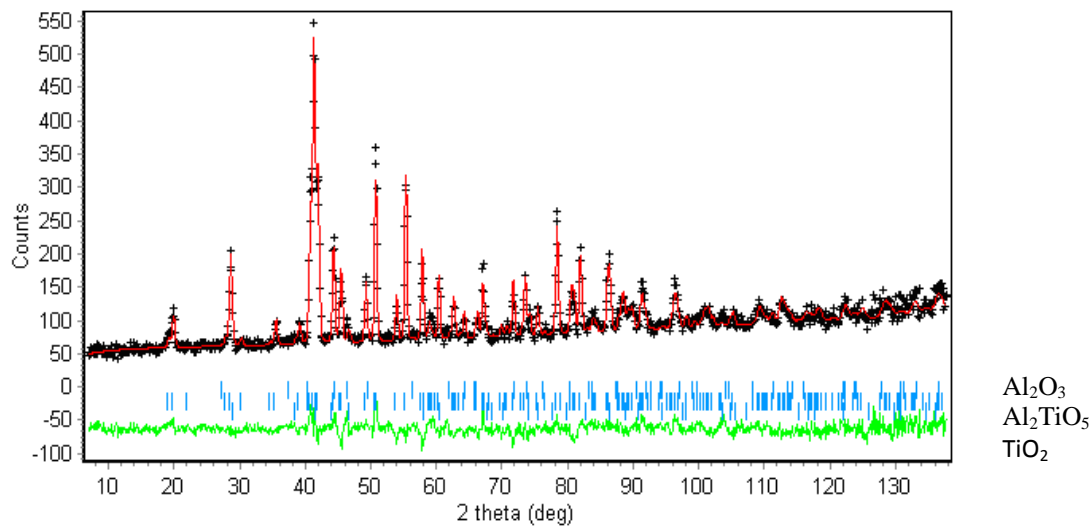


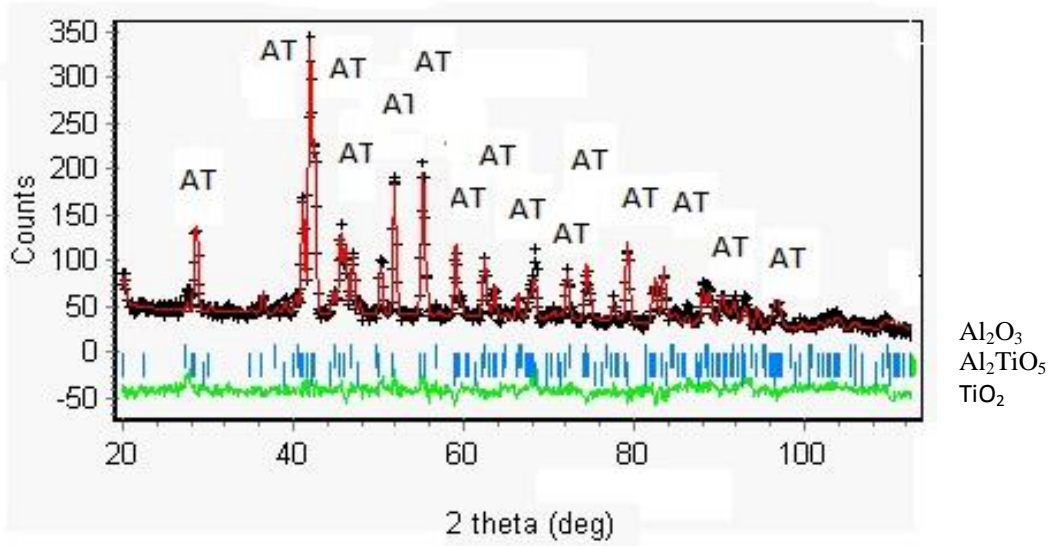
Figure 5.4: Neutron diffraction Rietveld difference plot for Al_2TiO_5 in air at 1400°C for 2 h.

Table 5.3: Figures-of-merit from Rietveld refinement of ND data for Al_2TiO_5 in air from room temperature to 1400°C .

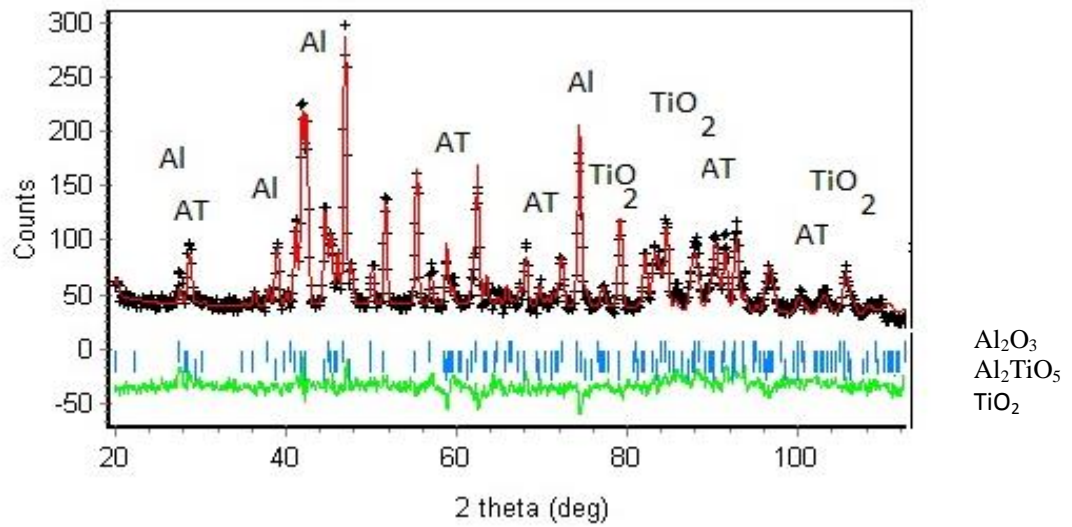
Temperature ($^\circ\text{C}$)	R_{wp}	R_{exp}	R_{B} for Al_2O_3	R_{B} for Al_2TiO_5	R_{B} for TiO_2	GOF
23	9.3	7.3	7.2	4.9	2.8	1.6
600	9.1	7.3	6.3	5.0	3.3	1.5
700	9.2	7.2	6.6	4.7	2.7	1.5
800	8.6	7.2	5.7	4.4	2.5	1.4
900	8.8	7.2	3.7	4.3	2.7	1.4
950	8.7	7.2	4.2	4.5	2.9	1.4
1000	9.0	7.2	3.7	4.5	1.9	1.5
1050	8.5	7.2	3.5	4.0	2.1	1.3
1100	8.7	7.2	4.3	3.9	1.8	1.4
1150	8.8	7.2	4.6	9.4	3.3	1.4
1200	9.0	7.3	4.1	4.3	4.4	1.5
1250	9.3	7.2	4.4	7.4	3.9	1.6
1300	9.4	7.1	5.1	5.2	3.9	1.7
1350	8.6	7.2	4.3	3.5	2.6	1.4
1400	8.8	7.4	3.2	6.5	2.1	1.4

(d) Isothermal stability of Al_2TiO_5 at 1100°C in atmosphere of 50% oxygen and 50% argon

The difference neutron diffraction plots of the refinement of Al_2TiO_5 at 1100°C in an atmosphere of 50% oxygen and 50% argon from 1 h to 16 h are investigated and their results are shown in Figure 5.5 (a) and (b). From Rietveld analysis, the qualities of fit are shown in the Table 5.4. Values such as R_p , R_{wp} , R_{exp} R_B factors for all phases and GOF are acceptable for the isothermal stability of Al_2TiO_5 .



(a)



(b)

Figure 5.5: ND diffraction Rietveld difference plots for isothermal stability Al_2TiO_5 at 1100°C in an atmosphere of 50% of oxygen and 50% of argon for (a) 1 h, and (b) 16 h . Legend: AT = Al_2TiO_5 , Al = Al_2O_3

Table 5.4: Figures-of-merit from Rietveld refinement with ND (MRPD) data for Al_2TiO_5 at 1100°C in the atmosphere of 50% oxygen and 50% argon from 1 h to 16 h.

Time (h)	R_{wp}	R_{exp}	R_{B} for Al_2O_3	R_{B} for Al_2TiO_5	R_{B} for TiO_2	GOF
1	10.74	6.33	8.08	6.24	4.22	2.8
4	10.27	6.21	8.00	5.29	4.10	2.8
8	10.63	6.19	5.92	5.45	4.98	2.9
12	10.82	6.17	5.91	5.89	5.23	3.0
16	11.21	6.28	8.38	7.26	4.29	3.1

Appendix 1-B: Supplementary Information on “In-Situ Diffraction study of Self-Recovery in Aluminium Titanate”.

Appendix 1-C: Supplementary Information on “Reformation of Phase Composition in Decomposed Aluminium Titanate”

LOW, I.M. & OO, Z. 2008. In-Situ Diffraction Study of Self-Recovery in Aluminium Titanate. *Journal of the American Ceramic Society*, 91, 1027-1029.

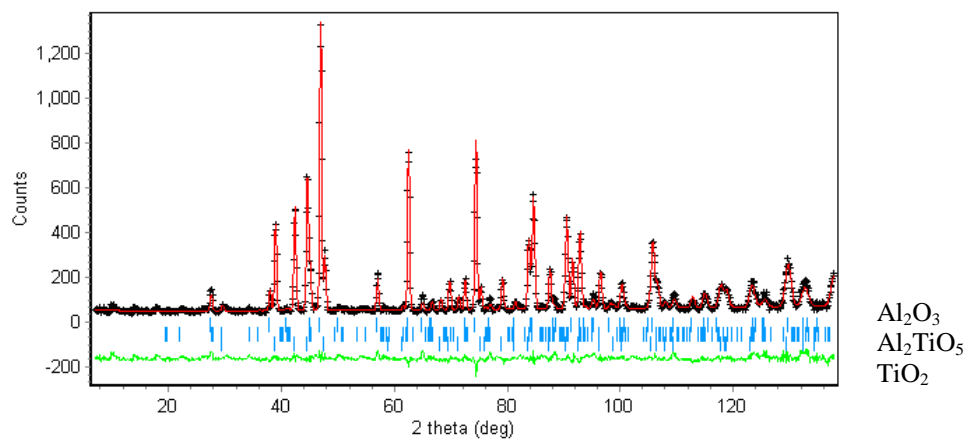
LOW, I.M & OO, Z. 2008. Reformation of Phase Composition in Decomposed Aluminium Titanate. *Materials Chemistry and Physics*, 111, 9-12.

Supporting Information

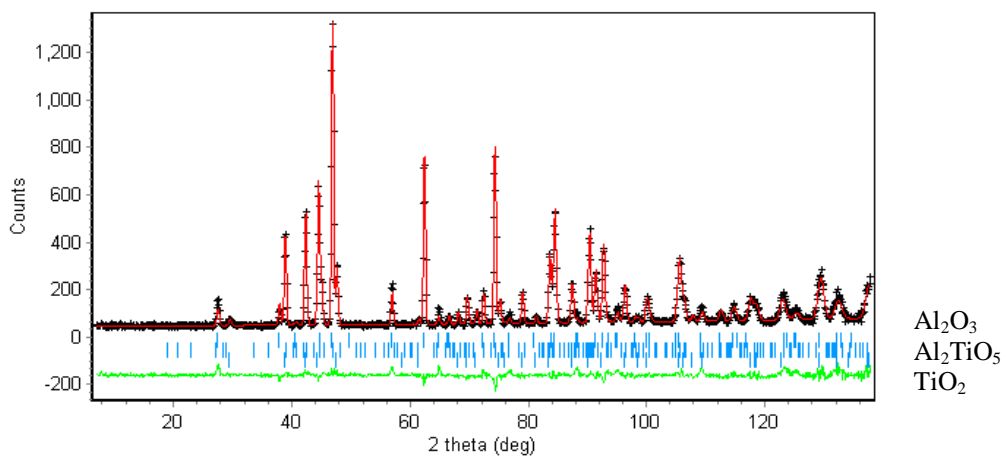
(a) Diffraction studies on self-recovery in Al_2TiO_5

The characteristics of self-recovery in Al_2TiO_5 were observed when it is annealed at $\geq 1300^\circ\text{C}$ in air using in-situ high-temperature neutron diffraction.

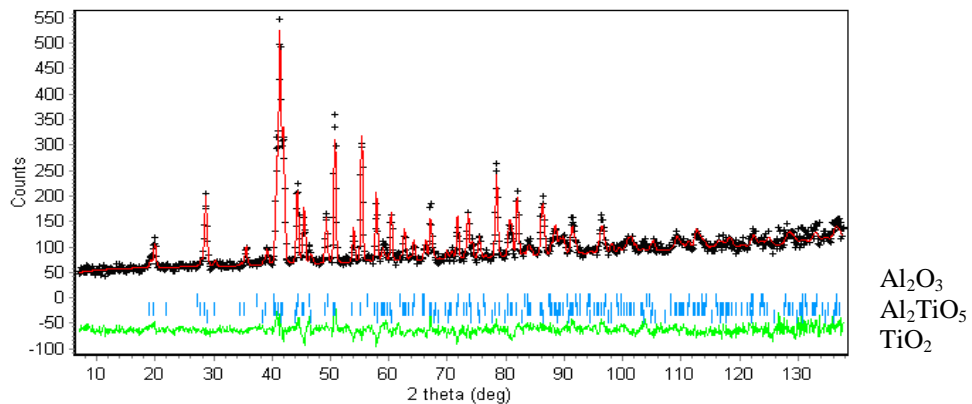
The various diffraction plots for room temperature; 1400°C and 1500°C are presented in Figure 5.6. The observed data is shown by a (+) sign, and the calculated data by a solid line (red). Vertical blue bars represent the Bragg peak positions for Al_2O_3 , Al_2TiO_5 , and TiO_2 from the top to the bottom respectively. The difference plots between observation and calculation are shown by green line. Table 5.5 shows the Figures-of-merit for Rietveld quality refinement results for self-recovery in the reformation of Al_2TiO_5 from room temperature to 1500°C . The relative phase abundances are shown in Table 5.6.



(a)



(b)



(c)

Figure 5.6: ND Rietveld difference plots for Al_2TiO_5 at (a) room temperature, (b) 1450°C for 2 h, and (c) 1500°C for 2 h. Wavelength for ND is 1.665\AA .

Table 5.5: Figures-of-merit from Rietveld refinement of ND data for reformation of Al_2TiO_5 from 20°C to 1500°C.

Temperature (°C)	R_{wp}	R_{exp}	GOF	R_B Al_2O_3	R_B Al_2TiO_5	R_B TiO_2
20	8.9	4.7	3.5	4.3	5.7	2.0
300	7.9	4.8	2.7	4.5	6.7	2.7
600	7.6	4.8	2.7	4.5	6.7	2.7
900	7.8	4.9	2.7	4.5	6.7	2.7
1200	7.8	4.8	2.7	4.5	6.7	2.7
1300	7.5	4.8	2.7	4.5	6.7	2.6
1400	7.3	4.8	2.7	4.5	6.7	2.7
1450	7.2	4.8	2.2	4.2	5.1	3.2
1500	7.2	4.8	2.2	3.5	5.2	2.4

Table 5.6: Relative phase abundances from Rietveld refinement with ND (MRPD) for the self-recovery in Al_2TiO_5 from room temperature to 1500°C

Temperature (°C)	$\alpha\text{-Al}_2\text{O}_3$ (wt%)	Al_2TiO_5 (wt%)	TiO_2 (wt%)
20	55.76 (1.08)	0.87 (0.31)	43.37 (0.89)
300	63.0 (0.94)	2.0 (0.30)	35.0 (0.80)
600	63.0 (0.90)	2.0 (0.30)	35.0 (0.80)
900	63.0 (0.90)	2.0 (0.30)	35.0 (0.80)
1200	63.0 (0.90)	2.0 (0.30)	35.0 (0.80)
1300	33.0 (0.91)	42.0 (0.22)	25.0 (0.75)
1400	14.0 (0.85)	78.0 (0.26)	8.0 (0.50)
1450	1.80 (0.13)	97.16 (2.38)	1.04 (0.16)
1500	1.42 (0.12)	97.64 (2.4)	0.94 (0.16)

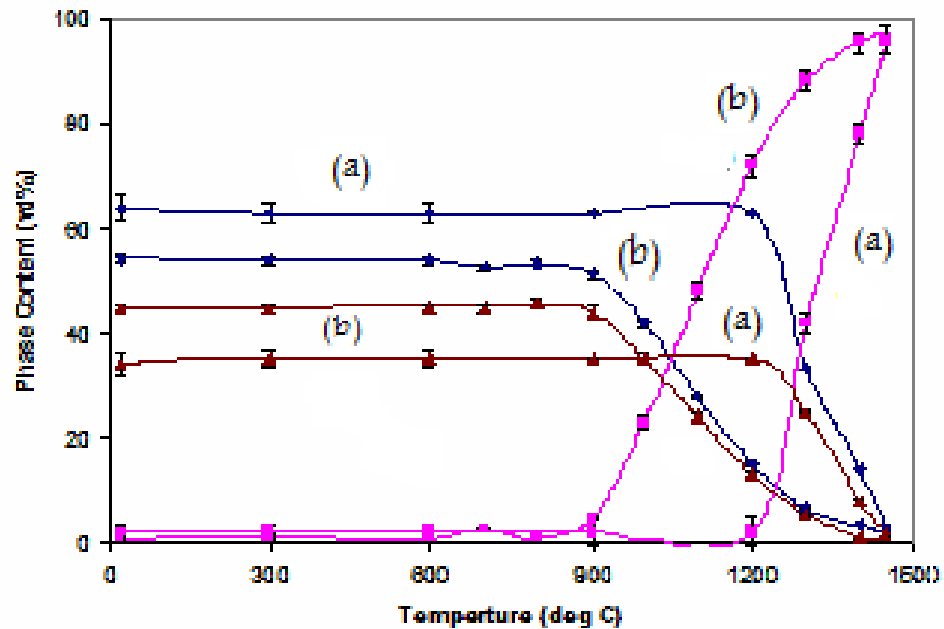


Figure 5.7: Phase abundance versus temperature for the formation of Al_2TiO_5 from room temperature to 1500°C . (a) re-heating from room temperature to 1450°C , and (b) controlled cooling from 1450°C to room temperature. Error bars indicate two estimated standard deviations $\pm 2\sigma$.

Legend: $\text{Al}_2\text{TiO}_5 = \blacksquare$ $\text{Al}_2\text{O}_3 = \blacklozenge$ $\text{TiO}_2 = \blacktriangle$

The neutron diffraction results of reformation are as follows:

- (a) Re-heating from 20°C to 1450°C , it is evident that more than 98 wt% of Al_2TiO_5 reformed.
- (b) Controlled cooling to 20°C from 1450°C , the subsequent decomposition of reformed Al_2TiO_5 .

It can be seen that, the sample remained quite stable during cooling from 1450° to 1200°C . However, on further cooling from 1200° to 1000°C , ~ 20 wt% of Al_2TiO_5 commenced to decompose at 1000°C . No further decomposition was observed from 600°C to room temperature.

Appendix 1-D: Supplementary Information on (i) “Effect of Vacuum Annealing on the Phase Stability of Ti_3SiC_2 ”, (ii) “Diffraction Studies of a Novel Ti_3SiC_2 -TiC System with Graded Interfaces”

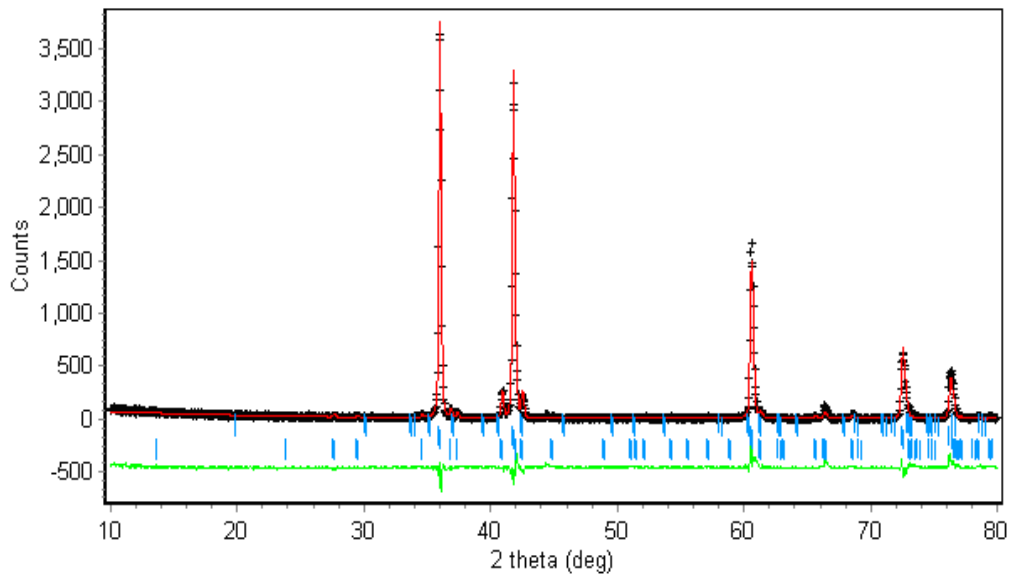
LOW, I.M., OO, Z. & PRINCE, K.E. 2007. Effect of Vacuum Annealing on the Phase Stability of Ti_3SiC_2 , *Journal of the American Ceramic Society*, 90, 2610-2614.

LOW, I.M., OO, Z. 2002. Diffraction Studies of a Novel Ti_3SiC_2 -TiC System with Graded Interfaces, *Journal of the Australian Ceramic Society*. 38, 112-116.

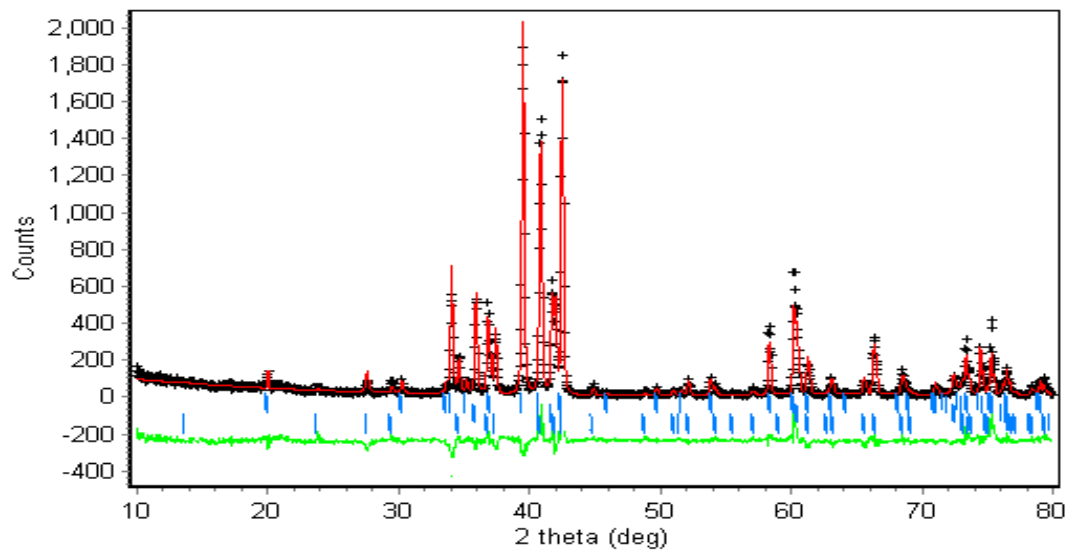
Supporting Information

The thermal stability of titanium silicon carbide (Ti_3SiC_2) in vacuum at high temperature was studied using XRD, ND, SIMS, and SRD.

XRD data collected were utilized to map the phase composition depth profiles at the near surface for vacuum-annealed Ti_3SiC_2 samples. The models of Kisi et al. (ICSD #86213) for Ti_3SiC_2 , Christensen et al. (ICSD #1546) for TiC and Nowotny et al. (ICSD #44386) model for $\text{Ti}_5\text{Si}_3\text{C}_x$ were used for the Rietveld analysis to evaluate the effect of vacuum-annealing on the phase stability of Ti_3SiC_2 . Figure 5.8 (a) and 5.8 (b) show XRD Rietveld difference plots for Ti_3SiC_2 at the first depth of 0 μm and the sixth depth of 50 μm respectively. Measured and calculated patterns are indicated by crosses (black) and solid line (red) respectively. Vertical bars (blue) represent the allowable peak positions for each of the phases (from top to bottom: Ti_3SiC_2 , TiC, $\text{Ti}_5\text{Si}_3\text{C}_x$). Intensity differences between the two patterns are shown along the bottom of the plot (green). The best fitting quality for Rietveld refinement with XRD data for vacuum-annealed Ti_3SiC_2 depth profile is shown in Table 5.7. The residuals values of refinements are R-weighted pattern (R_{wp}) ranged from 14.59 to 18.59 and R-expected (R_{exp}) ranged from 11.18 to 12.30 respectively, and the GOF (γ^2) is from 2.1 to 2.9. The good quality of refinement for depth-profiling of Ti_3SiC_2 by XRD is shown in Table 5.8.



(a)



(b)

Figure 5.8: (a) and (b): XRD Rietveld difference plot for Ti_3SiC_2 first-depth ($0 \mu\text{m}$ thick) and sixth-depth ($50 \mu\text{m}$ thick)

Legend: + = Measured pattern, Solid Red = Calculated pattern, Blue = (Vertical lines) Allowable peak positions for each of the phases, Green = Intensity differences between the two patterns

Table 5.7: Relative phase abundances determined by Rietveld analysis for XRD data: Composition depth profiles of vacuum-annealed Ti_3SiC_2 .

Depth (μm)	Ti_3SiC_2 (wt%)	TiC (wt %)	$\text{Ti}_5\text{Si}_3\text{C}$ (wt%)
0	0.27(0.27)	95.98(2.21)	3.16(0.27)
10	0.24(0.07)	90.1(1.2)	9.67(0.26)
20	0.29(0.07)	74.91(1.11)	24.8(0.45)
30	5.59(0.28)	33.77(1.34)	60.64(1.09)
40	31.43(0.92)	18.34(0.98)	50.23(1.51)
50	42.68(1.22)	13.32(0.82)	44.01(1.55)
60	61(1.30)	13.69(0.65)	25.31(1.00)
70	92.5(2.51)	4.21(0.31)	3.29 (0.44)

Table 5.8: Figures-of-merit for Rietveld refinements based on XRD depth-profiling data for thermal stability of Ti_3SiC_2 .

Depth (μm)	R_{wp}	R_{exp}	R_{B} TiC	R_{B} Ti_3SiC_2	R_{B} $\text{Ti}_5\text{Si}_3\text{C}_x$	GOF
0	18.03	12.15	4.74	9.04	16.6	2.2
10	18.06	12.30	4.42	7.96	9.9	2.1
20	14.59	12.21	7.20	8.18	11.7	2.9
30	15.45	11.96	1.60	8.09	13.46	2.9
40	18.59	11.18	2.00	7.09	10.08	2.7
50	16.97	11.70	1.6	6.27	9.84	2.1
60	16.93	11.60	5.1	7.3	10.1	2.3

Appendix 1-E: Supplementary Information on “Dynamic Study of the Thermal Stability of Impure Ti_3SiC_2 in Argon and Air by Neutron Diffraction”

OO, Z., LOW, I.M. & O’CONNOR, B.H. 2006. Dynamic Study of the Thermal Stability of Impure Ti_3SiC_2 in Argon and Air by Neutron Diffraction, *Physica B*, 385-386, 499-501.

Supporting Information

(a) The thermal stability of impure Ti_3SiC_2 in argon

The neutron diffraction difference plot for the Ti_3SiC_2 annealed in argon at 1200°C is shown in Figure 5.9, and the difference plots from room temperature to 1400°C are shown in Figure 5.10. The measured and calculated patterns are indicated by crosses (black) and solid line (red) respectively. The consistency between measurements and calculations is shown in green. Vertical bars (blue) represent the Bragg peak positions for each the phases from the top to the bottom are Ti_3SiC_2 , TiC , $\text{Ti}_5\text{Si}_3\text{C}$, $\alpha\text{-Al}_2\text{O}_3$, TiO_2 .

The results of best-fit Rietveld refinement and relative phase compositions as determined by using MRPD are shown in Table 5.9 and Table 5.10 respectively. According to the results, there was no apparent dissociation of Ti_3SiC_2 to form TiC at temperatures below 1200°C . It can be seen that dissociation began slowly at $1200^\circ\text{-}1300^\circ\text{C}$ but the process progressed rapidly from 1400° to 1500°C . The formation of TiO_2 was also observed at 1300°C . The transient phase $\text{Ti}_5\text{Si}_3\text{C}$ is believed to convert eventually into stable TiC at elevated temperature.

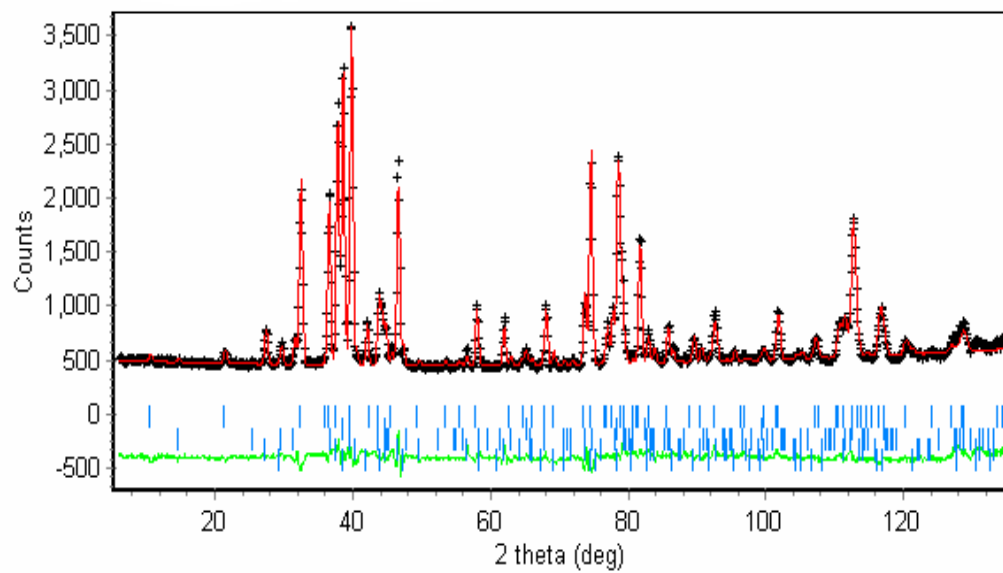


Figure 5.9: Neutron diffraction Rietveld difference plot for Ti₃SiC₂ annealed at 1200°C in argon for 2 h.

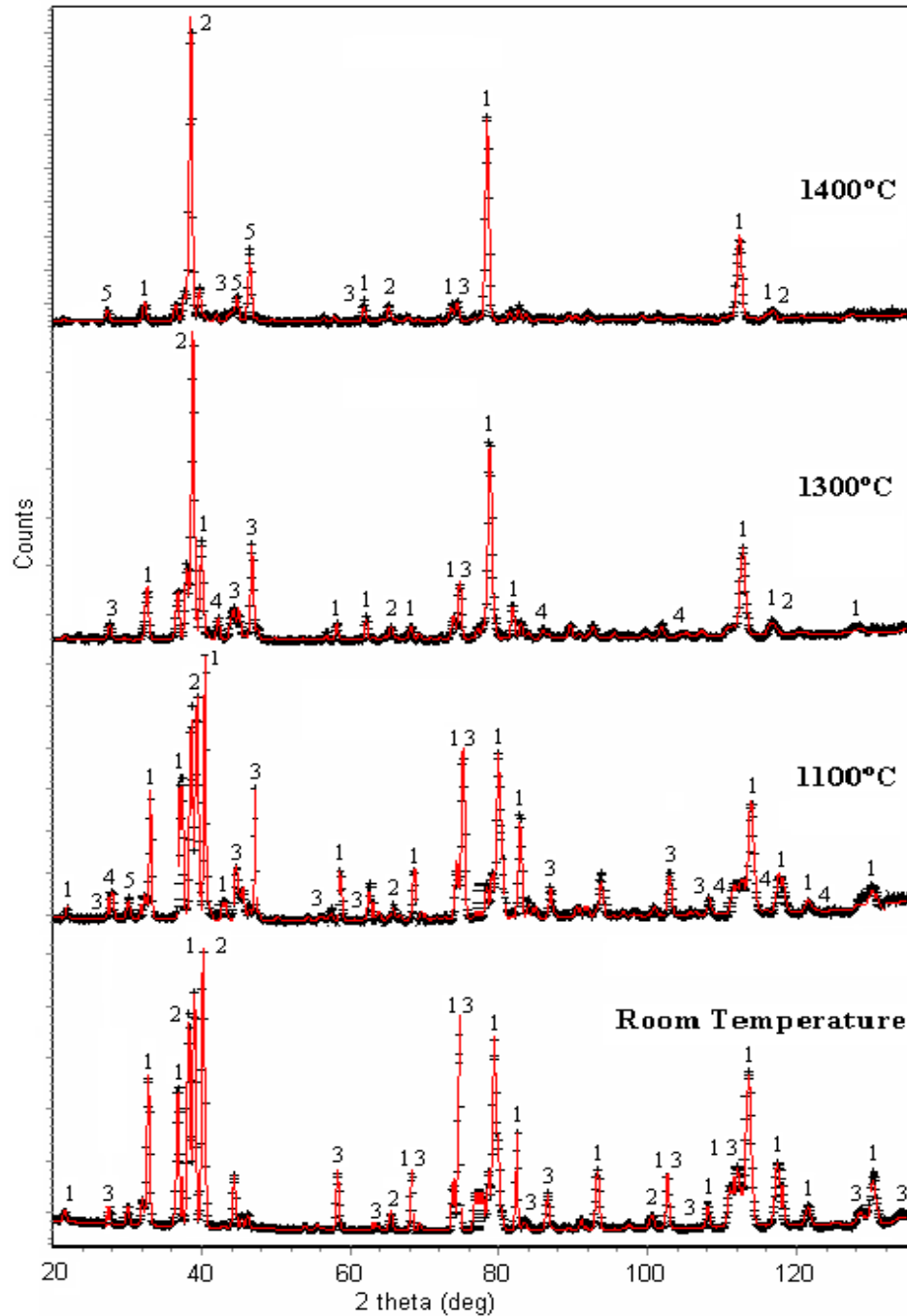


Figure 5.10: Stacking ND diffraction patterns for the Ti_3SiC_2 during heat treatment in argon from room temperature to 1400°C. The measured and calculated patterns are indicated by crosses (black) and solid line (red) respectively.

Legend: 1 = Ti_3SiC_2 , 2 = TiC, 3 = $\text{Ti}_5\text{Si}_3\text{C}$, 4 = Al_2O_3 , 5 = TiO_2

Table 5.9: Figures-of-merit from Rietveld refinement with ND (MRPD) data for Ti_3SiC_2 annealed in argon from room temperature to 1400°C

Temperature (°C)	R_{wp}	R_{exp}	GOF	R_{B} Ti_3SiC_2	R_{B} TiC	R_{B} $\text{Ti}_5\text{Si}_3\text{C}$	R_{B} Al_2O_3	R_{B} TiO_2
23	3.9	1.07	13.3	3.37	1.8	2.36	-	-
1000	5.0	2.0	6.2	3.6	0.42	2.23	2.98	3.51
1100	4.86	2.0	5.9	3.17	0.22	1.6	2.27	3.14
1200	4.49	2.0	5.2	3.09	0.23	1.94	1.88	2.25
1250	5.04	1.94	6.7	3.15	0.4	5.59	2.68	2.15
1300	5.28	1.92	7.5	3.14	0.51	1.92	1.59	2.17
1350	9.08	4.28	4.5	4.17	0.67	8.99	3.91	4.75
1400	8.36	4.32	3.7	3.47	0.82	6.27	3.08	5.1

Table 5.10: Relative phase abundances determined from Rietveld refinement using MRPD data for Ti_3SiC_2 annealed in argon from 20°C to 1400°C.

Temperature (°C)	Ti_3SiC_2 (wt%)	TiC (wt%)	$\text{Ti}_5\text{Si}_3\text{C}$ (wt%)	TiO_2 (wt%)
23	68.5 (1)	19.4 (1)	12.1 (0.7)	-
1000	67.6 (1.3)	17.51 (1.6)	11.5 (0.8)	3.36 (1.02)
1100	64.8 (1.3)	17.67 (1.7)	11.17 (1.1)	6.33 (0.3)
1200	61.4 (1.3)	21.1 (1.6)	9.79 (1.6)	7.48 (0.3)
1250	56.76 (1.3)	29.38 (1.8)	5.41 (1.1)	8.48 (0.4)
1300	51.52 (1.1)	39.01 (1.0)	0.63 (0.1)	10.1 (0.5)
1350	38.84 (1.8)	54.89 (3.6)	5.58 (1.8)	0.68 (0.3)
1400	25.97 (1.2)	64.73 (3.5)	7.04 (1.6)	2.24 (0.3)

(b) Oxidation of Ti_3SiC_2 in air

The neutron diffraction profile description plots for the Ti_3SiC_2 oxidized in air at 1350°C are shown in Figure 5.11 (a & b). Tables 5.11 and 5.12 show the relative phase abundances (wt%) Ti_3SiC_2 oxidized in air from room temperature to 1350°C . This was analyzed by the Rietveld method and figures of merit, where the best fit is located between 2.3 and 4.7 from room temperature to 1350°C . The Bragg factor R_B ranges from 0.6 to 5.5 which show all results are acceptable for the quality refinement. The crystal structure models used in the calculation were taken from the Inorganic Crystal Structure Data Base (ICSD-Fach Informations Zentrum and Gmelin Institut, Germany): ICSD (#86213 for Ti_3SiC_2), (#1546 for TiC), (#64987 for TiO_2), (#44095 for SiO_2 (Cristobalite)), (#29343 for SiO_2 (Tridymite)), (#1089 for TiSi_2), (#60483 for TiO) and (#1089 for TiSi_2) respectively.

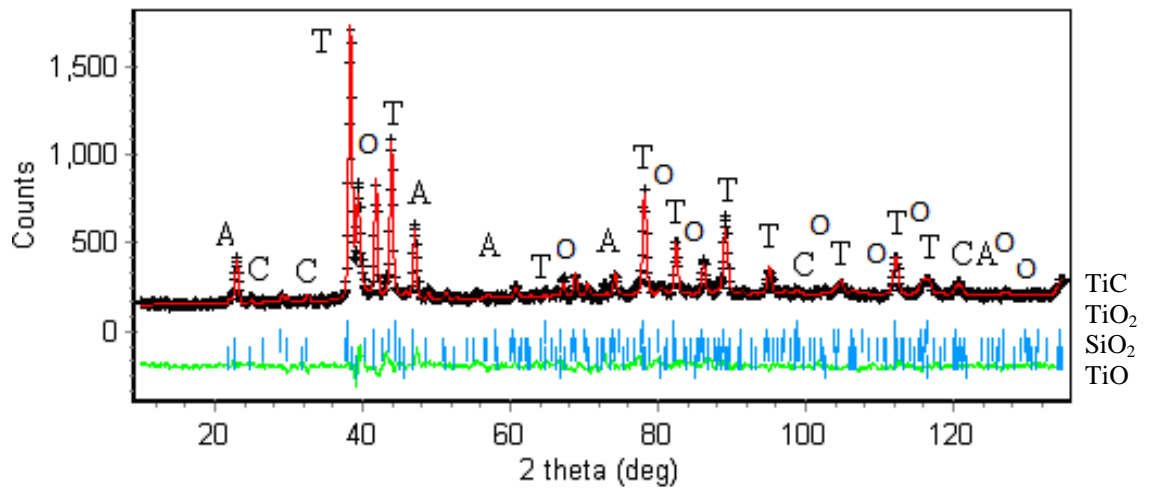


Figure 5.11: (a) Neutron diffraction Rietveld difference plot for the Ti_3SiC_2 oxidised in air at 1350°C .

Legend: From top to bottom T = TiC, A = TiO_2 (rutile), C = SiO_2 (Cristobalite), O = TiO.

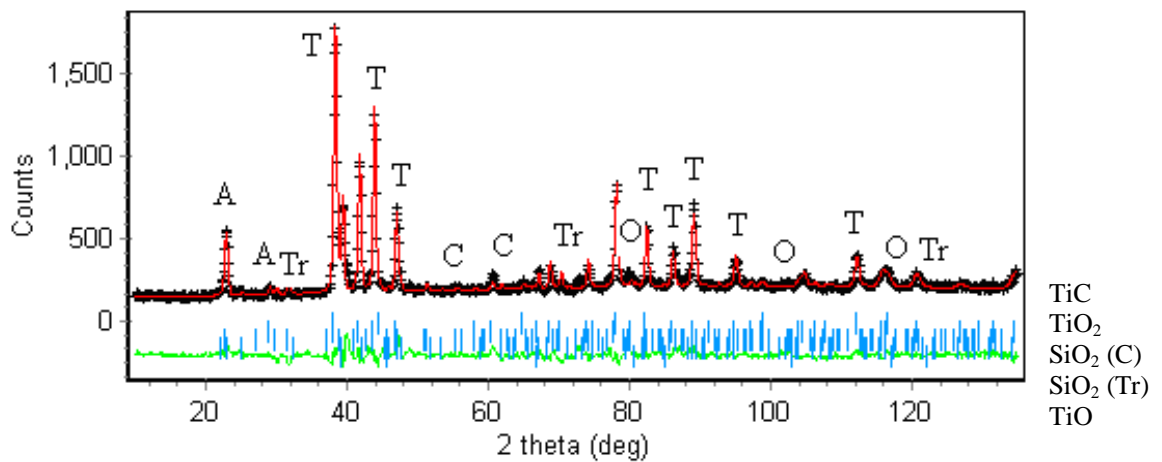


Figure 5.11: (b) Neutron diffraction Rietveld profile plot for the Ti_3SiC_2 oxidised in air cooling from 1350°C to room temperature.

Legend: From top to bottom T = TiC, A = TiO_2 (rutile) C = SiO_2 , (Cristobalite), Tr = SiO_2 (Trydimite) and O = TiO.

Table 5.11: Relative phase abundances determined from Rietveld refinement using MRPD, in-situ ND results for Ti_3SiC_2 oxidized in air from room temperature to 1350°C and from 1350°C to room temperature on cooling.

Temperature (°C)	Ti_3SiC_2 (wt%)	TiC (wt%)	TiO_2 (wt%)	SiO_2 Crist (wt%)	SiO_2 Trid (wt%)	TiO (wt%)
23	91.99 (0.82)	7.73 (0.11)	0.28 (0.09)	-	-	-
500	91.61 (1.16)	6.97 (0.16)	1.42 (0.14)	-	-	-
750	71.29 (1.26)	5.36 (0.24)	23.35 (0.99)	-	-	-
1000	46.75 (0.95)	2.71 (0.28)	50.54 (0.93)	-	-	-
1100	20.83 (1.38)	5.38 (0.86)	73.79 (1.74)	-	-	-
1200	16.43 (1.06)	9.71 (0.65)	72.5 (1.76)	-	-	1.36 (0.42)
1300	8.39 (1.1)	11.01 (0.83)	69.28 (2.03)	-	-	11.32 (1.85)
1350	-	12.63 (0.45)	45.73 (1.13)	9.35 (0.49)	-	32.3 (0.85)
1350-cool	-	10.59 (0.71)	45.76 (2.84)	12.53 (0.96)	0.41 (0.07)	30.71 (4.0)

Table 5.12: Figures-of-merit from Rietveld refinement with ND (MRPD) data for Ti_3SiC_2 oxidized in air from room temperature to 1350°C

Run number	Temperature (°C)	R_{wp}	R_{exp}	GOF	R_{B} Ti_3SiC_2	R_{B} TiC	R_{B} TiO_2	R_{B} TiO	R_{B} SiO_2
13986	23	2.2	3.5	2.3	2.2	3.2	2.7	-	-
13987	500	6.6	3.4	3.7	3.7	0.8	4.6	-	-
13988	750	6.6	3.4	3.8	4.4	1.1	3.5	-	-
13989	1000	6.2	3.1	3.9	4.6	0.6	2.7	-	-
13990	1100	6.5	3.0	4.7	2.4	1.4	2.6	-	-
13991	1200	6.8	3.0	4.0	2.7	0.3	3.1	2.4	-
13992	1300	7.7	3.0	4.0	4.0	1.9	3.5	1.2	-
13993	1350	7.2	3.0	4.1	-	1.1	3.2	5.5	5.1

(c) Further evidence of oxidation in Ti_3SiC_2

At high oxygen partial pressure, impure Ti_3SiC_2 oxidizes readily to stoichiometric oxide phase rutile (TiO_2) and cristobalite (SiO_2). Ti_3SiC_2 is not phase pure possibly because of thermal dissociation during sintering in the vacuum furnace. In-situ neutron diffraction results for impure Ti_3SiC_2 is shown in Table 5.11, with the phase abundance of cristobalite (SiO_2) of 9.35 wt% at 1350°C and 12.53 wt% at lower temperatures. The phase abundance of TiO increases from 1.36 wt% at 1200°C to 32.3 wt% at 1350°C, while that of TiO_2 drops from 72.5 wt% at 1200°C to 45.73 wt% at 1350°C.

To understand more about oxidation of Ti_3SiC_2 , commercially pure sample (Maxthal 312) of Ti_3SiC_2 was investigated. In-situ neutron diffraction plots for Ti_3SiC_2 were obtained for cylindrical bar Maxthal 312 samples, 15 mm in diameter and 50 mm in length, oxidized in air at 1400°C (Figure 5.12 (a-c)). The Maxthal 312 samples have the following physical properties: density of 4.47 g/cm³, porosity of ~1% and about 10 wt% in TiC content. Table 5.13 shows the relative phase composition (wt%) of Ti_3SiC_2 (Maxthal 312) obtained by Rietveld analysis. Table 5.14 presents the figures of merits where the GOF values are found to fall between 1.2 and 1.7 for heating from 23°C to 1400°C and cooling from 1400°C to 23°C. The Bragg factor R_B ranges from 1.09 to 3.0, which show all results, are acceptable for the quality refinement. The crystal structures models used in the calculation were taken from the Inorganic Crystal Structure Data Base (ICSD-Fach Informations Zentrum and Gmelin Institut, Germany) –ICSD (# 86213 for Ti_3SiC_2), (#1546 for TiC), (#64987 for TiO_2 , - rutile), (#44095 for SiO_2 Cristobalite), (#43801 for SiO_2 (Tridymite), (#60483 for TiO) and (#1089 for TiSi_2) respectively.

Comparing the results in Table 5.11 and Table 5.13, it was found that the oxidation characteristics, composition profiles and phase transition are temperature-dependent. The results also strongly suggested that the Ti diffused outward to form the outer layer TiO_2 and oxygen was transported inward to form the inner duplex layer TiO_2 and SiO_2 . The carbon from Ti_3SiC_2 was liberated into the air in the form of CO or CO_2 .

According to the analysis above, anatase formed at 650°C and rutile formed rapidly at above ~750°C (See Figure 5.13). The outer homogeneous layer of TiO₂ (rutile) became the protective film on the surface of the inner duplex layers of SiO₂ and TiO₂. At 1450°C, formation of SiO₂ (cristobalite) was observed. When cooling from 1450°C to room temperature, cristobalite transformed to tridymite in the lower temperature range.

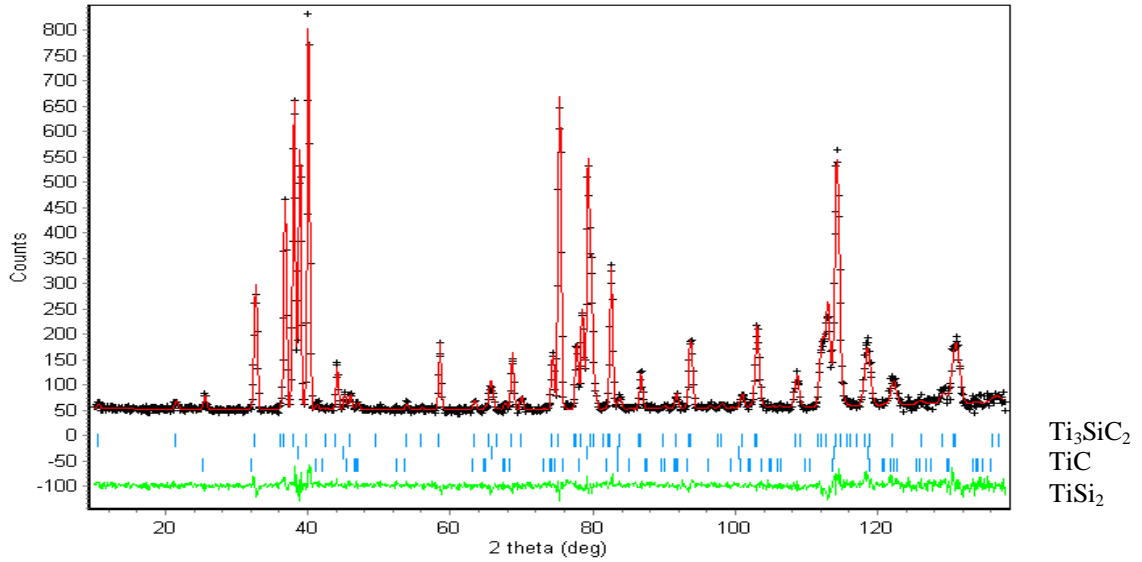


Figure 5.12: (a) Neutron diffraction Rietveld difference plot for the as-received Maxthal Ti_3SiC_2 at air for room temperature.

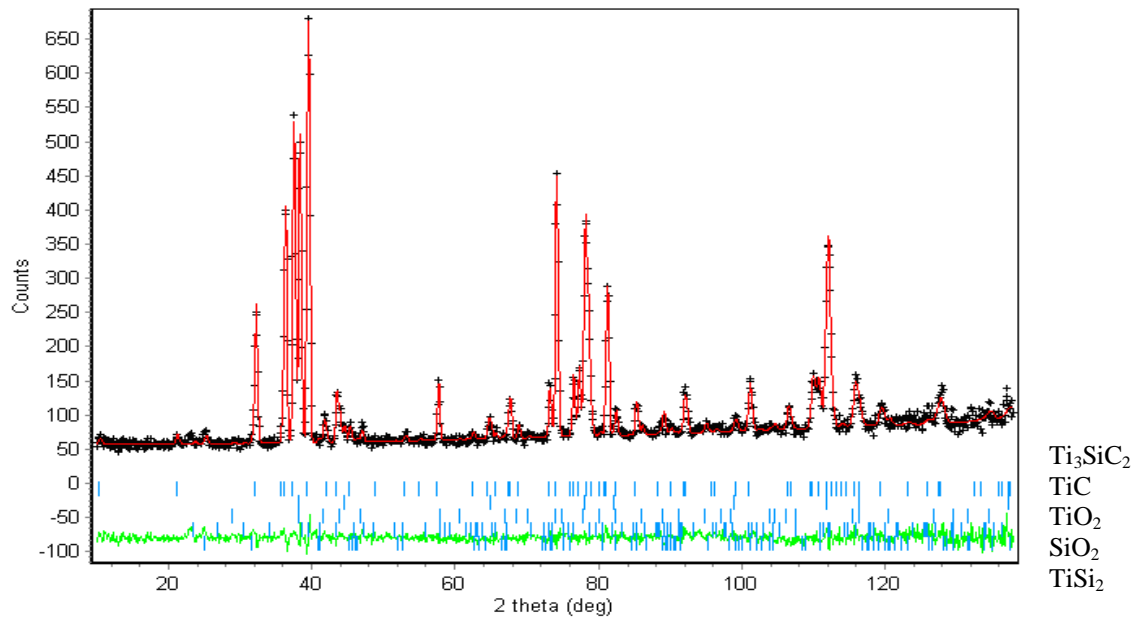


Figure 5.12: (b) Neutron diffraction Rietveld difference plots for Maxthal Ti_3SiC_2 oxidized in air at 1400°C for 2 h.

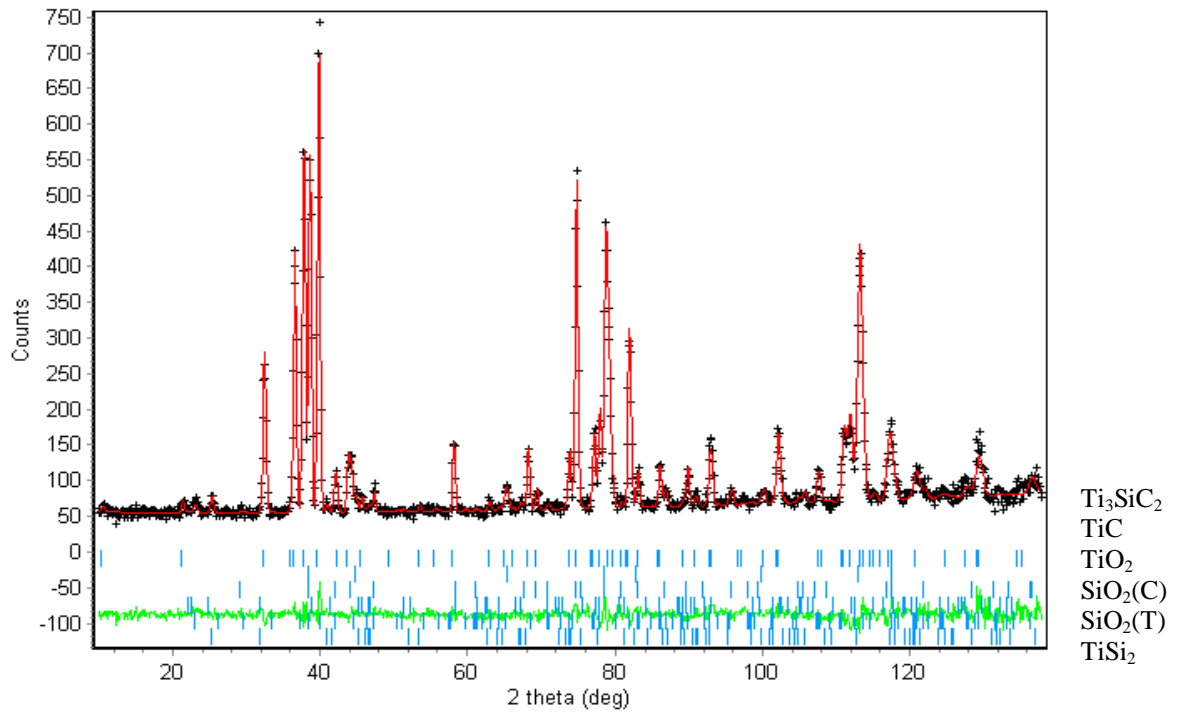


Figure 5.12: (c) Neutron diffraction Rietveld difference plots for Maxthal Ti_3SiC_2 oxidized in air at 1400°C and then cooled to 23°C .

Legend: $\text{SiO}_2(\text{C})$ = Cristobalite, $\text{SiO}_2(\text{T})$ = Tridymite

Table 5.13: Relative phase abundance determined from Rietveld analysis refinement using ND results for Ti_3SiC_2 (Maxthal 312) oxidized in air from 23°C to 1400°C and cooled from 1400°C to 23°C

Temperature (°C)	Ti_3SiC_2 (wt%)	TiC (wt%)	TiO_2 (wt%)	TiSi_2 (wt%)	SiO_2 (T) (wt%)	SiO_2 (C) (wt%)
23	79.23 (0.51)	15.38 (0.19)	-	5.39 (0.3)	-	-
600	79.99 (0.80)	14.82 (0.17)	-	5.19 (0.32)		
800	80.65 (1.21)	13.9 (0.35)	0.70 (0.01)	4.75 (0.43)		
1000	80.14 (0.93)	14.3 (0.27)	0.69 (0.01)	4.87 (0.32)		
1100	80.14 (0.93)	14.9 (0.29)	0.29 (0.1)	4.68 (0.32)		
1200	79.12 (0.87)	14.76 (0.27)	0.99 (0.1)	5.13 (0.31)		
1300	80.86 (1.09)	15.12 (0.32)	0.7 (0.1)	3.00 (0.35)	-	0.32 (0.01)
1400	79.14 (1.02)	14.61 (0.31)	3.39 (0.14)	2.67 (0.33)	-	0.2 (0.01)
1400-cool	75.09 (0.84)	14.29 (0.26)	5.29 (0.14)	4.57 (0.14)	0.07 (0.02)	0.71 (0.1)
23	73.02 (0.71)	14.54 (0.21)	6.24 (0.14)	5.15 (0.31)	0.14 (0.05)	0.89 (0.1)

SiO_2 (T) = Tridymite

SiO_2 (C) = Cristobalite

Table 5.14: Figures-of-merit from Rietveld refinement with ND data for Ti_3SiC_2 (Maxthal 312) oxidized in air from room temperature to 1400°C

Temp (°C)	R_{wp}	R_{exp}	GOF	R_{B} Ti_3SiC_2	R_{B} TiC	R_{B} TiO ₂	R_{B} TiSi ₂	R_{B} SiO ₂ (T)	R_{B} SiO ₂ (C)
23	6.15	5.40	1.4	2.83	1.20	-	3.22	-	-
600	5.98	5.10	1.3	2.67	1.28	-	2.67	-	-
800	8.14	7.18	1.2	2.30	0.72	3.64	3.66	-	-
1000	6.02	5.07	1.4	1.76	1.14	4.23	2.33	-	-
1100	5.92	5.05	1.3	1.50	0.68	2.92	2.32	-	-
1200	5.54	5.02	1.2	1.26	0.28	1.78	2.65	-	-
1300	6.64	5.01	1.7	1.09	1.30	2.93	3.92	-	2.56
1400	5.95	4.98	1.4	1.36	0.34	3.27	3.46	-	2.09
1400 to cool	6.14	5.01	1.5	2.93	1.18	2.61	2.61	3.07	3.63

SiO₂(T) = Tridymite

SiO₂(C) = Cristobalite

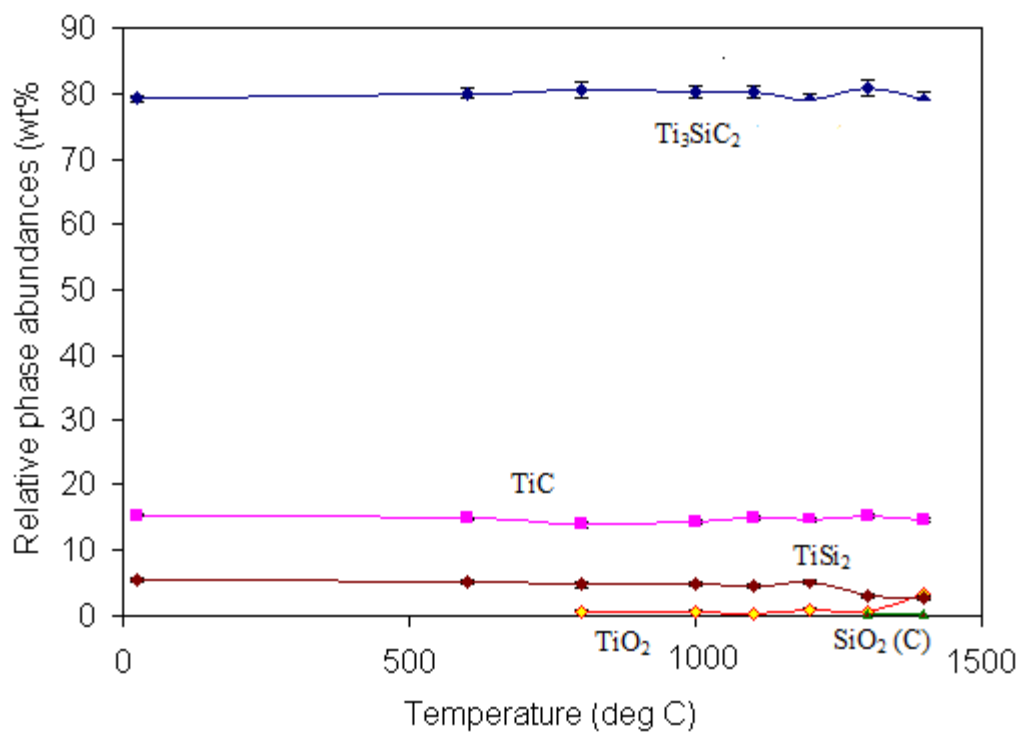


Figure 5.13: Variations of phase evolution during the in-situ oxidation of Ti_3SiC_2 (Maxthal 312) as revealed by neutron diffraction.

Legend: $\text{Ti}_3\text{SiC}_2 = \blacklozenge$, $\text{TiC} = \blacksquare$, TiO_2 rutile = \blacktriangle , $\text{TiSi}_2 = \blacklozenge$, SiO_2 cristobalite = \bullet

(d) XRD studies and microstructural analysis of Ti_3SiC_2 oxidation

For more evidence on the existence of oxidation in Ti_3SiC_2 , a Nikon optical microscope was used to analyze the microstructural details of Ti_3SiC_2 at 1300°C , as shown in Figure 5.14. The XRD analysis confirms the depth-profiling of phase difference plots and abundances in Ti_3SiC_2 as shown in Figures 5.15 and 5.16 respectively. The figures show that TiO_2 appeared at the outer layer, a mixture of TiO_2 and SiO_2 at the inner layer and Ti_3SiC_2 at the bulk. Tables 5.15 and 5.16 present the phase abundances and best fitting of oxidization behavior of Ti_3SiC_2 oxidized at 1300°C for 20 min in air.

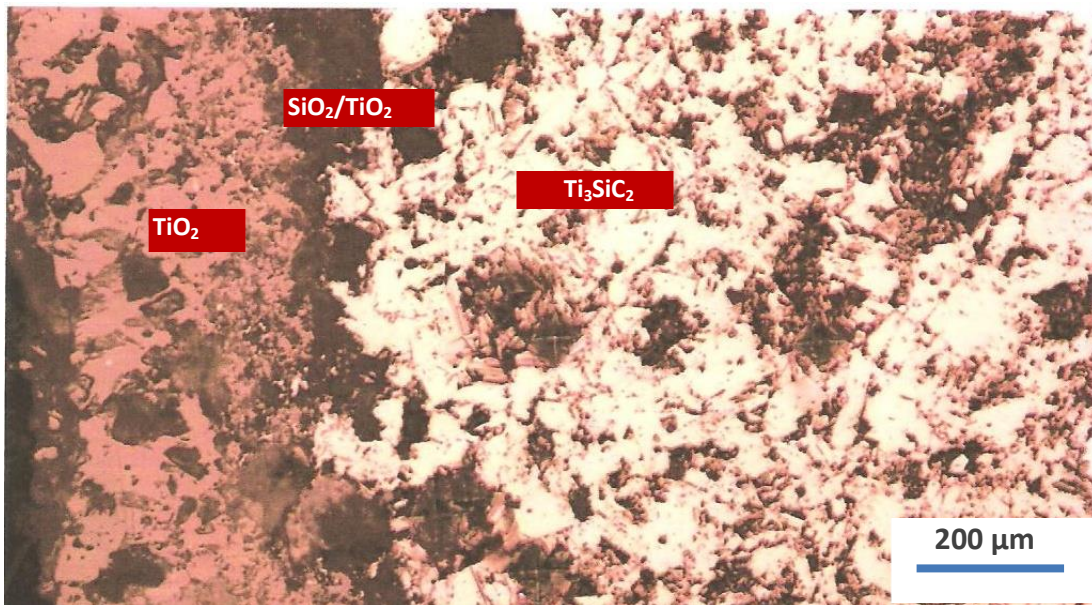


Figure 5.14: Optical micrograph showing the microstructural details of Ti_3SiC_2 oxidized at 1300°C for 20 min in air.

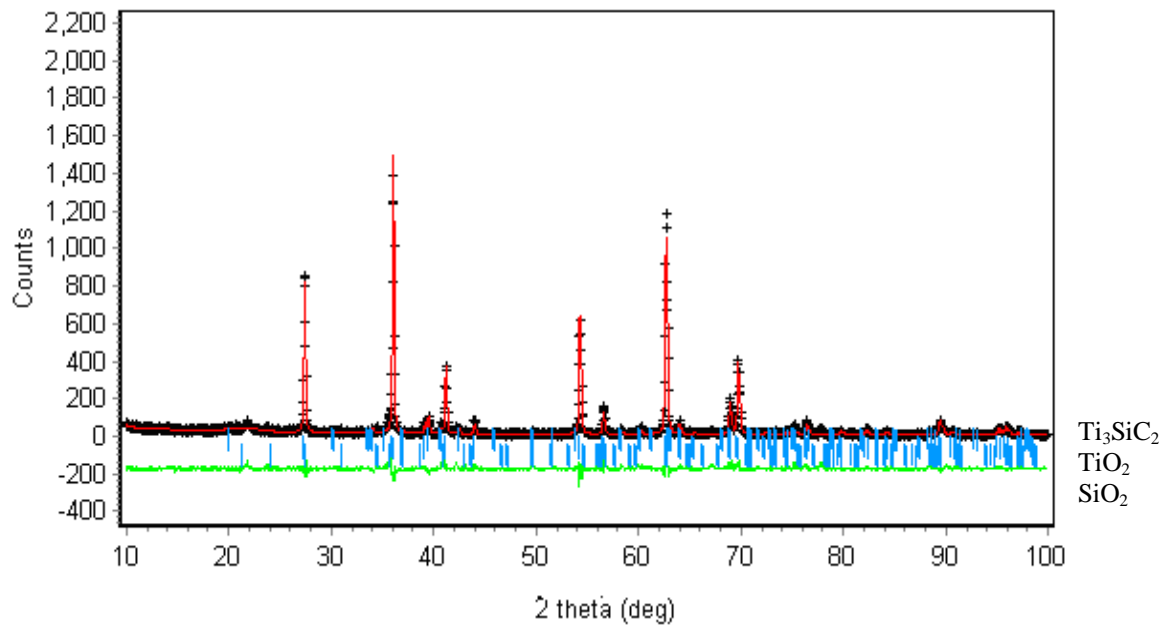


Figure 5.15: XRD Rietveld diffraction pattern for Ti₃SiC₂ (40 micron).

Table 5.15: Relative phase compositions determined from Rietveld refinement with XRD data for depth-profiling of phase abundances in Ti_3SiC_2 oxidized at 1300°C for 20 min in air.

Depth (μm)	Ti_3SiC_2 (wt%)	TiO_2 (rutile) (wt%)	SiO_2 (wt%)	esd for Ti_3SiC_2	esd for TiO_2	esd for SiO_2	GOF
0	0	100	0	0	0	0	5.0
25	0	100	0	0	0	0	3.7
40	3.23	84.71	12.06	0.37	1.41	1.27	2.0
50	18.54	80.74	0.72	0.63	1.8	0.23	2.8
60	35.16	64.33	0.51	0.7	1.12	0.01	2.8
70	60.12	39.88	0	1.07	0.91	0	3.4

Table 5.16: Figures-of-merit from Rietveld refinement with XRD data for Ti_3SiC_2 oxidized at 1300°C for 20 min in air.

Depth (μm)	R_{wp}	R_{exp}	R_{B} Ti_3SiC_2	R_{B} TiO_2	R_{B} SiO_2 (C)
0	15.60	16.28	-	5.0	-
25	15.43	16.39	-	5.6	-
40	16.20	16.88	6.3	5.9	7.9
50	15.09	16.07	6.0	4.6	5.7
60	14.02	15.80	5.6	6.1	6.0
70	15.54	16.55	6.0	6.5	7.5

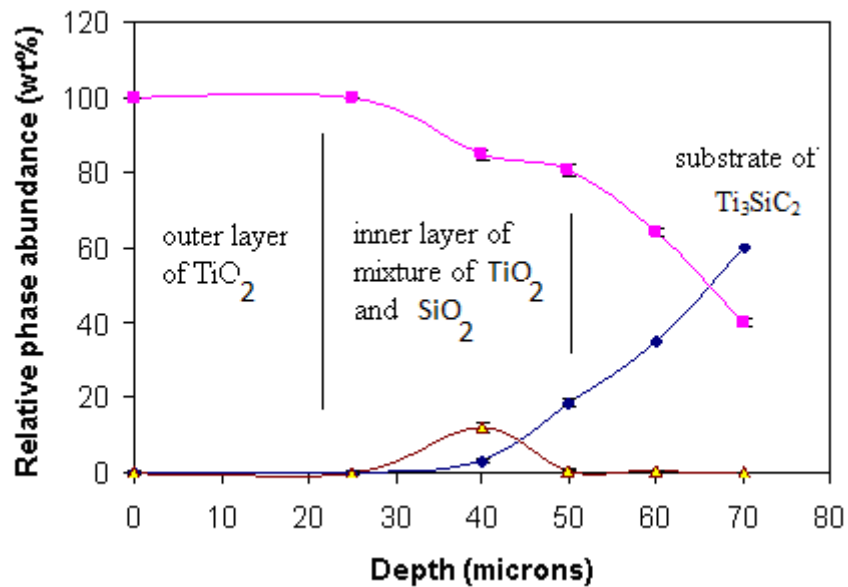


Figure 5.16: XRD depth-profiling of phase abundances for Ti₃SiC₂ oxidized at 1300°C for 15 min in air

Legend: TiO₂ = ■, Ti₃SiC₂ = ◆, SiO₂ (Cristobalite) = ▲

5.2 Appendix 1-F: Supplementary Information on “All Publications Used as Part of Thesis”

5.2.1 Rietveld Data Analysis

The Rietveld analysis method (Rietveld, 1967) for the X-ray diffraction, neutron diffraction and synchrotron radiation patterns is well established. This method uses crystal structure and diffraction peaks profile to generate x-ray or neutron diffraction patterns via a process of least square refinement which minimizes the differences between the observed and the calculated patterns. Crystal structure data including atom coordinates and unit cell parameters were taken from the Inorganic Crystal Structure Database (ICSD) (see Appendices I-G). The computations involved adjustment of the specimen displacement, phase scale factors, zero adjustment, polynomial fit parameters for the pattern-background, refinable lattice parameters, individual atom thermal parameters, overall thermal parameters, instrumentation parameters such as U, V, W, asymmetry parameter AS and 2θ – scale offset and peak profile functions (pseudo-Voigt with asymmetry).

In the least- squares procedure, the best fitted model is obtained when the residual R is minimized, where R is defined as, (Young, 1993),

$$R = \sum_i W_i (Y_{io} - Y_{ic})^2 \quad (5.1)$$

where Y_{io} is the observed intensity and Y_{ic} is the calculated intensity at point i , and W_i is the weighting factor for point i in the pattern which is normally set as the reciprocal of the measured intensity at point i given by:

$$w_i = \frac{1}{\sigma_i^2} \quad (5.2)$$

The calculated intensity Y_{ic} at each point i in the pattern for a number of phases k is determined by summing all the contributions of neighbouring reflection and the background. The intensity of diffracted beams is dependent on diffractometer optics. X-ray diffraction (XRD), synchrotron radiation diffraction (SRD) and neutron diffraction (ND) were employed in this research.

By using Bragg-Brentano optics to examine infinitely thick specimen, the calculated, Y_{ic} formulated by Warren (1969) is as follows:

$$y_{ic} = KA_i \sum_{jk} m_{jk} L_{jk} |F_{jk}|^2 G_{ijk} P_{jk} \frac{C_k}{V_k} + y_{ib} \quad (5.3)$$

K is the instrument constant, which is dependent on instrumental parameters and incident beam characteristics but independent of the specimen, A_i is the absorption factor, m_{jk} is the multiplicity factor, L_{jk} is the Lorentz-polarization factor for the reflection jk , F_{jk} is the structure factor, G_{ijk} is a normalized peak profile function, P_{jk} is the preferred orientation function, C_k is the volume fraction of k and V_k is the corresponding cell volume, and Y_{ib} is the background contribution for point i .

The calculated intensity of diffracted beams with Debye-Scherrer optics (SRD and ND) for cylindrical, semi-transparent specimens (Kisi, 1994) is given by

$$y_{ic} = KA_i(r, \theta) v \sum_{jk} m_{jk} L_{jk} |F_{jk}|^2 G_{ijk} P_{jk} \frac{C_k}{V_k} + y_{ib} \quad (5.4)$$

where $A_i(r, \theta)$ is the attenuation factor for specimen radius r and Bragg angle θ , and v , is the volume of the specimen.

Hunter and Howard (1998) have changed the simplified forms of equations 5.2 and 5.3 as follows: for Bragg-Brentano

$$y_{ic} = A_i \sum_{jk} s_k m_{jk} L_{jk} |F_{jk}|^2 G_{ijk} P_{jk} + y_{ib} \quad (5.5)$$

s_k is the Rietveld scale factor, and it is given by:

$$s_k = \frac{KC_k}{\mu V_k} \quad (5.6)$$

for Debye-Scherrer,

$$y_{ic} = A_i(r, \theta) \sum_{jk} s_k m_{jk} L_{jk} |F_{jk}|^2 G_{ijk} P_{jk} + y_{ib} \quad (5.7)$$

Where s_k is the Rietveld scale factor, which is given by

$$s_k = \frac{vKC_k}{V_k} \quad (5.8)$$

The structure factor, F_k is given by

$$F_k = \sum_{j=1}^n f_j \exp[2\pi i(h'_k r_j - h'_k B_j h_k)] \quad (5.9)$$

where f_j is the scattering factor or scattering length of atom j , and h_k , r_j and B_j are matrices representing the Miller indices, atomic coordinates and anisotropic thermal vibration parameters respectively.

The background intensity y_{ib} may be modeled using the polynomial (Rietveld, 1969):

$$y_{ib} = \sum_{m=-1}^n B_m (2\theta)^m \quad (5.10)$$

where B_m is refinable parameters and 2θ is the diffraction angle. The background model were 3rd order for X-ray diffraction (XRD), 3rd order for neutron diffraction (ND) data, and 5th order for synchrotron radiation diffraction (SRD). There are basically two approaches for dealing with the background in a powder diffraction pattern. It can either be estimated by linear interpolation between selected points of peaks or subtracted, or it can be modelled by an empirical or semi-empirical function containing several refinable parameters. For a simple pattern, where most peaks are resolved to the baseline, both approaches tend to work well and the fit is easily verified with a plot. For complex patterns with a high degree of reflection overlap, the majority of the peaks are not resolved to the baseline. For this reason, the estimation of the background is difficult.

In the pseudo-Voigt peak shape function, G_{ik} is given by

$$G_{ik} = \gamma \frac{C_0^{1/2}}{H_k \pi} [1 + C_0 X_k^2]^{-1} + (1 + \gamma) \frac{C_1^{1/2}}{H_k \pi^{1/2}} \exp[-C_1 X_{ik}^2] \quad (5.11)$$

where $C_0 = 4$, $C_1 = 4 \ln 2$, $X_{ik} = (2\theta_i - 2\theta_k) / H_k$, γ is a mixing parameter which varies from 0 to 1 and represents the fraction of Lorentzian character in this composite function.

The variation of the full-width-at-half-maximum (*FWHM*) of the Gaussian component of the peak shape as a function of 2θ is usually modelled with the equation derived by Caglioti et al. (1958) for low-resolution neutron data,

$$FWHM^2 = U \tan^2 \theta + V \tan \theta + W \quad (5.12)$$

where U , V and W are refineable parameters.

Peak asymmetry can be modelled using the semi-empirical function (Rietveld, 1969).

$$A_{ik} = 1 - A_s [\text{sign}(2\theta_i - 2\theta_k)] (2\theta_i - 2\theta_k)^2 \cot \theta_k \quad (5.13)$$

where A_s is asymmetry parameter determined from refinement.

Refinement trials of two types were conducted – the first with random orientation (RO) assumed for all phases, and second with the Dollase method (1986) who proposed correcting the intensities I_k of Bragg peaks for preferred orientation (PO), using the preferred correction.

$$P_k = (r^2 \cos^2 \alpha_k + r^{-1} \sin^2 \alpha_k)^{-3/2} \quad (5.14)$$

where r is the refineable preferred orientation (PO) parameters.

Pattern-background polynomial parameters were used to fit the background of data collections. Polynomial coefficient B_0 , B_1 , B_2 and B_3 and diffraction angle 2θ is related as follow:

$$y_{bi} = B_0 + B_1(2\theta_i) + B_2(2\theta_i)^2 + B_3(2\theta_i)^3 \quad (5.15)$$

B_0 , B_1 , B_2 , and B_3 was satisfactory for the pattern background refinement, but sometimes higher orders B_4 and B_5 were needed depending on data behavior collection from XRD, ND and SRD.

Refinement strategies on Rietveld phase composition were determined in powder mixtures using the “ZMV” expressions (O’Connor and Li, 1998)

Relative phase compositions:

$$W_k = \frac{S_k (ZMV)_k}{\sum_i S_i (ZMV)_i} \quad (5.16)$$

where W_k the weight fraction of phase k , S_k is the Rietveld phase scale factor, Z is the number of formula per unit cell, M is the mass of formular weight and V is the unit cell volumes.

The estimated standard deviation (*esd*) parameter, σ_j was performed, as depicted in the following equation:

$$\sigma_j = \left[M_{jj}^{-1} \frac{\sum_{i=1}^N w_i (y_{io} - y_{ic})^2}{N - P} \right] \quad (5.17)$$

M_{jj} is the diagonal element of the inverse of matrix M_{jk} , which is given by the equation below:

$$M_{jk} = -\sum_i w_i \left[(y_{io} - y_{ic}) \frac{\partial^2 y_{ic}}{\partial x_j \partial x_k} - \frac{\partial y_{ic}}{\partial x_j} \frac{\partial y_{ic}}{\partial x_k} \right] \quad (5.18)$$

x_j and x_k are adjustable parameters.

The figures-of-merit or *R*-values after refining, some formulae are presented as follows.

Bragg *R* factor for every phase:

$$R_B = \frac{\sum |I_{ko} - I_{kc}|}{\sum I_{ko}} \quad (5.19)$$

where I_{ko} and I_{kc} are observed and calculated intensities for Bragg reflection *k*.

Profile *R* factor

$$R_p = \frac{\sum_i |y_{io} - y_{ic}|}{\sum y_{io}} \quad (5.20)$$

Weighted profile *R* factor

$$R_{wp} = \left[\frac{\sum w_i (y_{io} - y_{ic})^2}{\sum w_i y_{io}^2} \right]^{1/2} \quad (5.21)$$

Expected *R* factor

$$R_{\text{exp}} = \left[\frac{N - P}{\sum w_i y_{io}^2} \right]^{1/2} \quad (5.22)$$

where N = number of observations and P = number of least – squares parameters being estimated.

The *GOF* is determined by the following equation.

$$GOF = \left(\frac{R_{wp}}{R_{\text{exp}}} \right)^2 \quad (5.23)$$

Equation (5.23) is the last statement of the Rietveld analysis because the best value of *GOF* should be 1.0. However, some researchers have suggested that the value should be less than four for phase abundance data analysis (Kisi, 1994). The difference plots between the observation and the calculation patterns play an important role for assessing the determination of good refinement. The two patterns should give a flat difference for a well-refined model. The difference plots may show indication of the presence of undetected phases or inaccuracies in the background or peak shape modeling.

Table 5.17: List of structure models, ICSD numbers and authors used for the Rietveld Analysis

Structural model	ICSD number	Author
α -Al ₂ O ₃	73725	Maslen et al.
Al ₂ TiO ₅	71356	Epicier et al.
TiO ₂ (Rutile)	64987	Shintani et al.
Ti ₃ SiC ₂	86213	Kisi et al.
TiC	1546	Christensen
TiO	60483	Loehman et al.
SiO ₂ (Cristobalite)	44095	Feng Liu et al.
SiO ₂ (Tridymite)	29343	Fleming et al.
TiSi ₂	1089	Jeitschko et al.
Ti ₅ Si ₃ C _x	44386	Nowotny et al.*
Ti ₅ Si ₃ C	unknown	Riley [#]

* For X-Ray Diffraction

[#] For Neutron Diffraction

5.3 Appendix I-G: Supplementary Information on (i) “Effect of Vacuum Annealing on the Phase Stability of Ti_3SiC_2 ”, (ii) “Diffraction Studies of a Novel Ti_3SiC_2 -TiC System with Graded Interfaces”

LOW, I.M., OO, Z. & PRINCE, K.E. 2007. Effect of Vacuum Annealing on the Phase Stability of Ti_3SiC_2 , *Journal of the American Ceramic Society*, 90, 2610-2614.

LOW, I.M. & OO, Z. 2002. Diffraction Studies of a Novel Ti_3SiC_2 -TiC System with Graded Interfaces, *Journal of the Australian Ceramic Society*, 38, 112-116.

5.3.1 POLARIS Medium-Resolution, High Intensity Powder Diffractometer

In situ ToF diffraction patterns were collected using the Polaris medium resolution and high intensity diffractometer at the UK pulsed spallation neutron source ISIS, at the Rutherford Appleton Laboratory in the UK. In-Situ ToF diffraction is used to monitor the structural evolution of phase decomposition in Ti_3SiC_2 at high temperature in real time.

For a ToF neutron diffraction measurement, the time of flight, t , as a reflection of its d -spacing is determined by three instruments or diffractometer constants, namely, DIFC, DIFA and ZERO.

$$t = \text{DIFC} \times d + \text{DIFA} \times d^2 + \text{ZERO} \quad (5.24)$$

DIFC is a constant relating to the theoretical time-of-flight of a measured Bragg reflection to its d -spacing and can be calculated by Bragg Law,

$$\lambda = 2d \sin \theta \quad (5.25)$$

with the de Broglie wavelength,

$$\lambda = \frac{h}{mv} = \frac{ht}{mL} \quad (5.26)$$

To have the expression for time-of-flight,

$$t = \left(\frac{2m}{h}\right)L \sin \theta \times d \quad (5.27)$$

where t = total time-of flight, m = mass of the neutron (1.67×10^{-27} kg), L = total time flight path from moderator to sample to detector, d = spacing, θ = $\frac{1}{2}$ of Bragg reflection angle (2θ), h = Planck's constant 6.62×10^{-34} Js.

After substituting and simplification, the Equation (5. 27) becomes,

$$t = 505.56L \sin \theta \times d \quad (5.28)$$

where t is in μs , L is in m , and d is in \AA

Therefore, it is found that,

$$\text{DIFC} = 505.56L\sin\theta \quad (5.29)$$

DIFA describes the wavelength dependence of the neutron absorption cross-section of an atom. Shorter wavelength neutrons will experience less absorption than the larger wavelength neutrons. Thus, the average penetration of the sample, the apparent total flight path and the scattering angle will vary with the neutron wavelength and the observed ToF. DIFA introduces a minor correction to the calculated ToF of a reflection to allow for peak shift due to absorption in the sample. Empirically it has been found that the quadratic equation depends on d^2 and it provides a good fit to observe shifts in reflection positions. Note that DIFA is initially set to a fit value but refinable.

The constant “ZERO” accounts for all differences between the various timing signals in the accelerator and the instrument data acquisition system, and also allows for the finite response times in the detector electronic. “ZERO” is a fixed value of the samples measured by the beamline scientists. The values of these diffractometer constants and the measurement conditions using POLARIS at ISIS are 4571.08 for DIFC constant, -0.69 (refinable) for DIFA value and 1.9 (fixed) for ZERO. The operational conditions used in the experimental work are tabulated in Table 5.18.

Table 5.18: (a), (b) and (c) Operational conditions when using in POLARIS

Table 5.18 (a)

Requirement	Setting
• sample dimension	: 10mm × 10mm × 40mm (rectangular bar shape)
• sample collection temperature	: 20°C and at every 100 °C between 1100°C and 1500°C at a rate of 20°C per minute
• data collection time	: 15 min for elevated temperature and 1 h for room temperature diffraction patterns
• d – spacing range	: 0.4 - 3.2 Å
• time channel size dT/ T	: 0.0005

Table 5.18 (b)

Requirement	Setting
Radiation	
• neutron beam	: Polychromatic white neutron beam (316K)
• moderator	: H ₂ O
• incident wavelength	: 0.6 to 6.2 Å
• resolution, $\Delta d/d$: 0.007
• Neutron flight path	: 12.75 to 12.85 m

Table 5.18 (c)

Requirement	Setting
Beam size	
• incident beam	: 10 × 40 mm
• scatter beam	: 11-mm gap in collimating slit
Atmosphere	
• Vacuum furnace	: ~ 10 ⁻⁴ torr
Detector	: fiber coated ZnS : Ag/6LiF Scintillation detector
Data collection format	: GSAS, General Structure Analysis System

5.3.2 X-Ray Diffraction (XRD)

X-ray diffraction (XRD) patterns of oxidized and vacuum-annealed Ti_3SiC_2 samples at various temperatures were obtained with an automated Siemens D500 Bragg-Brentano instrument (Eindhoven, the Netherlands).

A crystal structure of a crystalline material can be analyzed using XRD. When a beam of X - ray of a single wavelength strikes the materials, X- rays are scattered in all directions. The X-rays are diffracted when conditions satisfy the Bragg's Law.

$$2d \sin \theta = \lambda \quad (5.30)$$

Angle θ is half the angle between the diffracted beam and the original beam direction, λ is the wavelength of the x-rays, d is the inter planer spacing between the plane that causes the constructive reinforcement of the beam. In a diffractometer, a moving X-rays detector records the 2θ angle at which the beam is diffracted giving a characteristic diffraction patterns (Callister, 2003).

Table 5.19: Operational conditions when using XRD

Requirement	Setting
• sample dimension	: 3 mm thick (thin flat plate)
• X-rays beam	: Cu K α radiation
• required voltage and current	: 40 kV, 30 mA
• incident wavelength	: $\lambda = 0.15418$ nm
• 2θ range	: $5^\circ - 130^\circ$
• step size	: 0.04
• counting time	: 2.4 sec per step
• sample holder	: Al

5.4 Appendix I-H: Supplementary Information on (i) “Effect of Vacuum Annealing on the Phase Stability of Ti_3SiC_2 ”, (ii) “Dynamic Study of the Thermal Stability of Impure Ti_3SiC_2 in Argon and Air by Neutron Diffraction”

LOW, I.M., OO, Z. & PRINCE, K.E. 2007. Effect of Vacuum Annealing on the Phase Stability of Ti_3SiC_2 , *Journal of the American Ceramic Society*, 90, 2610-2614.

OO, Z., LOW, I.M. & O’CONNOR, B.H. 2006. Dynamic Study of the Thermal Stability of Impure Ti_3SiC_2 in Argon and Air by Neutron Diffraction. *Physica B*, 385-386, 499-501.

5.4.1 Secondary Ion Mass Spectroscopy (SIMS)

Secondary ion mass spectroscopy (SIMS) is one of the methods for gathering compositional information about the surface and near-surface regions of solid materials. It is also particularly suitable for the measurement of concentration profiles. The Cameca ims-5f SIMS of the Australian Nuclear Science and Technology Organization (ANSTO) facility was used to achieve the mapping of elemental and characterization of phase relations and properties in air-oxidized Ti_3SiC_2 .

SIMS involves the bombardment of a sample surface with a primary ion beam followed by mass spectrometry of the emitted secondary ions, as shown in Figure 5.18; SIMS is a semi destructive surface analytical technique. It has the advantage of being able to produce ions from solid samples without the intermediate stage of vaporization.

During SIMS analysis, the sample surface is slowly sputtered away by the primary ion beam, which can be focused to a spot of less than $1\mu\text{m}$ in diameter and can also be directed, enabling microanalysis and the measurement of the lateral distribution of elements on a microscopic scale. There are two modes available, static and dynamic. In the static mode a low sputtering rate gives only surface information and minimizes damage to the sample. Dynamic SIMS involves a high sputter rate, which leads to the formation of a crater in the sample. This produces information as a function of depth, called a depth profile. Continuous detection of these sputtered secondary ions allows SIMS to create a depth profile of the surface ($10\mu\text{m}$).

The SIMS line-scans and depth-profiles of air-oxidized Ti_3SiC_2 samples were obtained, while monitoring the yield of ^{48}Ti , ^{12}C , ^{28}Si and ^{16}O at the near-surface. The samples were gold-coated to avoid charging. According to the principle of SIMS, to study the characterization of phase relations and properties in air-oxidized Ti_3SiC_2 , positive secondary ion depth profiles were taken using 150 nA (for depth profiling) or 2nA (for line scan) primary Cs^+ ion current at 3 keV net impact energy, rastered over a $250 \times 250\mu\text{m}^2$ area. The ion current rates in all mass channels were normalized to the Cs^+ secondary ion counts rate to minimize the effect of variation in the primary ion beam

current, and as a mechanism for reducing matrix effects. Depth-profiling was conducted on samples with surface oxide layers of less than 10 μm . Line-scans were conducted on the cross-section of samples with relatively thick surface oxide layers ($>50 \mu\text{m}$).

Since a sample will gradually erode with time, a depth profile can be obtained by recording the detector signal as a function of time. The depth-profiling of oxidized Ti_3SiC_2 samples was obtained through the elemental imaging of Ti, Si, C and oxygen on the near-surface.

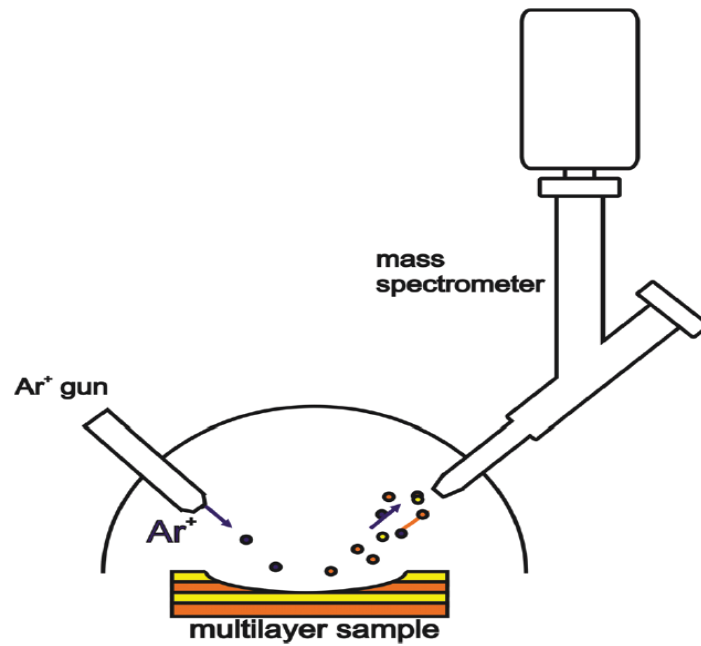


Figure 5.17: Schematic diagram for the Secondary Ion Mass Spectroscopy (SIMS)

Source: Institute for Research in Materials, Dalhousie University Canada.

(<http://www.hiden.com.cn>)

5.5 Appendix I-I: Supplementary Information on “Reformation of Phase Composition in Decomposed Aluminium Titanate”

LOW, I.M & OO, Z. 2008. Reformation of Phase Composition in Decomposed Aluminium Titanate. *Materials Chemistry and Physics*, 111, 9-12.

5.5.1 Differential Thermal Analysis (DTA) and Thermogravimetric Analysis (TGA)

The simultaneous DTA/TGA is used to study the phase decomposition and reactions during heating and cooling. It can also show whether the reaction mechanism is endothermic or exothermic reactions corresponding to the thermal energy changes in the sample.

Table 5.20: Operational condition when using DTA/TGA

Requirement	Setting
* instrument	: SETARAM
* atmosphere	: Air
* sample weight	: 10 mg
* temperature	: 1450 °C
* heating rate	: 10°C min ⁻¹
* crucible	: Al ₂ O ₃

.5.5.2 Scanning Electron Microscopy (SEM)

Microstructural characteristics were examined using the SEM Phillips XL30 at the Department of Imaging and Applied Physics, Curtin University, Australia. Scanning Electron Microscopy (SEM) has been used for generating high resolution images of the samples, mainly showing the cross-sectional microstructure of the materials. For this reason, scanning electron microscopy has been limited to observing microstructure and the microcracks of as-sintered Al_2TiO_5 (AT).

5.6 Appendix I-J: Supplementary Information on (i) “Effect of Atmospheres on the Thermal Stability of Aluminum Titanate”, (ii) “Reformation of Phase Composition in Decomposed Aluminium Titanate”, (iii) “In Situ Diffraction study of Self-Recovery in Aluminum Titanate” and (iv) “Dynamic Study of the Thermal Stability of Impure Ti_3SiC_2 in Argon and Air by Neutron Diffraction”

LOW, I.M. OO, Z. & O’CONNOR, B.H. 2006. Effect of Atmospheres on the Thermal Stability of Aluminum Titanate, *Physica B*, 385-386, 502-504.

LOW, I.M & OO, Z. 2008. Reformation of Phase Composition in Decomposed Aluminium Titanate. *Materials Chemistry and Physics*, 111, 9-12.

LOW, I.M. & OO, Z. 2008. In Situ Diffraction study of Self-Recovery in Aluminum Titanate. *Journal of the American Ceramic Society*, 90, 1027-1029.

OO, Z., LOW, I.M. & O’CONNOR, B.H. 2006. Dynamic Study of the Thermal Stability of Impure Ti_3SiC_2 in Argon and Air by Neutron Diffraction. *Physica B*, 385-386, 499-501.

5.6.1 MRPD-Medium Resolution Powder Diffraction (Neutron Diffraction)

The ND data collection was performed using a medium resolution powder diffractometer (MRPD) located at the Australian Nuclear Science and Technology Organization in Lucas Heights, NSW.

Neutron Diffraction is a crystallographic method for the determination of atomic and/or magnetic structure of materials (Hill and Howard, 1987). It offers bulk information of the sample materials, routinely used in complex and extreme environment.

Table 5.21: Operational conditions when using MRPD to analyze Al_2TiO_5

Requirement	Setting
* instrument	: MRPD diffractometer, Lucas Heights, NSW, Australia
* wavelength (λ)	: 1.667 Å
* range (2θ)	: 4 – 138°
* sample size	: 20 mm length \times 12mm in diameter
* step Size	: 0.1°
* counting time	: ~ 40 – 50 sec per step
* monochromator	: 8 Ge crystals (115 reflection),
* detectors	: 32 ^3He detectors 4° apart.
* analysis method	: Rietveld analysis

Table 5.22: Operational conditions when using MRPD to analyze Ti_3SiC_2

Requirement	Setting
* instrument	MRPD diffractometer, Lucas Heights, NSW, Australia
* wavelength (λ)	: 1.665 Å
* range (2θ)	: 10 – 135°
* step Size	: 0.1°
* counting time	: ~ 40 – 50 sec per step
*monochromator	: 8 Ge crystals (115 reflection),
*detectors	: 32 ^3He detectors 4° apart.
*analysis method	: Rietveld analysis

5.7 Appendix I-K: ICSD Crystal Structure Data

The following ICSD information is available in

Bergerhoff, G. & Brown, I.D. in "Crystallographic Databases", F.H. Allen et al. (Editor) Chester, International Union of Crystallography, (1987).

Alpha-Alumina (Al₂O₃)

Data for	ICSD #73725
Chemical Name	Aluminum Oxide
Structure	Al ₂ O ₃
Mineral Name	Corundum
Unit Cell	4.75450(5), 4.75450(5), 12.9820(6), 90°. 90°.120°
Space Group	R -3 C H
SG Number	167
Symmetry	Trigonal/ Rhombohedral

Atomic positions

Atom	Number	Wyckoff Site	x	y	z
Al	1	12c	0	0	0.35227
O	1	18e	0.6939	0	0.25

Reference:

Maslen, E. N., Streltsov, V. A., Streltsova, N. R., Ishizawa, N. & Satow, Y. 1993. Synchrotron X-ray Study of the Electron Density in Alpha-Al₂O₃, *Acta Crystallographica*, B49, 973-980.

Aluminium Titanium Oxide (Al₂TiO₅)

Data for	ICSD # 71356
Chemical Name	Dialuminum Titanium oxide
Structure	(Al ₂ Ti)O ₅
Mineral Name	Aluminum Titanate
Unit cell parameters	3.591, 9.429, 9.636, 90°, 90°, 90°
Space Group	Cm Cm
SG Number	63
Symmetry	Orthorhombic

Atomic positions

Atom	Number	Wyckoff Site	x	y	z
Ti	1	4C	0	0.1863	0.25
Al	1	4C	0	0.1863	0.25
Al	2	8F	0	0.1351	0.5613
Ti	2	8F	0	0.1351	0.5613
O	1	4C	0	0.759	0.25
O	2	8F	0	0.048	0.118
O	3	8F	0	0.317	0.075

Reference:

Epicier, T., Thomas, G., Wohlfromm, H. & Moya, J. S. 1991. High Resolution Electron Microscopy Study of the Cationic Disorder in Al₂TiO₅, *Journal of Materials Research*, **6**, 138-145.

Rutile (TiO₂)

Data for	ICSD # 64987
Chemical name	Titanium oxide
Structure	TiO ₂
Mineral Name	Rutile
Unit Cell	4.5845(1), 4.5845(1), 2.9533(1), 90°, 90°, 90°
Space Group	P 42 /m n m
SG Number	136
Symmetry	Tetragonal

Atomic positions

Atom	Number	Wyckoff site	x	y	z
Ti	1	2a	0	0	0
O	1	4f	0.3049	0.3049	0

Reference:

Shintani, H., Sato, S. & Saito, Y. 1975. Electron-Density Distribution in Rutile Crystals, *Acta Crystallographica*, B 31, 1981-1982.

Titanium Silicide Carbide (Ti₃SiC₂)

Data for	ICSD # 86213
Chemical name	Titanium Silicide Carbide
Structure	Ti ₃ SiC ₂
Unit Cell	3.30575(1), 3.0575 (1), 1.762349(30), 90° 90° 120°
Space Group	P 63 /m m c
SG Number	194
Symmetry	Hexagonal

Atomic positions

Atom	Number	Wyckoff site	x	y	z
Ti	1	2a	0	0	0
Ti	2	4f	0.6667	0.3333	0.1355(1)
Si	1	2b	0	0	0.75
C	1	4f	0.3333	0.6667	0.722(1)

Reference:

Kisi, E. H., Crossley, J. A. A., Myhra, S. & Barsoum, M. W. 1998. Structure and Crystal Chemistry of Ti₃SiC₂, *Journal of Physics and Chemistry of Solids*, 59, (9), 1437-1443.

Titanium Carbide (TiC)

Data for	ICSD # 1546
Chemical name	Titanium Carbide(1/1)
Structure	TiC
Unit Cell	4.328(2), 4.4328(2), 4.4328(2), 90° 90° 90°
Space Group	F m -3m
SG Number	225
Symmetry	Cubic

Atomic positions

Atom	Number	Wyckoff site	x	y	z
Ti	1	4a	0	0	0
C	1	4b	0.5	0.5	0.5

Reference:

Christensen, A. N. 1978. The Temperature Factor Parameters of some Transition Metal Carbides and Nitrides by Single Crystal X-ray and Neutron Diffraction, *Acta Chemica Scandinavica, Series A.* 32, 89-90.

Silicon Oxide (Cristobalite) SiO₂

Data for	ICSD # 44094
Chemical name	Silicon oxide-Ht
Structure	SiO ₂
Mineral Name	Cristobalite
Unit Cell	4.9586, 4.9586, 6.9074, 90° 90° 90°
Space Group	P 41 21 2
SG Number	92
Symmetry	Tetragonal

Atomic positions

Atom	Number	Wyckoff site	X	Y	Z
Si	1	4a	0.3028	0.3028	0
O	1	8b	0.2383	0.1093	0.1816

Reference:

Feng, L., Garofalini, S. H., King-Smith, D. & Vanderbilt, D. 1994. First-Principles Study of Crystalline Silica, *Physical Review B – Condensed Matter and Materials Physics*, 49, 12528-12534.

Tridymite (SiO₂)

Data for	ICSD # 29343
Chemical name	Silicon oxide- Subcell
Structure	SiO ₂
Mineral Name	Tridymite 2H low
Unit Cell	5.01, 5.01, 8.18, 90° 90° 120°
Space Group	P 63 2 2
SG Number	182
Symmetry	Hexagonal

Atomic positions

Atom	Number	Wyckoff site	x	y	z
Si	1	4f	0.3333	0.6667	0.47
O	1	2c	0.3333	0.6667	0.25
O	2	6g	0.425	0	0

Reference:

Fleming, J. E. & Lynton, H. 1960. A Preliminary Study of the Crystal Structure of Low Tridymite, *Physics and Chemistry of Glasses*, 1, 148-154.

Titanium Oxide (TiO)

Data for	ICSD # 60483
Chemical name	Titanium Oxide
Structure	TiO
Mineral Name	Titanium Oxide
Unit Cell	4.2493
Space Group	Fm-3m
SG Number	225
Symmetry	Cubic FCC

Atomic positions

Atom	Number	x	y	Z	Occupancy
Ti	1	0.000	0.000	0.000	0.000
O	1	0.500	0.500	0.500	0.000

Reference:

Loehman, R. E., Rao, C. N. R. & Honig, J. M. 1969. Crystallography and Defect Chemistry of Solid Solutions of Vanadium and Titanium Oxides, *Journal of Physical Chemistry*, 73, 1781-1784.

Titanium Silicon Carbide ($\text{Ti}_5\text{Si}_3\text{C}$)

Chemical Name	Titanium Silicon Carbide
Structure	$\text{Ti}_5\text{Si}_3\text{C}$
Unit Cell	7.4067 5.3062
Space Group	P 63/ m c m
SG Number	193

Atomic positions

Atom	Number	Wyckoff site	x	y	z
Ti	1	4d	0.3333	0.6667	0
Ti	2	6g	0.25	0	0.25
Si	1	6g	0.615	0	0.25
C	1	2b	0	0	0

Reference:

(Adopted from) RILEY, D. P. 2003. In-situ Neutron Diffraction Analysis of Titanium Silicon Carbide (Ti_3SiC_2) during Self-Propagating High-Temperature Synthesis *PhD Thesis*, The University of Newcastle, Australia.

Titanium Silicon (TiSi₂)

Data for	ICSD #1089
Chemical name	Titanium Silicon
Structure	TiSi ₂
Unit Cell	8.267, 4.800, 8.550 90. 90. 90
Vol	339.3
Space Group	Fddd (70)
SG Number	167
Symmetry	Orthorhombic

Reference:

Jeitschko, W. 1977. Refinement of the Crystal Structure of TiSi₂ and some Comments on Bonding in TiSi₂ and Related Compounds, *Acta Crystallographica*, Sec B, 33. 2347-2348.

6. APPENDIX II-A: STATEMENT OF CONTRIBUTIONS OF OTHERS

- 6.1 Appendix II-A: Statement of Contribution of Others for “LOW, I.M. OO, Z. & O’CONNOR, B.H. 2006. Effect of Atmospheres on the Thermal Stability of Aluminium Titanate. *Physica B*, 385-386, 502-504”.**

Statement of Contribution of Others for “Effect of Atmospheres on the Thermal Stability of Aluminium Titanate

27 June 2013

To Whom It May Concern

I, Mr Zeya Oo, contributed by samples preparation and all Rietveld analysis of ND data to the paper publication entitled


LOW, I.M. **OO, Z.** & O’CONNOR, B.H. 2006. Effect of Atmospheres on the Thermal Stability of Aluminium Titanate. *Physica B*, 385-386, 502-504,

Under taken with Zeya Oo

A handwritten signature in black ink, appearing to read 'Zeya Oo', with a horizontal line drawn underneath.

(Signature of Co-author 1)

Zeya Oo

A handwritten signature in black ink, appearing to read 'I.M. Low', with a horizontal line drawn underneath.

(Signature of First author)

I.M Low

Statement of Contribution of Others for “Effect of Atmospheres on the Thermal Stability of Aluminium Titanate

27 Jun 2013

To Whom It May Concern

I, Prof B. H. O Connor, contributed by specialist technical advice and manuscript editing to the paper/publication entitled

LOW, I.M. **OO, Z.** & O’CONNOR, B.H. 2006. Effect of Atmospheres on the Thermal Stability of Aluminium Titanate. *Physica B*, 385-386, 502-504,

Under taken with Zeya Oo



(Signature of Co-Author 2)

B.H. O’Connor



(Signature of Co-Author 1)

Zeya Oo

Statement of Contribution of Others for “Effect of Atmospheres on the Thermal Stability of Aluminium Titanate

27 June 2013

To Whom It May Concern

I, Prof B. H. O Connor, contributed by specialist technical advice and manuscript editing to the paper/publication entitled

LOW, I.M. **OO, Z.** & O’CONNOR, B.H. 2006. Effect of Atmospheres on the Thermal Stability of Aluminium Titanate. *Physica B*, 385-386, 502-504,

Under taken with Zeya Oo



(Signature of Co-Author 2)

B.H. O’Connor



(Signature of First-Author)

I. M. Low

6.2 Appendix II-B: “Statement of Contribution of Others” for LOW, I.M. & OO, Z. 2008. In Situ Diffraction study of Self-Recovery in Aluminium Titanate. *Journal of the American Ceramic Society*, 91[3], 1027-1029”.

Statement of Contribution of Others for “In Situ Diffraction study of Self-Recovery in Aluminium Titanate”

27 June 2013

To Whom It May Concern

I, Mr Zeya Oo, contributed by samples preparation and all Rietveld analysis of ND data to the paper/publication entitled

LOW, I.M. & OO, Z. 2008. In Situ Diffraction study of Self-Recovery in Aluminium Titanate. *Journal of the American Ceramic Society*, 91[3], 1027-1029”.

Undertaken with Zeya Oo

A handwritten signature in black ink, appearing to read 'Zeya Oo', with a horizontal line underneath.

(Signature of Co-Author)

Zeya Oo

A handwritten signature in black ink, appearing to read 'I. M. Low', with a horizontal line underneath.

(Signature of First Author)

I. M. Low

6.3 Appendix II-C: “Statement of Contribution of Others” for “LOW, I. M. & OO, Z. 2008. Reformation of Phase Composition in Decomposed Aluminium Titanate. *Materials Chemistry and Physics*, 11, 9-12”.

Statement of Contribution of Others for “Reformation of Phase Composition in Decomposed Aluminium Titanate”

27 June 2013

To Whom It May Concern

I, Mr Zeya Oo, contributed by samples preparation, microstructure evaluation, and all Rietveld analysis of ND data to the paper/publication entitled


LOW, I. M. & OO, Z. 2008. Reformation of Phase Composition in Decomposed Aluminium Titanate. *Materials Chemistry and Physics*, 11, 9-12”.

Undertaken with Zeya Oo



(Signature of Co-Author)

Zeya Oo



(Signature of First Author)

I. M. Low

- 6.4 Appendix II-D: “Statement of Contribution of Others” for “LOW, I.M. and OO, Z. 2002. Diffraction Studies of a Novel Ti_3SiC_2 -TiC system with Graded Interfaces. *Journal of the Australian Ceramic Society*, 38, 2, 2002, 112-116”.**

Statement of Contribution of Others for “Diffraction Studies of a Novel Ti₃SiC₂-TiC system with Graded Interfaces”

27 June 2013

To Whom It May Concern

I, Mr Zeya Oo, contributed by samples preparation, microstructure evaluation, and all Rietveld analysis of ND data and XRD data to the paper/publication entitled

LOW, I.M. & OO, Z. 2002. Diffraction Studies of a Novel Ti₃SiC₂-TiC system with Graded Interfaces. *Journal of the Australian Ceramic Society*, 38, 2, 2002, 112-116.

Undertaken with Zeya Oo

A handwritten signature in black ink, appearing to read 'Zeya Oo', with a stylized flourish at the end.

(Signature of Co-Author)

Zeya Oo

A handwritten signature in black ink, appearing to read 'I. M. Low', with a horizontal line under the 'w'.

(Signature of First Author)

I. M. Low

6.5 Appendix II-E: “Statement of Contribution of Others” for “LOW, I.M., OO, Z., & PRINCE, K. E. 2007. Effect of Vacuum Annealing on the Phase Stability of Ti_3SiC_2 . *Journal of the American Ceramic Society*, 90, 2610-2614”.

Statement of Contribution of Others for “Effect of Vacuum Annealing on the
Phase Stability of Ti_3SiC_2 ”

27 June 2013

To Whom It May Concern

I, Dr. K. E. Prince, contributed by specialist technical advice and instrument usage to the paper/preparation entitled

LOW, I.M., OO, Z., & PRINCE, K. E. 2007. Effect of Vacuum Annealing on the Phase Stability of Ti_3SiC_2 . *Journal of the American Ceramic Society*, 90, 2610-2614.

Undertaken with Zeya Oo



(Signature of Co-Author 1)

Zeya Oo



(Signature of Co-Author 2)

K. E Prince

Statement of Contribution of Others for “Effect of Vacuum Annealing on the
Phase Stability of Ti_3SiC_2 ”

27 June 2013

To Whom It May Concern

I, Mr Zeya Oo, contributed by samples preparation, microstructure evaluation, and all Rietveld analysis of ND data and XRD data to the paper/publication entitled

LOW, I.M., **OO, Z.**, & PRINCE, K. E. 2007. Effect of Vacuum Annealing on the Phase Stability of Ti_3SiC_2 . *Journal of the American Ceramic Society*, 90, 2610-2614.

Undertaken with Zeya Oo



(Signature of Co-Author)

Zeya Oo



(Signature of First Author)

I. M. Low

Statement of Contribution of Others for “Effect of Vacuum Annealing on the
Phase Stability of Ti_3SiC_2 ”

27 June 2013

To Whom It May Concern

I, Dr. K. E. Prince, contributed by specialist technical advice and instrument usage to the paper/preparation entitled


LOW, I.M., OO, Z., & PRINCE, K. E. 2007. Effect of Vacuum Annealing on the Phase Stability of Ti_3SiC_2 . *Journal of the American Ceramic Society*, 90, 2610-2614.

Undertaken with Zeya Oo



(Signature of Co-Author 2)

K. E Prince



(Signature of First Author)

I. M. Low

6.6 Appendix II-F: “Statement of Contribution of Others” for “OO, Z., LOW, I.M. & O’ CONNOR, B. H. 2006. Dynamics Study of the Thermal Stability of Impure Ti_3SiC_2 in Argon and Air by Neutron Diffraction. *Physica B*, 385-386, 499-501”.

Statement of Contribution of Others for “Dynamics Study of the Thermal Stability of Impure Ti₃SiC₂ in Argon and Air by Neutron Diffraction”

27 June 2013

To Whom It May Concern

I, Prof. B. H. O Connor, contributed by specialist technical advice and manuscript editing to the paper/publication entitled

OO, Z., LOW, I.M. & O’CONNOR, B. H. 2006. Dynamics Study of the Thermal Stability of Impure Ti₃SiC₂ in Argon and Air by Neutron Diffraction. *Physica B*, 385-386, 499-501.

Undertaken with Zeya Oo



(Signature of Co-Author)

B. H. O’Connor



(Signature of First Author)

Zeya Oo

Statement of Contribution of Others for “Dynamics Study of the Thermal Stability of Impure Ti_3SiC_2 in Argon and Air by Neutron Diffraction”

27 June 2013

To Whom It May Concern

I, Prof. I. M. Low contributed by project supervision and manuscript editing to the paper/publication entitled

OO, Z., LOW, I.M. & O’CONNOR, B. H. 2006. Dynamics Study of the Thermal Stability of Impure Ti_3SiC_2 in Argon and Air by Neutron Diffraction. *Physica B*, 385-386, 499-501.

Undertaken with Zeya Oo



(Signature of Co-Author)

I. M. Low



(Signature of First Author)

Zeya Oo

7. APPENDIX III: COPYRIGHT FORMS

7.1 Appendix III-A : Elsevier Journal Articles

Copyright information relating to:

LOW, I. M., OO, Z. & O'CONNOR, B. H. 2006. Effect of Atmospheres on the Thermal Stability of Aluminium Titanate . *Physica B*, 385-386, 502-504.

LOW, I. M. & OO, Z. 2008. Reformation of Phase Composition in Decomposed Aluminium Titanate. *Materials Chemistry and Physics*, 111, 9-12.

OO, Z., LOW, I. M. & O'CONNOR, B. H. 2006. Dynamic Study of the Thermal Stability of Impure Ti_3SiC_2 in Argon and Air by Neutron Diffraction. *Physica B*, 385-386, 499-501.

Available on

<http://www.elsevier.com/wps/find/authorsview.authors/copyright>

What rights do I retain as a journal author*?

As a journal author, you retain rights for a large number of author uses, including use by your employing institute or company. These rights are retained and permitted without the need to obtain specific permission from Elsevier. These include:

- the right to make copies (print or electric) of the journal article for their own personal use, including for their own classroom teaching use;
- the right to make copies and distribute copies (including via e-mail) of the journal article to research colleagues, for personal use by such colleagues (but not for Commercial Purposes**, as listed below);
- the right to post a pre-print version of the journal article on Internet web sites including electronic pre-print servers, and to retain indefinitely such version on such servers or sites (see also our information on [electronic preprints](#) for a more detailed discussion on these points);
- the right to post a revised personal version of the text of the final journal article (to reflect changes made in the peer review process) on the author's personal or institutional web site or server, incorporating the complete citation and with a link to the Digital Object Identifier (DOI) of the article;
- the right to present the journal article at a meeting or conference and to distribute copies of such paper or article to the delegates attending the meeting;
- for the author's employer, if the journal article is a 'work for hire', made within the scope of the author's employment, the right to use all or part of the information in (any version of) the journal article for other intra-company use (e.g. training), including by posting the article on secure, internal corporate intranets;
- patent and trademark rights and rights to any process or procedure described in the journal article; *
- **the right to include the journal article, in full or in part, in a thesis or dissertation;**
- the right to use the journal article or any part thereof in a printed compilation of works of the author, such as collected writings or lecture notes (subsequent to publication of the article in the journal); and
- the right to prepare other derivative works, to extend the journal article into book-length form, or to otherwise re-use portions or excerpts in other works, with full acknowledgement of its original publication in the journal.

***Please Note:** *The rights listed above apply to journal authors only. For information regarding book author rights, please contact the **Global Rights Department**.*

Elsevier Global Rights Department
phone (+44) 1865 843 830
fax (+44) 1865 853 333
email: permissions@elsevier.com

7.2 Appendix III-B: Wiley Inter-Science Articles

Copyright information relating to:

LOW, I. M. & OO, Z. 2008. In Situ Diffraction Study of Self-Recovery in Aluminium Titanate. *Journal of the American Ceramic Society*, 91, 1027-1029.

LOW, I. M., OO, Z. & PRINCE, K. E. 2007. Effect of Vacuum Annealing on the Phase Stability of Ti_3SiC_2 , *Journal of the American Ceramic Society*, 90, 2610-2614.

**JOHN WILEY AND SONS LICENSE
TERMS AND CONDITIONS**

Sep 05, 2012

This is a License Agreement between Zeya Oo ("You") and John Wiley and Sons ("John Wiley and Sons") provided by Copyright Clearance Center ("CCC"). The license consists of your order details, the terms and conditions provided by John Wiley and Sons, and the payment terms and conditions.

All payments must be made in full to CCC. For payment instructions, please see information listed at the bottom of this form.

License Number	2933420405882
License date	Jun 20, 2012
Licensed content publisher	John Wiley and Sons
Licensed content publication	Journal of the American Ceramic Society
Licensed content title	In Situ Diffraction Study of Self-Recovery in Aluminum Titanate
Licensed content author	It-Meng Low,Zeya Oo
Licensed content date	Feb 4, 2008
Start page	1027
End page	1029
Type of use	Dissertation/Thesis
Requestor type	Author of this Wiley article
Format	Print and electronic
Portion	Full article
Will you be translating?	No
Order reference number	
Total	0.00 USD
Terms and Conditions	

TERMS AND CONDITIONS

This copyrighted material is owned by or exclusively licensed to John Wiley & Sons, Inc. or one of its group companies (each a "Wiley Company") or a society for whom a Wiley Company has exclusive publishing rights in relation to a particular journal (collectively WILEY). By clicking "accept" in connection with completing this licensing transaction, you agree that the following terms and conditions apply to this transaction (along with the billing and payment terms and conditions established by the Copyright Clearance Center Inc., ("CCC's Billing and Payment terms and conditions"), at the time that you opened your Rightslink account (these are available at any time at <http://myaccount.copyright.com>)

Terms and Conditions

1. The materials you have requested permission to reproduce (the "Materials") are protected by copyright.
2. You are hereby granted a personal, non-exclusive, non-sublicensable, non-transferable,

https://s100.copyright.com/CustomerAdmin/PLF.jsp?IID=2012061_1340250309882

9/5/2012

7.3 Appendix III-C: Journal of the Australian Ceramic Society Article

Copyright information relating to:

LOW, I. M. & OO, Z. 2002. Diffraction Studies of a Novel Ti_3SiC_2 -TiC System with Graded Interfaces. *Journal of the Australian Ceramic Society*. 38, 112-116.

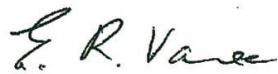
**PERMISSION TO USE COPYRIGHT MATERIAL FROM THE JOURNAL OF THE
AUSTRALIAN CERAMIC SOCIETY**

LOW, I.M. & OO, Z. 2002. Diffraction Studies of a Novel Ti_3SiC_2 -TiC System with Graded Interfaces, *Journal of the Australian Ceramic Society* 38, 2, 112-116.

I hereby give permission for Zeya Oo to include the above mentioned material in his higher degree thesis for the Curtin University, to communicate this material via the Australasian Digital Thesis Program. This permission is granted on a non-exclusive basis and for an indefinite period.

I confirm that I am the copyright owner of the specified article.

Permission to use this article is subject to the following conditions:

Signed : 
Name: E. R. VANCE
Position: ACS JOURNAL CO-EDITOR
Date: 15 OCTOBER 2012

8. BIBLIOGRAPHY (References cited in Appendices)

- CAGLIOTI, G., PAOLETTI, A. & RICCI, F. P. 1958. Choice of Collimators for a Crystal Spectrometer for Neutron Diffraction, *Nuclear Instruments*, 3, 223-228.
- CALLISTER, W. JR. 2003. Materials Science and Engineering, An Introduction. 6th Edition. John Wiley & Sons, Inc., New York.
- CHRISTENSEN, A. N. 1978. The Temperature Factor Parameters of Some Transition Metal Carbides and Nitrides by Single Crystal X-Ray and Neutron Diffraction, *Acta Chemica Scandinavica, Series A*, 32, 89-90.
- EPICIER, T., THOMAS, G., WOHLFROMM, H. & MOYA, J. S. 1991. High Resolution Electron Microscopy Study of the Cationic Disorder in Al_2TiO_5 , *Journal of Materials Research*, 6, 138-145.
- FENG, L., GAROFALINI, S. H., KING-SMITH, D. & VANDERBIL, T. D. 1994. First-Principles Study of Crystalline Silica, *Physical Review B – Condensed Matter and Materials Physics*, 49, 12528-12534.
- FLEMING, J. E. & LYNTON, H. 1960. A Preliminary Study of the Crystal Structure of Low Tridymite, *Physics and Chemistry of Glasses*, 1, 148-154.
- HILL, R. J., HOWARD, C. J. & HUNTER, B. A. 1995. Computer Program for Rietveld Analysis of Fixed Wavelength X-Ray and Neutron Powder Diffraction Patterns. Australian Atomic Energy Commission (now ANSTO) Report No. M112, Lucas Heights Research Laboratories, New South Wales, Australia.
- HUNTER, B. A. & HOWARD, C. J. 1998. A Computer Program (LHPM) for Rietveld Analysis of X-Ray and Neutron Powder Diffraction Patterns. Australian Nuclear Science and Technology Organization, Lucas Heights Research Laboratories, New South Wales, Australia, 1-27.
- JEITSCHKO, W. 1977. Refinement of the Crystal Structure of TiSi_2 and Some Comments on Bonding in TiSi_2 and Related Compounds, *Acta Crystallographica, Sec B*, 33, 2347-2348.
- KISI, E. H. 1994. Rietveld Analysis of Powder Diffraction Patterns, *Materials Forum*, 18, 135-153.

- KISI, E. H., CROSSLEY, J. A. A., MYHRA, S. & BAROSUM, M. W. 1998. Structure and Crystal Chemistry of Ti_3SiC_2 , *Journal of Physics and Chemistry of Solids*, 59, (9), 1437-1443.
- LOEHMAN, R. E., RAO, C. N. R. & HONIG, J. M. 1969. Crystallography and Defect Chemistry of Solid Solutions of Vanadium and Titanium Oxides, *Journal of Physical Chemistry*, 73, 1781-1784.
- MASLEN, E. N., STRELTSOV, V. A., STRELTSOVA, N. R., ISHIZAWA, N. & SATOW, Y. 1993. Synchrotron X-Ray Study of the Electron Density in Alpha Al_2O_3 , *Acta Crystallographica*, B 49, 973 – 980.
- NORBERG, S. T., ISHIZAWA, N., STEFAN, H. & YOSHIMURA, M. 2005. Redetermination of $\beta-Al_2TiO_5$ Obtained by Melt Casting, *Acta Crystallographica*, E61, i160-i162.
- O'CONNOR, B. H. & LI, D. Y. 2000. Influence of Refinement Strategies on Rietveld Phase Composition Determination, *Advances in X-Ray Analysis*, 42, 204-211.
- RIETVELD, H. M. 1967. Line Profiles of Neutron Powder-Diffraction Peaks for Structure Refinement, *Acta Crystallographica*. 22, 151-152.
- RIETVELD, H. M. 1969. A Profile Refinement Method for Nuclear and Magnetic Structures, *Journal of Applied Crystallography*, 2, 65-71.
- RILEY, D. P. 2003. In-Situ Neutron Diffraction Analysis of Titanium Silicon Carbide (Ti_3SiC_2) During Self-Propagating High-Temperature Synthesis, *PhD Thesis*, The University of Newcastle, Australia.
- RILEY, D. P., KISI, E. H., HANSEN, T. C. & HEWAT, A. W. 2002. Self-Propagating High-Temperature Synthesis of Ti_3SiC_2 : I, Ultra-High-Speed Neutron Diffraction Study of the Reaction Mechanism, *Journal of the American Ceramics Society*, 85, 2417-2424.
- SHINTANI, H., SATO, S. & SAITO, Y. 1975. Electron-Density Distribution in Rutile Crystals, *Acta Crystallographica*. B 31, 1981-1982.
- WARREN, B. E. 1969. X-Ray Diffraction, Addison-Wesley, Massachusetts, USA.
- YOUNG, R.A. (Ed). 1993. The Rietveld Method. *International Union of Crystallography*, Oxford University Press, Great Britain.